General Disclaimer

One or more of the Following Statements may affect this Document

- This document has been reproduced from the best copy furnished by the organizational source. It is being released in the interest of making available as much information as possible.

- This document may contain data, which exceeds the sheet parameters. It was furnished in this condition by the organizational source and is the best copy available.

- This document may contain tone-on-tone or color graphs, charts and/or pictures, which have been reproduced in black and white.

- This document is paginated as submitted by the original source.

- Portions of this document are not fully legible due to the historical nature of some of the material. However, it is the best reproduction available from the original submission.

Produced by the NASA Center for Aerospace Information (CASI)

(NASA-CR-152328) FORWARD VELOCITY EFFECTS ON FAN NOISE AND THE SUPPRESSION CHARACTERISTICS OF ADVANCED INLETS AS MEASURED IN THE NASA-AMES 40 BY 80 FOOT WIND TUNNEL Final Report (General Electric Co.) 63/71 N82-30030 HC A08 Uncla. 30131

PRECEDING PAGE BLANK NOT FILMED

FOREWORD

This report was prepared by the Advanced Engineering and Technical Programs Department, Aircraft Engine Group, General Electric Company, Evendale, Ohio, under the sponsorship of the National Aeronautics and Space Administration, Ames Research Center, Moffett Field, California, under Contract NAS2-8675. The program was initiated on 7 May 1975, and this report covers the work done up to 7 November 1979. Mr. Michael D. Falarski was the Technical Project Monitor for NASA, and Mr. Michael T. Moore was the Program Technical Manager for the General Electric Company. Acknowledgement is made of the many contributions to this program by L.E. Langenbrunner, E.O. McCann, R.S. Coffin, J.A. Gilbert, and D.L. Shepherd.

PRECEDING PAGE BLANK NOT FILMED

TABLE OF CONTENTS

Section		Page
1.0	SUMMARY	1
2.0	INTRODUCTION	2
3.0	TEST DESCRIPTION	3
	3.1 Test Facilities	3
	3.1.1 NASA ARC Outdoor Test Stand	3
	3.1.2 NASA ARC 40 by 80 Foot Wind Tunnel	3
	3.2 Test Vehicle	3
	3.2.1 JT15D Turbofan Engine	3
	3.2.2 Nacelle, Nozzle, and Mount	8
	3.3 Inlet Configurations	13
	3.3.1 Baseline Inlet	13
	3.3.2 CTOL Hybrid Inlet	13
	3.3.3 STOL Hybrid Inlet	17
	3.3.4 Deflector Inlet	21
	3.3.5 Canted Baseline Inlet	28
	3.4 Test Setup	28
	3.4.1 Outdoor Static Tests	28
	3.4.2 Wind Tunnel Tests	28
	3.5 Instrumentation	34
	3.5.1 External Noise	34
	3.5.2 Internal Noise	34
	3.5.3 Aerodynamic Performance	34
	3.6 Test Summary	38
	3.6.1 Outdoor Static Tests	38
	3.6.2 Wind Tunnel Tests	48
	3.7 Data Reduction	52
	3.7.1 Aerodynamic Performance Data	53
	3.7.2 Fixed-Microphone Data	53
	3.7.3 Traverse-Microphone Data	53
	3.7.4 Internal-Noise Data	54
4.0	DATA ANALYSIS	56
	4.1 Analysis Techniques	56
	4.1.1 Wind Tunnel/Static Transformation	56
	4.1.2 Wind Tunnel Background Noise	59
	4.1.3 Large-Scale Turbofan Noise	59

TABLE OF CONTENTS (Concluded)

Section		Page
	4.2 Fan/Inlet Aerodynamic Performance	61
	4.2.1 Hybrid Inlet Throat Mach Number Determination	61
	4.2.2 Inlet Pressure Recovery and Distortion	64
	4.2.2.1 Zero Angle of Attack	64
	4.2.2.2 Non-Zero Angle of Attack	73
	4.2.3 Fan Operating Charactristics	81
	4.3 Baseline Inlet Acoustic Considerations	81
	4.3.1 Static-to-Flight Effects	81
	4.3.2 Fan-Modification Effects	92
	4.4 Hybrid Inlet Acoustic Performance	92
	4.4.1 Comparisons with Baseline Inlet	94
	4.4.2 Angle-of-Attack Effects	104
	4.4.3 Forward-Velocity Effects	104
	4.4.4 Effects on Large-Scale-Fan Noise	115
	4.5 Deflector Inlet Acoustic Performance	120
	4.5.1 Comparisons with Baseline Inlet	120
	4.5.2 Angle-of-Attack Effects	122
	4.5.3 Forward-Velocity Effects	127
	4.5.4 Effects on Large-Scale-Fan Noise	127
	4.6 Canted-Baseline-Inlet Acoustic Characteristics	127
	4.6.1 Comparisons with Baseline Inlet	135
	4.6.2 Effects on Large-Scale-Fan Noise	138
5.0	CONCLUSIONS AND RECOMMENDATIONS	144
	5.1 Fan-Noise Testing Techniques	144
	5.2 Forward-Velocity Testing in the 40 by 80	144
	5.3 Hybrid-Inlet Suppression at Forward Velocity	146
	5.4 Deflector-Inlet Suppression at Forward Velocity	146
	5.5 Canted-Inlet Effects on Fan Noise	147
	APPENDIX ABBREVIATIONS AND SYMBOLS	149
	REFERENCES	150

LIST OF ILLUSTRATIONS

Figure		Page
1.	NASA ARC VTOL Test Stand.	4
2.	NASA ARC 40 by 80 Wind Tunnel.	5
3.	Production JT15D Turbofan Engine.	6
4.	JT15D Fan Configuration.	9
5.	JT15D in Quiet Nacelle Used for Advanced Inlet Tests.	10
6.	JT15D/Quiet Nacelle and Mount Assembly.	11
7.	Rear-View Photo of JT15D/Quiet Nacelle Mounted in NASA ARC 40 by 80 Wind Tunnel.	12
8.	Sketch of Baseline Inlet.	15
9.	Photo of JT15D/Baseline Inlet with Aeroacoustic Lip.	16
10.	Photo of JT15D/Baseline Inlet with Flight Lip and Fairings.	16
11.	Sketch of Conventional Takeoff/Landing (CTOL) Hybrid Inlet.	18
12.	Photo of JT15D/CTOL Hybrid Inlet with Aeroacoustic Lip.	19
13.	Photo of JT15D/CTOL Hybrid Inlet with Flight Lip and Fairings.	19
14.	CTOL Hybrid Inlet Treatment Details.	20
15.	Sketch of Short Takeoff/Landing (STOL) Hybrid Inlet.	22
16.	Photo of JT15D/STOL Hybrid Inlet with Aeroacoustic Lip.	23
17.	Photo of JT15D/STOL Hybrid Inlet with Flight Lip and Fairings.	23
18.	STOL Hybrid Inlet Treatment Details.	24
19.	Sketch of Deflector Inlet with Flight Lip and Nacelle.	25
20.	Photos of JT15D/Deflector Inlet with Flight Lip and Fairings.	26
21.	Deflector-Inlet Treatment Details.	27

LIST OF ILLUSTRATIONS (Continued)

Figure		Page
22.	Sketch of Canted Baseline Inlet.	29
23.	Photos of JT15D/Baseline Inlet and JT15D/Canted Baseline Inlet with Fairings.	30
24.	Test Setup for First Outdoor Static and Wind Tunnel Tests.	31
25.	Test Setup for Second Wind Tunnel and Outdoor Static Tests.	32
26.	Test Setup in NASA ARC 40 by 80 Wind Tunnel (1st Entry).	33
27.	Test Setup in NASA ARC 40 by 80 Wind Tunnel (2nd Entry).	35
28.	Internal-Noise Transducer Locations.	36
29.	Wall Static Pressure Tap Locations.	39
30.	Discharge Total Pressure Rake Locations.	44
31.	Inlet Total Pressure Rake Locations.	45
32.	Photos of JT15D Fan Showing Total Pressure Rakes.	46
33.	Verification of Traverse Microphone Data Processing.	55
34.	Wind Tunnel Convection-Correction Nomenclature.	57
35.	Background Noise for 40 by 80 Wind Tunnel	60
36.	Predicted Wall Mach Number Distribution for Both Hybrid Inlets at Design Point.	62
37.	Predicted Wall Static Pressure Coefficient for Both Hybrid Inlets at Design Point.	63
38.	Typical Curves for Determining Hybrid Inlet Throat Mach Number.	65
39.	CTOL Hybrid Inlet: Design-Point Aerodynamic Performance.	66
40.	STOL Hybrid Inlet: Design-Point Aerodynamic Performance.	67
41.	Hybrid Inlet Throat Mach Number Variation with Fan Speed.	68
42.	Hybrid Inlet Pressure Recovery and Distortion at Zero Angle of Attack.	71

LIST OF ILLUSTRATIONS (Continued)

Figure		Page
43.	Deflector Inlet Pressure Recovery and Distortion at Zero Angle of Attack.	74
44.	CTOL Hybrid Inlet Pressure Recovery and Distortion at Angle of Attack.	75
45.	STOL Hybrid Inlet Pressure Recovery and Distortion at Angle of Attack.	77
46.	Deflector Inlet Pressure Recovery and Distortion at Angle of Attack.	79
47.	JT15D Fan Flow/Speed Curve for Production and Hybrid Inlet Nozzles.	82
48.	JT15D Fan Pressure Ratio/Speed Curve for Production and Hybrid Inlet Nozzles.	83
49.	JT15D Fan Flow/Pressure Ratio Map.	84
50.	Narrowband Spectra for Baseline Inlet at Static and Forward-Velocity Conditions.	86
51.	Narrowband BPF Noise Level Variation with Fan Speed for Baseline Inlet.	89
52.	Narrowband Spectra for Baseline Inlet with Standard and Redesigned JT15D Fan.	93
53.	Blade-Passing-Frequency, 1/3-Octave-Band Noise Directivity for Baseline and CTOL Inlets at Forward Velocity.	95
54.	One-Third-Octave-Band Noise Spectra for Baseline and CTOL Inlets at 41 m/s (135 ft/s) Forward Velocity.	96
55.	Blade-Passing-Frequency, 1/3-Octave-Band Noise Directivity for Baseline and STOL Inlets at Forward Velocity.	97
56.	One-Third-Octave-Band Noise Spectra for Baseline and STOL Inlets at 41 m/s (135 ft/s) Forward Velocity.	98
57.	Narrowband Spectra for Baseline and CTOL Inlets for 41 m/s (135 ft/s) Forward Velocity.	100
58.	Narrowband Spectra for Baseline and STOL Inlets at 41 m/s (135 ft/s) Forward Velocity.	102

LIST OF ILLUSTRATIONS (Continued)

Figure		Page
59.	CTOL Hybrid Inlet Fan Noise Suppression Spectra at Forward Velocity.	105
60.	STOL Hybrid Inlet Fan Noise Suppression Spectra at Forward Velocity.	106
61.	One-Third-Octave-Band Noise Spectra for CTOL Inlet at Three Angles of Attack.	107
62.	One-Third-Octave-Band Noise Spectra for STOL Inlets at Three Angles of Attack.	109
63.	One-Third-Octave-Band Noise Spectra for CTOL Inlets at Various Forward Velocities.	111
64.	One-Third-Octave-Band Noise Spectra for STOL Inlet at Various Forward Velocities.	113
65.	CTOL Noise Directivity (CF6 Size) at Forward Velocity.	116
66.	STOL Noise Directivity (QCSEE Size) at Forward Velocity.	118
67.	Blade-Passing-Frequency, 1/3-Octave-Band Noise Directivity for Baseline and Deflector Inlets at Forward Velocity.	121
68.	One-Third-Octave-Band Noise Spectra for Baseline and Deflector Inlets at 41 m/s (135 ft/s) Forward Velocity.	123
69.	One-Third-Octave-Band Noise Spectra for Deflector Inlet at Two Angles of Attack.	124
70.	Deflector Inlet Fan Entrance Static Pressure Distortion at Two Angles of Attack.	126
71.	Deflector Inlet Fan Entrance Static Pressure Distortion at Two Forward Velocities.	128
72.	One-Third-Octave-Band Noise Spectra for Deflector Inlet at Two Forward Velocities.	129
73.	Deflector Inlet Noise Directivity (CF6 Size) at Forward Velocity.	131
74.	Advanced Inlets Fan Noise Suppression Comparison.	133
75.	Canted-Inlet Effect on Fan Entrance Static Pressure.	136

LIST OF ILLUSTRATIONS (Concluded)

Figure		Page
76.	Narrowband BPF Noise Level Variation with Fan Speed for Canted Baseline Inlet.	137
77.	Narrowband Spectra for Baseline Inlet and Canted Baseline Inlet at V_T = 344 m/s (1129 ft/s).	139
78.	One-Third-Octave-Band Noise Spectra for Baseline and Canted Baseline Inlets at 41 m/s (135 ft/s) Forward Velocity.	140
79.	Blade-Passing-Frequency, 1/3-Octave-Band Noise Directivity for Baseline and Canted Baseline Inlets at Forward Velocity.	141
80.	Canted Baseline Inlet Noise Directivity (CF6 Size) at Forward Velocity.	142

LIST OF TABLES

Table		Page
1.	Production JT15D Parameters.	7
2.	Inlet Design Parameters.	14
3.	Run Logs for Outdoor Static Tests.	47
4.	Run Log for First 40 by 80 Wind Tunnel Test.	49
5.	Run Log for Second 40 by 80 Wind tunnel Test.	50
6.	Measurement Angles Required for Static Equivalent Angles at 10° Increments.	59
7.	JT15D Fan and Hybrid Inlet Test Parameters.	70

1.0 SUMMARY

Two hybrid inlets and a deflector inlet were tested along with a baseline inlet in the NASA Ames Research Center 40-by-80 Foot Wind Tunnel (40 by 80) with a small turbofan engine in a quiet nacelle to determine the forward-velocity effects on fan noise and the suppression characteristics of advanced inlets. Data were obtained from outdoor static tests to determine the effects of static-to-flight environment changes on the fan noise. The effects of canting the baseline inlet to simulate wing-mounted engine inlets were also determined for fan noise.

The static-to-flight effects are shown to be the reductions in blade-passing tone levels due to reducing the rotor-turbulence interaction noise inherent in outdoor static and wind tunnel quasi-static testing. Because these tone levels have substantial variability and mask other sources at low fan speeds, the static-to-flight effects are virtually unpredictable. Testing in the 40 by 80 at forward velocities of 21 m/s (68 ft/s) and above reduced the rotor-turbulence tone noise below all other fan noise sources so that the forward-velocity effects on fan noise and the suppression characteristics of advanced inlets could be determined.

At a forward velocity of 41 m/s (135 ft/s), the CTOL hybrid inlet suppressed the high-tip-speed fan noise as much as 18 PNdB on a 61 m (200 ft) sideline scaled to a CF6 size engine. This suppression level remained essentially the same over a throat Mach number range of $0.62 \leq M_{TH} \leq 0.77$ due to the treatment effects at low M_{TH} and the flow-acceleration effects at high M_{TH}. At a forward velocity of 41 m/s (135 ft/s), the STOL hybrid inlet suppressed the low-tip-speed fan noise as much as 13 PNdB on a 61 m (200 ft) sideline QCSEE size engine. This suppression level changed only slightly over a throat Mach number range of $0.62 \leq M_{TH} \leq 0.77$ due to treatment effects at low M_{TH} and a combination of treatment and flow-acceleration effects at high M_{TH}. There were essentially no changes in the fan-noise suppression characteristics of the hybrid inlets at forward velocities ranging from 21 m/s (68 ft/s) to 59 m/s (194 ft/s) at angles of attack up to 15°.

At a forward velocity of 41 m/s (135 ft/s), the deflector inlet suppressed the fan noise over a tip-speed range of 311 m/s (1020 ft/s) to 405 m/s (1330 ft/s) by as much as 13 PNdb at 61 m (200 ft) overhead, scaled to a CF6 size engine. The combination of noise redirection and treatment effects kept these suppression levels relatively unchanged over the full range of tip speeds. However, changes in both forward velocity and angle of attack caused unpredictable changes in these suppression levels.

Canting the baseline inlet centerline downward 4° relative to the engine centerline caused as much as a 7 PNdB increase in noise level at 61 m (200 ft) overhead, scaled to a CF6 size engine, at a forward velocity of 41 m/s (135 ft/s). The noise increase occurs at the critical noise-emission angles of 50° to 60° at fan speeds that are in the approach power setting range of large turbofan engines. These noise-level changes were found to be independent of changes in forward velocity and angle of attack.

2.0 INTRODUCTION

Extensive research has been conducted to understand and suppress the forward-radiated noise from the fan of a turbofan engine. However, most of this research has been conducted under static test conditions with no simulation of forward speed or angle of attack. Because the fan noise is related to the inlet flow environment, the forward-radiated noise is expected to be affected by forward speed. Flight effects on fan noise have been observed by investigators who have compared turbofan flyover noise with static noise, but the details are obscured by the mixture of aircraft-noise and other engine-noise sources. Therefore, in order to properly understand the fan-noise suppression characteristics of advanced inlets, the investigation should include actual or simulated flight testing.

The NASA Ames Research Center (ARC) 40-by-80-Foot Wind Tunnel (40 by 80) offered a means of providing controlled, simulated-flight conditions for this type testing. ARC also had a small, high-bypass turbofan available to provide the fan noise. The hybrid inlet and deflector inlet concepts were the advanced inlets chosen to be evaluated for both aerodynamic and acoustic performance. To achieve fan-noise suppression, the hybrid inlet combines the usual acoustic treatment in the diffuser wall with flow acceleration at the throat at moderate Mach numbers ($0.6 \leq M_{TH} \leq 0.8$) using a smaller throat area and higher diffuser wall angles than conventional inlets. The deflector inlet utilizes the conventional acoustic treatment in the diffuser walls to achieve suppression and redirects or deflects the remaining sound upward with an asymmetric length that has the lower portion of the lip extended forward of the upper portion. The suppression characteristics of the advanced inlets were to be determined by comparing the acoustic signatures with those from a cylindrical baseline inlet that was designed as a standard reference for the unsuppressed fan noise.

The objectives of the program were to determine the low-speed flight effects as simulated by the 40 by 80 on the forward-radiated fan noise and on the suppression characteristics of two hybrid inlets and a deflector inlet relative to a baseline inlet. In addition, the change in forward-radiated fan noise due to canting the baseline inlet to simulate a typical wing-mounted turbofan inlet was evaluated. A corollary objective was to determine the effect on the fan-noise signature of modifying the engine by increasing the number of core inlet guide vanes to achieve a vane/blade ratio to assure that the interaction mode would not propagate. To investigate the engine/inlet operating characteristics and to supplement the 40 by 80 noise data, outdoor static tests were conducted at ARC.

This report contains a summary of the tests and data-reduction techniques in Section 3.0 along with a description of the test facilities, turbofan engine, inlets, instrumentation, and test setup. Section 4.0 contains a description of the data-analysis techniques and a discussion of the data-analysis results. The conclusions and recommendations complete the report and are contained in Section 5.0.

3.0 TEST DESCRIPTION

3.1 TEST FACILITIES

3.1.1 NASA ARC Outdoor Test Stand

Outdoor static tests were conducted on the VTOL test stand located in the northeast corner of ARC. Due to the remote location of the static test stand, the ambient noise levels are low. There are no community noise limits on the operation of the turbofan engine. A plan-view sketch of the VTOL test stand is shown in Figure 1. The operations trailer housed the engine operator's console as well as the acquisition systems for the noise data.

3.1.2 NASA ARC 40 by 80 Foot Wind Tunnel

The simulated-flight tests were conducted in the Large Scale Aerodynamics Branch 40-by-80-Foot Wind Tunnel (40 by 80) at ARC. A plan-view sketch of the 40 by 80 is shown in Figure 2. This facility has the capability, with an engine installed in the test section, to simulate flight speeds up to 91 m/s (300 ft/s). However, due to the fact the wind tunnel is a closed-circuit facility, operation of an engine with the wind off circulates airflow around the circuit creating a minimum-forward-velocity range of 4 m/s (13.5 ft/s) to 8 m/s (26.3 ft/s), depending on the fan airflow. The wind-off operation provided quasi-static conditions of a very low-speed flow across the test section.

The use of the 40 by 80 for previous acoustic testing was significantly enhanced by lining the floor and part of the walls of the test section with a 7.62 cm (3 inch) layer of polyurethane foam. The foam mat virtually removed reverberant reflections from the noise data at all frequencies above 500 Hz. To ensure consistency in the noise measurements, the same foam was placed on the ground between the microphone and the engine during the outdoor static tests.

3.2 TEST VEHICLE

3.2.1 JT15D Turbofan Engine

The test vehicle supplied by ARC was a JT15D turbofan engine; a cross section is shown in Figure 3. The physical and aerodynamic parameters for the production JT15D fan are listed in Table 1. The JT15D is a moderate-bypass-ratio engine with a single-stage, supersonic-tip-speed fan. With regard to forward-radiated fan noise, the JT15D has many of the design features (Reference 1) that have been incorporated into the approximately

ORIGINAL PAGE IS
OF POOR QUALITY

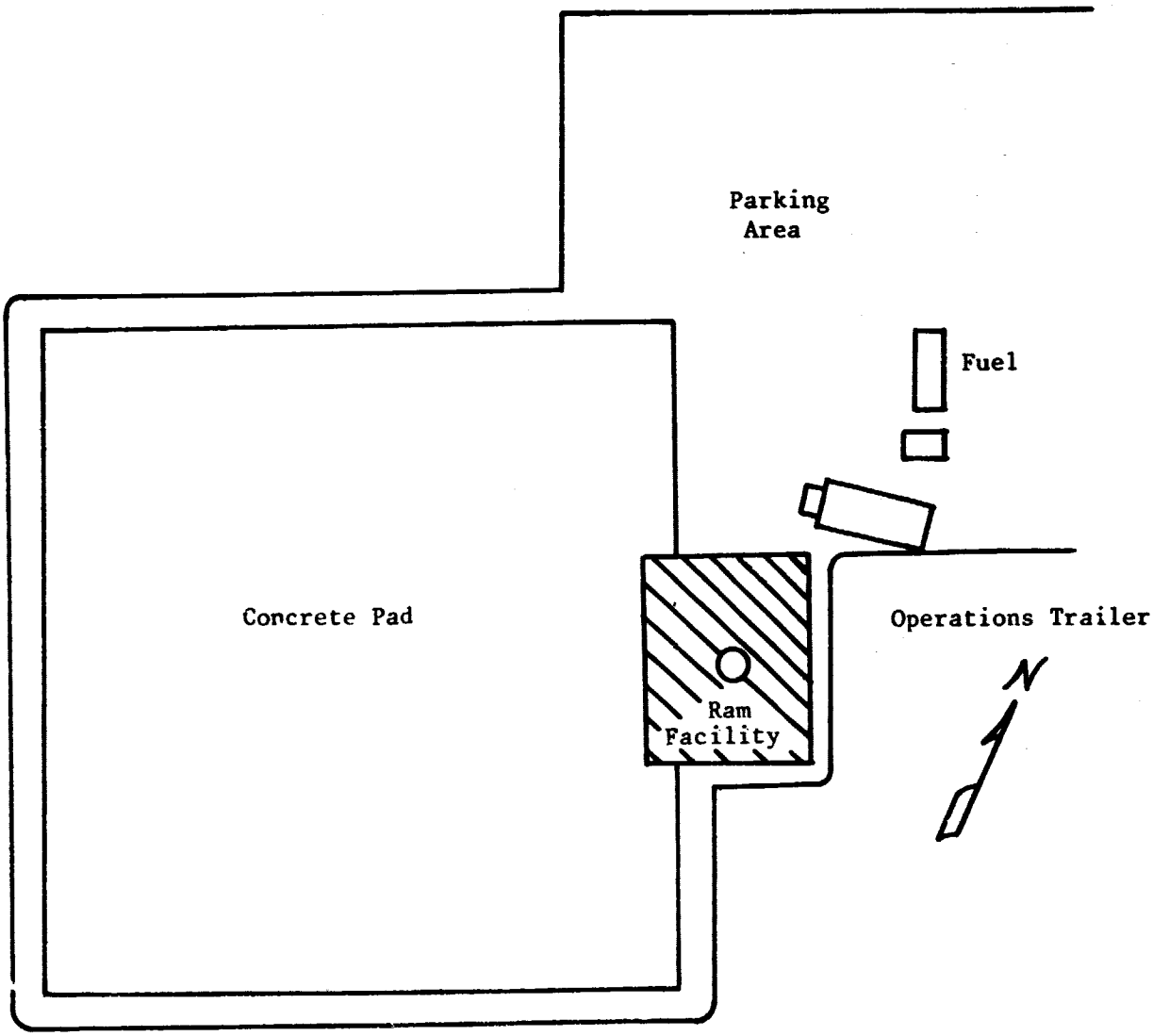

Figure 1. NASA ARC VTOL Test Stand.

ORIGINAL PAGE IS
OF POOR QUALITY

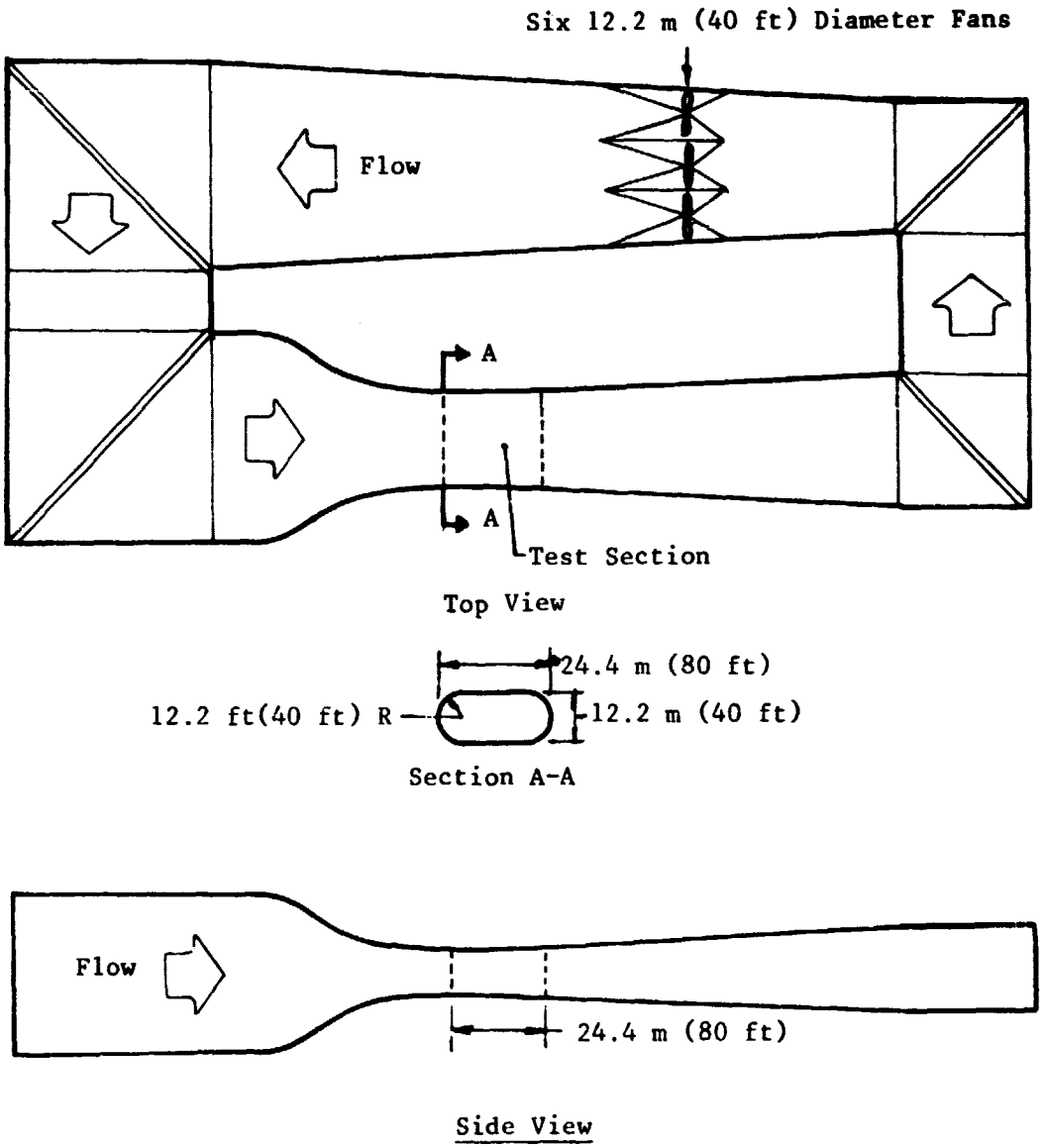

Figure 2. NASA ARC 40 by 80 Wind Tunnel.

ORIGINAL PAGE IS
OF POOR QUALITY

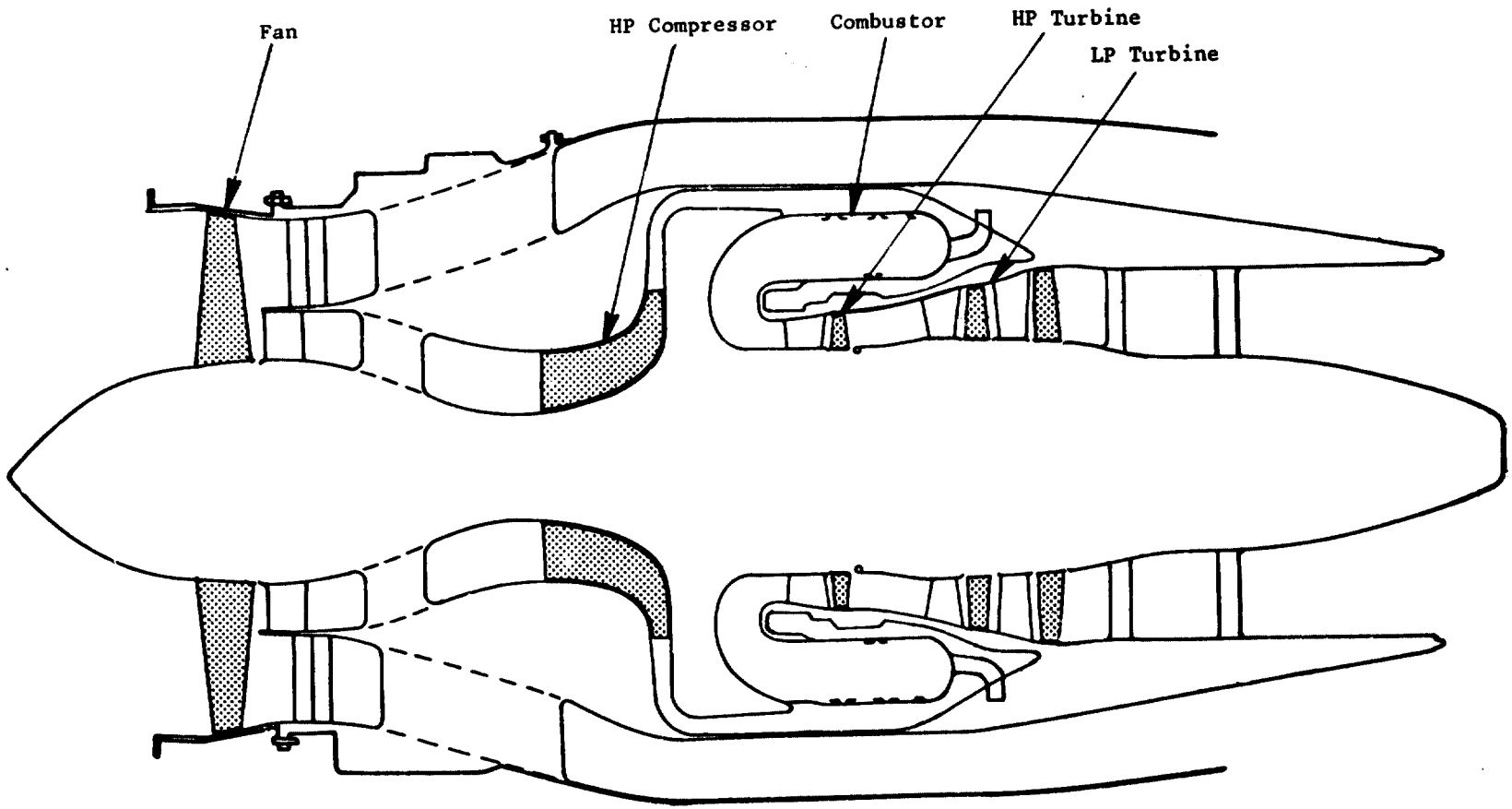

Figure 3. Production JT15D Turbofan Engine.

Table 1. Production JT15D Parameters.

Fan Pressure Ratio	1.5
Bypass Ratio	3.2
Hub/Tip Ratio	0.405
Rotor Diameter, cm (inches)	53 (21)
Maximum Fan RPM	16,000
Rotor Blades	28
Bypass Stator Vanes	66
Core Stator Vanes	33
Bypass Vane/Blade Ratio	2.36
Core Vane/Blade Ratio	1.18
Bypass Rotor-Stator Spacing	1.83
Core Rotor-Stator Spacing	0.50

four-times-larger modern turbofan engines in commercial service. Features such as the absence of inlet guide vanes, large spacing between the fan blades and outlet guide vanes, and at least twice as many outlet guide vanes as fan blades are common design features between the JT15D and the CF6, JT9D, and RB211 turbofan engines. However, during fan-noise research testing at ARC, Hodder (Reference 2) determined that considerable noise was being generated by the fan-tip interaction with the inlet temperature sensor wake and by the fan hub wake interaction with the core inlet guide vanes (IGV's). NASA ARC engineers have modified the inlet temperature sensor to eliminate the wake as a noise source. While verifying that the core IGV's are a noise source, ARC engineers have determined that the JT15D will operate at reduced fan speeds with the core IGV's removed. As a result of these tests, NASA ARC had the engine manufacturer redesign the core inlet guide vanes to increase the number to more than twice the number of fan blades and to increase the axial spacing between the vanes and blades without changing the engine aerodynamic performance over the full operating range.

During the outdoor static and wind tunnel testing of the advanced inlets, the same JT15D engine was used throughout but with three variations of the core IGV's. The three variations of the JT15D fan are shown in Figure 4 and are identified as

Standard JT15D = Production JT15D - Temperature Sensor

Modified JT15D = Standard JT15D - Core IGV's

Redesigned JT15D = Standard JT15D + Redesigned Core IGV's

The standard and modified JT15D were used during the first outdoor static and wind tunnel tests. The redesigned JT15D was used exclusively during the second series of wind tunnel and outdoor static tests.

3.2.2 Nacelle, Nozzle, and Mount

The JT15D engine used during the advanced inlet testing was housed in a special quiet nacelle that was designed by ARC engineers. The nacelle was completely lined with sound-absorbant material to minimize the radiation of engine-casing noise to the forward quadrant. A new coannular nozzle system for the JT15D was also designed by ARC engineers. The new, fan nozzle included a larger exit area, to provide the additional flow required by the hybrid inlets, and had both walls lined with acoustic treatment to suppress the aft-radiated fan noise. The JT15D with nacelle and nozzle system is shown in cross section in Figure 5, and the complete assembly is shown on the mount in Figure 6.

The mount is a leaned strut that supports the engine assembly 4.6 m (15 ft) over the wind tunnel floor as shown in Figure 7. The strut carries all the plumbing and instrumentation lines to the engine assembly and is fastened to a turntable. The axis of rotation is through the fan face; this allows angle of attack to be accomplished by rotating the engine assembly about the vertical axis without changing the distances from the fan face to

ORIGINAL PAGE IS
OF POOR QUALITY

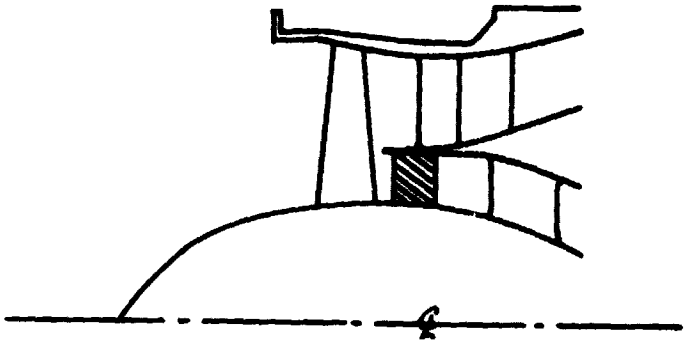

- Standard - 33 Core IGV's

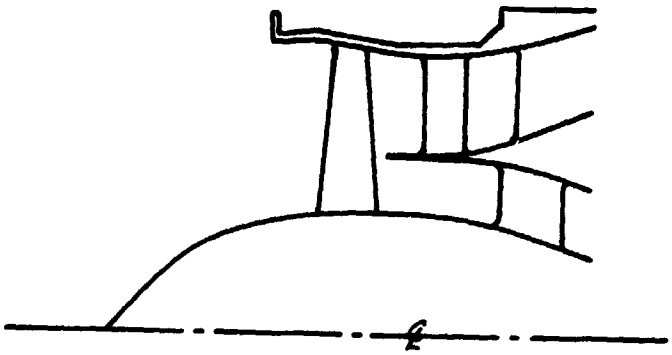

- Modified - No Core IGV's

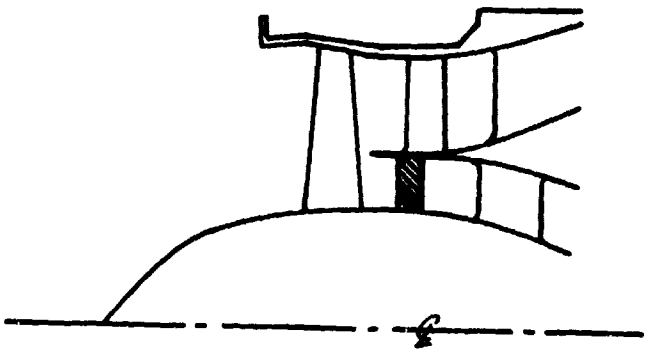

- Redesigned - 71 Core IGV's

- 28 Fan Blades
- 66 Bypass Vanes

Figure 4. JT15D Fan Configurations.

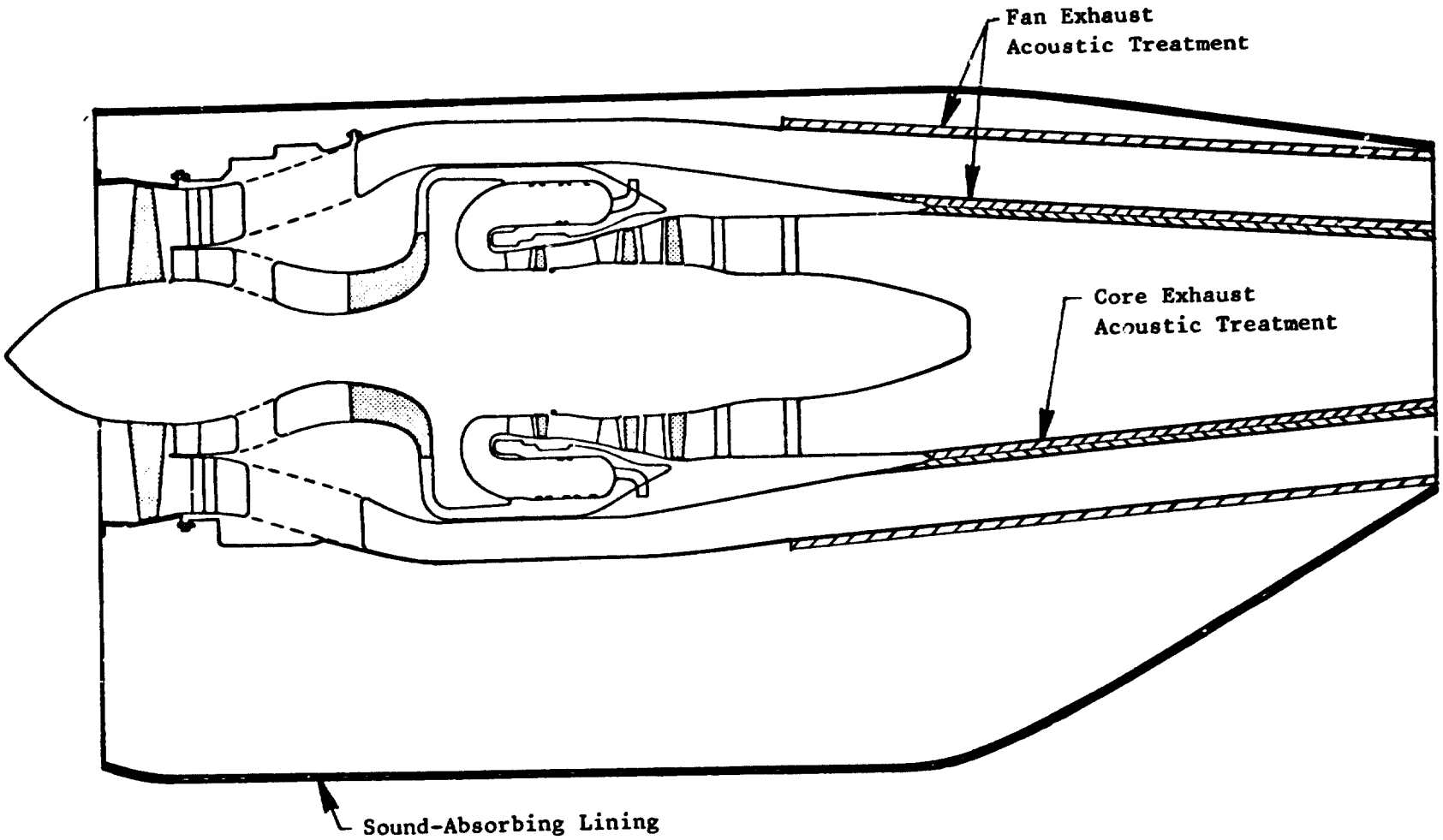

Figure 5. JT15D in Quiet Nacelle Used for Advanced Inlet Tests.

ORIGINAL PAGE IS
OF POOR QUALITY

ORIGINAL PAGE IS
OF POOR QUALITY

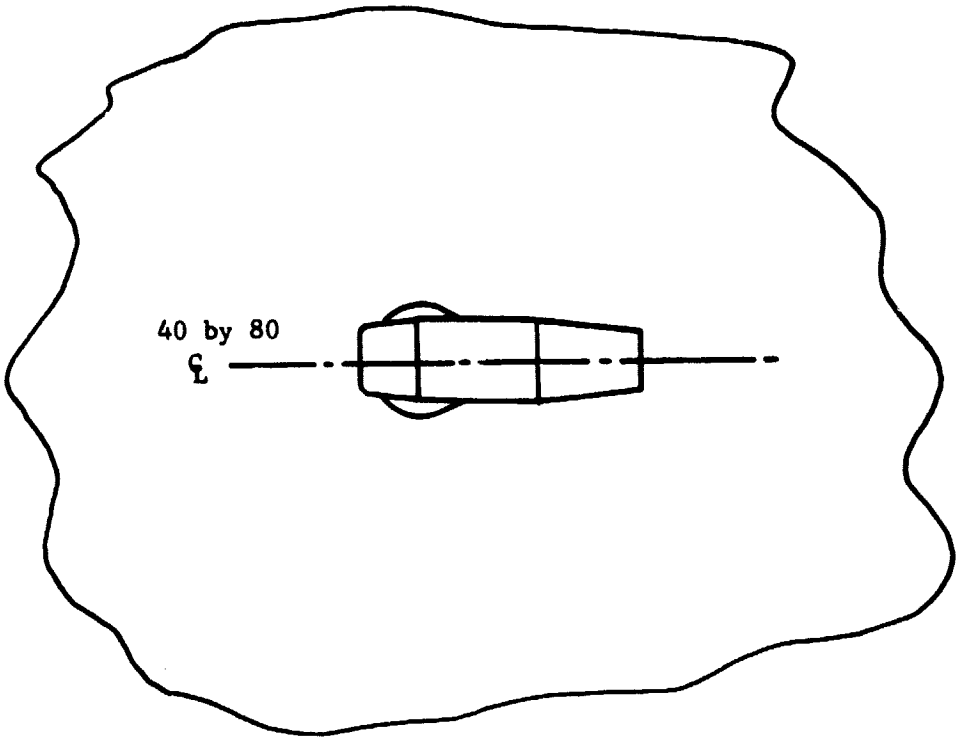

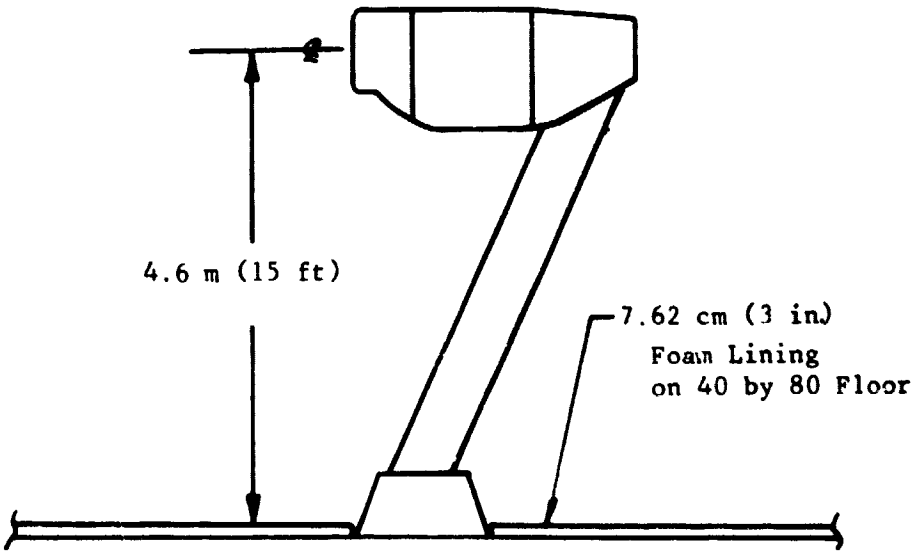

Figure 6. JT15D/Quiet Nacelle and Mount Assembly.

ORIGINAL PAGE
BLACK AND WHITE PHOTOGRAPH

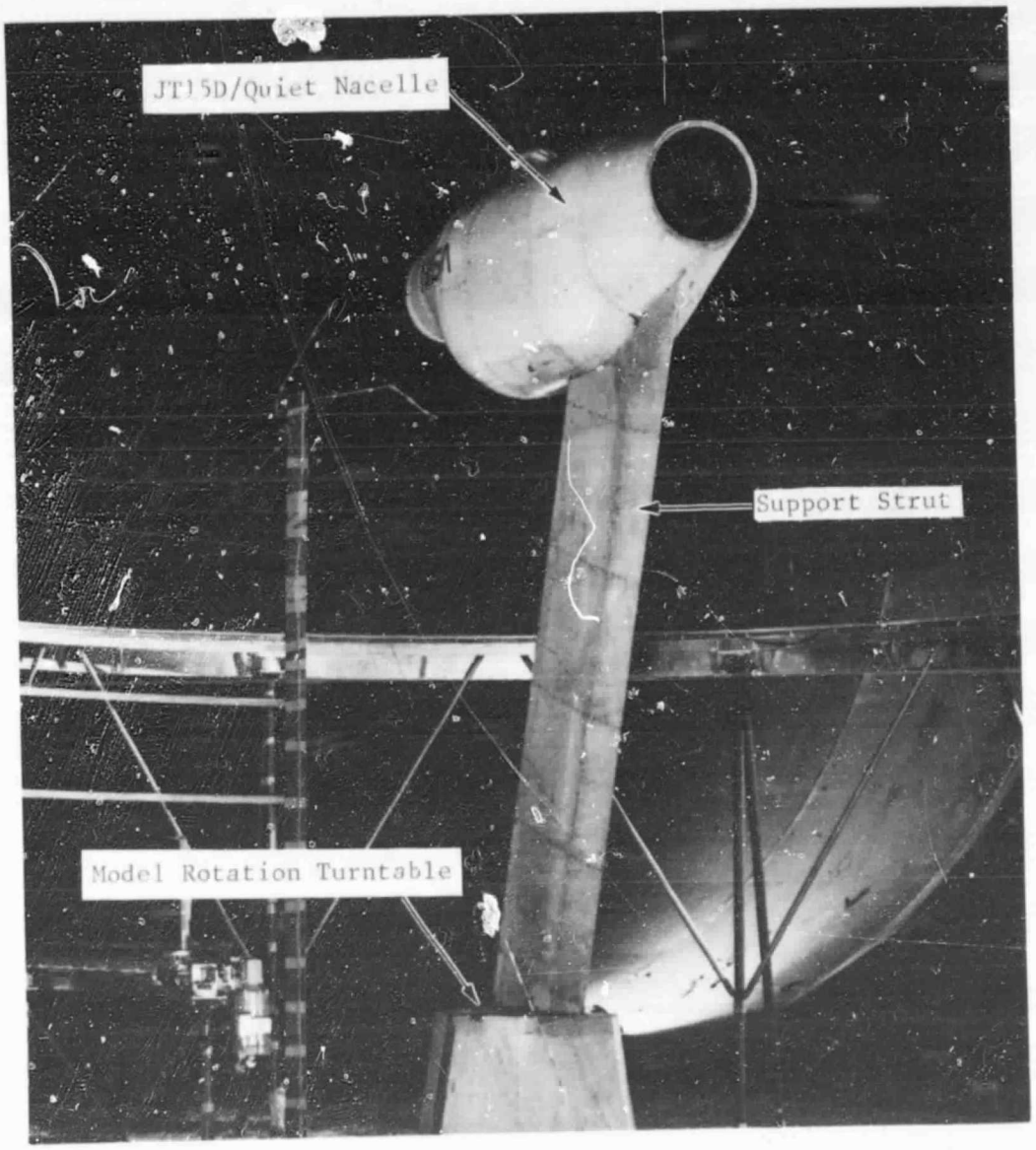

Figure 7. Rear-View Photograph of JT15D/Quiet Nacelle Mounted in NASA ARC 40 by 80 Wind Tunnel.

the noise-measurement field. The engine assembly and mount were installed on a nonrotating base at the VTOL test stand to duplicate the wind tunnel setup during outdoor static testing.

3.3 INLET CONFIGURATIONS

NASA ARC fabricated all the tested inlets based upon aerodynamic and mechanical designs provided by the General Electric Co. The advanced inlets were designed in both hard-wall and treated versions, and the baseline inlet was designed to be only a hard-wall reference. The conventional takeoff and landing (CTOL) hybrid inlet, the deflector inlet, and the baseline inlet were all designed for high-fan-speed operation; the short takeoff and landing (STOL) hybrid inlet was designed for low-fan-speed operation. The aerodynamic design points for all the inlets are listed in Table 2. Details of the inlet designs, including coordinates of the flow lines, can be found in Reference 3. A flight lip was designed to match the aerodynamic requirement at the respective design point for each of the inlets. Aeroacoustic lips were designed for each of the hybrid inlets and the baseline inlet. These lips provide the same aerodynamic profiles entering the inlet throats at static conditions that exist with the flight lips at the design-point forward velocity. The throat Mach number listed for each inlet is the one-dimensional calculation based on airflow and physical area. The acoustic design goals for the program were to achieve maximum perceived noise level (PNL) suppression when scaled to larger turbofan engines typical of those on modern commercial aircraft. From a practical standpoint, there was also a goal to design as much of the hardware as possible to be common between the inlets.

3.3.1 Baseline Inlet

The baseline inlet is cylindrical and is the same length as the CTOL hybrid inlet. The baseline inlet attaches to the JT15D fan casing with four drag links which compress a rubber seal completely around the circumference to ensure no leaks in the flow path at the interface. There is no provision for total pressure rakes at the fan face in this inlet.

An aeroacoustic bellmouth lip and a flight lip were provided as shown in the cross section sketches in Figure 8. The aeroacustic lip was used for outdoor static testing and is shown with the baseline inlet attached to the JT15D in the photo in Figure 9. The flight lip was designed to permit angle-of-attack operation up to 20° with minimal flow distortion. The flight lip was mated to the JT15D nacelle with a fairing for the wind tunnel testing. The JT15D engine assembly with the baseline inlet and flight lip attached is shown in the photo in Figure 10.

3.3.2 CTOL Hybrid Inlet

The CTOL hybrid inlet was designed around current, turbofan-powered, commercial-transport, aircraft requirements. The overall inlet is slightly

Table 2. Inlet Design Parameters.

Parameter	Baseline	CTOL	STOL	Deflector
V_o, m/s (ft/s)	82 (270)	82 (270)	41 (135)	82 (270)
α, Degrees	15	20	20	30
$\dot{w}$, kg/s (lb/s)	34 (75)	28.5 (63)	34 (75)	34 (75)
M_{th}	0.4	0.72	0.77	0.6
V_T, m/s (ft/s)	405 (1330)	405 (1330)	344 (1129)	405 (1330)
N_c, rpm	14,500	14,520	12,320	14,520
L/D	1.01	1.01	1.45	0.5/1.01
L/D Treated	-	0.79	0.79	0.79

ORIGINAL PAGE IS
OF POOR QUALITY

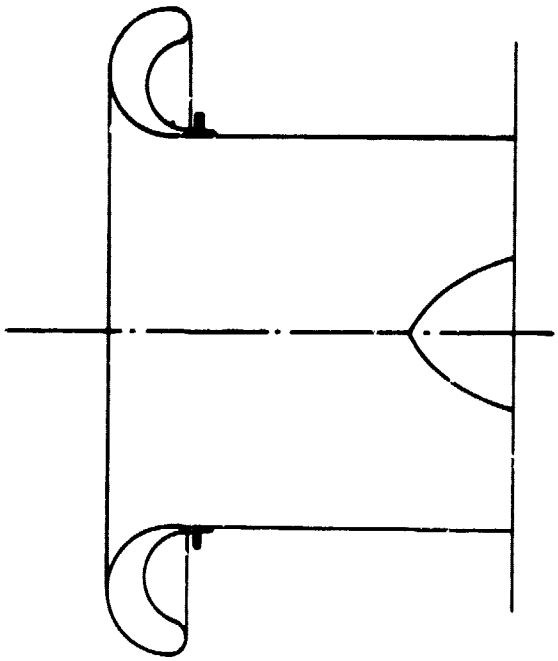

- Aeroacoustic Lip

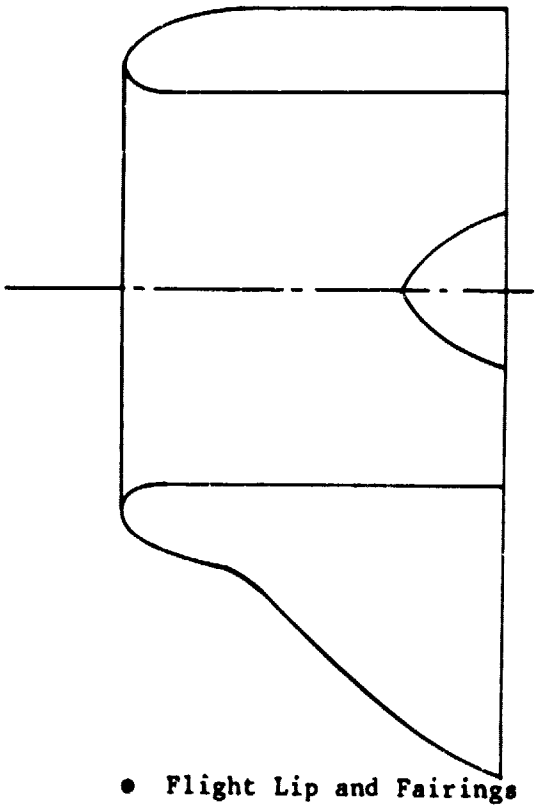

- Flight Lip and Fairings

Figure 8. Sketch of Baseline Inlet.

ORIGINAL PAGE
BLACK AND WHITE PHOTOGRAPH

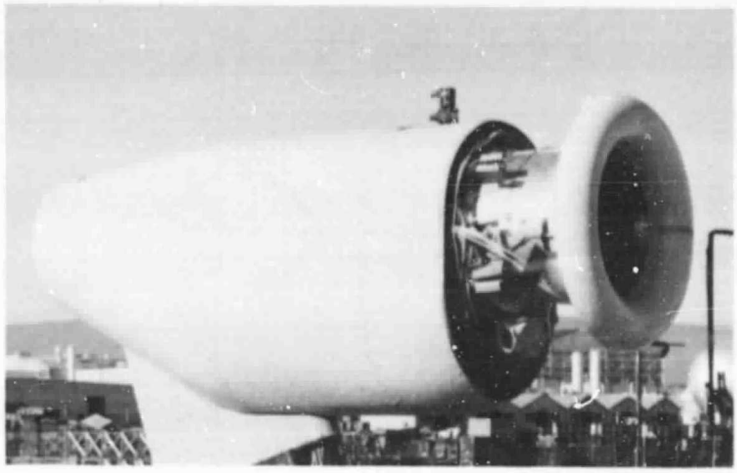

Figure 9. Photograph of JT15D/Baseline Inlet with Aero-acoustic Lip.

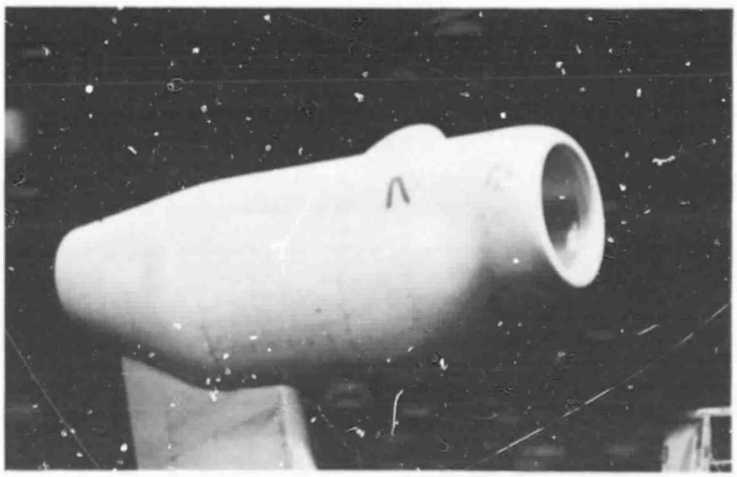

Figure 10. Photograph of JT15D/Baseline Inlet with Flight Lip and Fairings.

longer than desired due to the requirement to keep the diffuser flow attached up to 20° inlet angle of attack with the higher than conventional diffuser wall angles. The diffuser is divided into two sections; the aft diffuser is common with the STOL hybrid inlet. The aft diffuser mates with the JT15D engine and attaches with the same drag links as the baseline inlet. Both diffuser sections were built in treated and hard-wall versions; the hard-wall aft diffuser had provisions for total pressure rakes.

An aeroacoustic lip or a flight lip attaches to the forward diffuser to complete the throat of the inlet as shown in Figure 11. The aeroacoustic lip was used for outdoor static testing and is shown, together with the inlet, attached to the engine assembly in the photo in Figure 12. The flight lip was designed to permit angle-of-attack operation up to 20° and mates to the JT15D with a fairing for wind tunnel testing. The JT15D engine assembly with the CTOL hybrid inlet and flight lip attached is shown in the photo in Figure 13.

To satisfy the suppression requirements, particularly at low throat Mach numbers where acceleration suppression is minimal, the acoustic treatment was designed to attenuate noise over a wide range of frequencies. To accomplish this broadband suppression, a bulk absorber material with two different cavity depths was selected. The forward-diffuser treatment depth was selected to provide maximum suppression of the blade-passing frequency (BPF) noise, which would be in the 6300 Hz 1/3-octave band for most of the fan speeds to be tested. The resulting design, shown in Figure 14, was to compress 0.228 cm (0.090 in.) thickness of bulk absorber into pockets that were 0.127 cm (0.050 in.) deep and cover them with a 28% porosity facesheet.

The aft-diffuser treatment depth was chosen to provide maximum suppression of the supersonic rotor "buzz saw" noise. Based upon preliminary JT15D noise data, this type of noise was most severe in the 2000 Hz 1/3-octave band at the design fan speed for the CTOL hybrid inlet. A bulk absorber thickness of 1.6 cm (0.63 in.) covered with the same 28% porosity facesheet was the treatment design chosen for the aft diffuser as shown in Figure 14. The two treatment sections together provided a total treatment length to fan diameter ratio, $(L/D)_{TR}$, of 0.79 for the CTOL hybrid inlet.

3.3.3 STOL Hybrid Inlet

The STOL hybrid inlet was designed to meet the stringent noise requirements proposed for powered-lift STOL aircraft. The requirement to operate the JT15D at the low fan-tip speeds typical of STOL engines resulted in a low inlet-flow rate. The low flow rate at the design point resulted in a small throat area to achieve the design throat Mach number which, in turn, required a long inlet to maintain diffuser wall angles consistent with the CTOL hybrid inlet. As previously mentioned, the aft diffuser is common with the CTOL hybrid inlet. The forward diffuser was divided into two pieces so that the treated length, which is only about one-half the total length, could be replaced with a hard-wall section.

ORIGINAL PAGE IS
OF POOR QUALITY

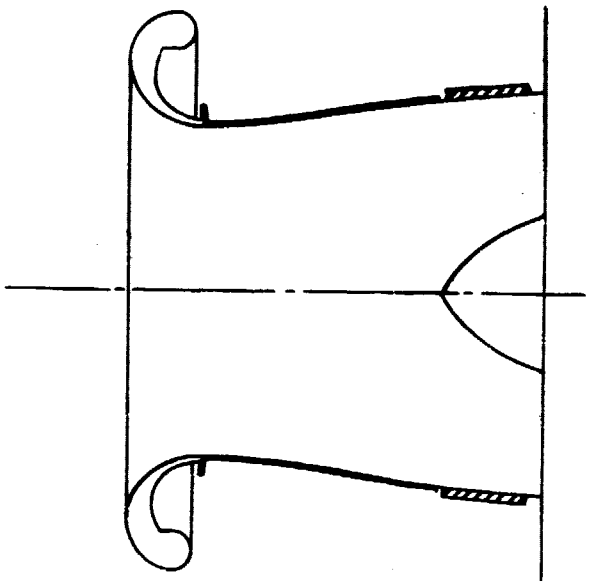

- Aeroacoustic Lip

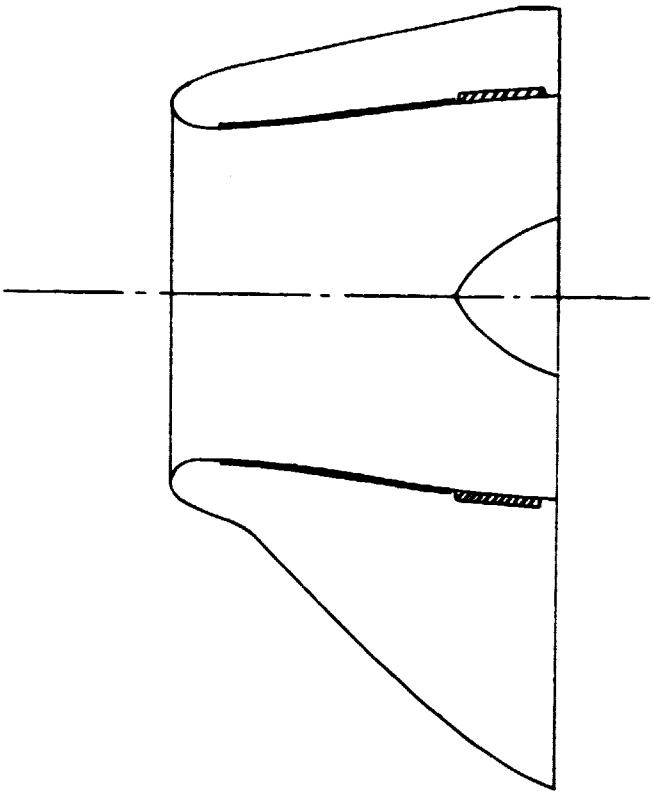

- Flight Lip and Fairings

Figure 11. Sketch of Conventional Takeoff/Landing (CTOL) Hybrid Inlet.

ORIGINAL PAGE
BLACK AND WHITE PHOTOGRAPH

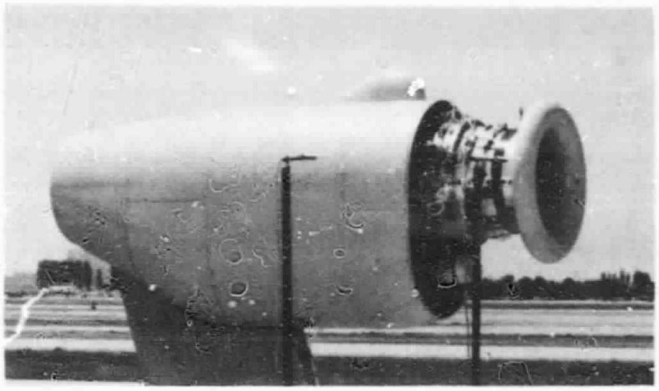

Figure 12. Photograph of JT15D/CTOL Hybrid Inlet with Aeroacoustic Lip.

Figure 13. Photograph of JT15D/CTOL Hybrid Inlet with Flight Lip and Fairings.

ORIGINAL PAGE IS
OF POOR QUALITY

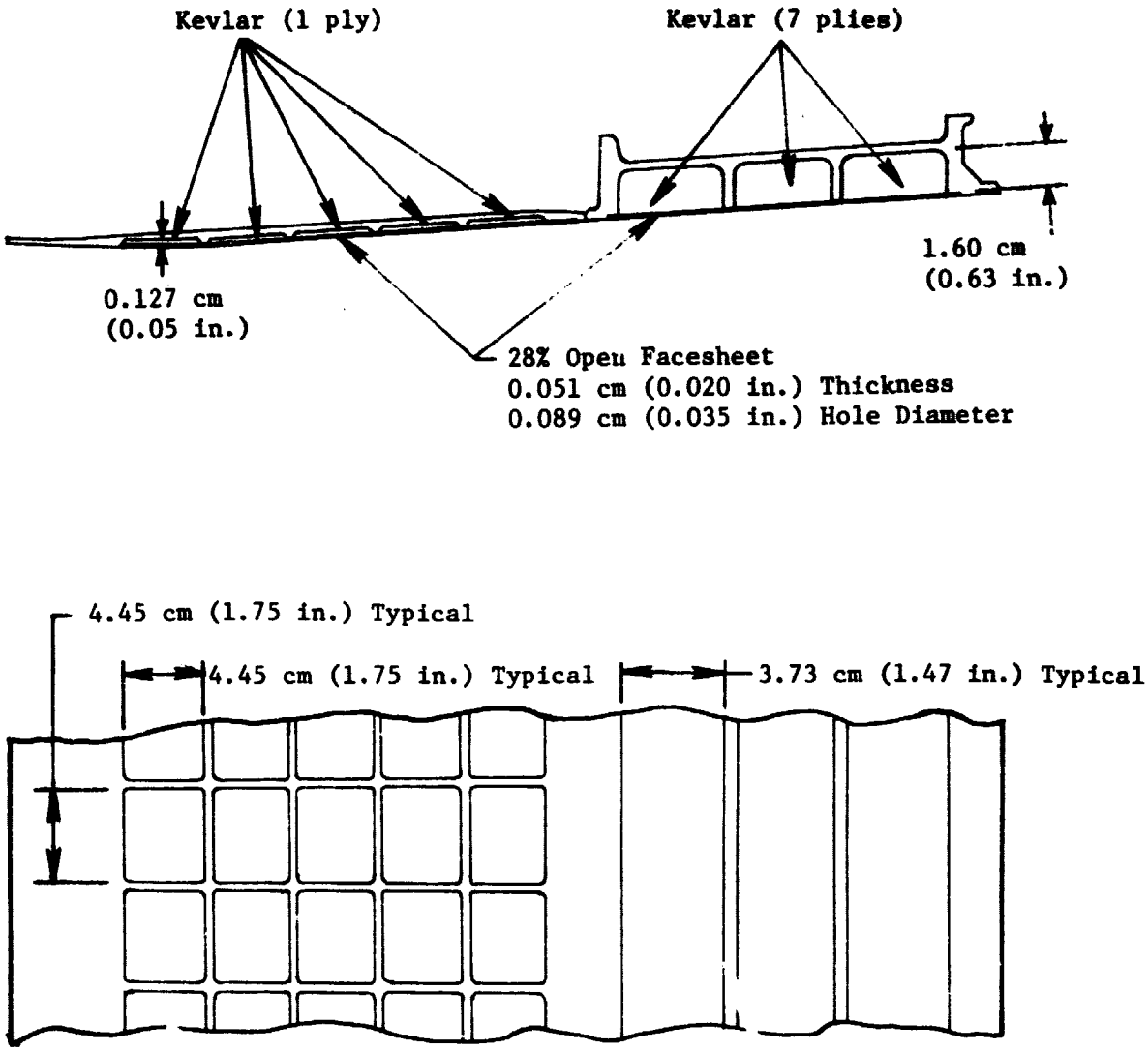

Figure 14. CTOL Hybrid Inlet Treatment Details.

An aeroacoustic lip and a flight lip were built. These attach to the forward diffuser as shown in Figure 15. The aeroacoustic lip was used for outdoor static testing and is shown, together with the inlet, attached to the engine assembly in the photo in Figure 16. The flight lip was designed to permit angle-of-attack operation up to 30° and mates to the JT15D with the same fairing as the CTOL hybrid inlet. The STOL hybrid inlet configuration attached to the JT15D engine assembly in preparation for wind tunnel testing is shown in the photo in Figure 17.

The acoustic treatment for the STOL hybrid inlet was designed using the same criterion of suppression over a wide frequency range that was applied to the CTOL hybrid inlet. The aft-diffuser treatment design that was chosen based on the high-tip-speed noise signature should also provide broadband suppression centered at 2000 Hz at the lower tip speeds associated with STOL engines. The forward-diffuser treatment length was chosen to be the same as the CTOL hybrid inlet for two reasons. The primary reason was to preserve commonality for treatment effectiveness comparisons, and the other reason was that a treatment length in excess of 0.79 fan diameters is impractical for aircraft applications.

The forward-diffuser treatment depth was chosen to provide maximum suppression of the noise at BPF. For most of the fan speeds to be tested with the STOL hybrid inlet, the BPF is in the 6300 Hz 1/3-octave band. Therefore, the forward-diffuser acoustic design turned out to be the same for the STOL hybrid inlet as for the CTOL hybrid inlet. A sketch of the STOL hybrid inlet treatment design is shown in Figure 18.

3.3.4 Deflector Inlet

The deflector inlet was designed around the requirements for current, turbofan-powered, commercial aircraft. Other considerations were to design the inlet as short as possible while using the hybrid inlet aft diffuser. To ensure that the inlet aerodynamic performance would be acceptable, particularly at angle of attack, the forward diffuser was cylindrical, and the flight lip was sized for low forward speeds. Cross-sectional sketches of the deflector inlet with a special fairing to attach it to the JT15D nacelle are shown in Figure 19. The deflector inlet and JT15D engine assembly are shown in two views in the photos in Figure 20. There was no aeroacoustic lip built for the deflector inlet.

The deflector inlet treatment design was based upon the CTOL hybrid inlet; in fact, the aft diffuser was the same hardware. The treatment in the forward diffuser is the same pocket-type design but covers only 180° of the wall because the diffuser is so short. The treatment design for the deflector inlet is shown in Figure 21 with the diffuser projected as a plane for clarity. A hard-wall version of the diffuser was not built, but untreated testing was accomplished by using the hard-wall aft diffuser and applying aluminum foil tape in streamwise overlapping strips to the treated portion of the diffuser.

ORIGINAL PAGE IS
OF POOR QUALITY

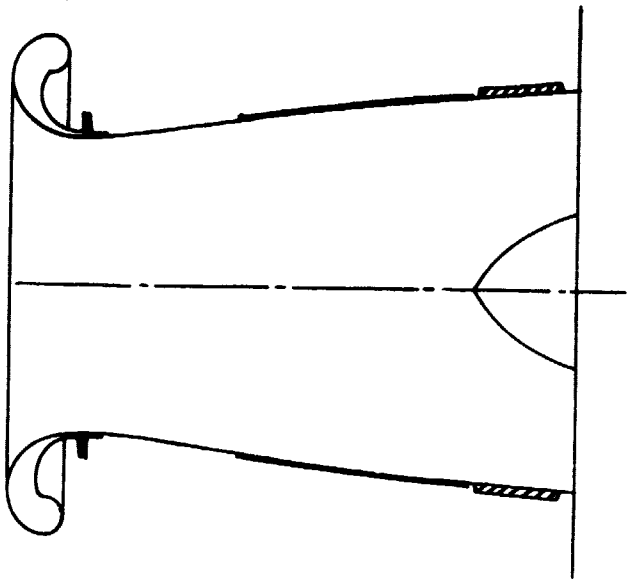

- Aeroacoustic Lip

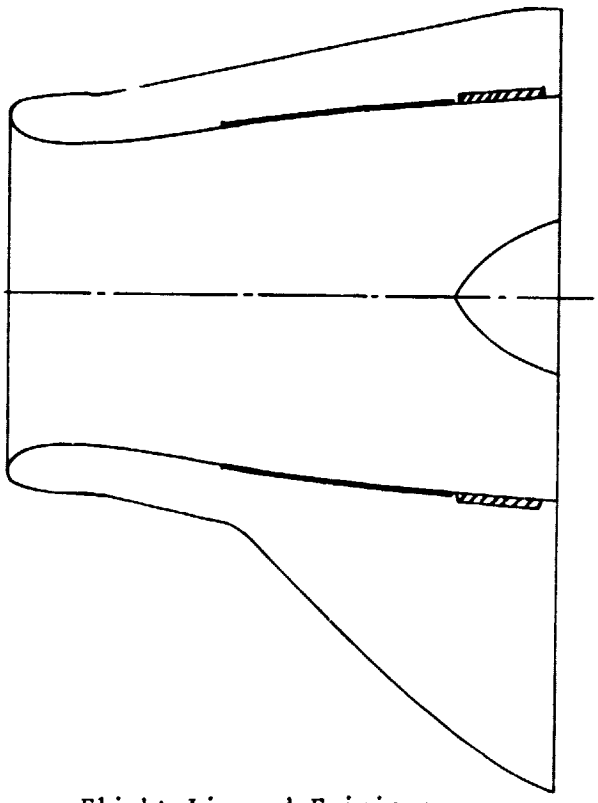

- Flight Lip and Fairings

Figure 15. Sketch of Short Takeoff/Landing (STOL) Hybrid Inlet.

ORIGINAL PAGE
BLACK AND WHITE PHOTOGRAPH

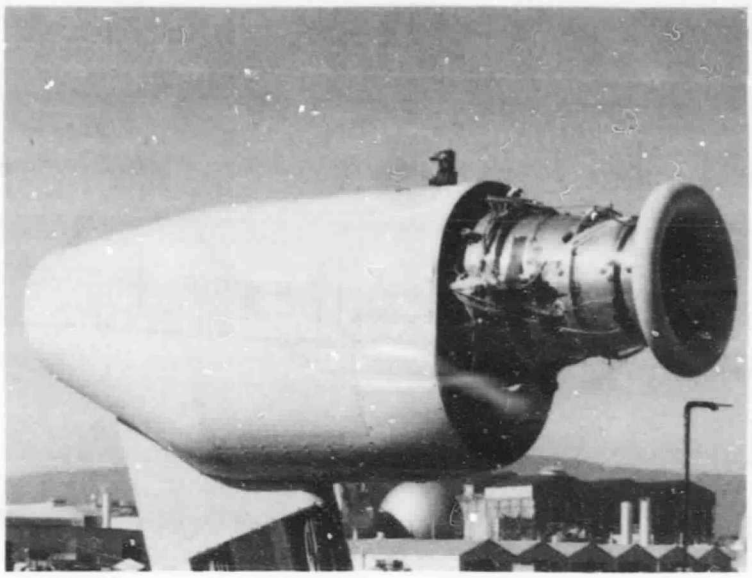

Figure 16. Photograph of JT15D/STOL Hybrid Inlet with Aeroacoustic Lip.

Figure 17. Photograph of JT15D/STOL Hybrid Inlet with Flight Lip and Fairings.

ORIGINAL PAGE IS
OF POOR QUALITY

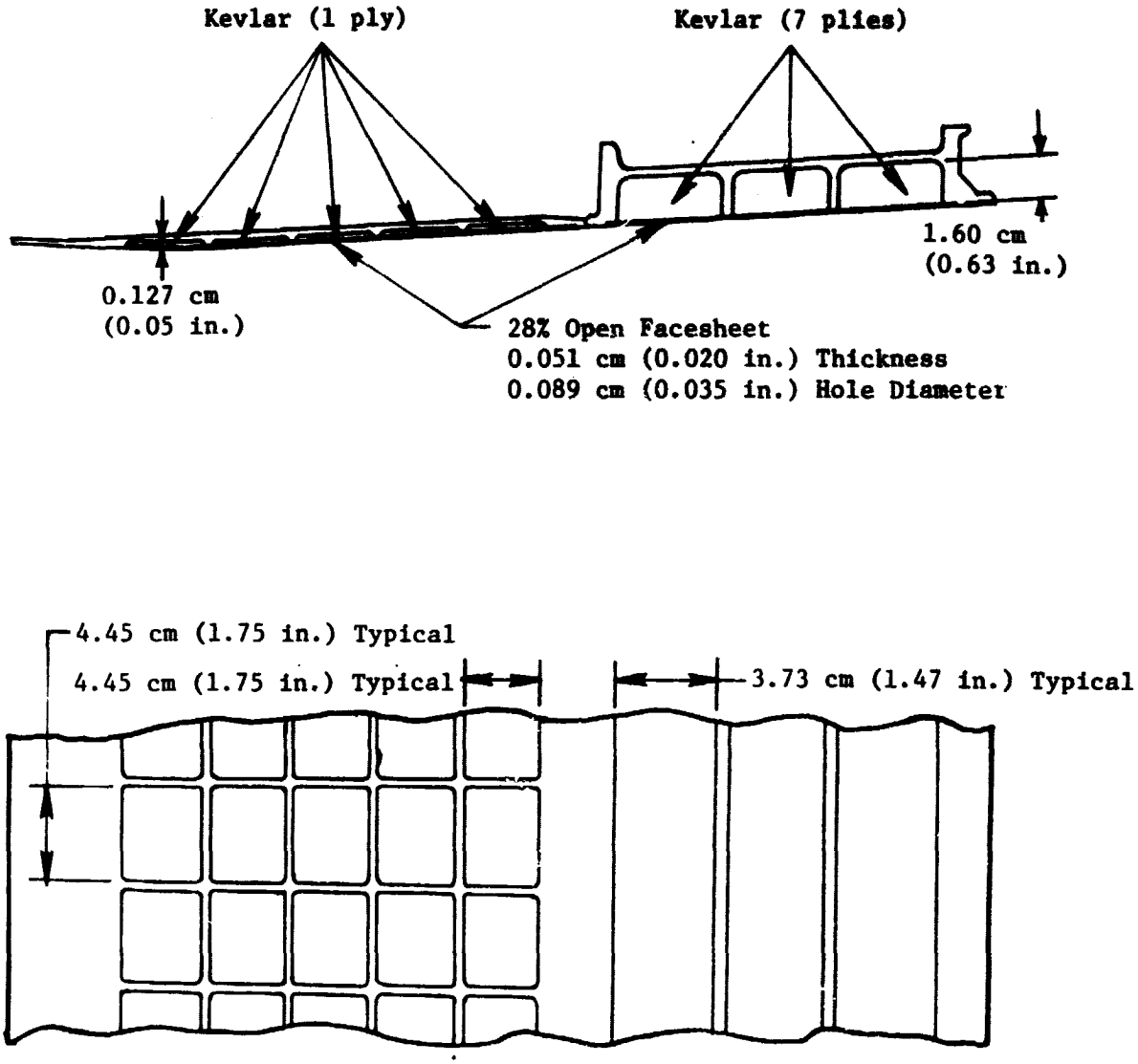

Figure 18. STOL Hybrid Inlet Treatment Details.

ORIGINAL PAGE IS
OF POOR QUALITY

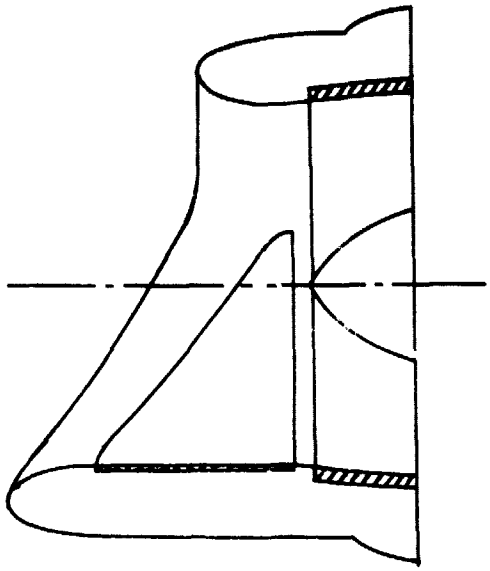

- Top View

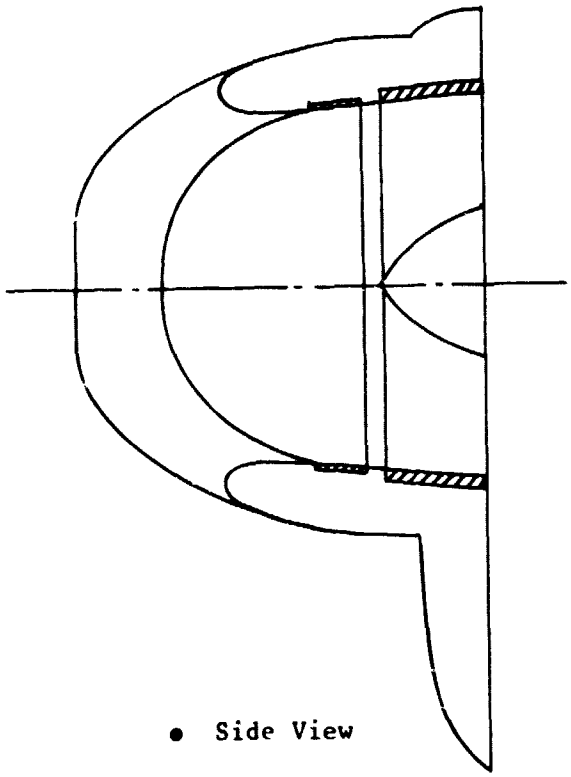

- Side View

Figure 19. Sketch of Deflector Inlet with Flight Lip and Fairings.

ORIGINAL PAGE
BLACK AND WHITE PHOTOGRAPH

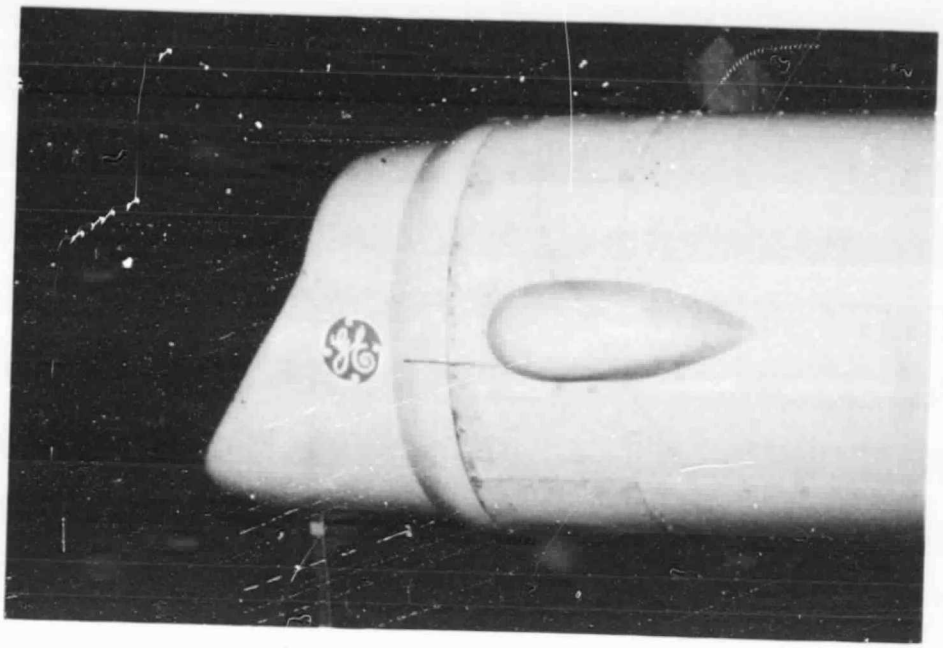

Top View

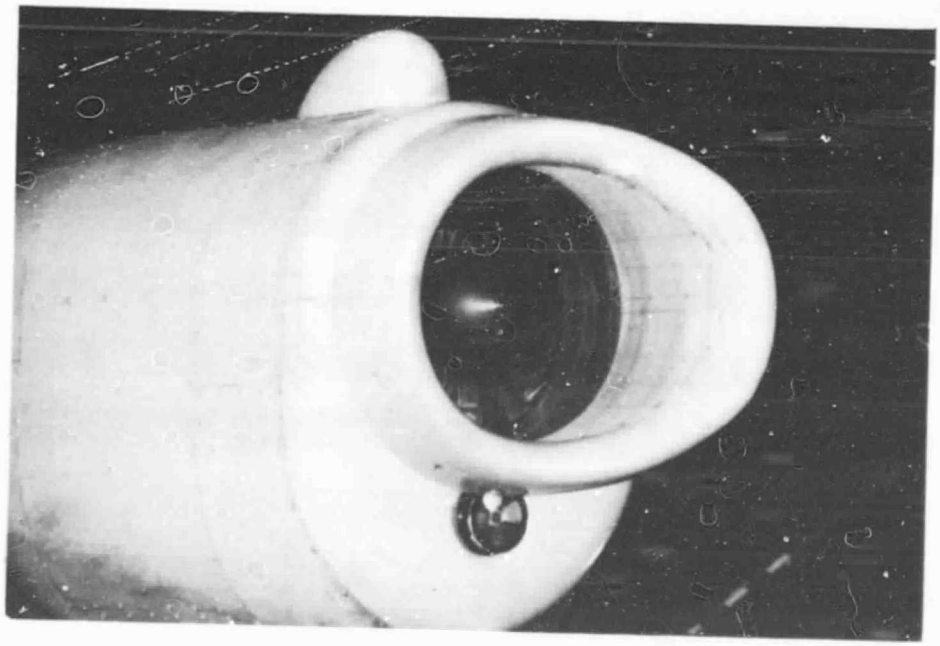

Front-Quarter View

Figure 20. Photographs of JT15D/Deflector Inlet with Flight Lip and Fairings.

ORIGINAL PAGE IS
OF POOR QUALITY

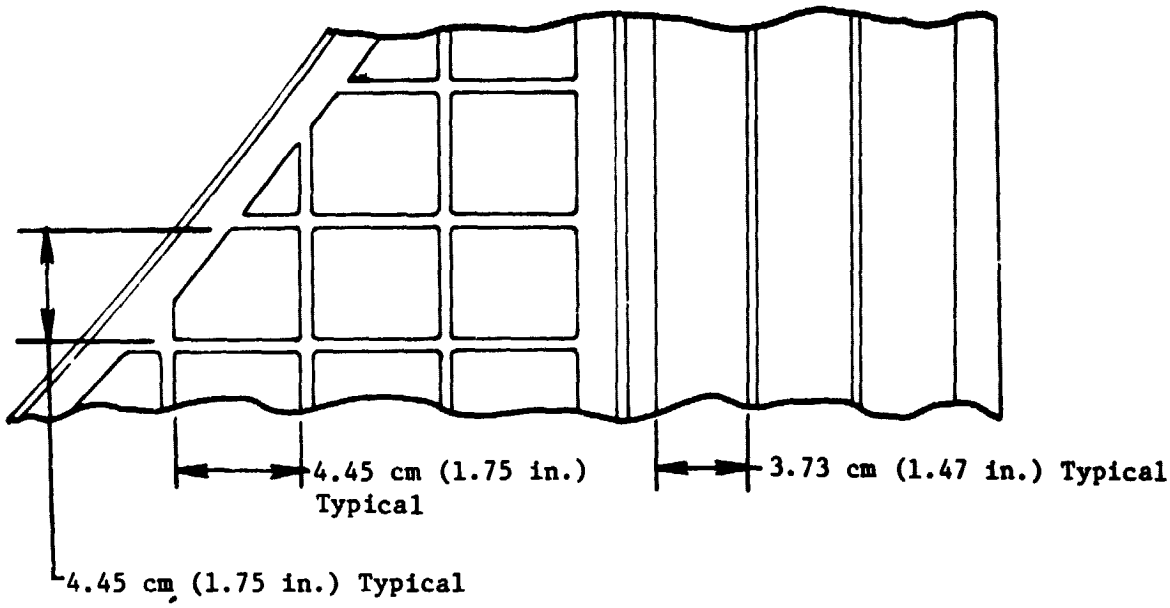

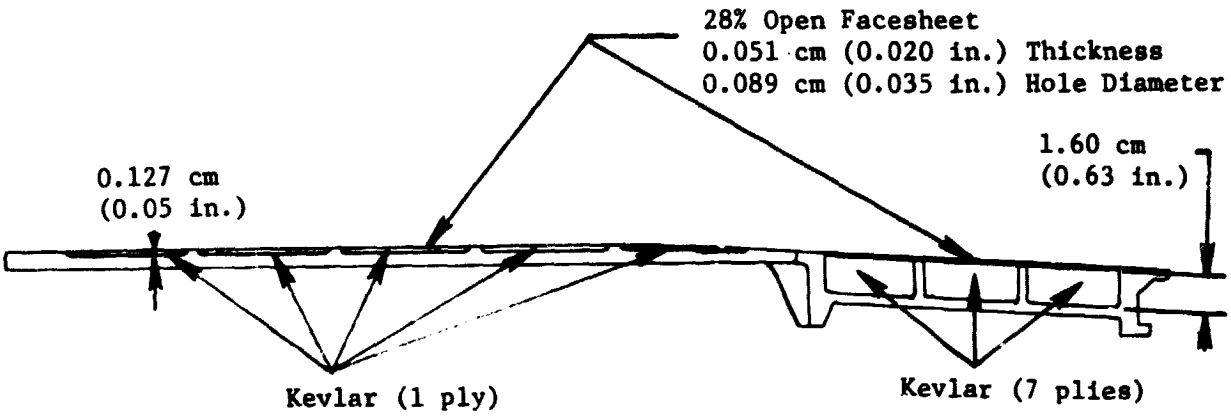

Figure 21. Deflector Inlet Treatment Details.

3.3.5 Canted Baseline Inlet

An actual aircraft-inlet design feature that is rarely simulated during inlet-noise testing is the downward cant of the inlet centerline relative to the engine centerline. Canted inlets are prevalent on the wing-mounted engines of modern commercial transports. To obtain an assessment of the potential effect of a canted the inlet on forward-radiated fan noise, a wedge was built to provide a 4° cant to the baseline inlet. The wedge was inserted between the cylindrical baseline inlet and the JT15D engine as shown in Figure 22. The gap between the external fairing and the nacelle, caused by canting the inlet, was covered with sheet metal for the wind tunnel testing. The canted baseline inlet configuration is shown compared with the straight baseline inlet in the photos in Figure 23. The canted baseline inlet was also tested with the aeroacoustic bellmouth lip during the outdoor static tests.

3.4 TEST SETUP

3.4.1 Outdoor Static Tests

The test vehicle was mounted during the wind tunnel tests by bolting the support strut to the ram facility located near the operations trailer at the VTOL test stand (see Figure 1). The engine centerline was 4.6 m (15 ft) above the ground and pointed in a northerly direction. The noise measurements were made on a 3.7 m (12 ft) arc at the engine centerline height and along a sideline that was 2.8 m (9 ft) below and 1.2 m (4 ft) to the left of the engine referenced to the fan face. To minimize ground-reflection interference in the noise measurements, large pieces of wind tunnel foam were used to cover the ground under the engine and the microphones.

During the first outdoor static test, fixed microphone locations were used that covered angles from 10° to 90° on the arc and 30° to 90° on the sideline as shown in Figure 24. During the second outdoor static test, traversing microphones were used that covered angles from -59° to 82° on the arc and 30° to 90° on the sideline as shown in Figure 25.

3.4.2 Wind Tunnel Tests

The test vehicle was mounted during the wind tunnel tests by bolting the support strut a turntable located in the center of the 40 by 80 test section. The engine centerline was 4.6 m (15 ft) above the wind tunnel floor with the turntable capable of yawing the test vehicle up to 40° for angle-of-attack operation. The floor and part of the walls were covered with the foam to minimize reflection interference in the noise data. Noise measurements were made at the same arc and sideline distances as in the outdoor static tests.

The first wind tunnel test used fixed microphone locations that covered 10° to 90° on the arc and 30° to 90° on the sideline. The photo in Figure 26

ORIGINAL PAGE IS
OF POOR QUALITY

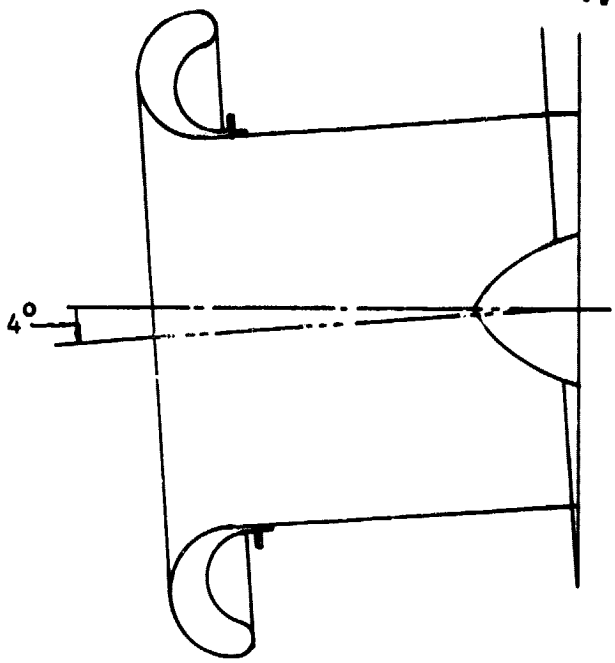

- Aeroacoustic Lip (Top View)

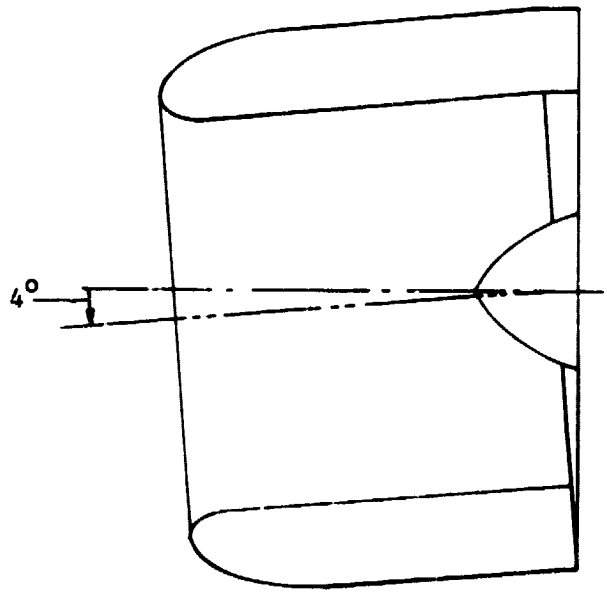

- Flight Lip and Fairings (Top View)

Figure 22. Sketch of Canted Baseline Inlet.

ORIGINAL PAGE
BLACK AND WHITE PHOTOGRAPH

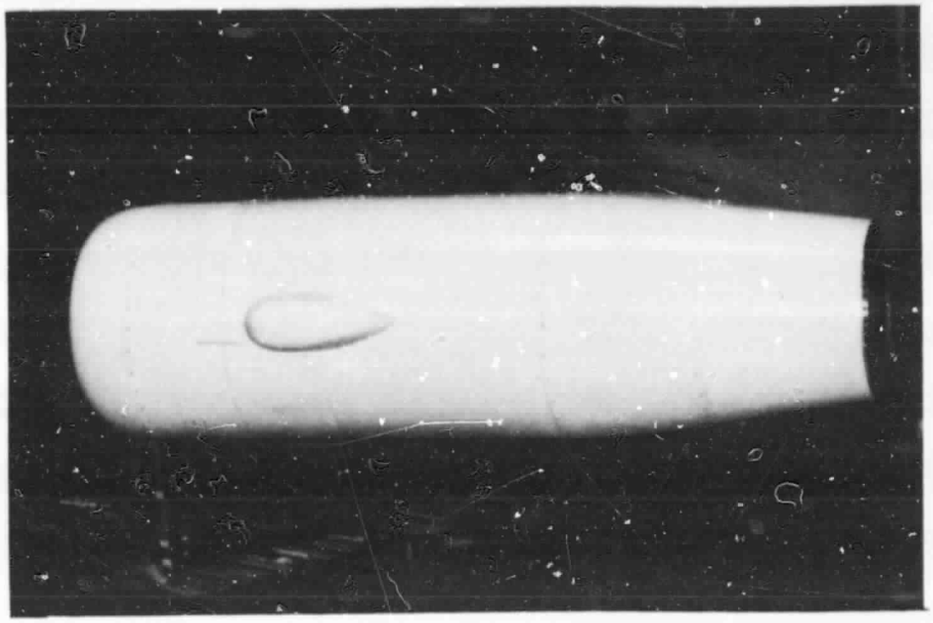

JT15D/Baseline Inlet

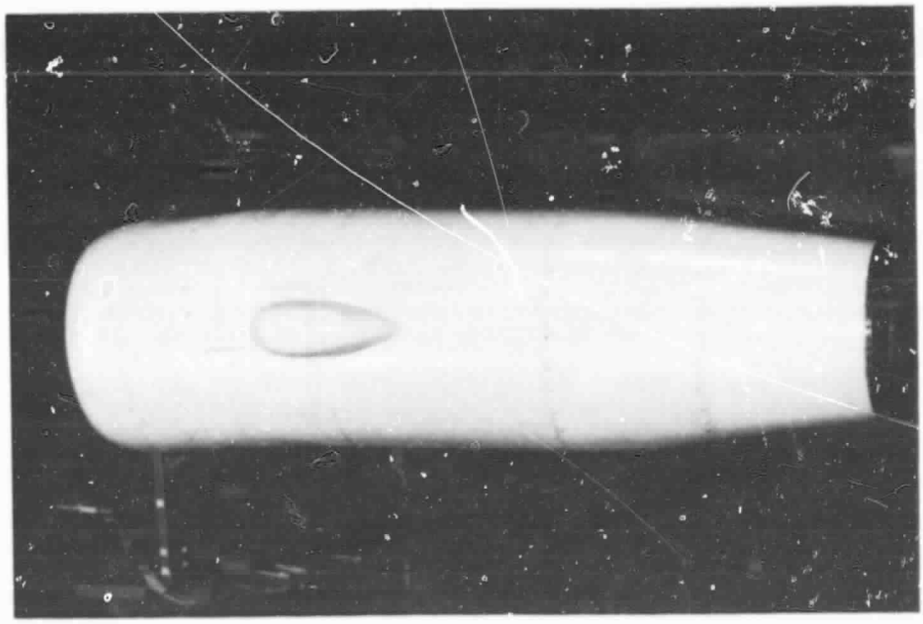

JT15D/Canted Baseline Inlet

Figure 23. Photographs of JT15D/Baseline Inlet and JT15D/Canted Baseline Inlet with Fairings.

ORIGINAL PAGE IS
OF POOR QUALITY

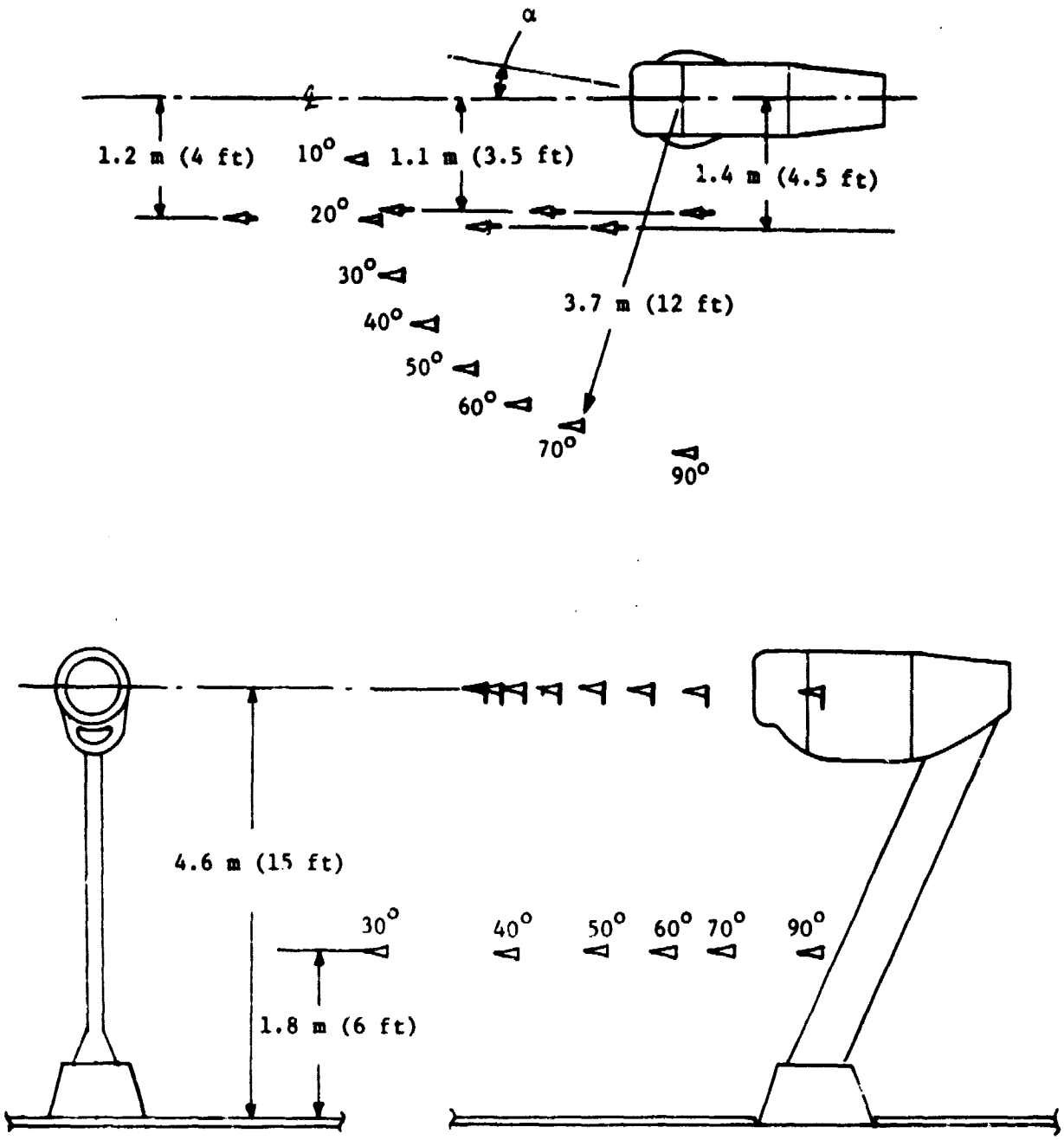

Figure 24. Test Setup for First Outdoor Static and Wind Tunnel Tests.

ORIGINAL PAGE IS
OF POOR QUALITY

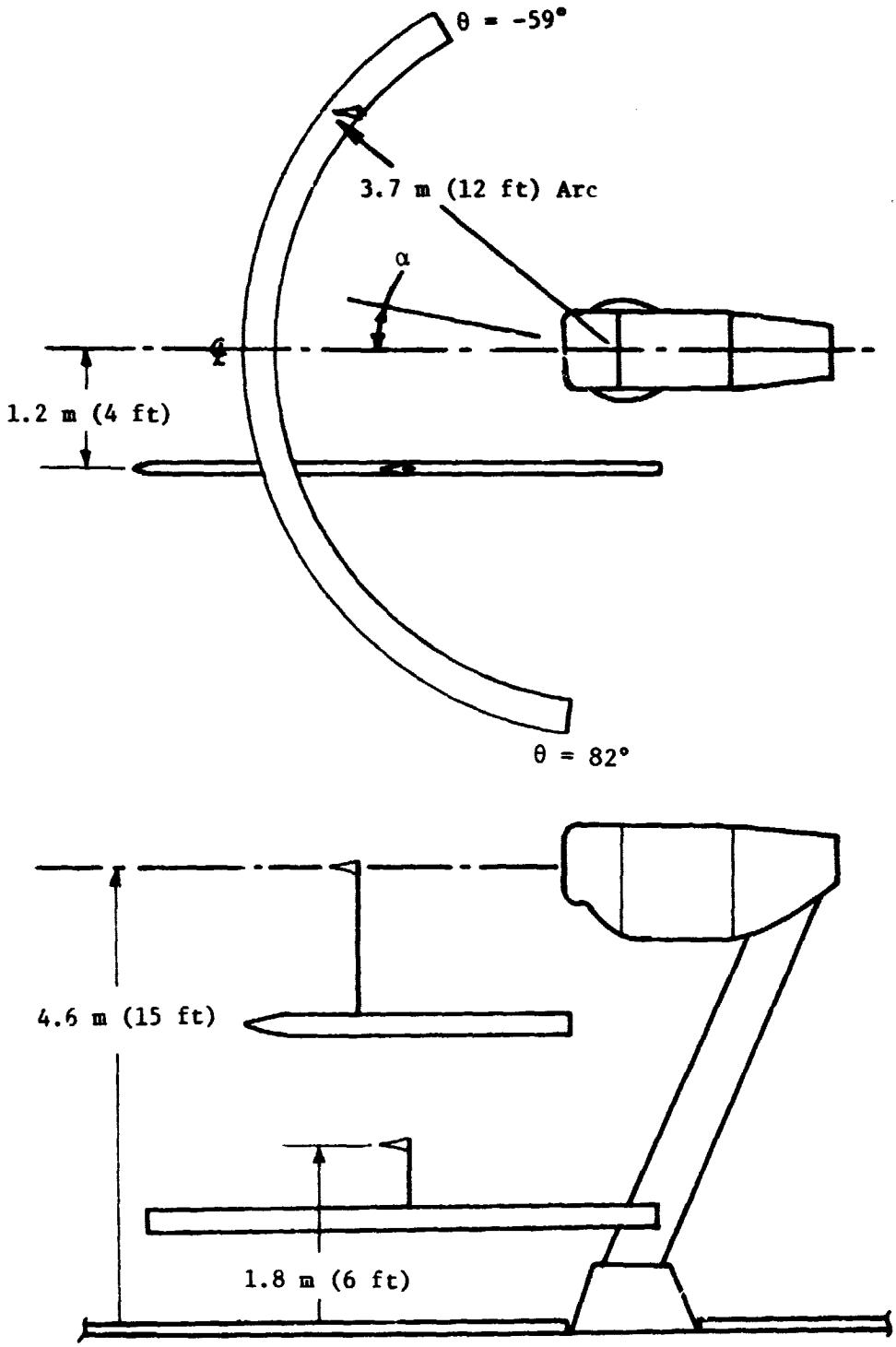

Figure 25. Test Setup for Second Wind Tunnel and Outdoor Static Tests.

ORIGINAL PAGE
BLACK AND WHITE PHOTOGRAPH

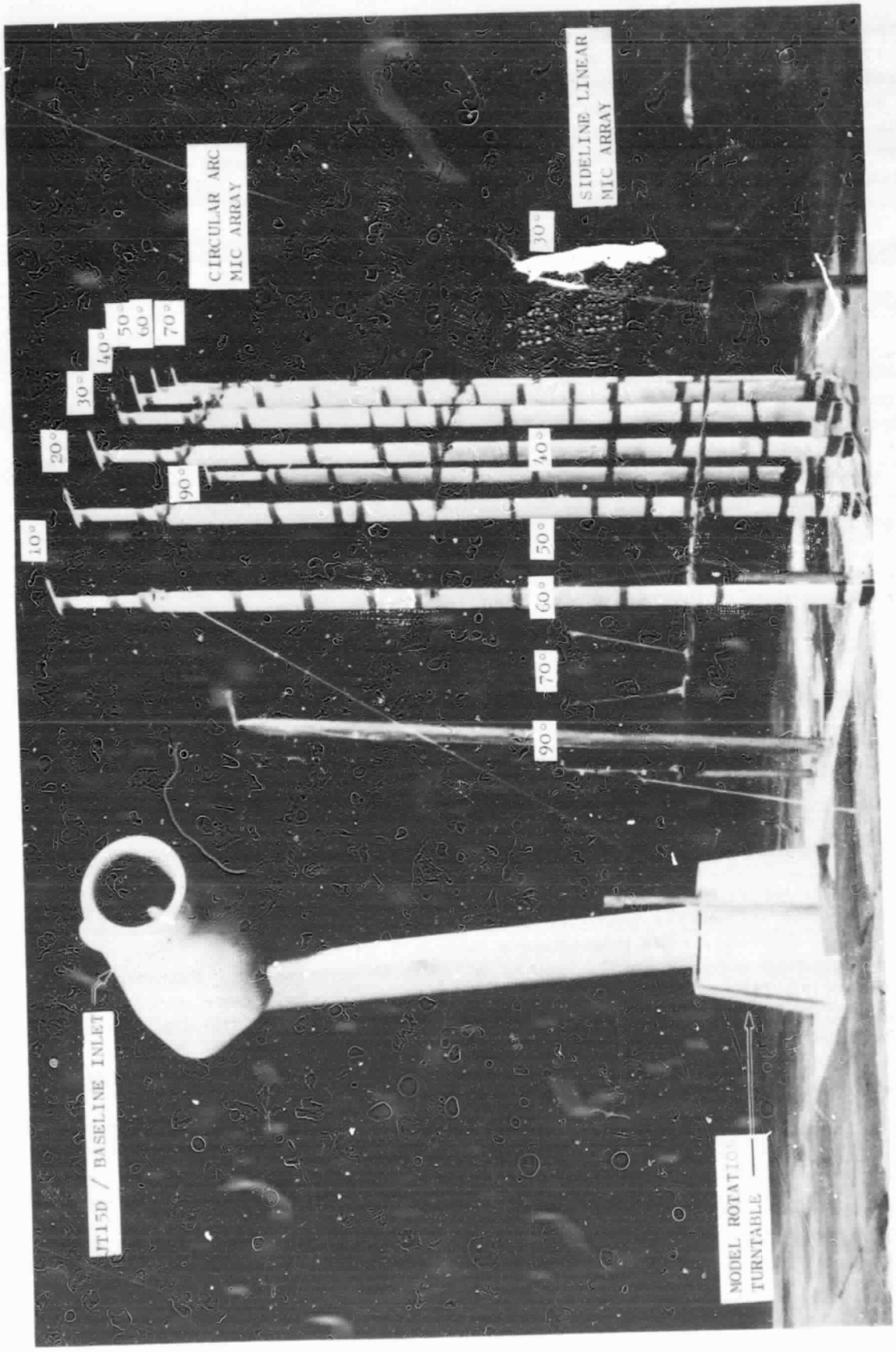

Figure 26. Test Setup in NASA ARC 40 by 80 Wind Tunnel (1st Entry).

shows the first wind tunnel test setup. In order to obtain better definition of the inlet-noise directivity at all angles of attack, the second wind tunnel test used traversing microphones that covered -59° to 82° on the arc and 30° to 90° on the sideline. Two near-field microphones that were 0.6 m (2 ft) from the engine centerline and 0.3 m (1 ft) forward of the inlet lip were used for some configurations. The photo in Figure 27 shows the second wind tunnel test setup.

3.5 INSTRUMENTATION

3.5.1 External Noise

All external noise measurements were made with B&K microphones. During all tests the microphones used were the 0.64 cm (0.25 in.) B&K 4135 with B&K UA0385 nose cones attached. By using the same microphone/nose-cone configuration for both outdoor static and wind tunnel tests, direct comparisons of the data can be made. However, B&K provides correction curves for noise arriving at the microphone at incidence angles from 0° to 180° and for the presence of nose cones. These curves were used to correct all the 1/3-octave-band data so that absolute sound pressure levels could be determined.

During the first outdoor static and wind tunnel tests, the fixed microphones were oriented pointing forward parallel to the engine centerline or wind tunnel centerline. The near-field and sideline traversing microphones were similarly pointed forward during the second outdoor static and wind tunnel tests. The circular-traversing microphones used during the second tests were attached to movable vanes that kept the microphones pointed upstream during forward speed testing in the wind tunnel. However, during quasi-static wind tunnel and outdoor static testing, the vanes were locked so that the microphones pointed away from the engine at all angles.

3.5.2 Internal Noise

Internal noise measurements were made on the diffuser walls of each inlet with Kulite (XTMS-1-190-25D) pressure transducers during all outdoor static and wind tunnel testing. The transducers have a 0.32 cm (0.125 in.) pressure-sensitive diaphragm mounted in the end of a 10-32 threaded bolt. Each inlet was provided with threaded holes through the diffuser walls; these enabled the transducers to be installed with the diaphragms flush with the inner surface. The locations of the transducers for each of the inlets are shown in Figure 28. Since the transducers were removable, the same sensors were used at the same relative location in each inlet to minimize data errors.

3.5.3 Aerodynamic Performance

Static pressure distributions along the surfaces of each inlet were an essential part of the data acquired for each test condition. For the hybrid

ORIGINAL PAGE
BLACK AND WHITE PHOTOGRAPH

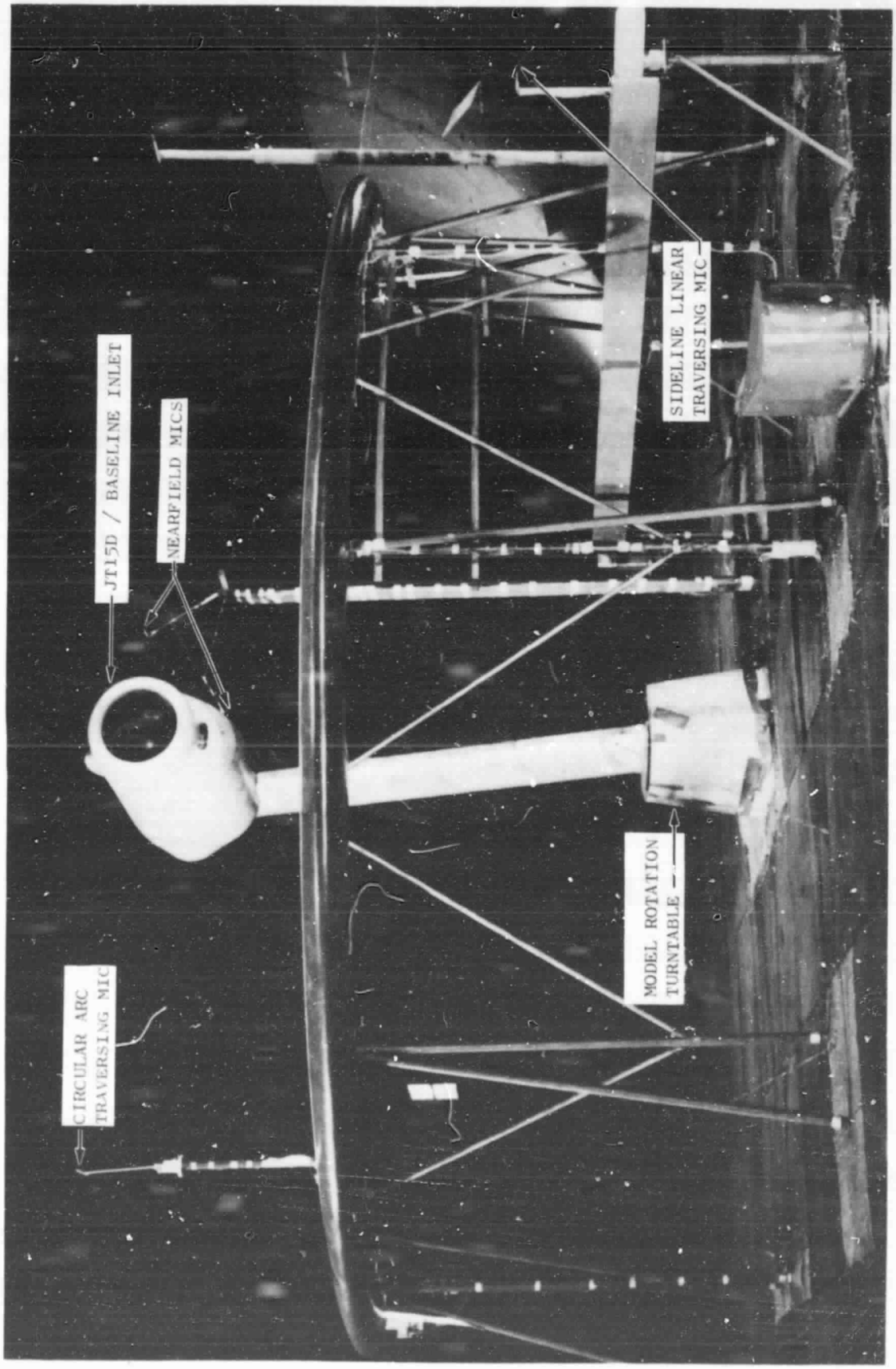

Figure 27. Test Setup in NASA ARC 40 by 80 Wind Tunnel (2nd Entry).

ORIGINAL PAGE IS
OF POOR QUALITY

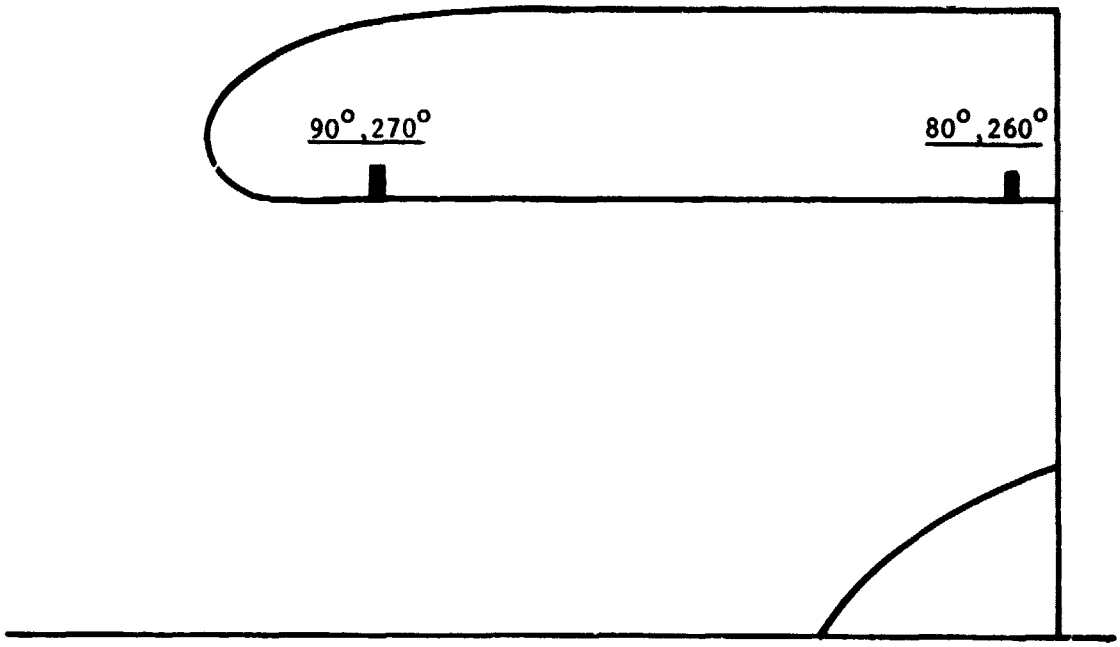

(a) Baseline Inlet

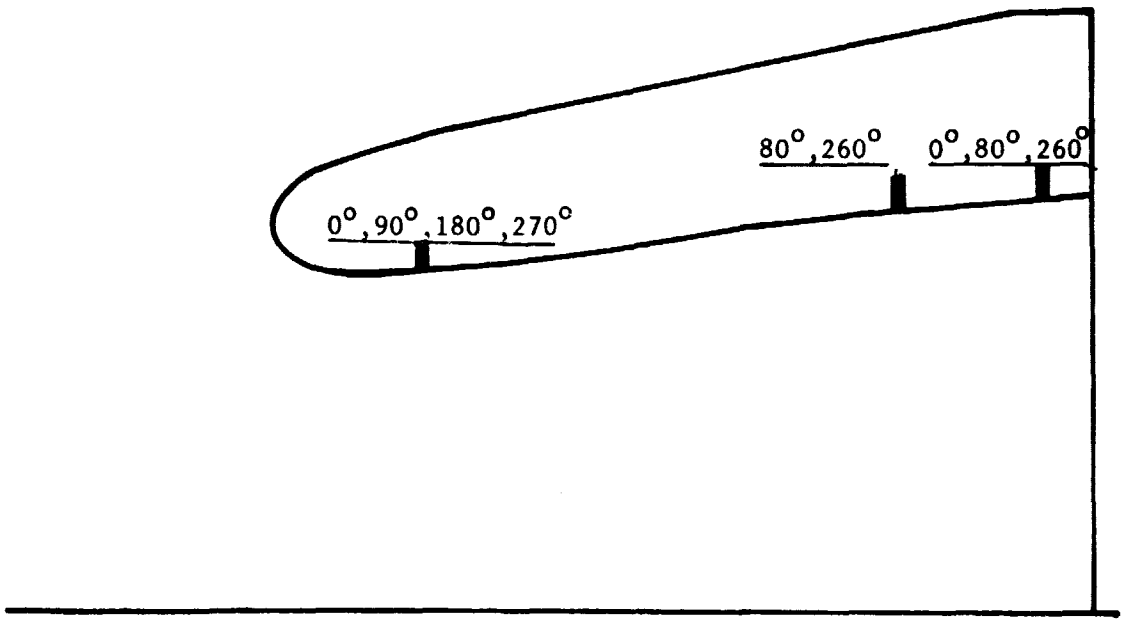

(b) CTOL Inlet

Figure 28. Internal-Noise Transducer Locations.

ORIGINAL PAGE IS
OF POOR QUALITY

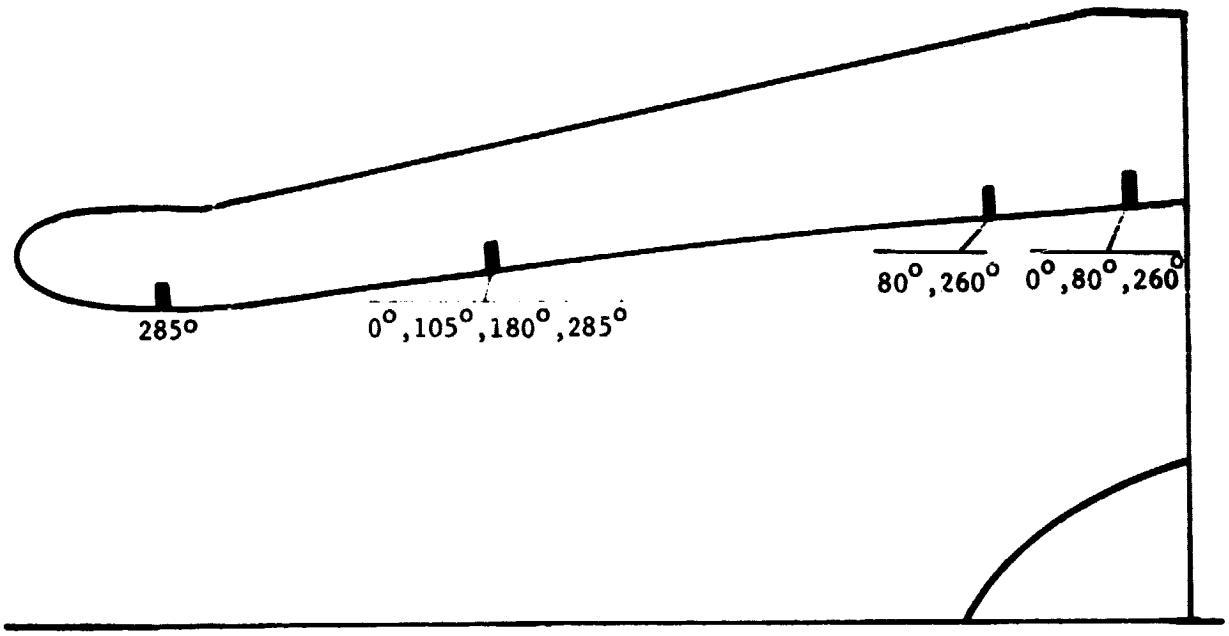

(c) STOL Inlet

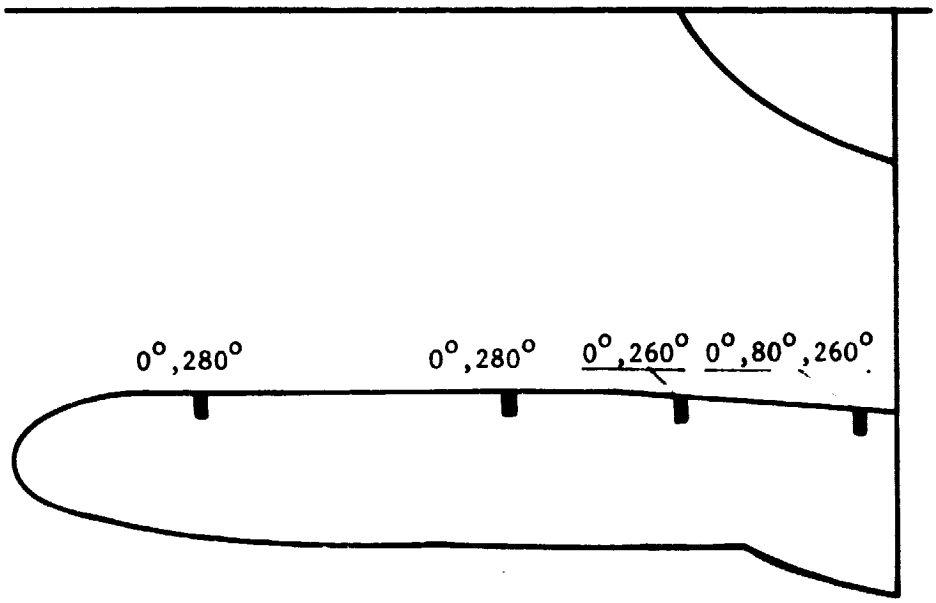

(d) Deflector Inlet

Figure 28. Internal-Noise Transducer Locations (Concluded).

inlets, the static pressures were used along with precomputed graphs to determine the one-dimensional throat Mach number and the airflow through the inlet. The static pressure tap locations for each of the inlets are shown in Figure 29. Selected wall static pressure data were monitored on-line to set throat Mach numbers at zero angle of attack and to determine the onset of diffuser wall separation while setting maximum angle-of-attack limits.

By using the inlet airflow data obtained from matching the General Electric computerized airflow predictions with the measured wall static pressures, the JT15D fan-airflow/speed relationship was determined. However, since the fan nozzle area was enlarged for these tests, there was no correlation of fan airflow to fan pressure ratio available. A special outdoor test using the baseline inlet with aeroacoustic lip was run with two fan-discharge rakes installed as shown in Figure 30. The JT15D fan pressure ratio was then measured at various fan speeds with the production fan nozzle as well as with the hybrid-inlet fan nozzle.

During the aerodynamic performance testing, the inlet total pressure loss and distortion were measured for both hybrid inlets and the deflector inlet with six 5-element total pressure rakes. The rakes were installed in the hard-wall aft diffuser section at six equally spaced angular locations as shown in Figures 31 and 32. The total pressure rakes were originally designed for a smaller duct and, as a result, do not have probe-element-immersion depths at centers of equal annular areas. However, this was not a problem since the distortion profiles were not expected to extend inward of the inner elements of the rakes, and the average total pressure calculations would be area-weighted to provide more representative inlet-pressure-loss results.

The total pressure rakes also had transducers installed in each element to measure dynamic total pressure distortion. The transducers indicated in Figure 31 were monitored and recorded during aerodynamic performance testing to aid in determining diffuser wall flow separation. During angle-of-attack sweeps, the maximum angle-of-attack limit was set just below the point at which the transducers indicated rapid changes in total pressure near the walls.

3.6 TEST SUMMARY

3.6.1 Outdoor Static Tests

The outdoor static tests were conducted at the VTOL test stand during the periods 22 July 1977 to 28 July 1977 and 2 November 1978 to 7 November 1978 using the same JT15D engine and inlet hardware. Both the standard JT15D and the modified engine (core IGV's removed) were used during the first test series; the redesigned version (new core IGV's) was used during the second test series. Complete summaries of the tests are contained in Table 3 including the details of each inlet configuration used with each engine. The objectives of the outdoor static tests were, first, to operationally check out the inlet/engine combination and, then, to obtain a limited amount of noise data for subsequent comparisons with the wind tunnel noise data. Since the primary objectives of

ORIGINAL PAGE IS
OF POOR QUALITY

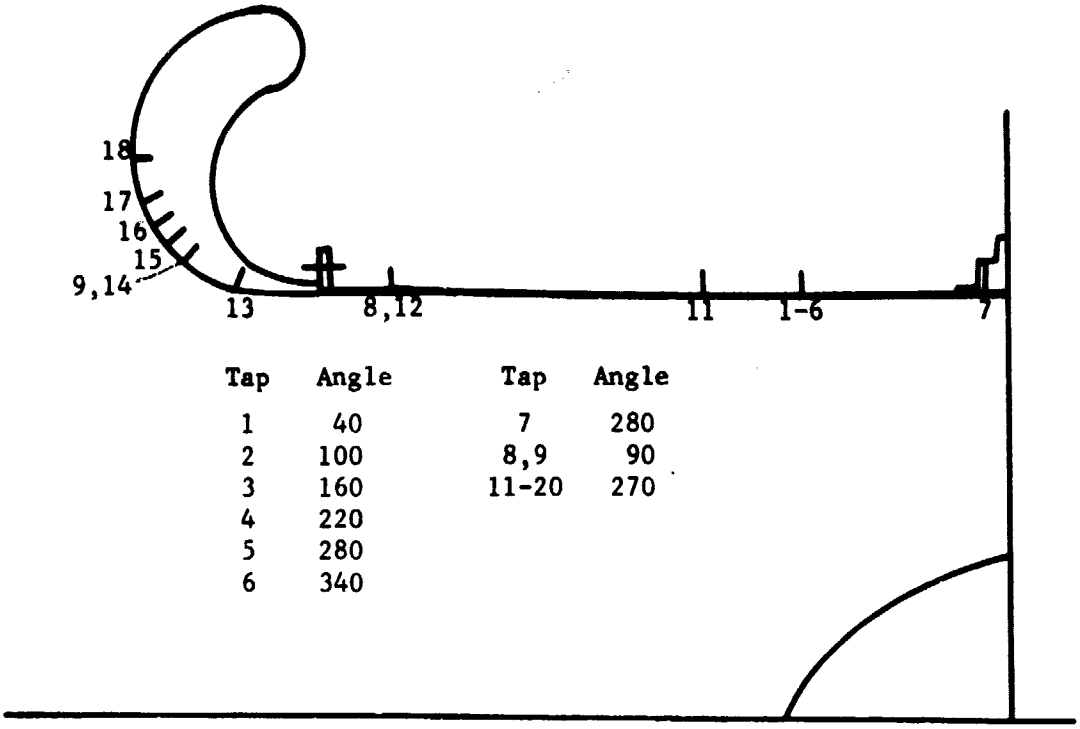

Tap	Angle	Tap	Angle
1	40	7	280
2	100	8,9	90
3	160	11-20	270
4	220		
5	280		
6	340		

(a) Baseline Inlet with Aeroacoustic Lip

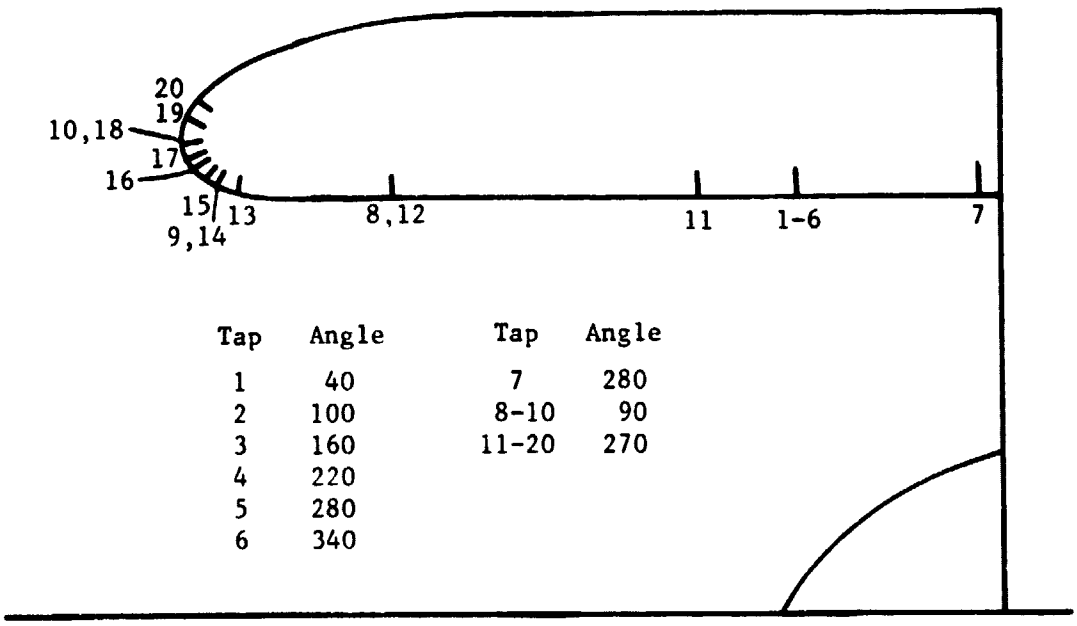

Tap	Angle	Tap	Angle
1	40	7	280
2	100	8-10	90
3	160	11-20	270
4	220		
5	280		
6	340		

(b) Baseline Inlet with Flight Lip

Figure 29. Wall Static Pressure Tap Locations.

ORIGINAL PAGE IS
OF POOR QUALITY

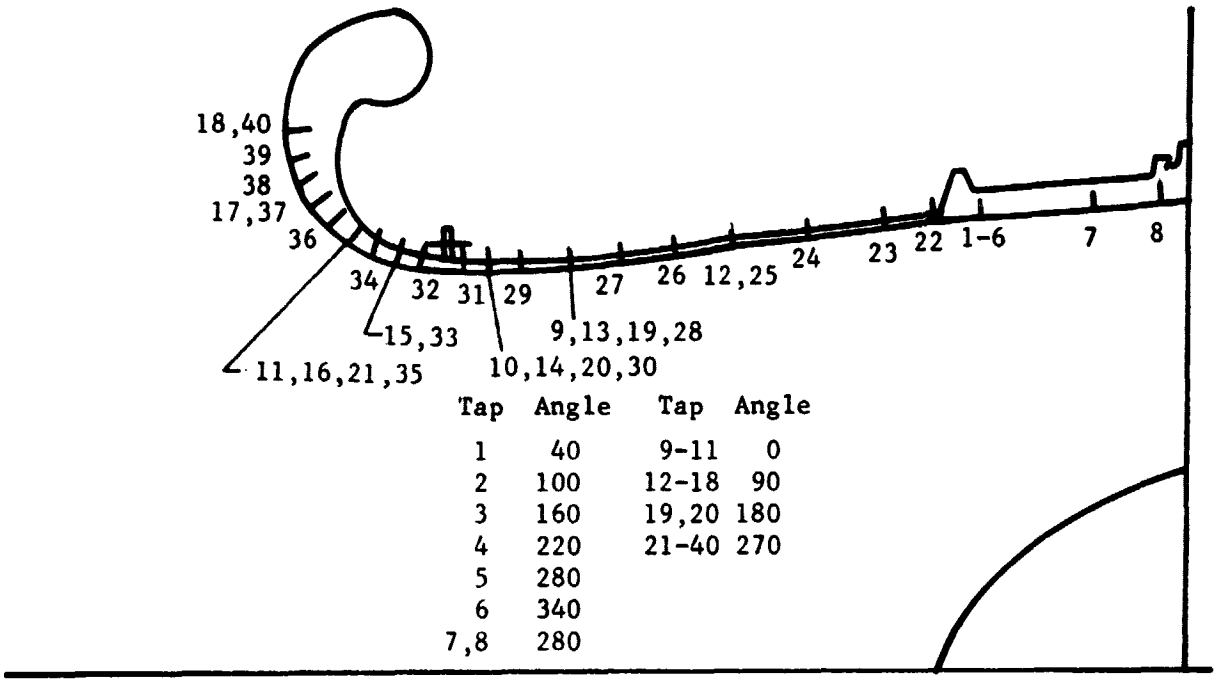

Tap	Angle	Tap	Angle
1	40	9-11	0
2	100	12-18	90
3	160	19,20	180
4	220	21-40	270
5	280		
6	340		
7,8	280		

(c) CTOL Inlet with Aeroacoustic Lip

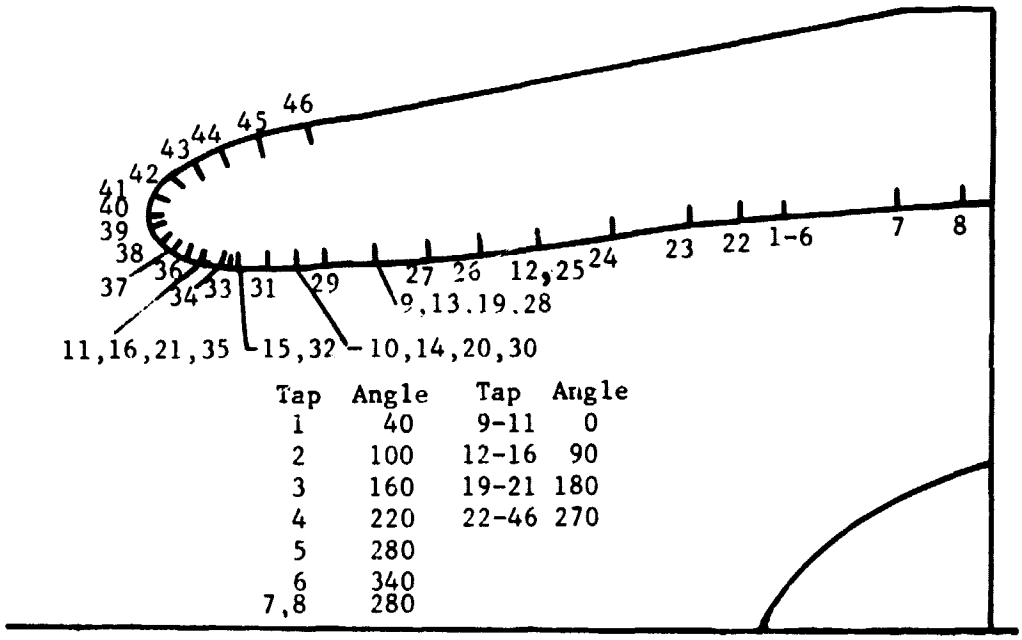

Tap	Angle	Tap	Angle
1	40	9-11	0
2	100	12-16	90
3	160	19-21	180
4	220	22-46	270
5	280		
6	340		
7,8	280		

(d) CTOL Inlet with Flight Lip

Figure 29. Wall Static Pressure Tap Locations (Continued).

ORIGINAL PAGE IS
OF POOR QUALITY

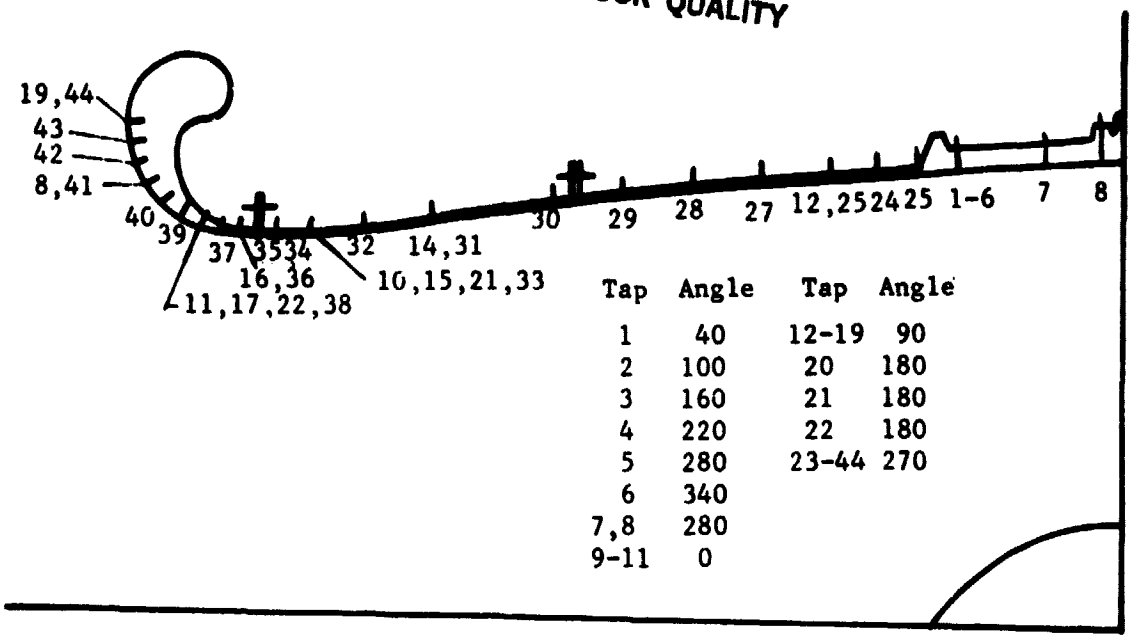

Tap	Angle	Tap	Angle
1	40	12-19	90
2	100	20	180
3	160	21	180
4	220	22	180
5	280	23-44	270
6	340		
7,8	280		
9-11	0		

(e) STOL Inlet with Aeroacoustic Lip

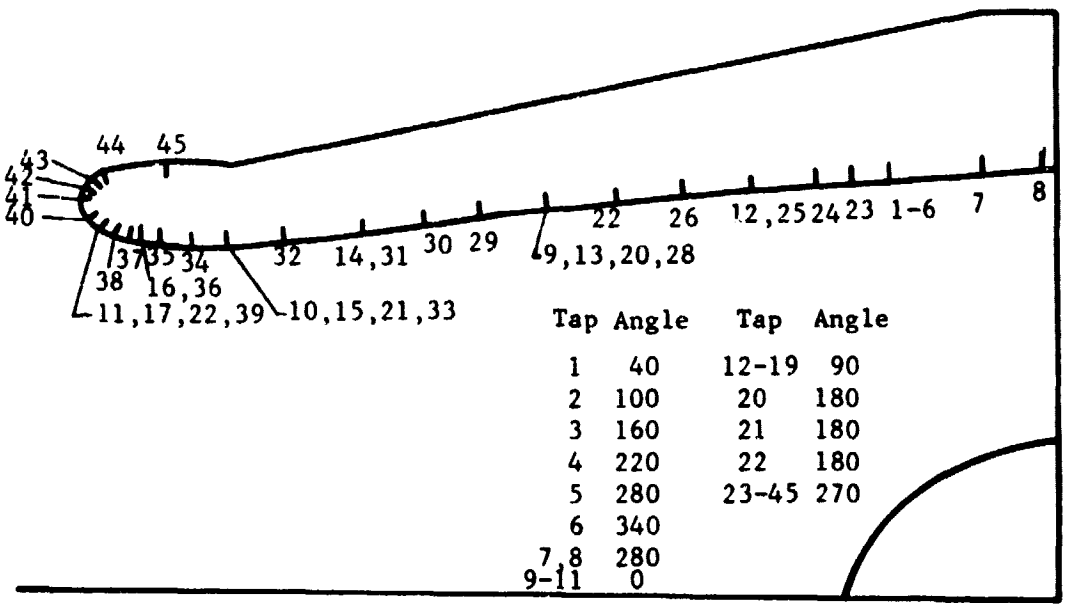

Tap	Angle	Tap	Angle
1	40	12-19	90
2	100	20	180
3	160	21	180
4	220	22	180
5	280	23-45	270
6	340		
7,8	280		
9-11	0		

(f) STOL Inlet with Flight Lip

Figure 29. Wall Static Pressure Tap Locations (Continued).

ORIGINAL PAGE IS
OF POOR QUALITY

Tap	Angle
2	40
3	100
4	160
5	220
6	280
7	340
8	280
9	280
10-16	20
17-24	90
25-33	270
34-40	300
41-47	340

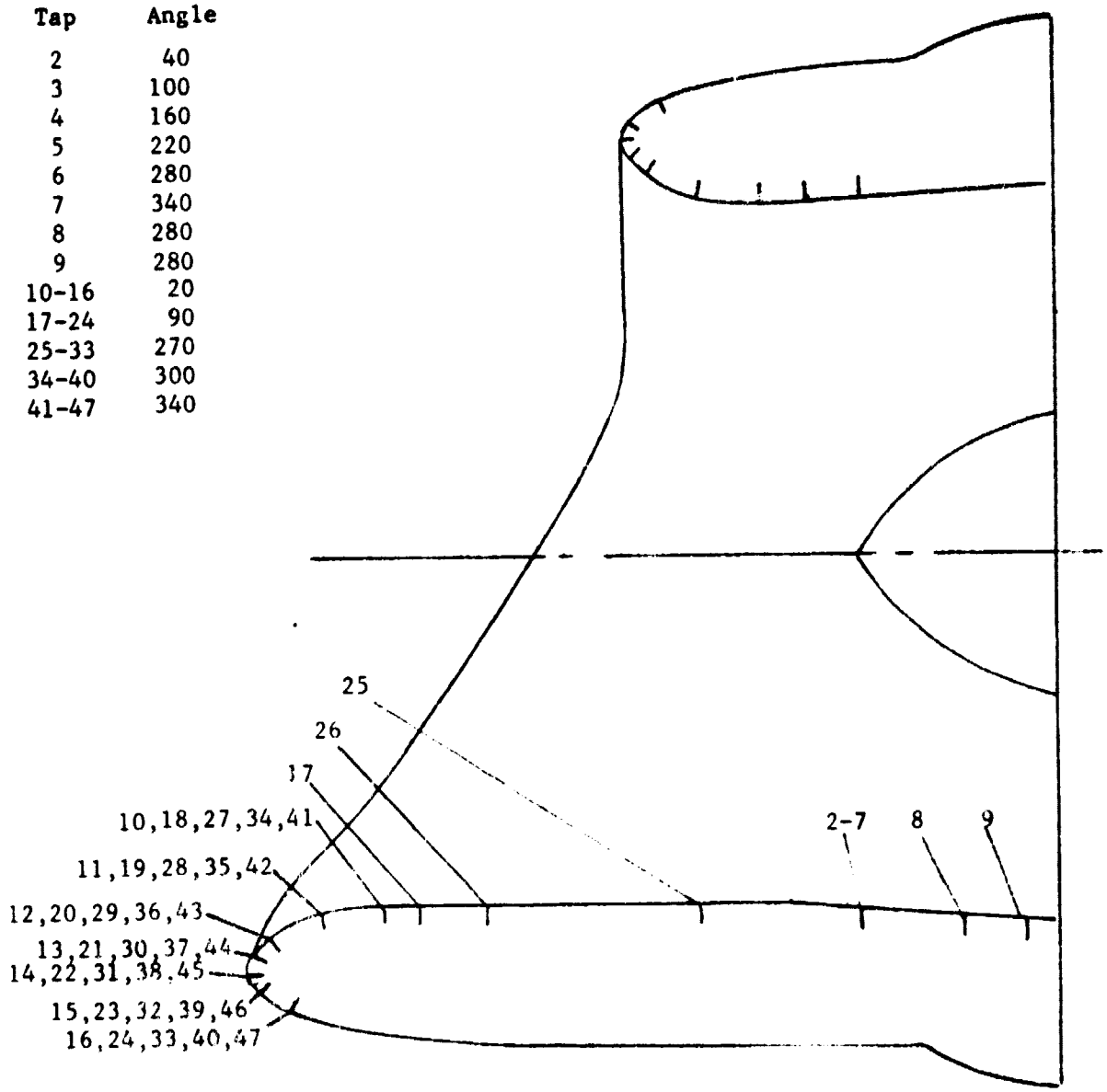

(g) Deflector Inlet

Figure 29. Wall Static Pressure Tap Locations (Continued).

ORIGINAL PAGE IS
OF POOR QUALITY

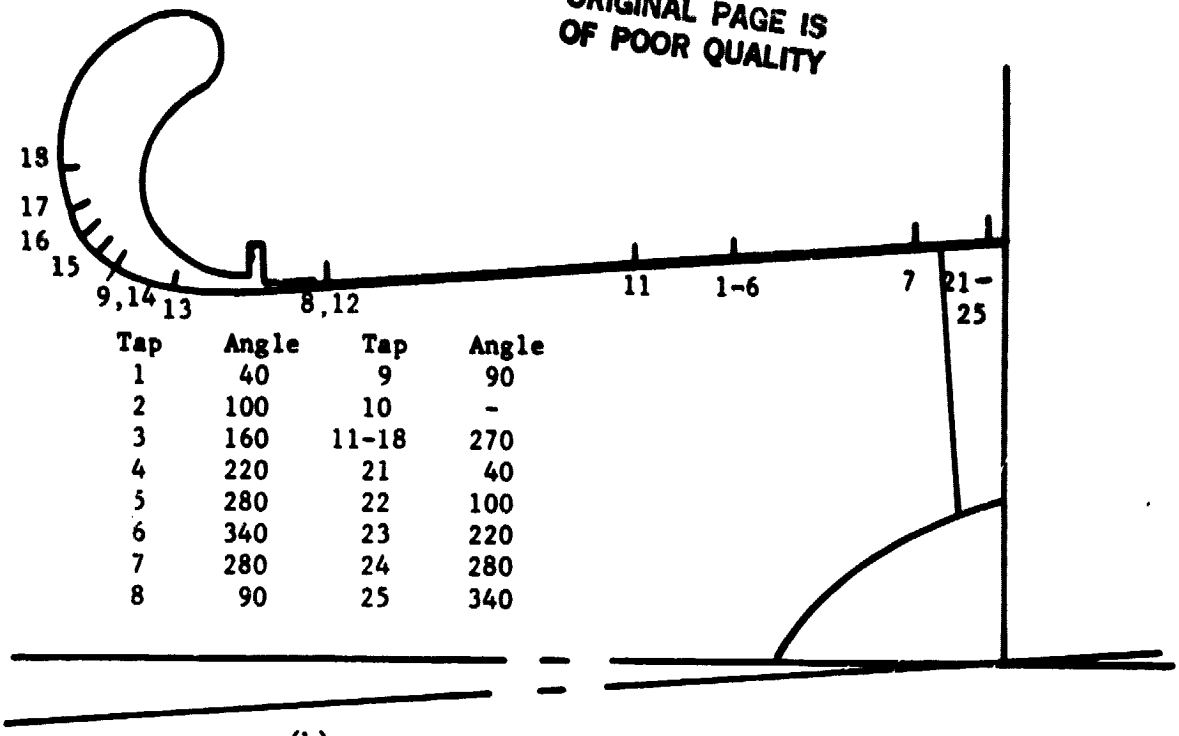

Tap	Angle	Tap	Angle
1	40	9	90
2	100	10	-
3	160	11-18	270
4	220	21	40
5	280	22	100
6	340	23	220
7	280	24	280
8	90	25	340

(h) Canted Baseline Inlet with Aeroacoustic Lip

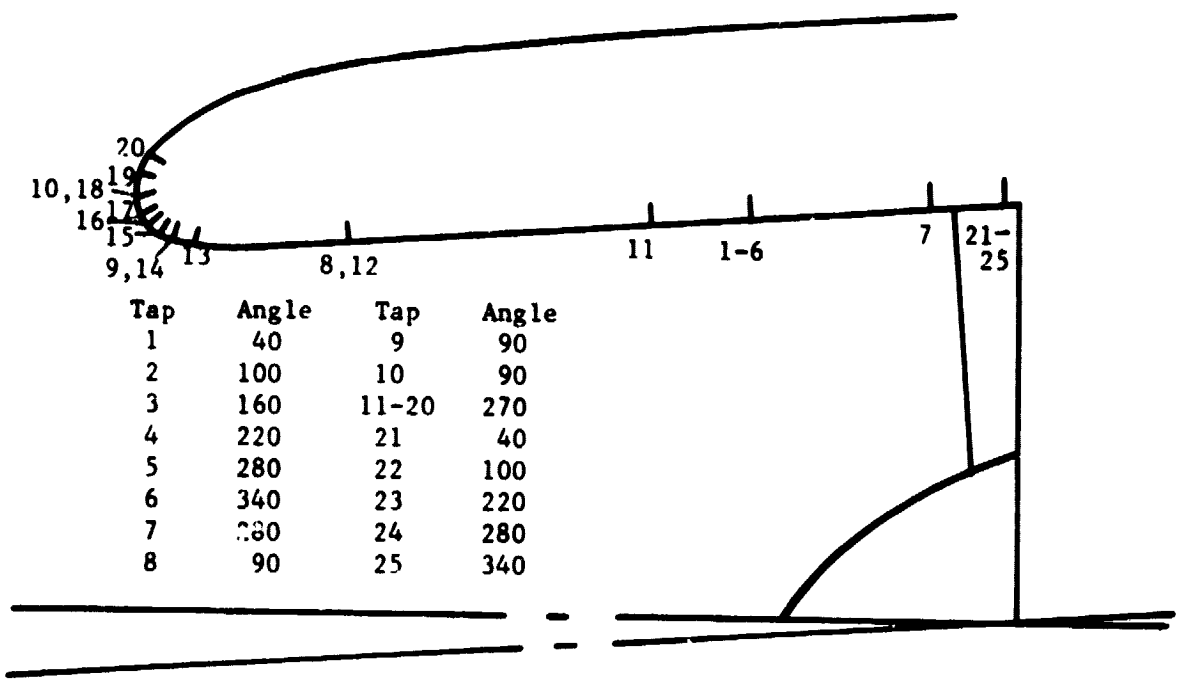

Tap	Angle	Tap	Angle
1	40	9	90
2	100	10	90
3	160	11-20	270
4	220	21	40
5	280	22	100
6	340	23	220
7	280	24	280
8	90	25	340

(i) Canted Baseline Inlet with Flight Lip

Figure 29. Wall Static Pressure Tap Locations (Concluded).

ORIGINAL PAGE IS
OF POOR QUALITY

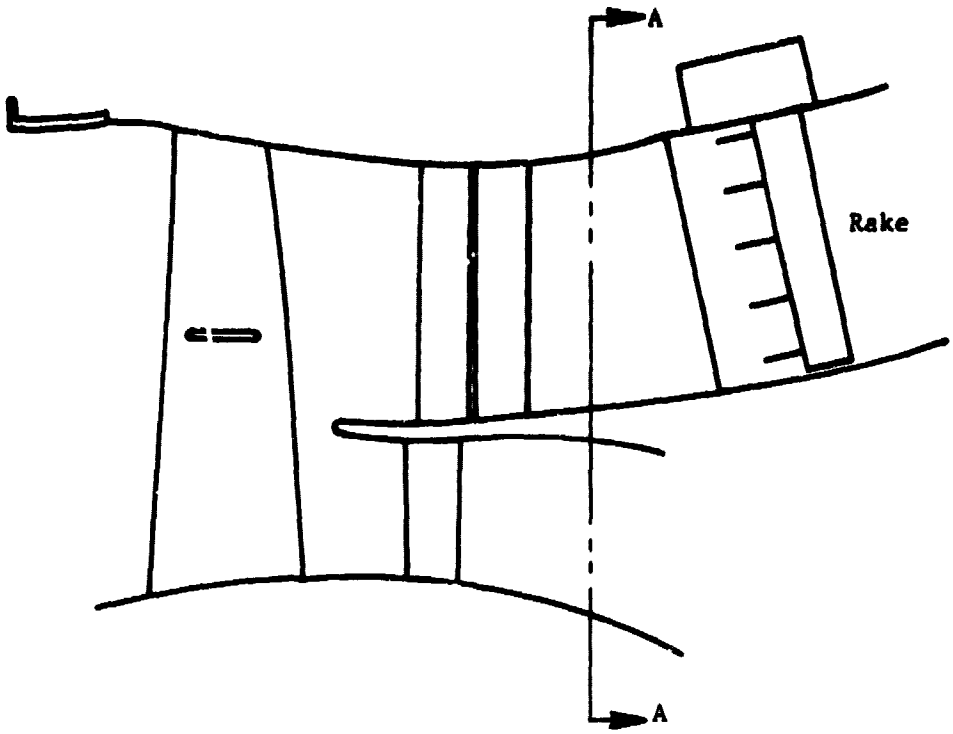

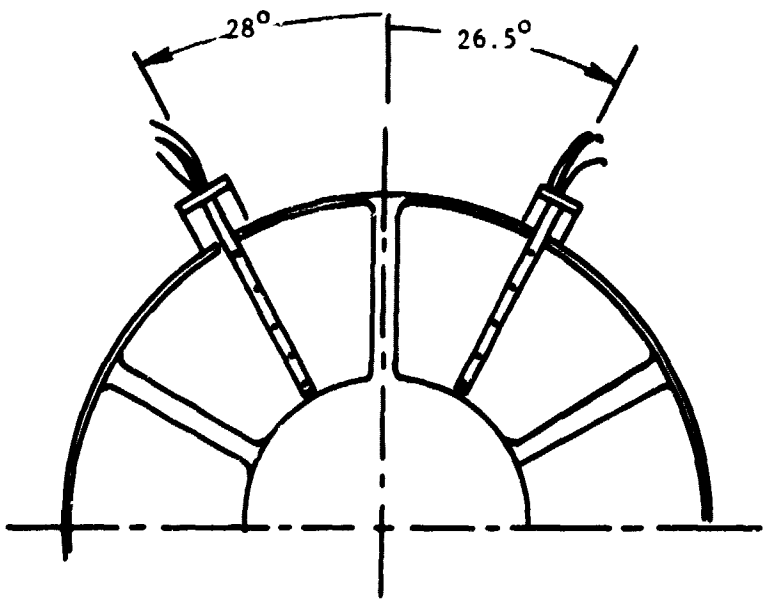

Section A-A

Figure 30. Discharge Total Pressure Rake Locations.

ORIGINAL PAGE IS
OF POOR QUALITY

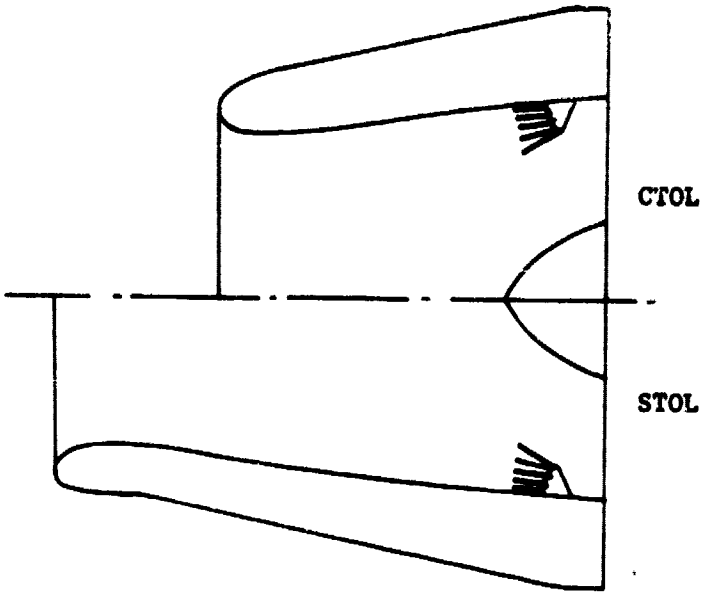

Section A-A

Note: Pressure transducers are just inside the tip of each pressure tube.

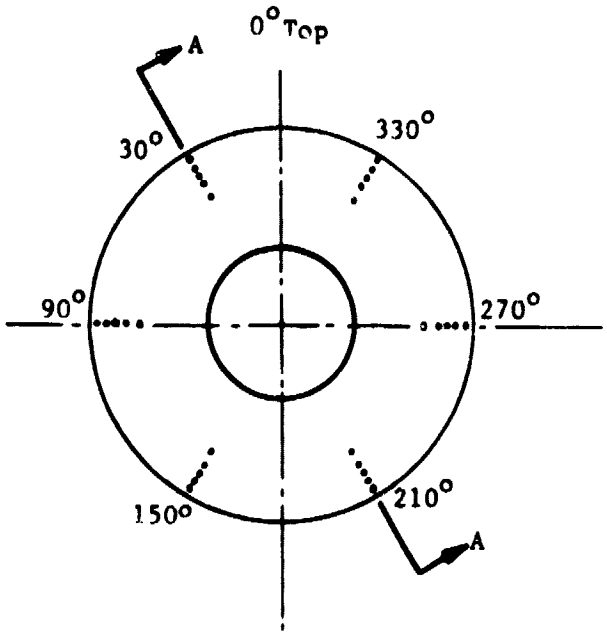

Forward Looking Aft

Figure 31. Inlet Total Pressure Rake Locations.

ORIGINAL PAGE
BLACK AND WHITE PHOTOGRAPH

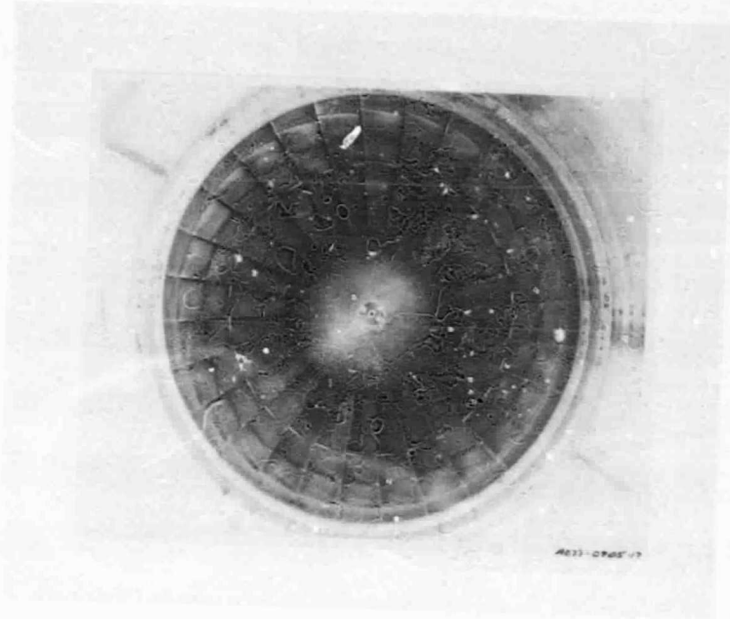

Without Rakes

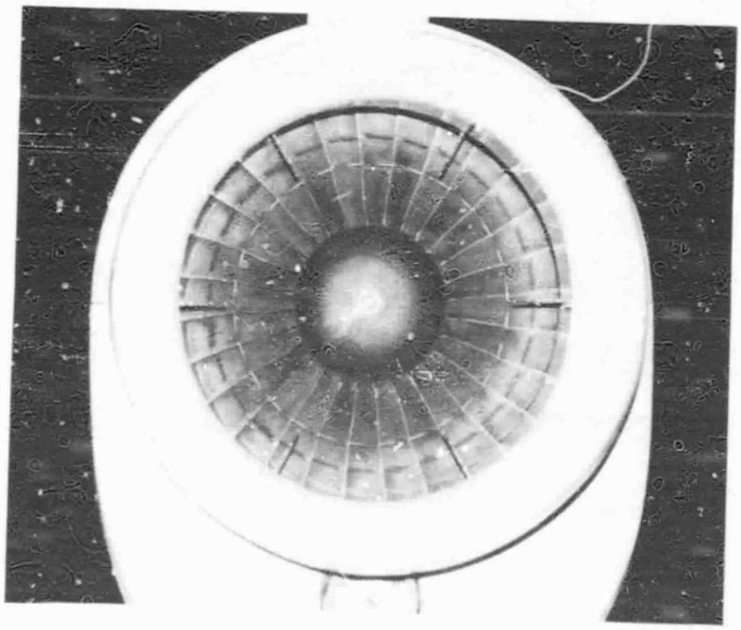

With Rakes

Figure 32. Photographs of JT15D Fan Showing Total Pressure Rakes.

Table 3. Run Logs for Outdoor Static Tests.

Run	JT15D	Inlet	Lip	Treated	Rakes	Mics	α	Vo	Points
First									
1	Std	STOL	A/A	Yes	X		0	≈0	9
2	Std	CTOL	A/A	Yes		X	0	≈0	8
3	Mod	STOL	A/A	Yes		X	0	≈0	8
4	Mod	STOL	A/A	Yes		X	0	≈0	4
5	Mod	Base	A/A	No		X	0	≈0	9
6	Mod	Base	A/A	No		X	0	≈0	3
7	Mod	Base	A/A	No		X	0	≈0	4
Second									
1	Red	Defl	FL	Yes		X	0	≈0	12
2	Red	Base	A/A	No		X	0	≈0	18
3	Red	Cant	A/A	No		X	0	≈0	15

the program were to determine forward-velocity effects on fan noise and inlet suppression, extensive outdoor static tests were not conducted.

The hybrid inlets were run first during the first outdoor static test, which preceded the wind tunnel tests, to provide the wall static pressure data necessary to establish the inlet airflow and throat Mach number correlations with fan speed. Subsequent tests with the baseline inlet were run at the same corrected fan speeds that were run with the STOL hybrid inlet. Thirty-six noise-data points were recorded covering a range of throat Mach numbers from $0.6 \leq M_{TH} \leq 0.8$ for each hybrid inlet and equivalent fan speeds for the baseline inlet. The baseline inlet was only run at low corrected fan speeds corresponding to the STOL hybrid inlet range because of the speed limitation on operation of the JT15D without the core IGV's.

The second outdoor static test was conducted after both wind tunnel tests were completed to provide baseline inlet data with the redesigned engine in the outdoor environment. In addition, the treated deflector inlet and the canted baseline inlet were run over the entire fan speed range to obtain data from those configurations in the outdoor environment. A total of 45 noise-data points were recorded for the three inlet configurations covering a range of corrected fan speeds from 11,000 rpm to 15,000 rpm.

For each noise-data point the fan corrected speed was set based upon throat Mach number, if applicable, and allowed to stabilize. All amplifier gain settings were optimized for the internal and external noise measurements, and then at least 30 seconds of data were tape-recorded. During traverse operation (second outdoor static test), the recorders ran continuously for the 3 to 4 minutes required to complete the traverse. To minimize errors in data reduction the traverse-microphone amplifier gain settings, which were preestablished based on peak overall noise levels, were not changed during data acquisition.

3.6.2 Wind Tunnel Tests

The wind tunnel tests were conducted in the 40 by 80 during the periods of 23 August 1977 to 1 September 1977 and 12 September 1978 to 5 October 1978 using the same JT15D engine and inlet hardware as the outdoor static tests. First the modified JT15D and then the standard JT15D were used in the first wind tunnel tests. The redesigned version of the JT15D was used exclusively during the second wind tunnel tests. Complete summaries of the wind tunnel tests are contained in Table 4 (first entry) and Table 5 (second entry) which include the details of each inlet configuration used with each engine. The primary objectives of the first entry were to completely determine the aerodynamic performance and to obtain preliminary acoustic performance of the hybrid inlets with the standard and modified JT15D engines. The objectives of the second entry were to determine the acoustic performance of the hybrid inlets, the deflector inlet, and the canted baseline inlet as well as measure the aerodynamic performance of the deflector inlet.

Table 4. Run Log for First 40-by-80-Foot Wind Tunnel Test.

Run	JT15D	Inlet	Lip	Treated	α	Vo	Run	JT15D	Inlet	Lip	Treated	α	Vo
1	Mod	STOL	A/A	Yes	0	10	30	Std	STOL	FL	No	0-30	40
2	Mod	STOL	FL	Yes		10	31	Std	STOL	FL	No	0-40	80
3	Mod	STOL	FL	Yes		40	32	Std	STOL	FL	No	0	10
4	Mod	STOL	FL	Yes		80	33	Std	STOL	FL	No	0-36	120
5	Mod	STOL	FL	Yes		120	34	Std	STOL	FL	No	0,15	120
6	Mod	STOL	FL	Yes		80	35	Std	STOL	FL	No	0,15	80
7	Mod	STOL	FL	Yes		10	36	Std	STOL	FL	No	0	10
8	Mod	STOL	FL	No		10	37	Std	STOL	FL	No	0,15	40
9	Mod	STOL	FL	No		40	38	Std	CTOL	FL	No		160
10	Mod	STOL	FL	No		80	39	Std	CTOL	FL	No		120
11	Mod	STOL	FL	No		120	40	Std	CTOL	FL	No		80
12	Mod	Base	FL	No		10	41	Std	CTOL	FL	No	0	10
13	Mod	Base	FL	No		40	42	Std	STOL	FL	Yes	0.15	120
14	Mod	Base	FL	No		80	43	Std	STOL	FL	Yes	0.15	120
15	Mod	Base	FL	No		120	44	Std	STOL	FL	Yes		80
16	Mod	Base	FL	No		80	45	Std	STOL	FL	Yes		40
17	Mod	Base	FL	No		10	46	Std	STOL	FL	Yes	0	10
18	Std	STOL	FL	Yes	0	10	47	Std	CTOL	FL	Yes	0,15	160
19	Std	STOL	FL	Yes	0-30	40	48	Std	CTOL	FL	Yes	0,15	80
20	Std	STOL	FL	Yes	0-40	80	49	Std	CTOL	FL	Yes	0	10
21	Std	STOL	FL	Yes	0-40	80	50	Std	CTOL	FL	Yes	0,15	120
22	Std	STOL	FL	Yes	0-35,5	120	51	Std	Base	FL	No	0,15	80
23	Std	STOL	FL	Yes	0-32	120	52	Std	Base	FL	No	0	40
24	Std	CTOL	FL	Yes	0	10	53	Std	Base	FL	No	0,15	120
25	Std	CTOL	FL	Yes	0-25	80	54	Std	Base	FL	No	0,15	160
26	Std	CTOL	FL	Yes	0-25	120	55	Std	Base	FL	No	0	10
27	Std	CTOL	FL	Yes	0-25	120	56	Std	Base	FL	No	0	10
28	Std	CTOL	FL	Yes	0-25	160	57	Std	Base	A/A	No	0	10
29	Std	STOL	FL	No	0	10	58	Std	CTOL	A/A	Yes	0	10

Note: Run 18-33 had total pressure rakes and no microphones.

Table 5. Run Log for Second 40-by-80-Foot Wind Tunnel Test.

Run	JT15D	Inlet	Lip	Treated	α	Vo	Run	JT15D	Inlet	Lip	Treated	α	Vo
1	Red	STOL	A/A	Yes	0	10	38	Red	CTOL	FL	No	15	80
2	Red	STOL	A/A	Yes	0	10	39	Red	CTOL	FL	No	15	115
3	Red	STOL	FL	Yes	0	10	40	Red	CTOL	FL	No	8	115
4	Red	STOL	FL	Yes	0	40	41	Red	CTOL	FL	No	15	115
5	Red	STOL	FL	Yes	15	40	42	Red	CTOL	FL	No	0	80,115
6	Red	STOL	FL	Yes	30	40	43	Red	CTOL	FL	No	8	80
7	Red	STOL	FL	Yes	0	80	44	Red	CTOL	FL	No	15	80
8	Red	STOL	FL	Yes	0	80	45	Red	Base	A/A	No	0	13
9	Red	STOL	FL	Yes	15	80	46	Red	Base	A/A	No	0	13
10	Red	STOL	FL	Yes	30	80	47	Red	Base	FL	No	0	14
11	Red	STOL	FL	Yes	0	115	48	Red	Base	FL	No	0	40
12	Red	STOL	FL	Yes	15	115	49	Red	Base	FL	No	15	40
13	Red	STOL	FL	Yes	25	115	50	Red	Base	FL	No	0	80
14	Red	STOL	FL	Yes	0	80,115	51	Red	Base	FL	No	8	80
15	Red	CTOL	FL	Yes	0	0	52	Red	Base	FL	No	15	80
16	Red	CTOL	FL	Yes	0	80	53	Red	Base	FL	No	0	115
17	Red	CTOL	FL	Yes	8	80	54	Red	Base	FL	No	8	115
18	Red	CTOL	FL	Yes	15	80	55	Red	Base	FL	No	15	115
19	Red	CTOL	FL	Yes	0	115	56	Red	Base	FL	No	15	115
20	Red	CTOL	FL	Yes	0	115	57	Red	Base	FL	No	15	115
21	Red	CTOL	FL	Yes	0	115	58	Red	Cant	FL	No	0	14
22	Red	CTOL	FL	Yes	8	115	59	Red	Cant	FL	No	0	11
23	Red	CTOL	FL	Yes	15	115	60	Red	Cant	FL	No	4	12
24	Red	CTOL	A/A	Yes	0	16	61	Red	Cant	FL	No	1	40
25	Red	CTOL	A/A	Yes	0	16	62	Red	Cant	FL	No	0	80
26	Red	STOL	FL	No	0	10	63	Red	Cant	FL	No	4	80
27	Red	STOL	FL	No	0	10	64	Red	Defl	FL	No	0	11
28	Red	STOL	FL	No	0	80	65	Red	Defl	FL	No	0	80
29	Red	STOL	FL	No	15	80	66	Red	Defl	FL	No	0-30	80
30	Red	STOL	FL	No	25	80	67	Red	Defl	FL	No	0-30	115
31	Red	STOL	FL	No	0	40	68	Red	Defl	FL	No	0	12
32	Red	STOL	FL	No	15	40	69	Red	Defl	FL	No	0	80
33	Red	STOL	FL	No	33	40	70	Red	Defl	FL	Yes	0	10
34	Red	CTOL	FL	No	0	15	71	Red	Defl	FL	Yes	0	80
35	Red	CTOL	FL	No	0	11	72	Red	Defl	FL	Yes	0	115
36	Red	CTOL	FL	No	0	40	73	Red	Defl	FL	Yes	15	115
37	Red	CTOL	FL	No	15	40	74	Red	Defl	FL	Yes	15	80

Note: Run 64-67 had total pressure rakes and no microphones.

The modified JT15D engine was moved from the VTOL test stand to the 40 by 80 to be run during the initial wind tunnel noise testing. The STOL hybrid and baseline inlets were tested at forward speeds up to 62 m/s (203 ft/s) over a corrected fan speed range of 11,000 rpm to 12,400 rpm; this is a throat Mach number range of $0.6 \leq M_{TH} \leq 0.8$ for the STOL hybrid inlet. No angle-of-attack testing was done due to the use of the modified JT15D engine.

The core IGV's were then reinstalled, and the aerodynamic performance testing was conducted using the standard JT15D engine. Performance data were acquired for the STOL hybrid inlet over the above throat Mach number and forward-velocity range and at angle of attack up to the separation limit or the 40° travel limit on the turntable. Performance data for the CTOL hybrid inlet were acquired over the throat Mach number range of $0.6 \leq M_{TH} \leq 0.8$ at forward velocities up to 82 m/s (270 ft/s) and at angles of attack up to the separation limit. No external-noise data were recorded during these tests since the presence of the rakes would have significantly altered the fan-noise levels. This permitted recording of the 16 rake pressure transducers in place of 16 microphones without additional recorder channels.

The noise testing of the hybrid and baseline inlets with the standard JT15D engine was performed during the remainder of the first wind tunnel test. The same throat Mach number and forward-speed ranges were tested for the hybrid inlets but only up to 15° angle of attack. The baseline inlet was tested at the same forward speed and angle-of-attack combinations as the hybrid inlets and operated at corresponding corrected fan speeds of 11,000 rpm to 12,500 rpm (STOL range) and 13,400 rpm to 15,000 rpm (CTOL range). A total of 602 data points were acquired with 122 noise points for the modified JT15D engine test; 173 aerodynamic performance points and 307 noise points were acquired for the standard JT15D engine.

The redesigned JT15D engine was installed in the 40 by 80 for the second wind tunnel test. The hybrid and baseline inlets were tested at forward speeds up to 59 m/s (194 ft/s) over the STOL and CTOL corrected-fan-speed ranges corresponding to the throat Mach number range of $0.6 \leq M_{TH} \leq 0.8$. The STOL hybrid inlet was tested at angles of attack up to 30°, and the CTOL hybrid and baseline inlets were tested at angle of attack up to 15°.

The canted baseline inlet was then tested over the same corrected-fan-speed ranges as the baseline inlet at forward speeds up to 41 m/s (135 ft/s). The configuration was first tested with the engine axis aligned with the flow, -4° angle of attack to the inlet, to simulate actual installed operation. The engine axis was then rotated 4° to align the inlet axis with the flow to acquire data at 0° inlet angle of attack for comparison.

The second wind tunnel test was concluded with the aerodynamic performance and noise testing of the deflector inlet. Aerodynamic data were acquired at forward speeds up to 59 m/s (194 ft/s) at angle of attack up to 30° over the same corrected-fan-speed range as the baseline inlet. After removal of the total pressure rakes and switching the recorder input to the microphones, the

noise testing was conducted. Noise data for the deflector inlet were acquired over the same forward speed and fan speed ranges at angle of attack up to 15°. A total of 511 data points were acquired during the second wind tunnel test including 50 aerodynamic performance points, 358 microphone-traverse noise points, and 103 fixed-position-microphone noise points.

For all wind tunnel testing the same procedure for setting test conditions and acquiring data was followed for all the noise-data points. The forward velocity in the 40 by 80 was set, and then the JT15D was put on point. This was done by setting either throat mach number from monitored static pressures or corrected fan speed based on fan-entrance temperature. The turntable was then rotated until the desired angle of attach was obtained. The fan speed was reset, if necessary, and then data was acquired. Steady-state data were recorded on the digital system, and then noise-data were tape recorded. For the first wind tunnel test the noise data were recorded for at least 30 seconds from the fixed-position microphones. For the second wind tunnel test the noise data were recorded continuously until both microphone traverses stopped. For selected conditions the traversing microphones were fixed at 30°, 50°, and 70° relative to the inlet axis, and 30 seconds of noise data were tape recorded at each angle.

During the aerodynamic performance portion of the first wind tunnel test, a slightly different procedure was used to determine the angle-of-attack limits for the hybrid inlets. After the wind tunnel conditions and the JT15D fan speed were set, data were acquired at angles of attack up to 15°. The turntable rotation was then continued until either the wall static pressure or the rake transducers indicated diffuser separation. The turntable rotation was immediately reversed to reattach the flow; the fan corrected speed was reset, and then steady-state data were taken at an angle of attack close to the separation value. In some cases diffuser separation did not occur before the turntable limit of 40° angle of attack was reached or a predetermined value of steady-state total pressure distortion at the fan entrance was exceeded.

3.7 DATA REDUCTION

The reduction and processing of the test data was shared between NASA and GE. The steady-state aerodynamic performance data for the inlets and the test facilities were calculated on-line by the NASA computers. Editing and correcting the data was performed by GE and NASA engineers, and the final computed test results were supplied by NASA to GE. The external and internal noise measurements were monitored on-line during the tests by GE personnel to ensure signal validity. The posttest noise-data reduction and processing were accomplished at the GE facilities. During most of the second wind tunnel test, high signal levels were observed on the downstream portion of the linear microphone traverse. It was determined that the source of the pressure disturbance was wakes shedding from the circular traverse rail. The fan-noise portion of the signal was swamped by this background noise; as a result, data from the traverse-rail microphone during the second wind tunnel test was unusable.

3.7.1 Aerodynamic Performance Data

As part of the pretest effort, GE engineers conducted an extensive axisymmetric compressible-flow analysis of the hybrid inlets. This analysis determined the relationships between the airflow rate, the total pressure recovery, the surface pressure distribution, and the throat Mach number for each hybrid inlet at both outdoor static and wind tunnel test conditions. The results of this analysis were incorporated into the on-line aerodynamic performance computer program used for all wind tunnel testing. This program computed throat Mach number for all zero-angle-of-attack test points using three selected wall static pressures from each hybrid inlet. During testing with the total pressure rakes, the program also computed the average total pressure distortion and area-weighted average total pressure for all hybrid-inlet and deflector-inlet test points. The General Electric Distortion Analysis Program was run off-line using the rake total pressures to compute more detailed total pressure distortion parameters as well as contour plots of the pressures. These computer programs were a valuable asset to the wind tunnel testing because preliminary results were available on-line for each test point, and final checked results were available at the completion of the tests.

3.7.2 Fixed-Microphone Data

The fixed-microphone data from the first outdoor static and wind tunnel tests were reduced into 1/3-octave-band spectra from 100 Hz to 20 kHz using a 16-second average time and corrected to standard day conditions by conventional data-reduction techniques. Since these data were the preliminary noise measurements, they were not corrected for wind tunnel background noise or convection effects. Some of the data were reduced to 20 Hz narrowbands from 0 to 20 kHz for use in comparisons with the data from the second wind tunnel test.

3.7.3 Traverse-Microphone Data

The 3.7 m (12 ft) arc microphone data from the second wind tunnel and outdoor static tests were reduced to 1/3-octave-band spectra from 400 Hz to 16 kHz by special techniques developed to process moving-microphone data. While the traverse was moving, narrowband spectra were continuously computed with an angular spacing that depended upon the averaging time in the spectral calculations. The averaging time used was 0.2 seconds; this provides the smallest angular resolution between spectra on the 3.7 m (12 ft) arc and keeps the statistical errors below ±1 dB in the sound pressure levels. For each data point, the narrowband spectra are computed every 3.3° around the arc and and are then converted to 1/3-octave-band spectra corrected to standard-day conditions.

To verify the traverse-microphone data-reduction technique, the data acquired when the traverse was stopped at 30°, 50°, and 70° for selected points were compared to the traverse data at those angles at the same test conditions.

Typical comparisons of the spectra computed from fixed-microphone data reduction to spectra computed form traverse-microphone data reduction are shown in Figure 33. The baseline inlet was used because it changes more with frequency and angle than data from the hybrid inlets does; therefore, it represents a tougher test case for comparisons of the methods. These comparisons indicate that the traverse-microphone data-reduction method provides spectrum levels within ±2 dB of those computed by conventional techniques. In addition, the traverse-microphone data has an advantage over fixed-microphone data in that no errors exist due to calibrating and recovering data from several microphones.

3.7.4 Internal Noise Data

Selected internal-noise data from the outdoor static and the wind tunnel tests were reduced to 20 Hz narrowband spectra from 0 to 20 kHz using digital fast Fourier transform techniques. The 2.0-second average time used resulted in statistical errors less than ±0.5 dB in the sound pressure level. The narrowband spectra were then converted to 1/3-octave-band spectra from 100 Hz to 16 kHz for comparison with the 3.7 m (12 ft) arc microphone data.

ORIGINAL PAGE IS
OF POOR QUALITY

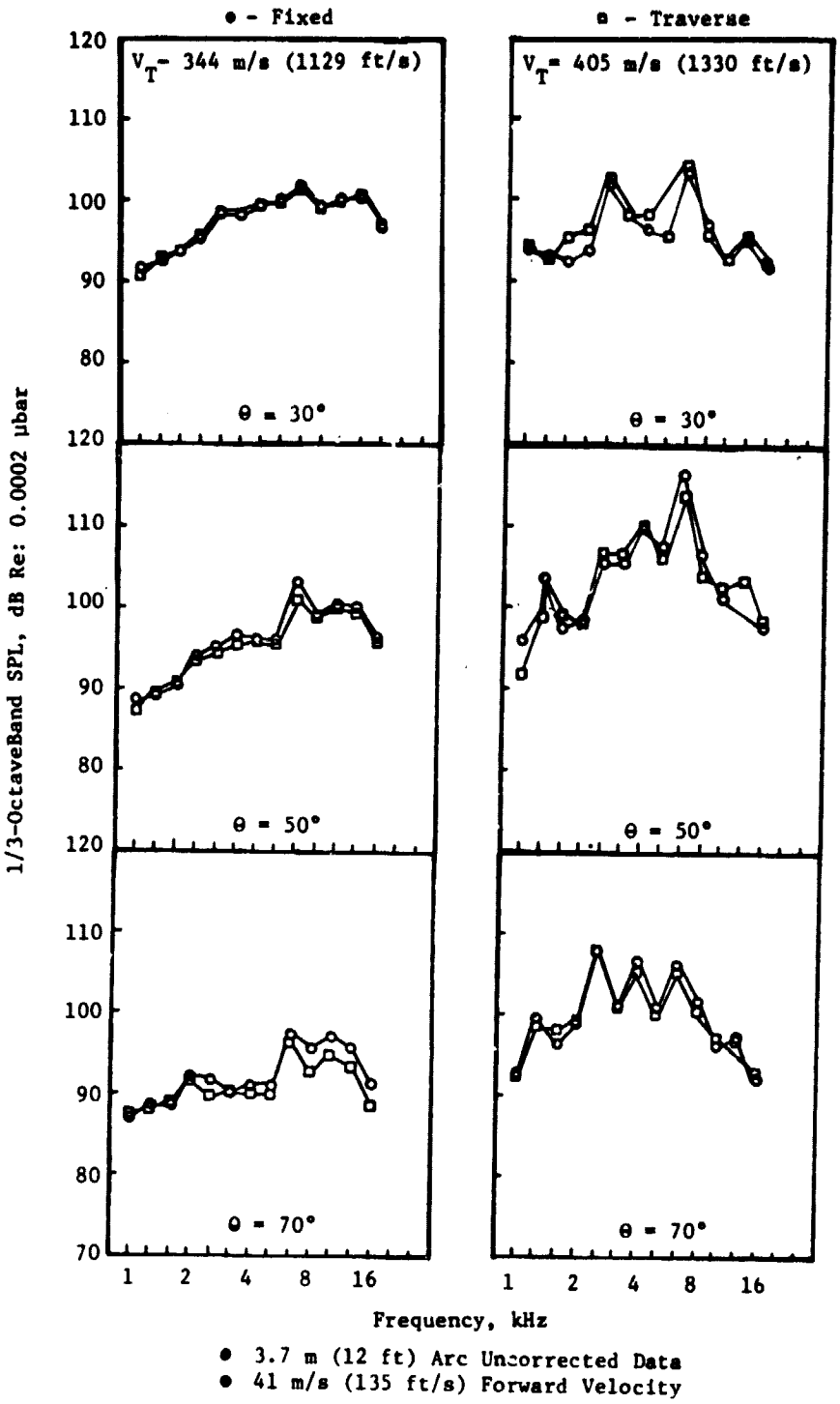

Figure 33. Verification of Traverse-Microphone Data Reduction.

4.0 DATA ANALYSIS

4.1 ANALYSIS TECHNIQUES

The techniques used to analyze noise data from the outdoor static and wind tunnel tests use both narrowband and 1/3-octave-band spectra formats. The narrowband format is used primarily for comparison of noise levels from different configurations or test conditions at the blade-passing frequency. These types of analyses provide detailed information about the relative tone levels that are often obscured by the 1/3-octave-band format. However, the bulk of the data analyses utilize techniques that yield results in the 1/3-octave-band format.

The analysis technique used for the wind tunnel data involves several steps. The first step is to account for convection effects that transform the angles and correct the levels of the traverse-microphone measured spectra to equivalent static conditions. The next steps are to select spectra at forward angles from 10° to 90° from the inlet axis, apply microphone angle-of-incidence corrections, and substract the wind tunnel background noise from the selected spectra. Finally, the sound-level spectra are corrected to standard-day conditions, scaled to the large turbofan engine, and extrapolated to the 61 m (200 ft) sideline. The spectra are then weighted and summed to obtain perceived noise levels (PNL) at the forward arc angles in 10° increments for use in determining directivity patterns. Tables of 1/3-octave-band spectra for the corrected and scaled data along with plots of selected 1/3-octave-band spectra, 1/3-octave-band directivity, and PNL directivity patterns from the second wind tunnel tests are presented in Reference 3.

4.1.1 Wind Tunnel/Static Transformation

As the noise from the fan propagates forward in the wind tunnel the waves are convected downstream by the flow velocity as shown in Figure 34. This convection has the effect of causing the angular location and propagation distance of the wind-on data to change relative to the static data. To properly assess the effects of forward velocity on the fan noise, the convection effects should be removed from the wind-on data to provide a consistent basis for comparisons.

The static equivalent angle, ϕ (see Figure 34), for the 3.7 m (12 ft) arc measurements relative to the wind tunnel axis is given in terms of the measurement angle, Ω, by the expression

$$\phi = \tan^{-1}\left(\frac{\sin \Omega}{M_c + \cos \Omega}\right) \qquad (1)$$

ORIGINAL PAGE IS
OF POOR QUALITY

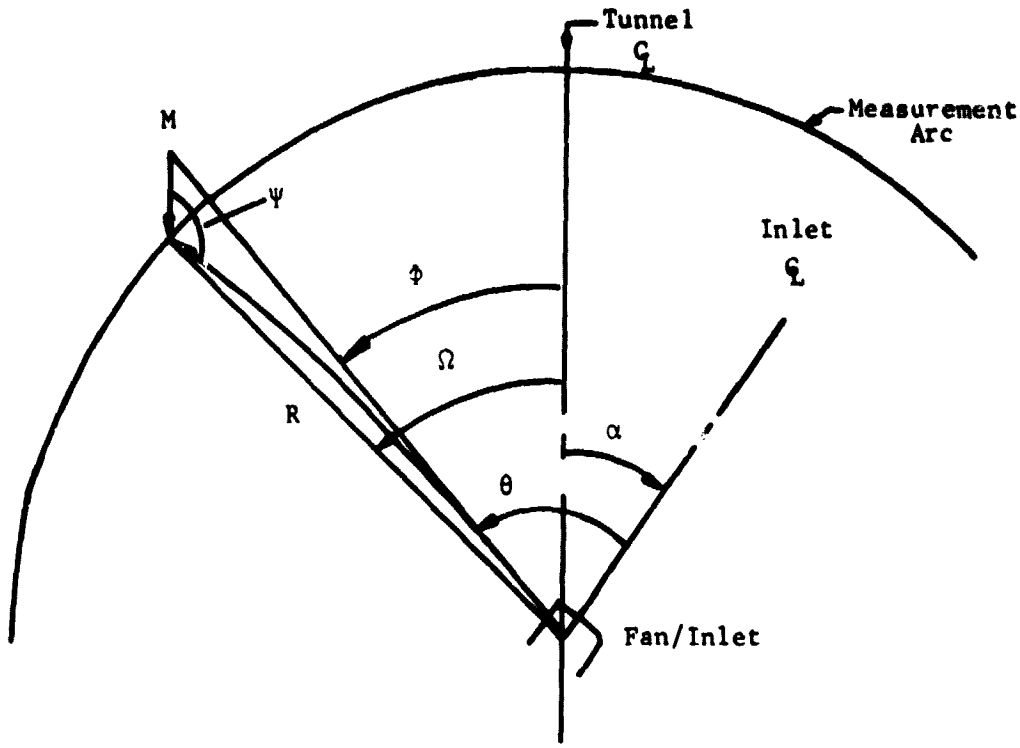

Ψ - Microphone Incidence Angle

θ - Noise Emission Angle

α - Inlet Angle of Attack

Ω - Measurement Angle

Φ - Static Equivalent Angle

R - Measurement Radius

M - Tunnel Flow Mach Number

Figure 34. Wind Tunnel Convection Correction Nomenclature.

where M_o is the wind tunnel flow Mach number. The noise emission angle, θ, relative to the inlet axis is then given by

$$\theta = \phi + \alpha \tag{2}$$

where α is the inlet angle of attack. Finally, the noise incidence angle, ψ, at the microphone to be used for corrections is given by

$$\psi = 180 - \Omega \tag{3}$$

which is applicable at all angles since the microphone always points upstream.

The noise propagation distance during wind-on conditions was effectively lengthened by the convection effects. The ratio of the measured to the static equivalent distance is given by

$$\frac{R + \Delta R}{R} = \frac{\sin \Omega}{\sin \theta} \tag{4}$$

where R is the actual distance to the traverse arc, 3.7 m (12 ft). Substitution of Equation (1) into Equation (4) provides the expression

$$\frac{R + \Delta R}{R} = \sin \Omega \left[\left(\frac{M_o + \cos \Omega}{\sin \Omega} \right)^2 + 1 \right]^{1/2} \tag{5}$$

which relates the distance ratio to the measurement angle and the wind tunnel flow Mach number. The distance ratio is then used to increase the measured sound pressure levels at a specific angle; this corrects the wind-on data to equivalent static conditions. The formula for this level correction is

$$\Delta SPL = 10 \log \left(\frac{R + \Delta R}{R} \right)^2 \tag{6}$$

where ΔSPL is added to each 1/3-octave band in the spectra.

The application of the convection corrections and the microphone incidence-angle corrections are facilitated by the use of a traversing-microphone system to acquire the fan-noise data. For each data point the traverse-microphone data-reduction program computes 1/3-octave-band spectra at each 3.3° around the arc from -59° to +82° relative to the wind tunnel centerline. The program then computes Equation (1) for each spectrum and selects spectra at 10° increments from θ = 10° to θ = 90° for further corrections. The spectra are then corrected for microphone incidence angle and frequency response based on the microphone manufacturer's calibrations. The spectra are then ready for wind tunnel background noise and standard-day temperature and humidity conditions.

A graphical solution to Equation (1) was used to determine the measurement angle to use for each 10° static equivalent angle for selection of narrowband spectra. These values appear in Table 6. Unfortunately, the convection correction was not anticipated when the traverse rail was set up, and the last value of traverse-microphone data usable for zero angle-of-attack data is 70°. This is the reason all the directivity curves presented later end at a noise-emission angle of 70°.

Table 6. Measurement Angles Required for Static Equivalent Angles at 10° Increments.

V_o, m/s	M_o	ϕ								
		10	20	30	40	50	60	70	80	90
20.6	0.059	10.6	21.15	31.7	42.2	52.6	62.9	73.2	83.3	93.4
41.2	0.118	11.2	22.3	33.4	44.3	55.2	65.8	76.3	86.6	96.8
59.2	0.170	11.7	23.4	34.7	46.3	57.5	68.5	79.2	89.6	99.8

4.1.2 Wind Tunnel Background Noise

The wind tunnel background noise was determined by acquiring data with the traverse microphone with the engine off at each of the forward velocities used during the test. Averaging several of these data points, the background noise was found to be essentially constant at all measurement points along the traverse arc. The spectral shape remained basically the same with the level increasing as the wind tunnel velocity was increased. The background-noise spectra for the wind tunnel velocities tested are shown in Figure 35. The background-noise spectra were then logarithmically subtracted from the wind-on data measured along the 3.7 m (12 ft) arc.

The final corrections applied to the spectra were to account for the nonstandard-day test environment. The temperature and humidity measured in the flow at the engine inlet are used along with the tables in Reference 4 to determine corrections to the 3.7 m (12 ft) arc data. The corrections adjust the sound level at each 1/3-octave band for the differences in atmospheric attenuation between the actual test conditions and standard-day, reference conditions.

4.1.3 Large-Scale Turbofan Noise

In order to compare the fan noise and inlet suppression with large, high-bypass-turbofan systems the JT15D noise must be scaled to the large size. The

ORIGINAL PAGE IS
OF POOR QUALITY

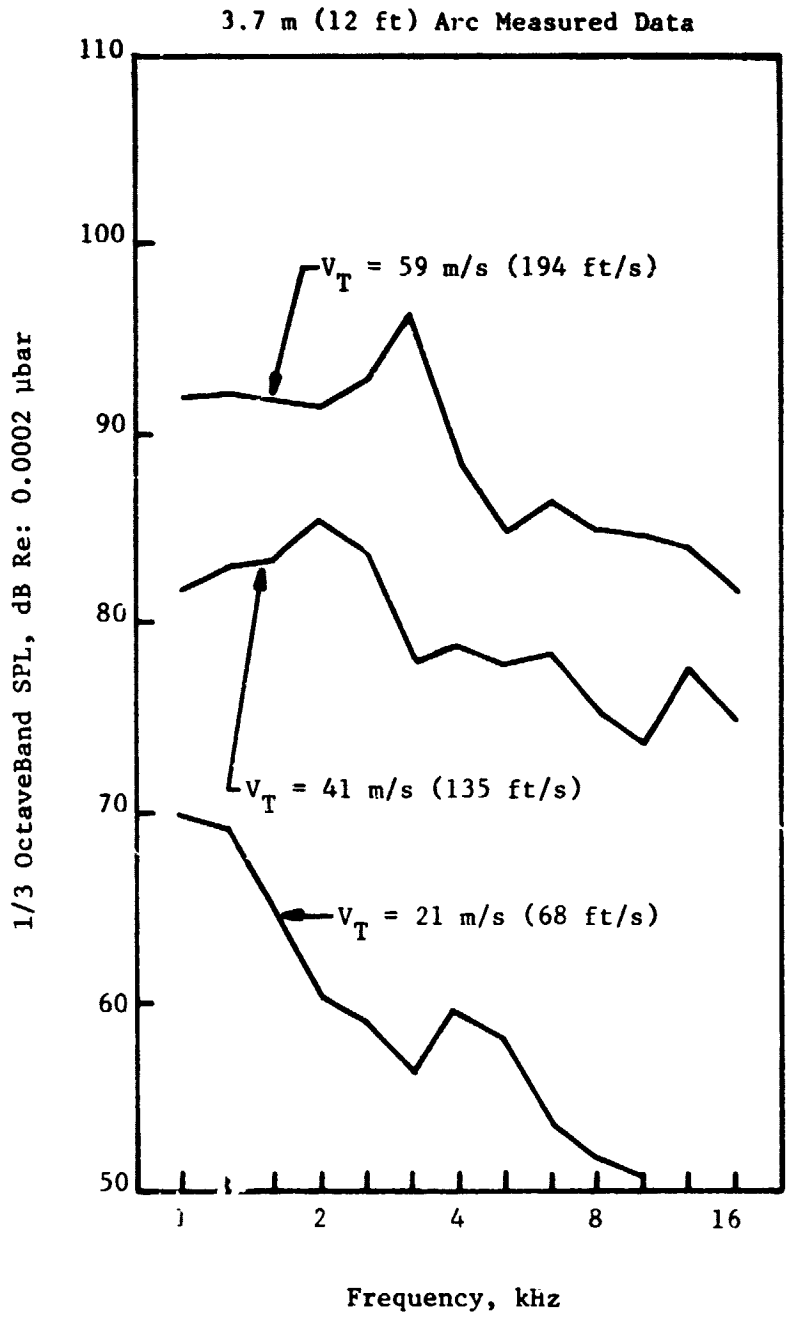

Figure 35. Background Noise for 40 by 80 Wind Tunnel.

systems chosen for the comparisons were the CF6 for the CTOL hybrid-inlet, canted-inlet, and deflector-inlet data and the QCSEE for the STOL hybrid-inlet data. The CF6 fan has an entrance diameter of 219.5 cm (86.4 in.) and 38 blades; the QCSEE fan has an entrance diameter of 180.3 cm (71 in.) and 28 blades.

The scaling procedure involves first transferring the data back to the source at a reference diameter of 0.3 m (1 ft). This is done by removing the standard-day atmospheric attenuation and adding the spherical-divergence factor for the distance from the measurement arc. The 1/3-octave-band sound pressure levels are then increased by the airflow ratio between the engines; this is proportional to the ratio of the square of the engine diameters. The frequency scales are then reduced, by the diameter ratio between the engines, to ensure that the Strouhal number remains constant. In order to place the blade-passing-frequency noise in the proper 1/3-octave band for the large engine the frequency-shift factor is modified by the ratio of the blade number between the engines.

Once the fan noise has been scaled at the source to the large engine, the data is extrapolated to a distance of 61 m (200 ft) parallel to the inlet centerline. This distance can be either to a sideline or overhead as long as no angle of attack is involved. The distances to this line along the rays at 10° increments are computed and used to determine the standard-day atmospheric attenuation, from Reference 4, and the spherical-divergence values to be substracted from the spectra. The scaled and extrapolated spectra are then summed to obtain the overall sound pressure levels and weighted to obtain the perceived noise levels at each 10° angle.

4.2 FAN/INLET AERODYNAMIC PERFORMANCE

Prior to discussion of the results of the acoustic-data analysis, a detailed summary of the aerodynamic performance of the various inlets is presented. This summary serves not only to demonstrate the adequacy of the aerodynamic prediction methods but also to verify that the low-noise-inlet concepts tested provide good performance while suppressing fan noise. Also presented are the limits of operation at angle of attack at each forward velocity as determined by breakdown of the fan/inlet aerodynamics or other physical constraints.

4.2.1 Hybrid Inlet Throat Mach Number Determination

The General Electric Streamtube Curvature (STC) (Reference 5) axisymmetric-flow-analysis computer program was used to generate the internal contours for the CTOL and STOL hybrid inlets. The STC analyses also provided local wall Mach number and wall static pressure versus axial distance along the inlet for each combination of forward velocity and throat Mach number tested. Typical plots of these data at the design point (see Table 2) for each inlet are shown in Figures 36 and 37. These data were cross-plotted to

ORIGINAL PAGE IS
OF POOR QUALITY

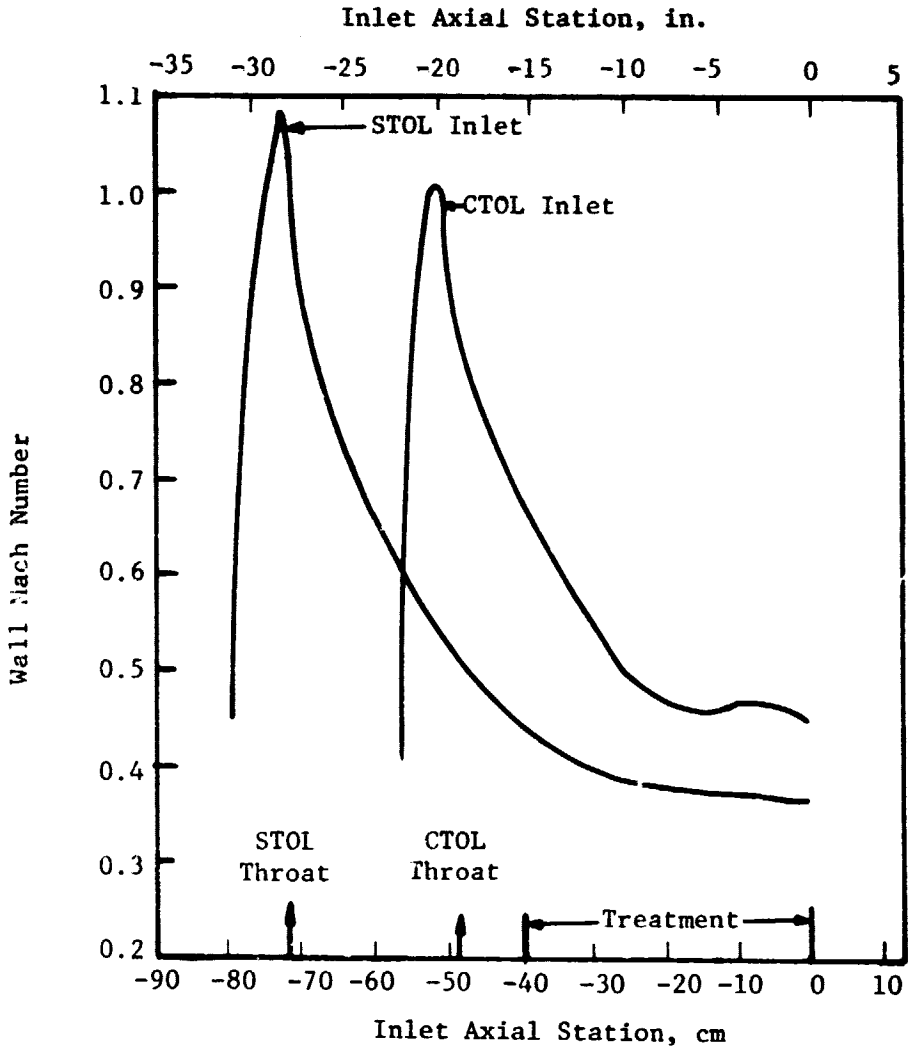

Figure 36. Predicted Wall Mach Number Distribution for Both Hybrid Inlets at Design Point.

ORIGINAL PAGE IS
OF POOR QUALITY

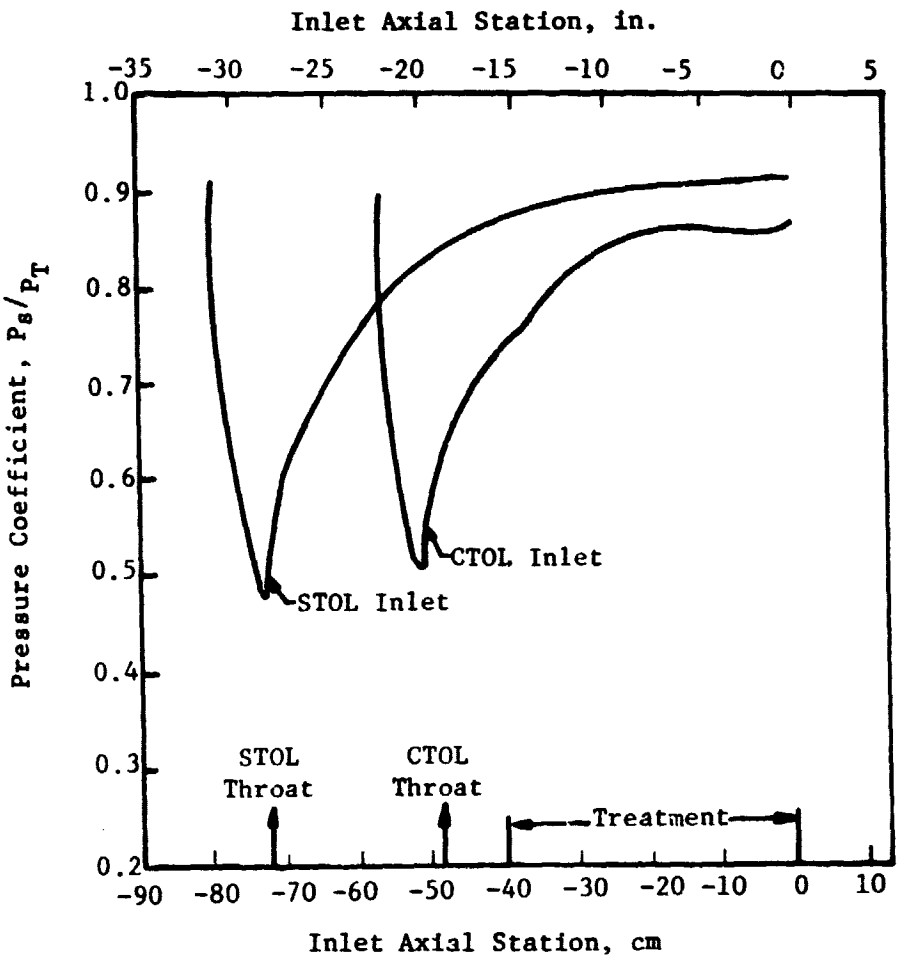

Figure 37. Predicted Wall Static Pressure Coefficient for Both Hybrid Inlets at Design Point.

obtain trends of the throat Mach number versus wall stall pressure at selected points on the inlet wall where static pressure taps were located. These plots were used to set throat Mach number during the tests and were programmed into the on-line, steady-state, data-reduction program to compute throat Mach number from the test data. The plots for the design point for each inlet are shown in Figure 38.

To demonstrate the adequacy of the STC predictions, the measured wall Mach numbers and wall static pressures were compared with the predictions at the design point for each inlet. These comparisons, shown in Figures 39 and 40, demonstrate that the STC predictions are very good from the inlet highlight aft to the middle of the diffuser. Toward the aft end of the diffuser the boundary layer growth and viscous effects become dominant factors causing the inviscid predictions from the STC program to be slightly in error.

During the first wind tunnel tests the on-line throat Mach numbers were computed by averaging the throat Mach number values determined from three of the static pressure taps. The three taps used were in a line near the throat of each hybrid inlet. For the posttest data analysis, the throat Mach number was determined by averaging the values from 10 of the static pressure taps. The 10 taps used were distributed circumferentially as well as axially to provide better coverage of the diffusers. The result was a much tighter correlation of throat Mach number with corrected fan speed as shown in Figure 41. With the throat Mach number primarily dependent on corrected fan speed, the operation of the second wind tunnel test could then be considerably simplified by setting corrected fan speed rather than static pressures. The specific values of corrected fan speed and the corresponding values of corrected fan tip speed, inlet throat Mach number, inlet airflow, and fan pressure ratio that were used are listed in Table 7.

4.2.2 Inlet Pressure Recovery and Distortion

During the aerodynamic performance portion of the wind tunnel tests, the pressure recovery and distortion were measured for the hybrid and deflector inlets. These data were acquired over the complete range of fan speeds, forward velocities, and angles of attack for which acoustic data were to be acquired. In addition, these data were acquired while the limits of angle-of-attack operation were being determined at each combination of throat Mach number and forward velocity.

4.2.2.1 Zero Angle of Attack

The hybrid-inlet pressure recovery and distortion at zero angle of attack for various forward velocities are plotted versus throat Mach number in Figure 42. The recovery and distortion characteristics for the hybrid inlets at low throat Mach number are slightly worse than conventional inlets at comparable throat Mach number due to the additional length of the diffusers. As the throat Mach number increases, a gradual drop in recovery and rise in distortion occur due to the increasing diffusion rates. Pressure distortion

ORIGINAL PAGE IS
OF POOR QUALITY

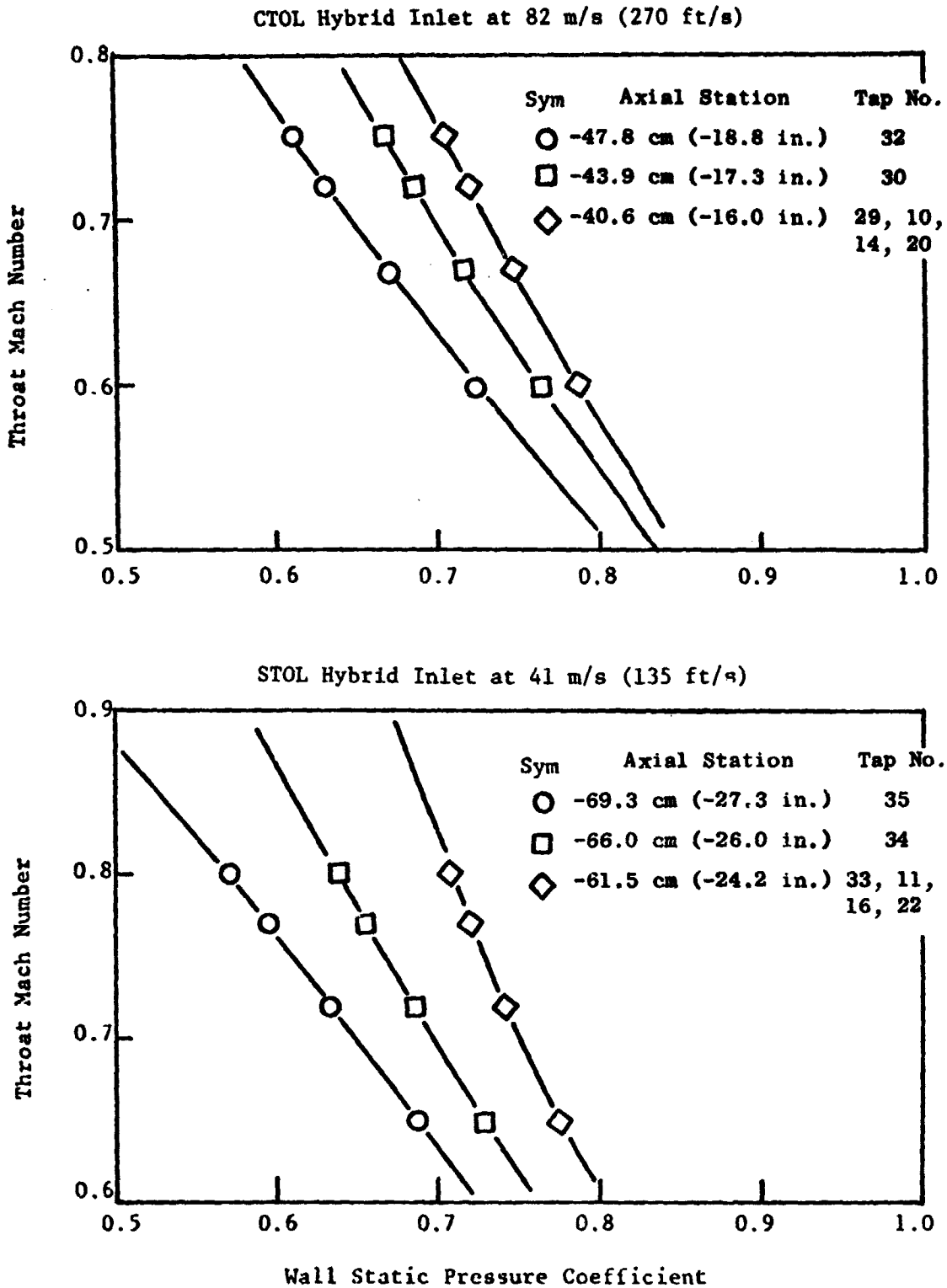

Figure 38. Typical Curves for Determining Hybrid Inlet Throat Mach Number.

ORIGINAL PAGE IS
OF POOR QUALITY

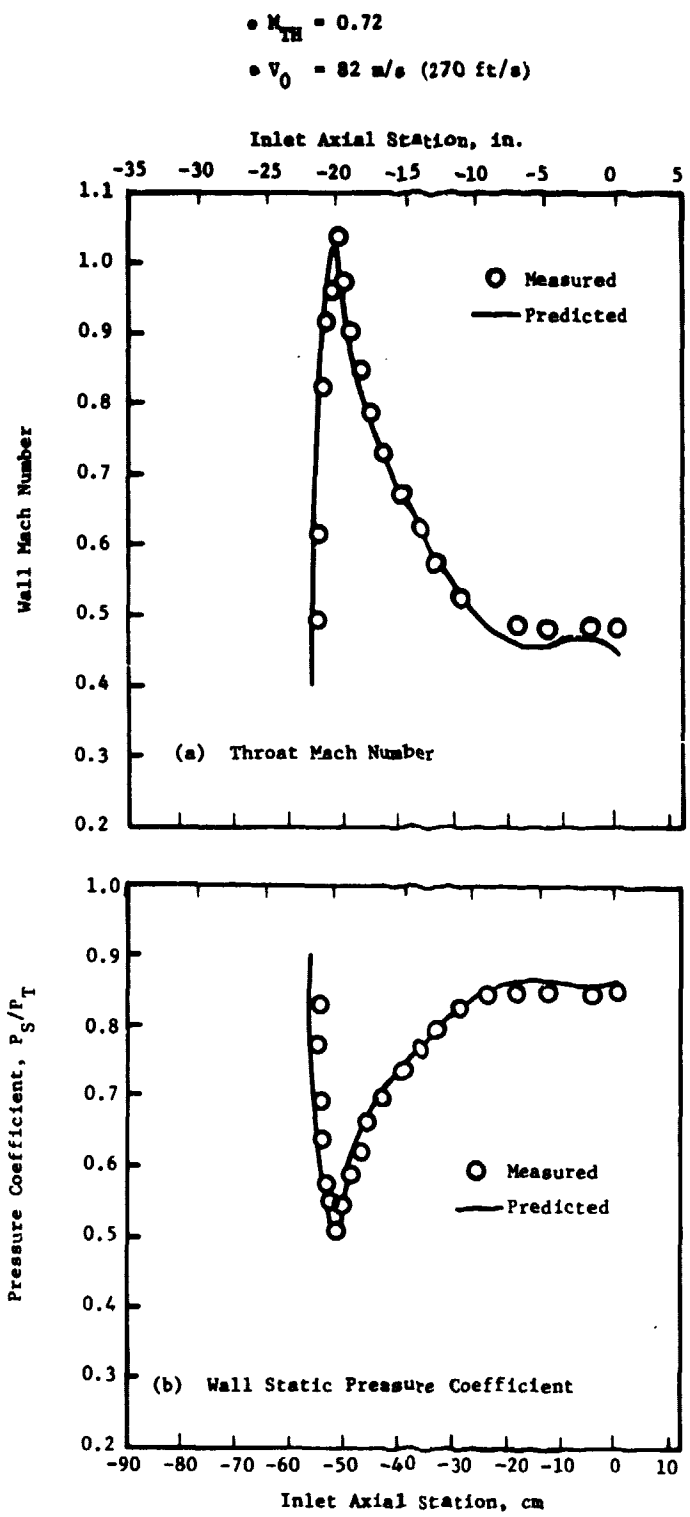

Figure 39. CTOL Hybrid Inlet Design Point Aerodynamic Performance.

ORIGINAL PAGE IS
OF POOR QUALITY

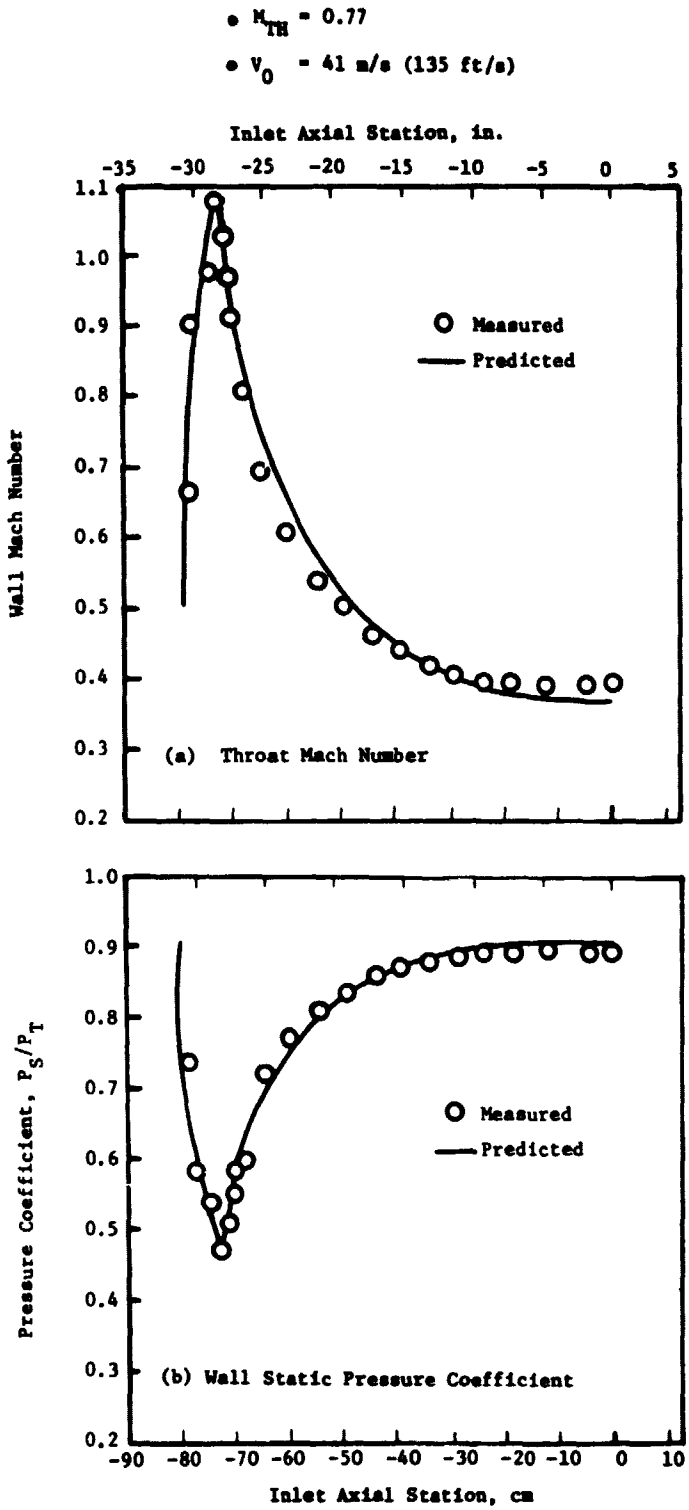

Figure 40. STOL Hybrid Inlet Design Point Aerodynamic Performance.

ORIGINAL PAGE IS
OF POOR QUALITY

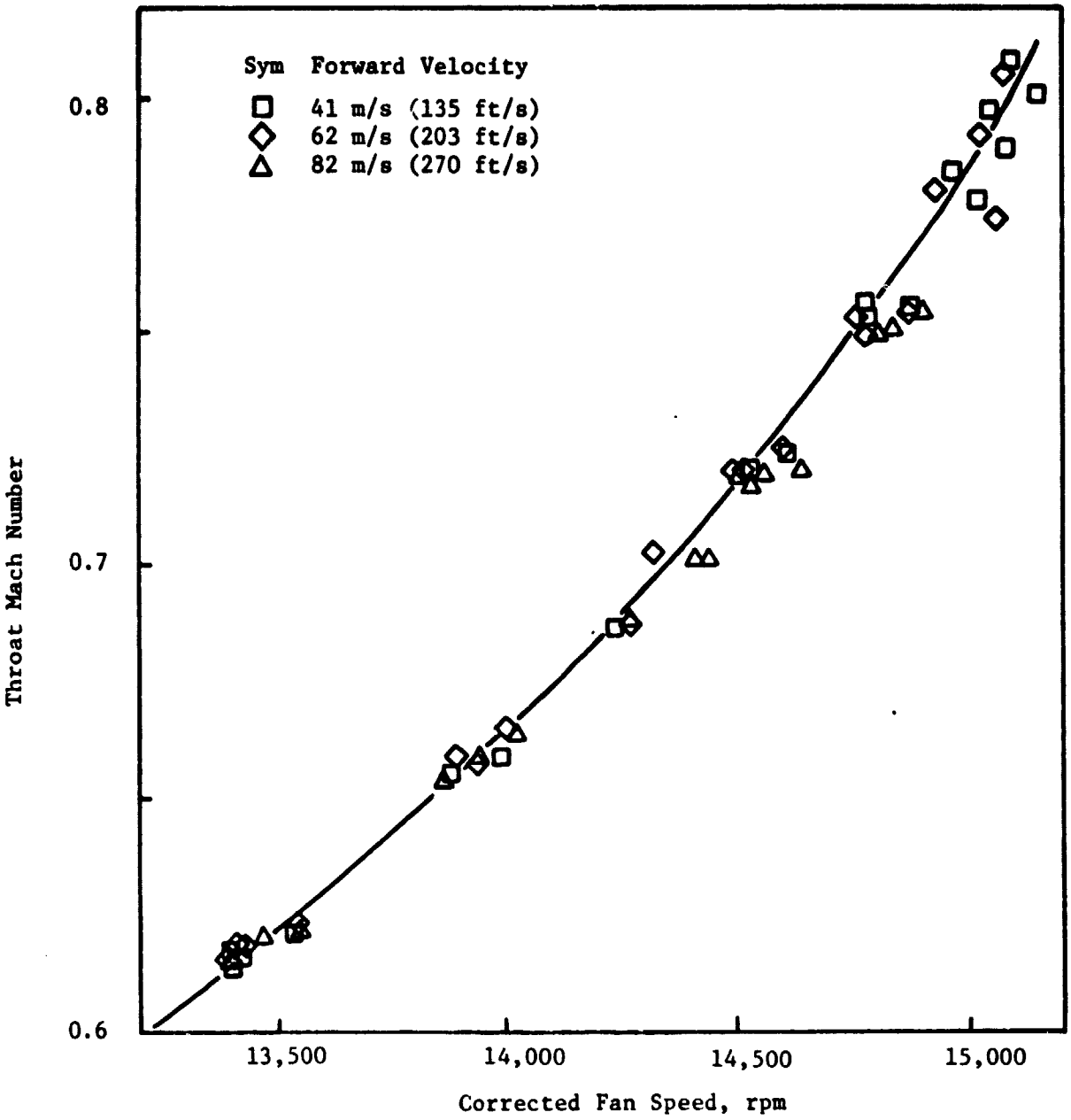

(a) CTOL Hybrid Inlet

Figure 41. Hybrid Inlet Throat Mach Number Variation with Fan Speed.

ORIGINAL PAGE IS
OF POOR QUALITY

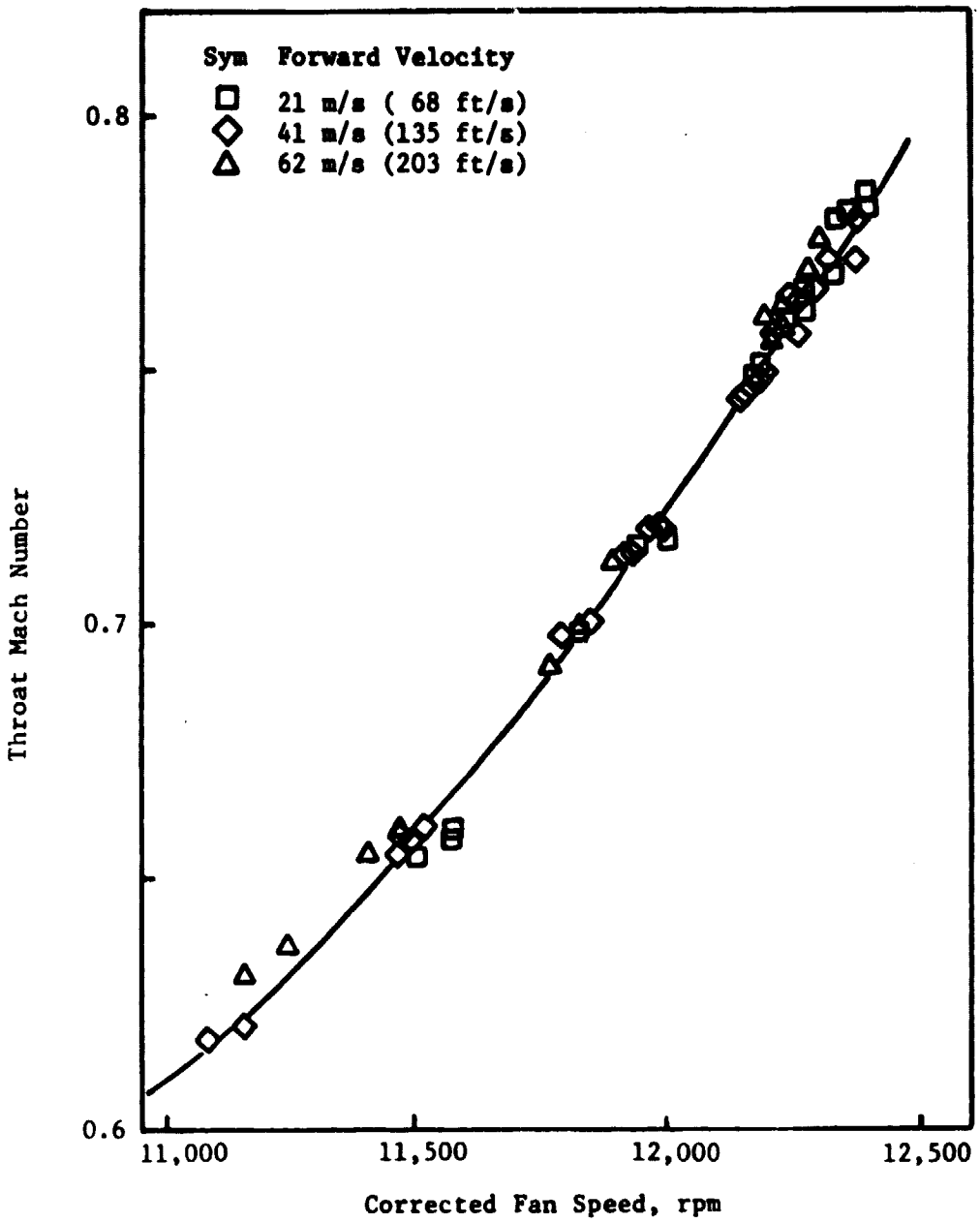

(b) STOL Hybrid Inlet

Figure 41. Hybrid Inlet Throat Mach Number Variation with Fan Speed (Concluded).

Table 7. JT15D Fan and Hybrid Inlet Test Parameters.

Nc, rpm	m/s	V_T, ft/s	M_{TH} Baseline	M_{TH} STOL	M_{TH} CTOL	$\dot{W}$ kg/s	$\dot{W}$ lb/s	PR	BPF 1/3-OB kHz
11,140	311	1020	0.29	0.62	0.46	25.4	56.1	1.158	5.0
11,525	322	1056	0.30	0.66	0.49	26.6	58.6	1.171	5.0
11,985	335	1098	0.31	0.72	0.51	27.5	60.7	1.187	5.0
12,320	344	1129	0.33	0.77	0.54	28.4	62.7	1.200	6.3
13,475	376	1235	0.37	---	0.62	31.2	69.1	1.245	6.3
13,953	390	1278	0.38	---	0.66	32.6	71.8	1.266	6.3
14,520	405	1330	0.40	---	0.72	34.0	74.9	1.294	6.3
14,895	416	1365	0.42	---	0.77	34.9	77.0	1.312	6.3

ORIGINAL PAGE IS
OF POOR QUALITY

ORIGINAL PAGE IS
OF POOR QUALITY

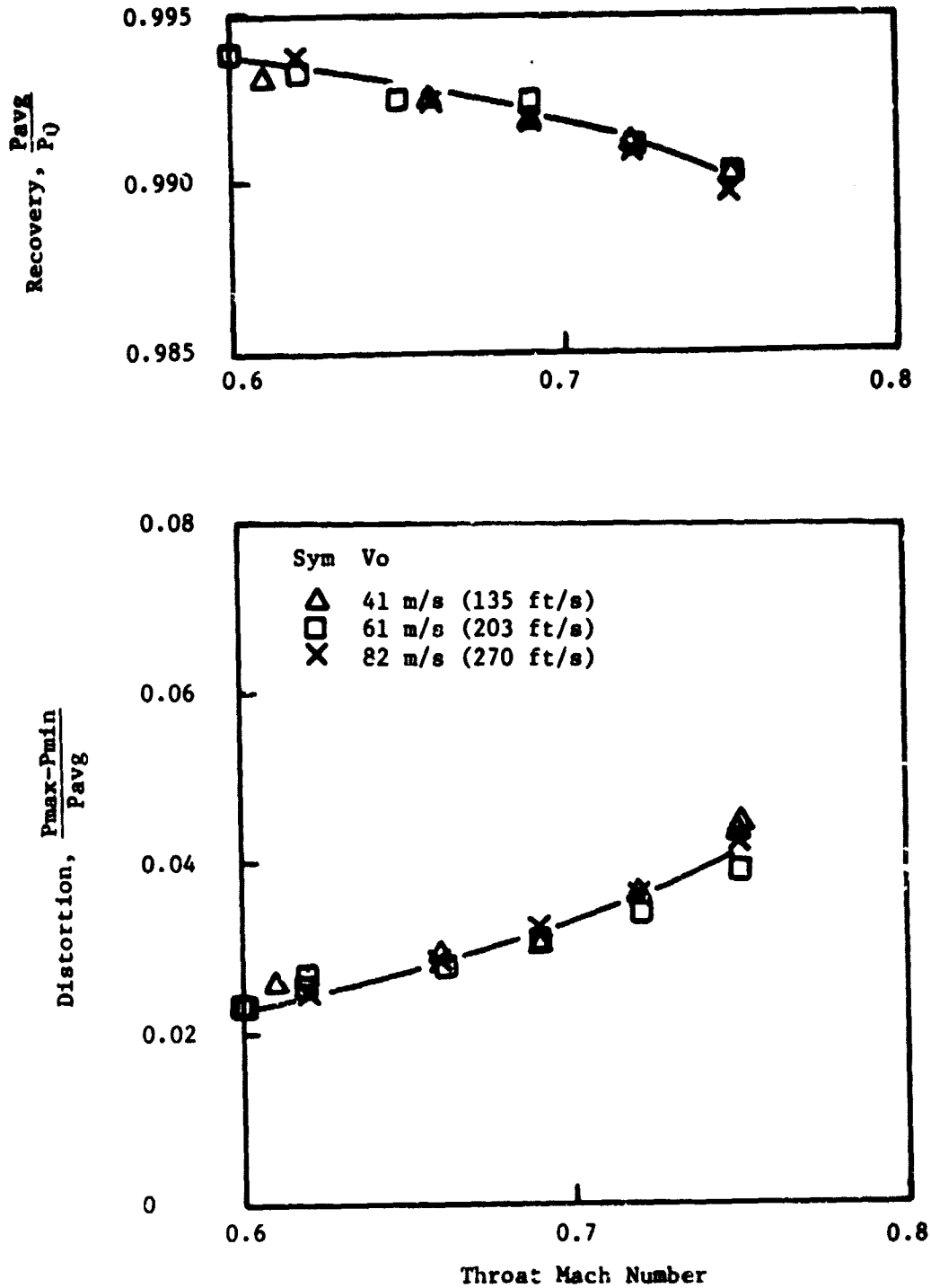

(a) CTOL Hybrid Inlet

Figure 42. Hybrid Inlet Pressure Recovery and Distortion at Zero Angle of Attack.

ORIGINAL PAGE IS
OF POOR QUALITY

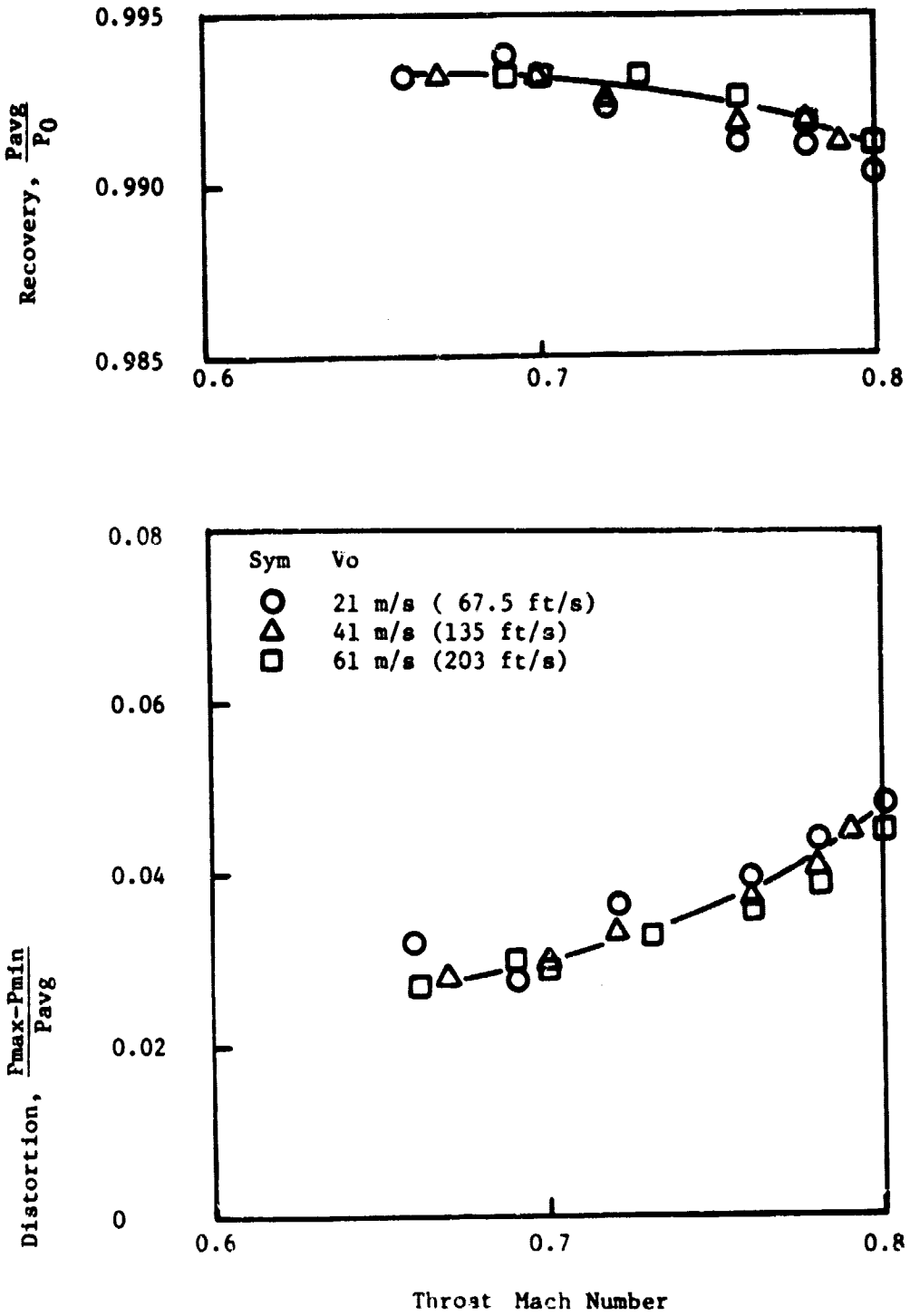

(b) STOL Hybrid Inlet

Figure 42. Hybrid Inlet Pressure Recovery and Distortion at Zero Angle of Attack (Concluded).

less than 5% is generally considered acceptable for an inlet. Note that there are no abrupt changes in these trends as the throat Mach number increases above the design values and that forward velocity has little or no effect on these characteristics; this indicates good diffuser and flight lip design.

The deflector inlet pressure recovery and distortion are plotted versus corrected fan speed in Figure 43 for zero angle-of-attack operation at two forward velocities. Since the deflector inlet has a short diffuser, the pressure recovery and distortion characteristics are more similar to those of conventional inlets. The diffuser is not only short, it also has a shallow diffusion angle that keeps the recovery and distortion relatively constant as fan speed is increased. As with the hybrid inlets, the lip was designed for high-angle-of-attack operation, and there is no appreciable effect of forward velocity on the deflector inlet recovery and distortion characteristics.

4.2.2.2 Non-Zero Angle of Attack

The pressure recovery and distortion for the design and the lowest throat Mach number are plotted versus angle of attack for the CTOL hybrid inlet in Figure 44 and for the STOL hybrid inlet in Figure 45. The levels remain virtually constant at all throat Mach numbers and forward velocities up to 15° angle of attack due primarily to the efficacy of the lip design. At higher angles of attack the flow around the lip begins to break down as either the throat Mach number or the forward velocity is increased. As these parameters are increased, the Mach number around the lip increases on the windward side of the inlet causing locally high pressure losses. The result is lower pressure recovery and higher pressure distortion as the flow enters the engine.

At each combination of forward velocity and fan speed, data were acquired at incrementally higher angles of attack until the objective angle for noise testing was reached or until the diffuser flow separated. Based on these data, the STOL hybrid inlet could be tested at angles of attack up to 30° at forward velocities up to 41 m/s (135 ft/s), and the CTOL hybrid inlet could be tested at angles of attack up to 15° at forward velocities up to 82 m/s (270 ft/s). The STOL hybrid inlet encountered diffuser flow separation at 30° angle of attack at the throat Mach number of 0.77 at a forward velocity of 62 m/s (203 ft/s). This was the only limit on angle-of-attack operation of either hybrid inlet.

The pressure recovery and distortion for the deflector inlet at two forward velocities are plotted versus angle of attack in Figure 46. At both low and high corrected fan speed the performance of the inlet is virtually constant up to 20° angle of attack. There is a very slight effect of forward velocity on the pressure distortion; however, the values are too low to place any significance on the trend. As can be seen by these results, one of the good features of a deflector inlet is excellent angle-of-attack capability.

ORIGINAL PAGE IS
OF POOR QUALITY

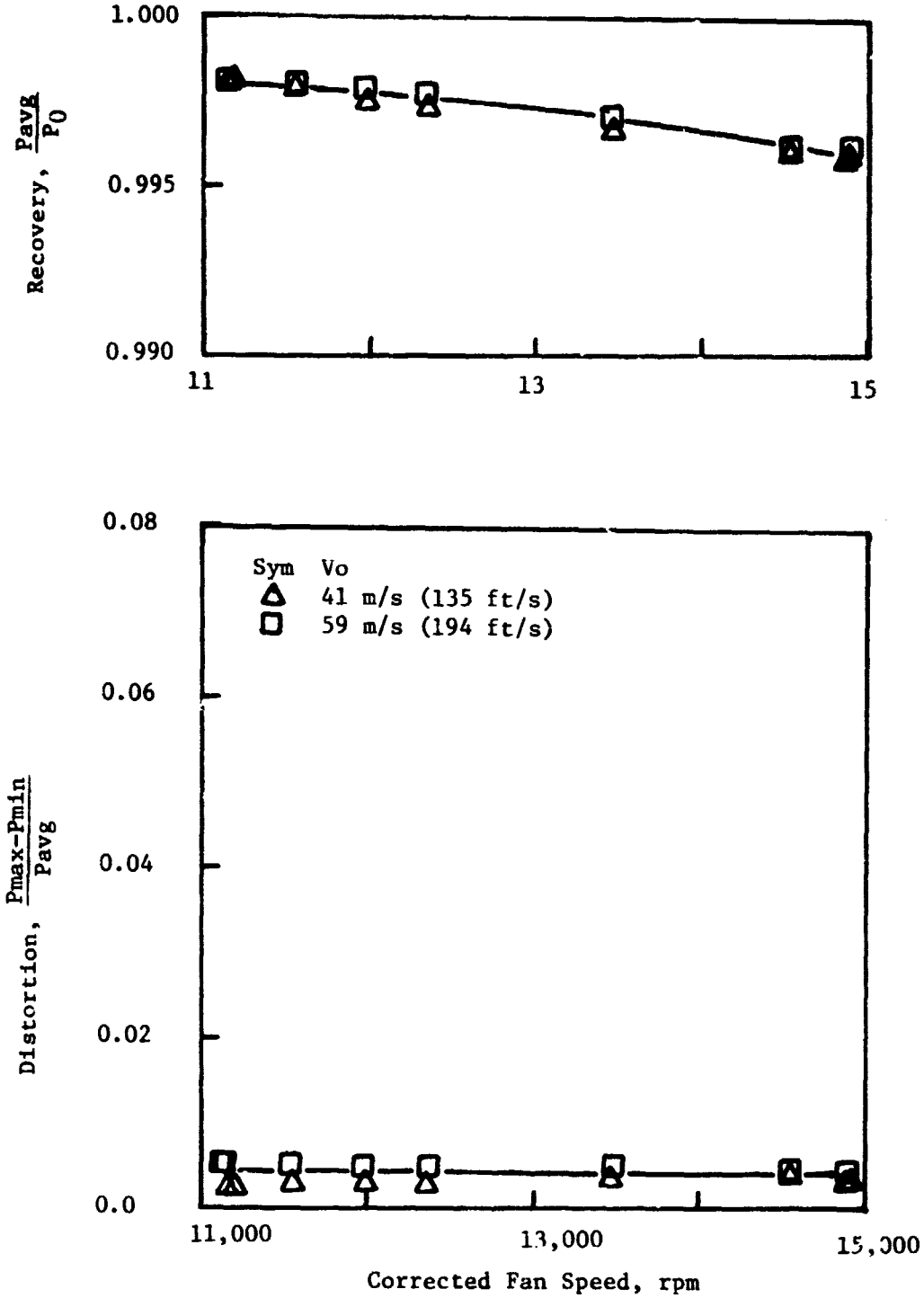

Figure 43. Deflector Inlet Pressure Recovery and Distortion at Zero Angle of Attack.

ORIGINAL PAGE IS
OF POOR QUALITY

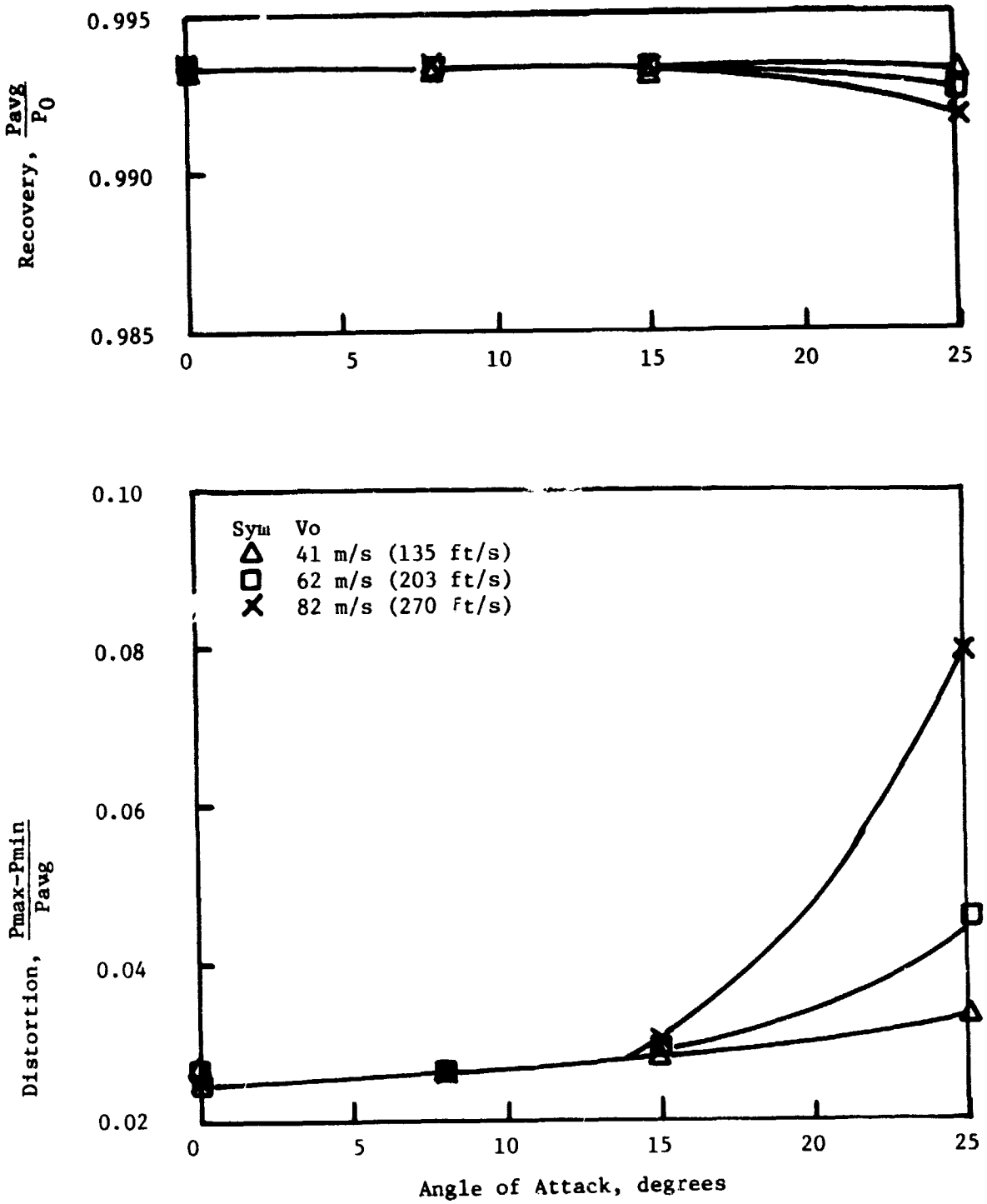

(a) $M_{TH} = 0.62$

Figure 44. CTOL Hybrid Inlet Pressure Recovery and Distortion at Angle of Attack.

ORIGINAL PAGE IS
OF POOR QUALITY

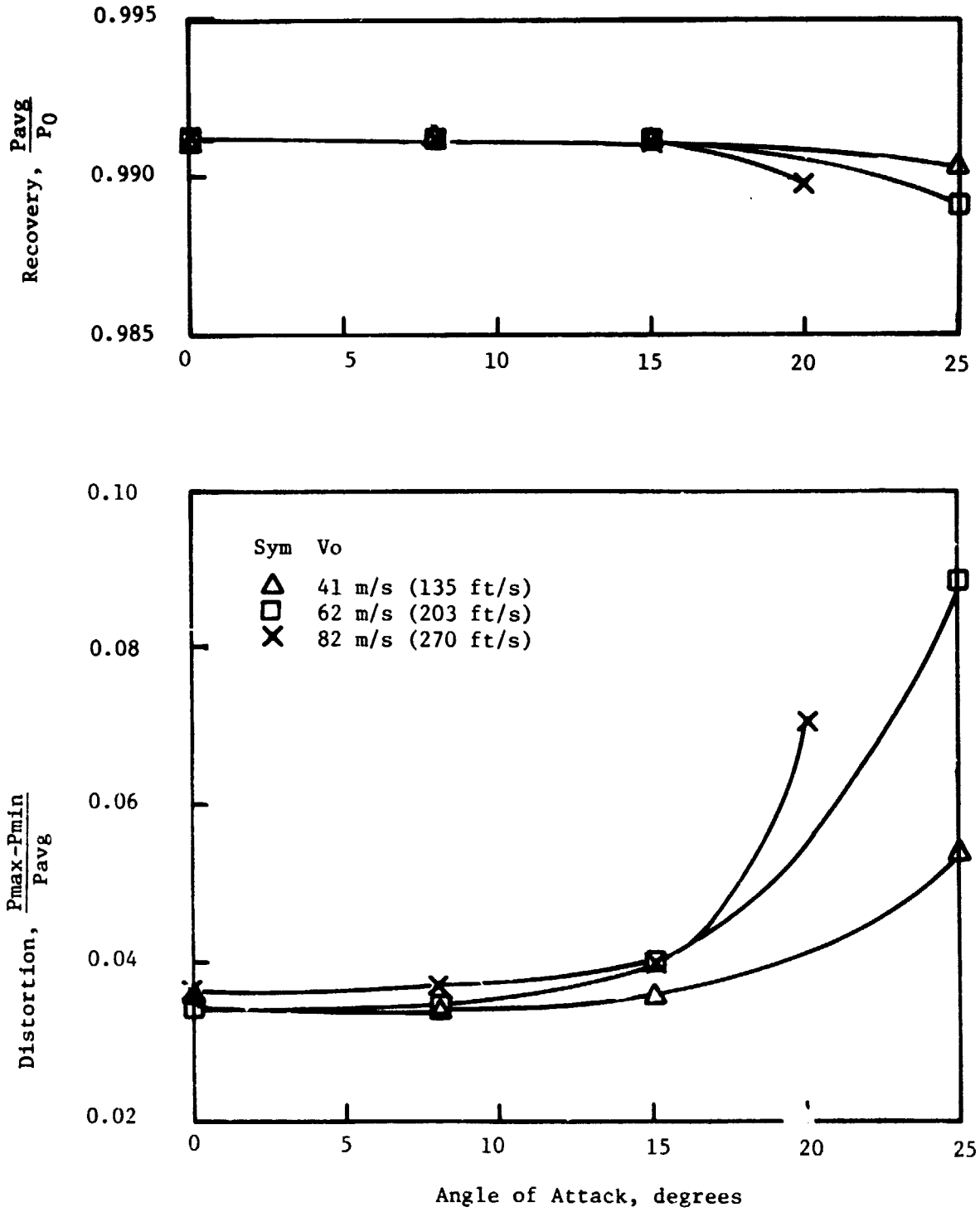

(b) $M_{TH} = 0.72$

Figure 44. CTOL Hybrid Inlet Pressure Recovery and Distortion at Angle of Attack (Concluded).

ORIGINAL PAGE IS
OF POOR QUALITY

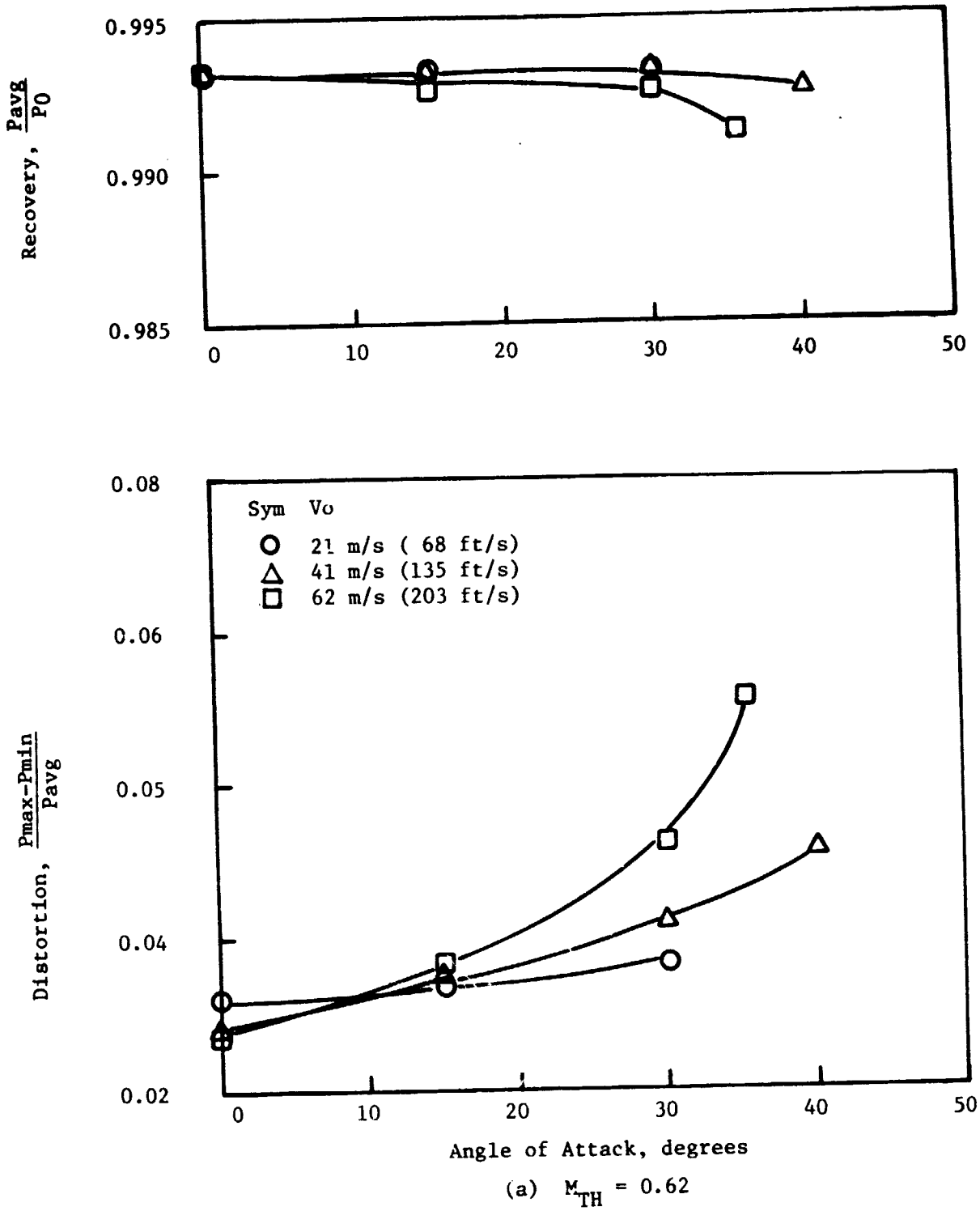

(a) $M_{TH} = 0.62$

Figure 45. STOL Hybrid Inlet Pressure Recovery and Distortion at Angle of Attack.

ORIGINAL PAGE IS
OF POOR QUALITY

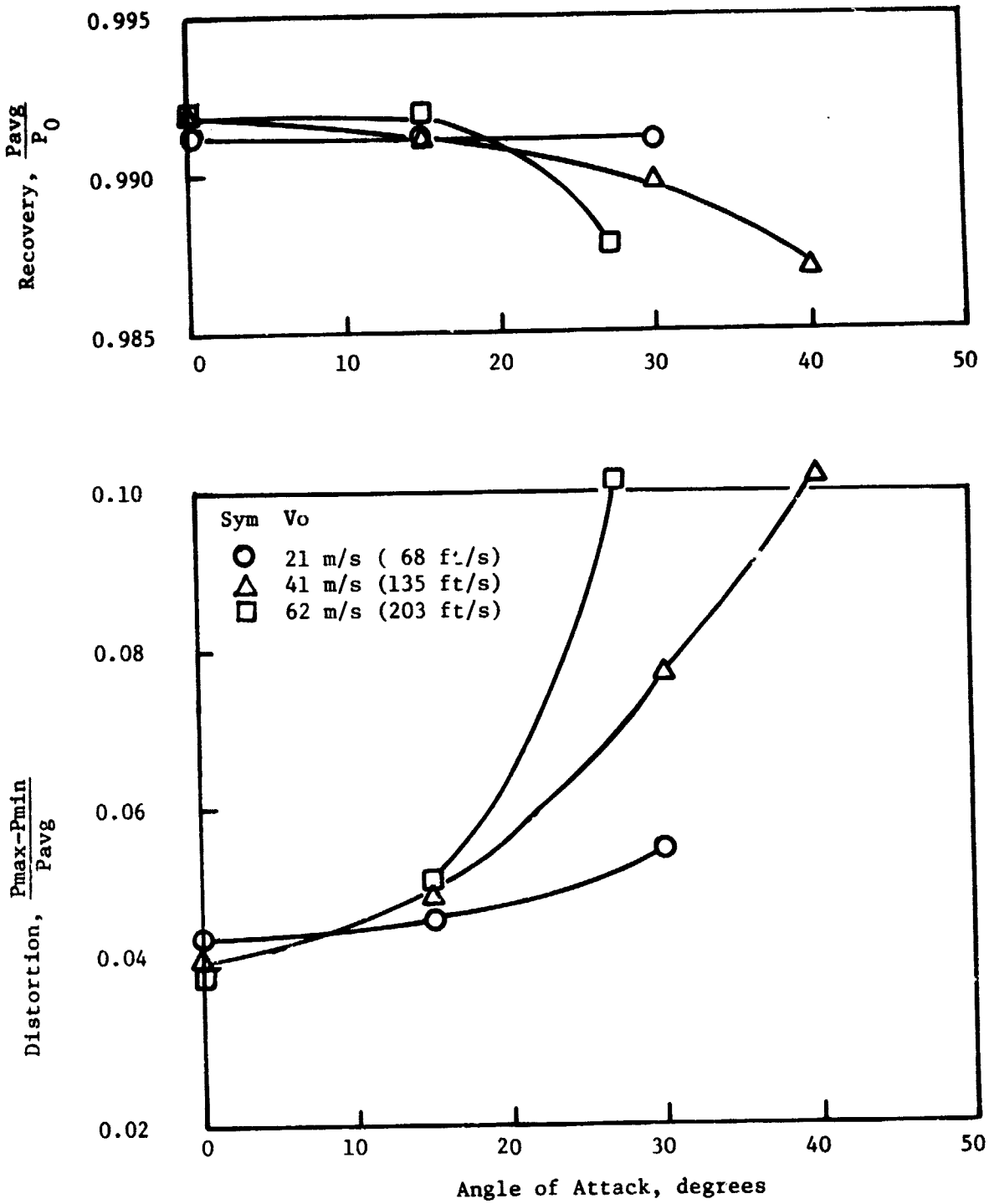

(b) $M_{TH} = 0.77$

Figure 45. STOL Hybrid Inlet Pressure Recovery and Distortion at Angle of Attack (Concluded).

ORIGINAL PAGE IS
OF POOR QUALITY

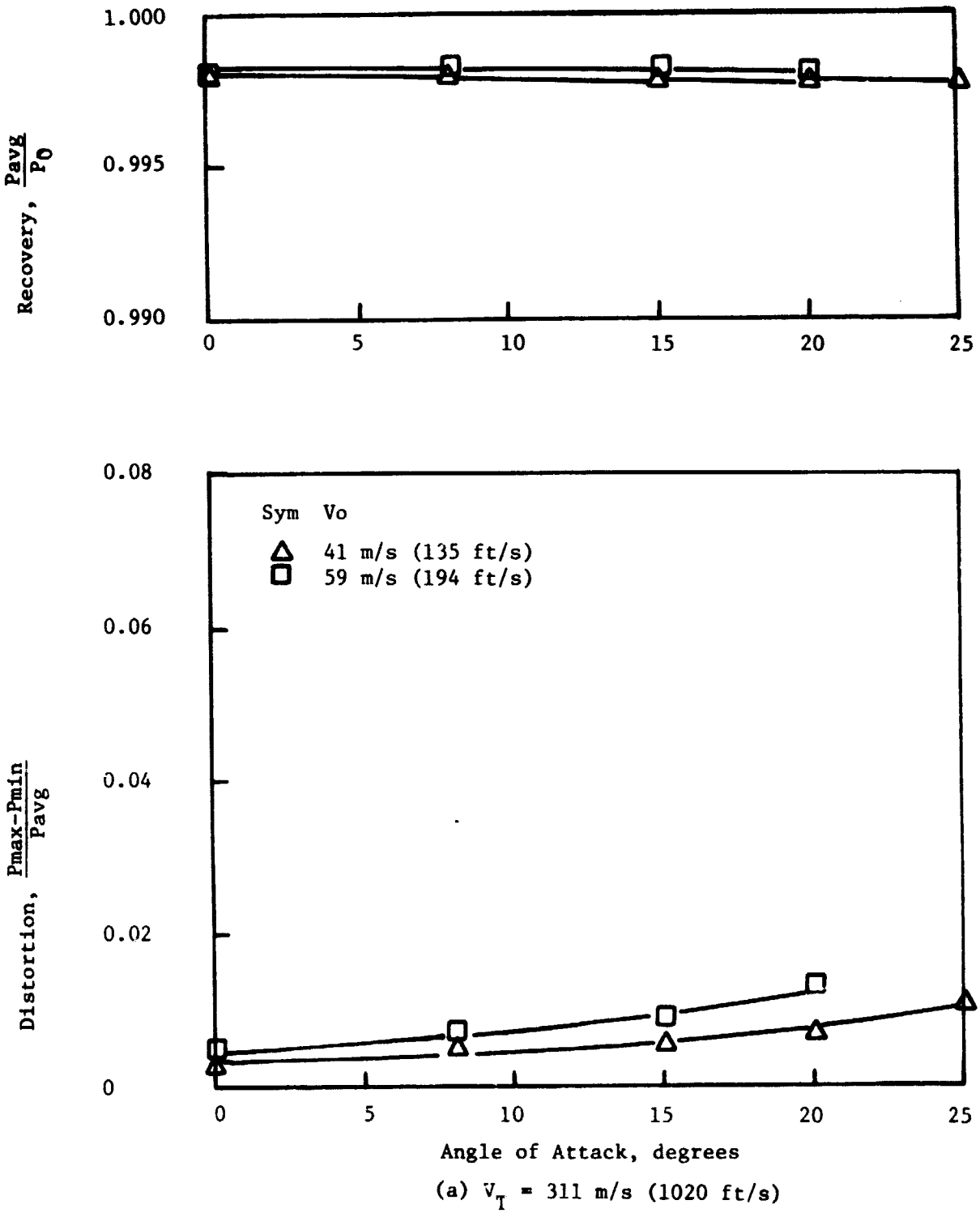

(a) V_T = 311 m/s (1020 ft/s)

Figure 46. Deflector Inlet Pressure Recovery and Distortion at Angle of Attack.

ORIGINAL PAGE IS
OF POOR QUALITY

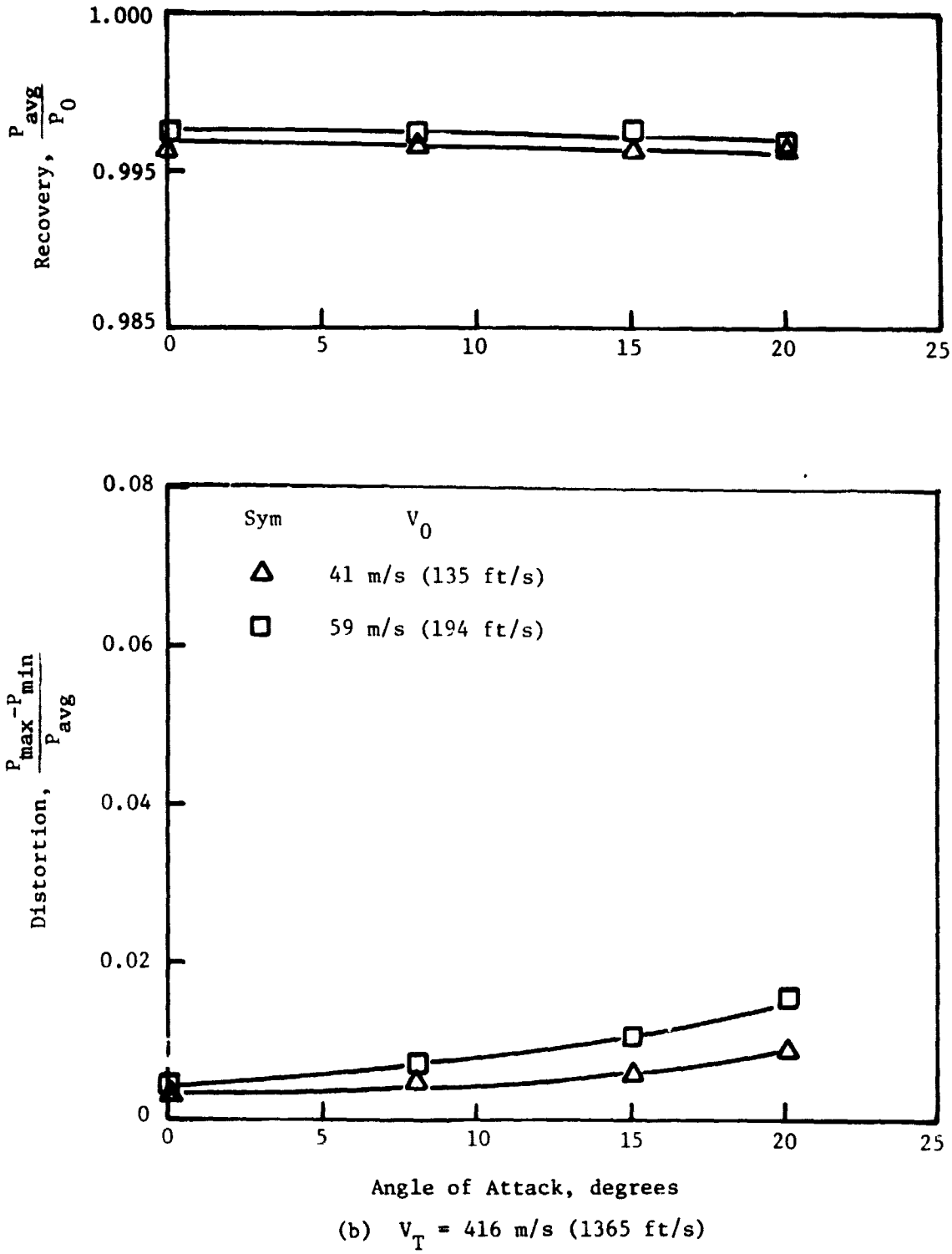

(b) V_T = 416 m/s (1365 ft/s)

Figure 46. Deflector Inlet Pressure Recovery and Distortion at Angle of Attack (Concluded).

4.2.3 Fan Operating Characteristics

Another output of the STC program is the airflow for each hybrid inlet as a function of throat Mach number. These calculations were combined with the recovery data and the throat Mach number/corrected-fan-speed data to obtain the plot of corrected airflow versus corrected fan speed shown in Figure 47. The lower curve in Figure 47 is for the smaller, production, fan-exhaust nozzle and was provided by NASA ARC.

To provide additional data on the JT15D fan operating characteristics, NASA ARC conducted a test to measure the fan pressure ratio versus corrected fan speed with both the hybrid-inlet fan nozzle and the production fan nozzle. The cylindrical baseline inlet was used for the bellmouth, and the GE-supplied rakes shown in Figure 30 were used to measure the fan discharge pressure. The data were supplied to GE and are shown in Figure 48. These data, together with the airflow data from the hybrid inlets, were then combined to provide a fan map of pressure ratio versus corrected airflow with speed lines drawn between the curves representing the two nozzle configurations. The fan map shown in Figure 49 may be used when comparing noise data from other JT15D tests that have used the production nozzle.

4.3 BASELINE INLET ACOUSTIC CONSIDERATIONS

In order to discuss the suppression characteristics of advanced inlets, the reference levels of fan noise must first be established. Similarly, to discuss the forward-velocity effects on the suppression, the static-to-flight effects on the reference fan-noise levels must also be determined. The baseline cylindrical inlet was used with the redesigned JT15D to provide the data for the reference noise levels and was tested both outdoors and in the wind tunnel to provide the data for the static-to-flight effects on the reference noise levels.

4.3.1 Static-to-Flight Effects

In earlier tests at NASA Ames (Reference 2), the modified JT15D engine was used to investigate static-to-flight effects on fan noise. Those results linked atmospheric turbulence to the generation of fan tone noise by showing a substantial reduction in noise levels at blade-passing frequencies when the engine was static tested with a device that reduced inflow turbulence into the inlet. These tests were restricted to low corrected fan speeds to assure no other fan tone noise sources were present and demonstrated reduction of the fan tone noise at blade-passing frequency down to the level of the broadband noise at the surrounding frequencies. For this particular fan, the noise from rotor interaction with the bypass stator vanes does not propagate throughout the entire speed range. However, this much static-to-flight effect due to cleaning up the inlet will not necessarily be realized at higher corrected fan speeds when the fan tip speed exceeds sonic velocity and the rotor-generated tone noise begins to propagate. Since the corrected fan speeds run during the baseline inlet tests covered the range from slightly below to well

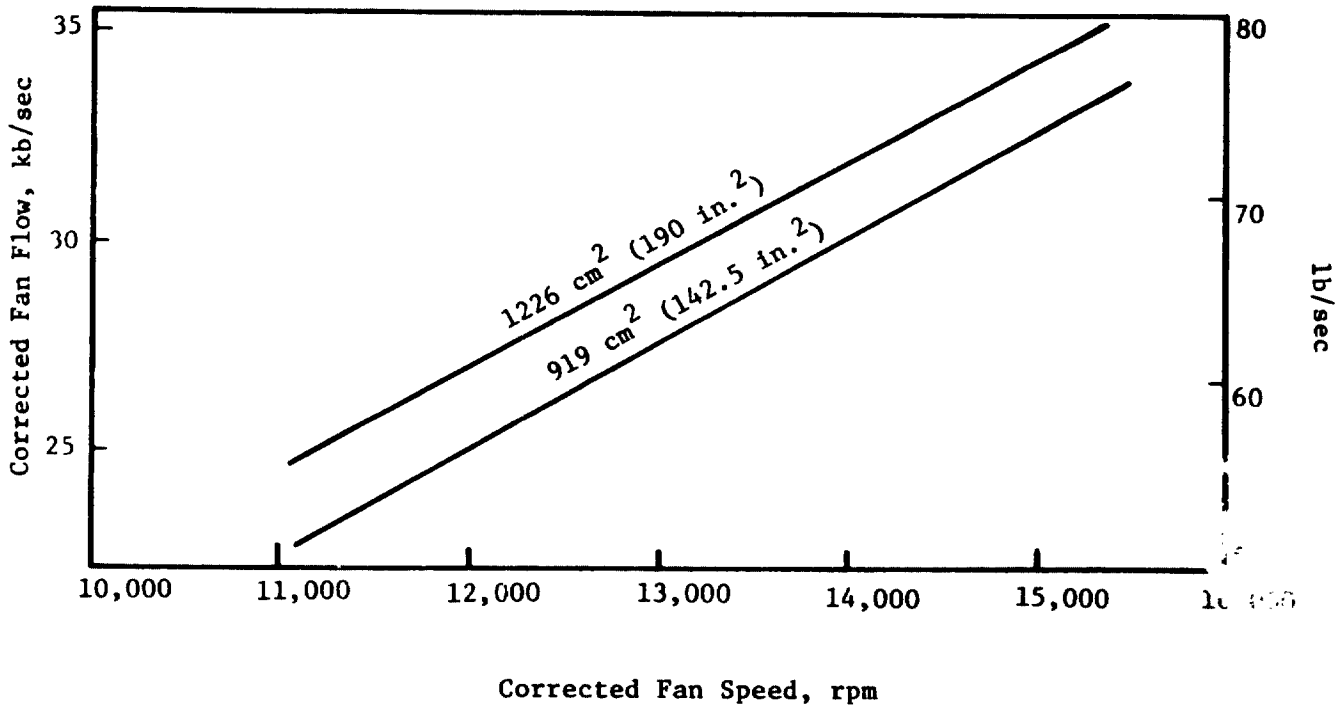

Figure 47. JT15D Fan Flow/Speed Curve for Production and Hybrid Inlet Nozzles.

ORIGINAL PAGE IS
OF POOR QUALITY

ORIGINAL PAGE IS
OF POOR QUALITY

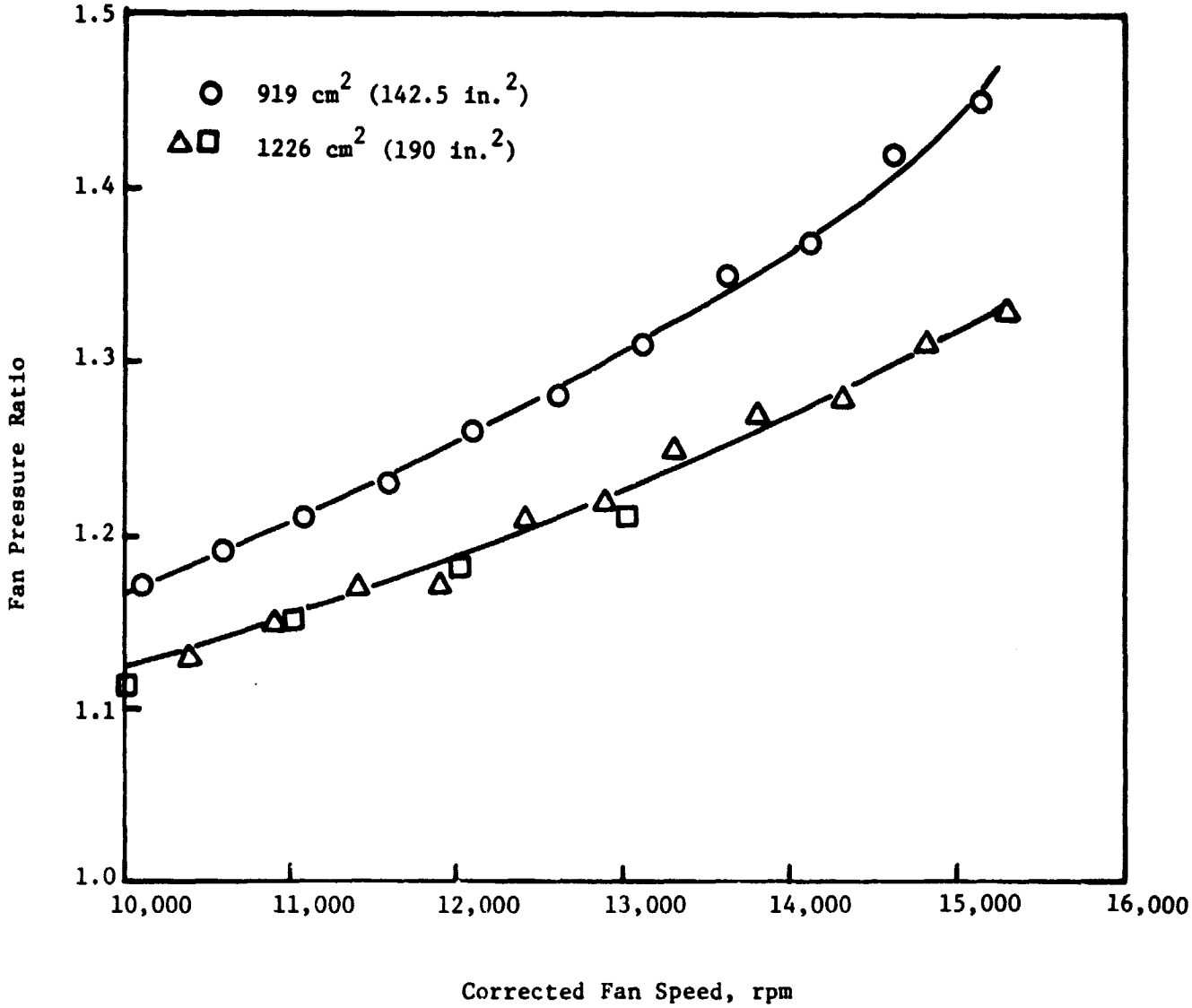

Figure 48. JT15D Fan Pressure Ratio/Speed Curve for Production and Hybrid Inlet Nozzle.

ORIGINAL PAGE IS
OF POOR QUALITY

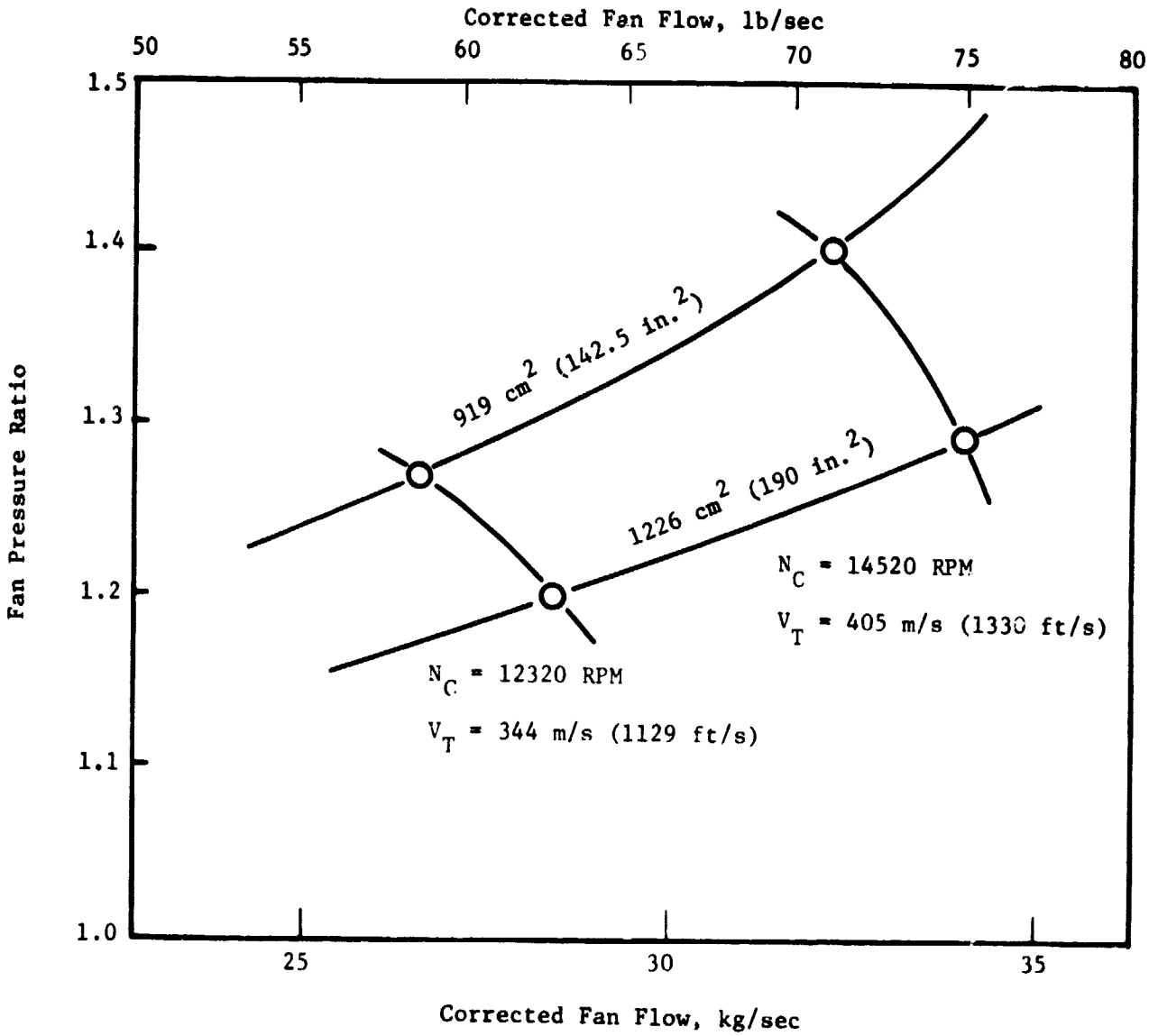

Figure 49. JT15D Fan Flow/Pressure Ratio Map.

above sonic tip speed, the relative strength of the rotor-turbulence tone noise to the rotor-alone tone noise will be determined for the JT15D along with the complete spectrum of reference fan noise.

The direct comparison of the outdoor static and wind tunnel quasi-static data with the wind tunnel data at a forward velocity of 41 m/s (135 ft/s) is shown for three corrected fan speeds in Figure 50. Presentation of the 2 kHz segments of the 20 Hz narrowband spectra that include the blade-passing frequency at 10° increments in noise-emission angle shows the static-to-flight effect on the tone levels and the tone directivity. These data confirm the conclusion in Reference 6 that the rotor-turbulence noise only affects the tone levels of the spectra. The largest static-to-flight effect occurs at the lowest fan corrected speed because the rotor-alone noise has just begun to propagate and only shows up in the far field above the broadband noise at noise emission angles of 40° and larger. As the fan tip speed is increased the rotor-alone noise increases and develops a directivity pattern for the BPF tone that peaks sharply near 50°to 60° with as much as 20 dB difference between the peak and the on-axis levels. Since the rotor-turbulence noise is more uniformly distributed to all angles, it adds to the rotor-alone noise at the off-peak angles and contributes to the static-to-flight effects on fan noise even at high corrected fan speeds. To show how the rotor-turbulence tone noise adds to the rotor-alone tone noise as the latter becomes stronger, the narrowband blade-passing-frequency tone level variations with fan tip speed for the baseline inlet in the outdoor static and 40 by 80 quasi-static and forward-velocity test environment are presented in Figure 51. The tone levels at the peak-noise-emission angle and at the 30° and 70° noise-emission angles from the three test conditions are compared. Note that the peak-noise-emission angle changes considerably between the outdoor static and the 40 by 80 data below the fan tip speed for which the rotor-turbulence and rotor-alone tone noise levels are approximately equal. Note also, that while there is basically no change in the peak-angle noise level above that fan tip speed, there is considerable change in the levels at off-peak angles due to these static-to-flight effects.

Another conclusion from Reference 6 is that the rotor-turbulence tone noise has considerable variability due to the random nature of the atmospheric turbulence in outdoor static tests. The data from the second outdoor static tests, where the wind varied only slightly in velocity and direction, confirmed this conclusion. The shaded regions in Figure 51 represent the range of tone level measured during the outdoor static tests at those angles. This means that the static-to-flight effects will vary considerably and that the outdoor static data cannot be used as reference noise levels unless, of course, turbulence conditions are controlled. The wind tunnel quasi-static data have less variation in tone levels, but these data are also influenced by turbulence. According to Reference 6, the forward velocity in the 40 by 80 has to be at least 21 m/s (68 ft/s) for this size engine in order for the rotor-turbulence interaction tone noise to be less than the broadband noise. Therefore, for more reliable fan-noise suppression results, the baseline inlet data from the wind tunnel tests at forward velocities of 21 m/s (68 ft/s) or higher will be used as reference noise levels. Specifically, the

ORIGINAL PAGE IS
OF POOR QUALITY

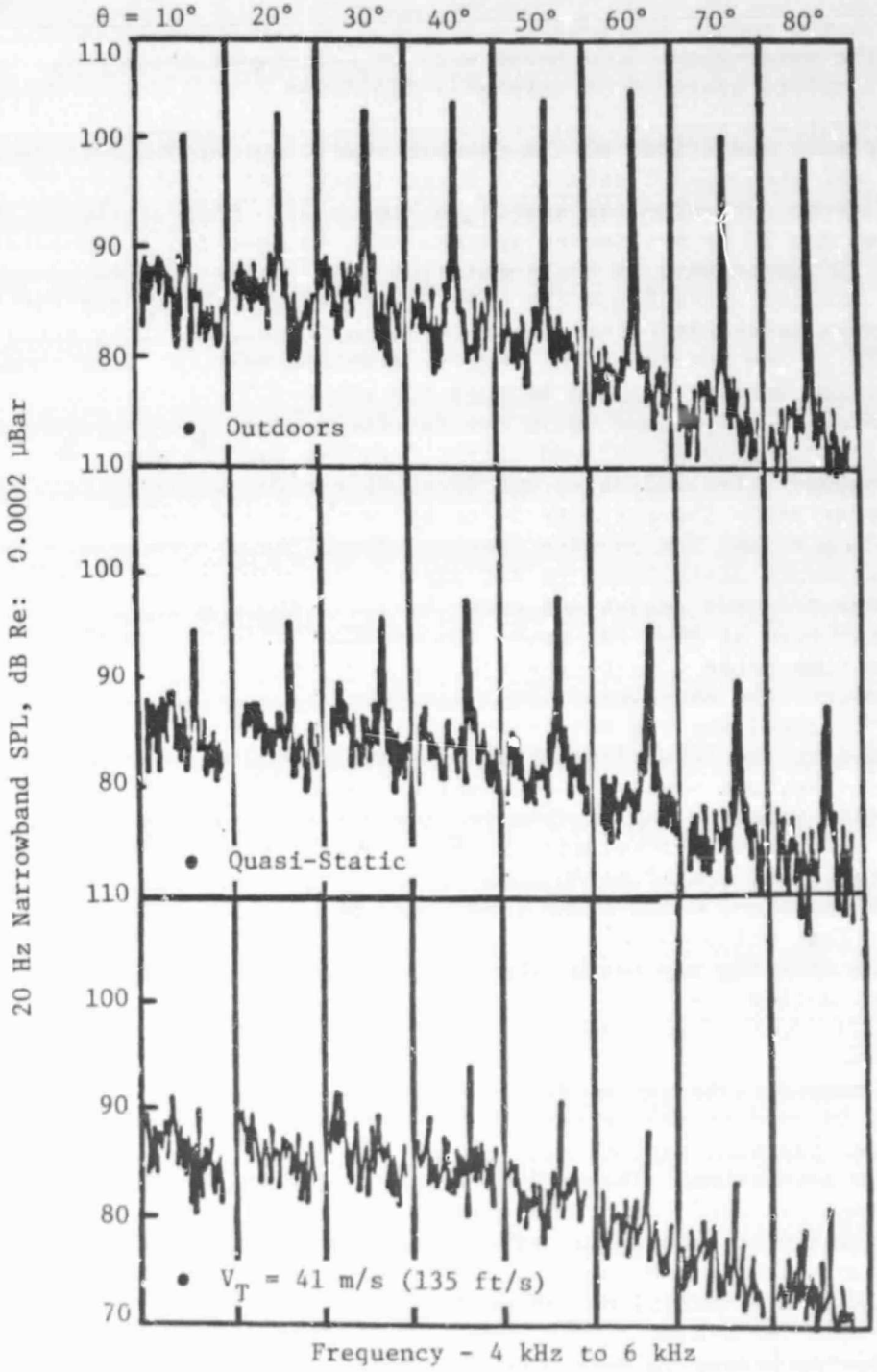

• 3.7 m (12 ft) Arc Uncorrected Data

(a) V_T = 311 m/s (1020 ft/s)

Figure 50. Narrowband Spectra for Baseline Inlet at Static and Forward-Velocity Conditions.

ORIGINAL PAGE IS
OF POOR QUALITY

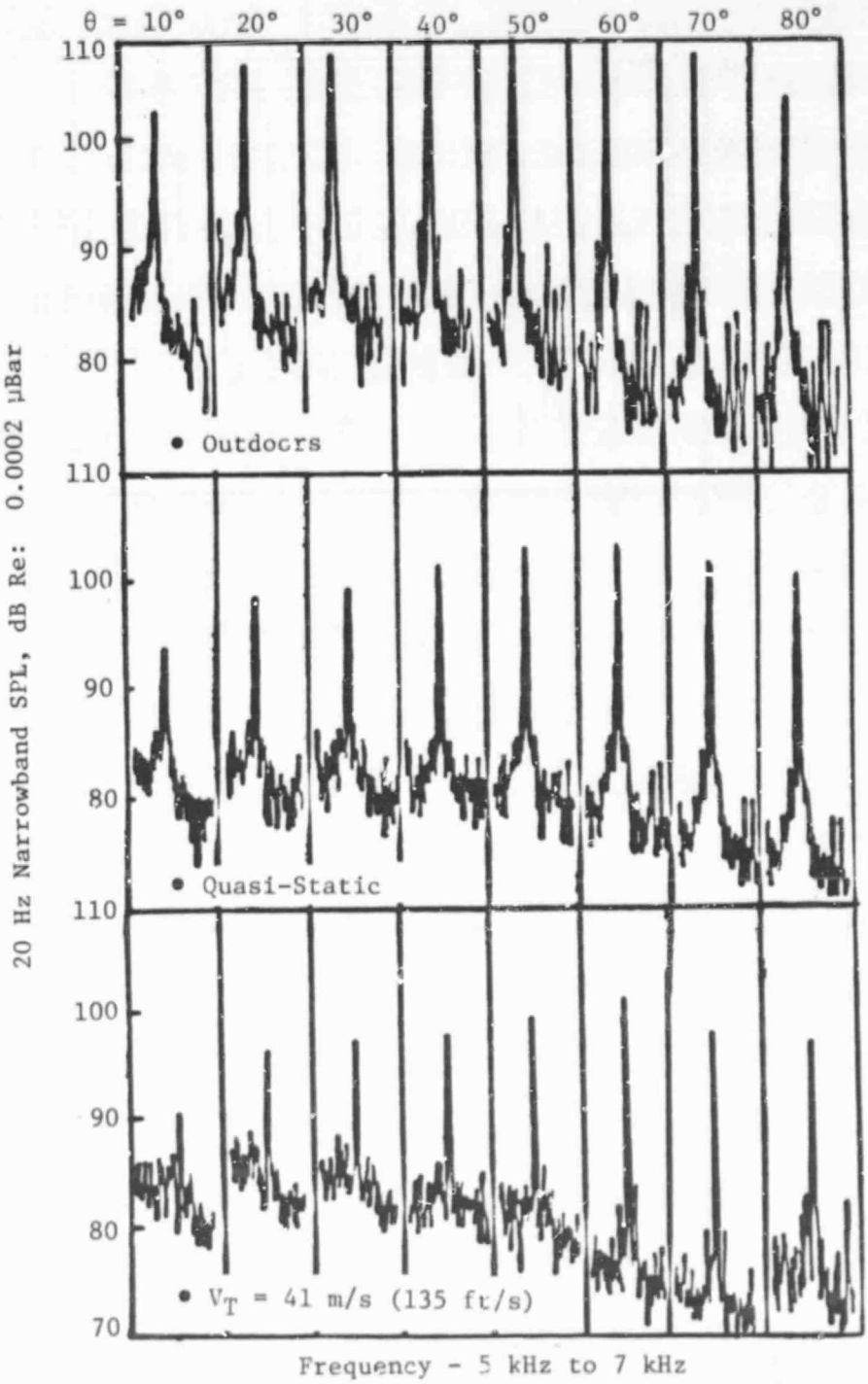

• 3.7 m (12 ft) Arc Uncorrected Data

(b) V_T = 334 m/s (1129 ft/s)

Figure 50. Narrowband Spectra for Baseline Inlet at Static and Forward-Velocity Conditions (Continued).

ORIGINAL PAGE IS
OF POOR QUALITY

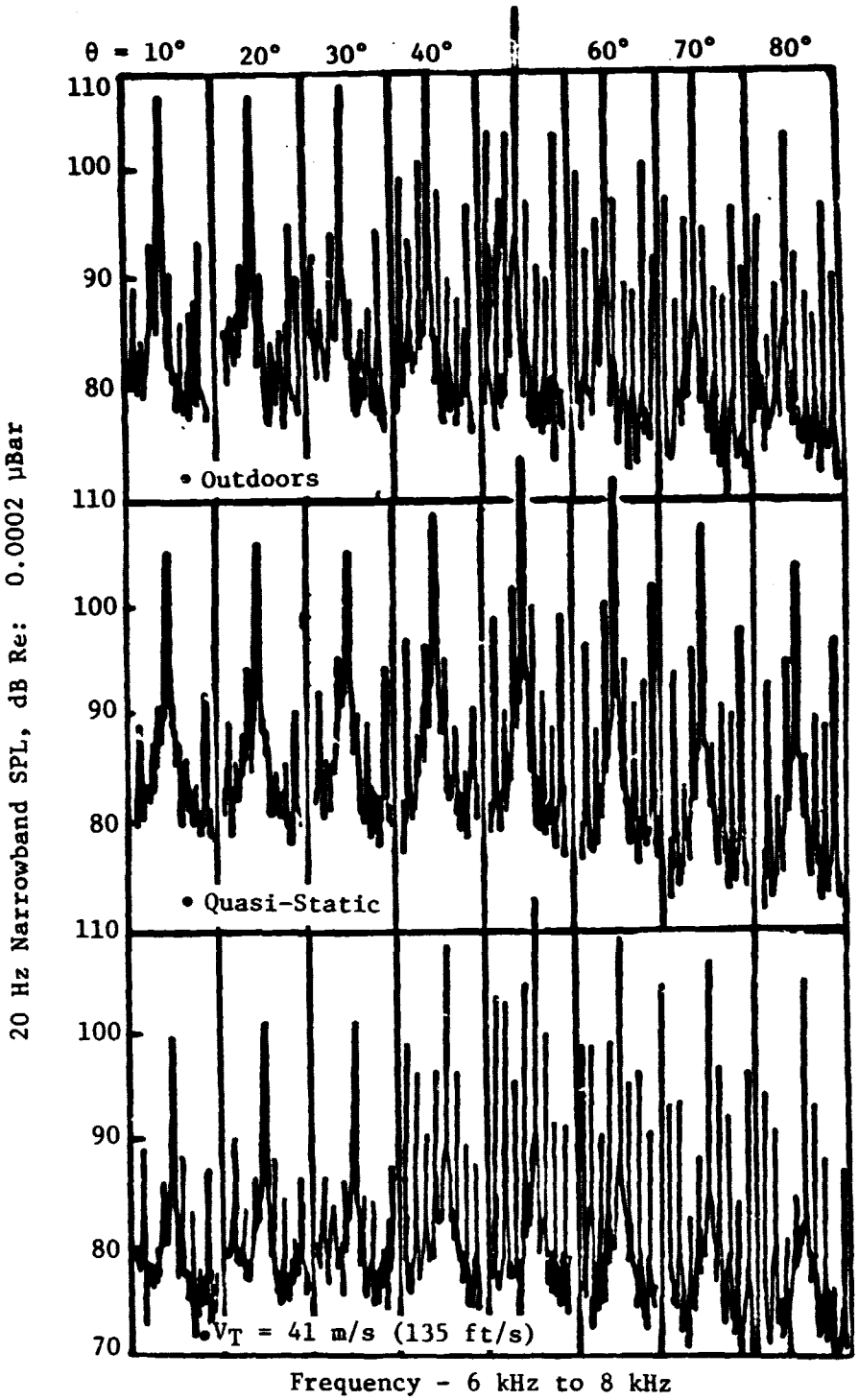

• 3.7 m (12 ft) Arc Uncorrected Data

(c) V_T = 405 m/s (1330 ft/s)

Figure 50. Narrowband Spectra for Baseline Inlet at Static and Forward-Veloctiy Conditions (Concluded).

C-2

ORIGINAL PAGE IS
OF POOR QUALITY

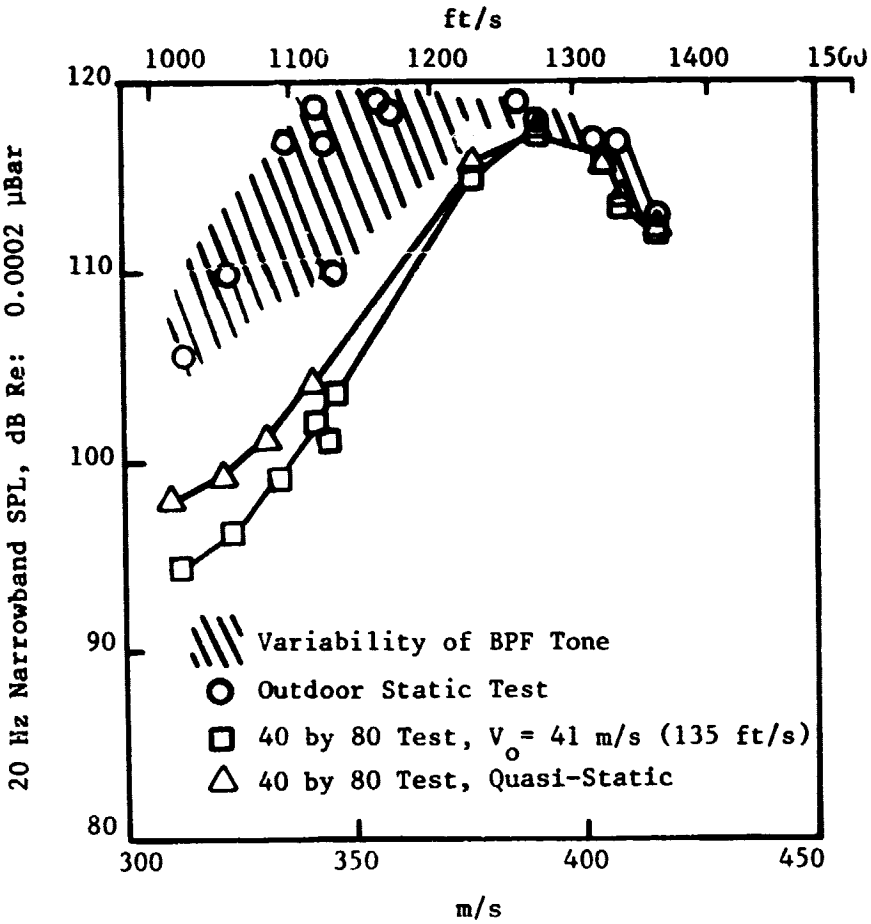

Corrected Fan Tip Speed

• 3.7 m (12 ft) Arc Uncorrected Data

(a) Peak SPL Angle

Figure 51. Narrowband BPF Noise Level Variation with Fan Speed for Baseline Inlet.

ORIGINAL PAGE IS
OF POOR QUALITY

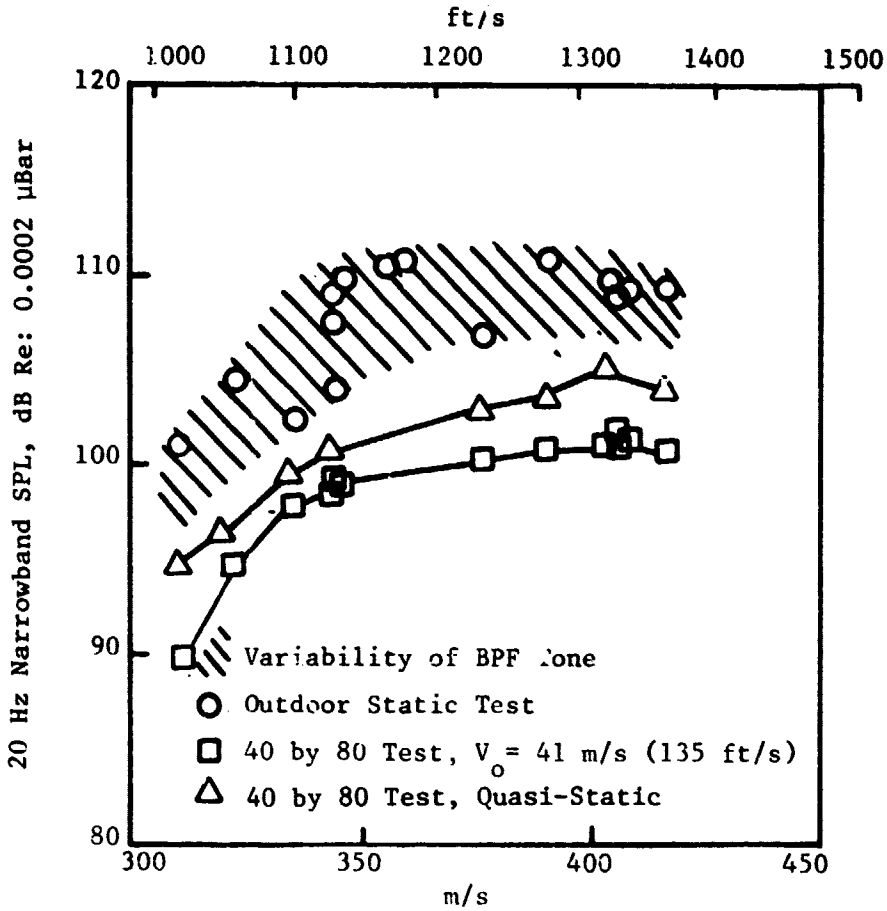

Corrected Fan Tip Speed

● 3.7 m (12 ft) Arc Uncorrected Data

(b) 30° Noise Emisison Angle

Figure 51. Narrowband BPF Noise Level Variation with Fan Speed for Baseline Inlet (Continued).

ORIGINAL PAGE IS
OF POOR QUALITY

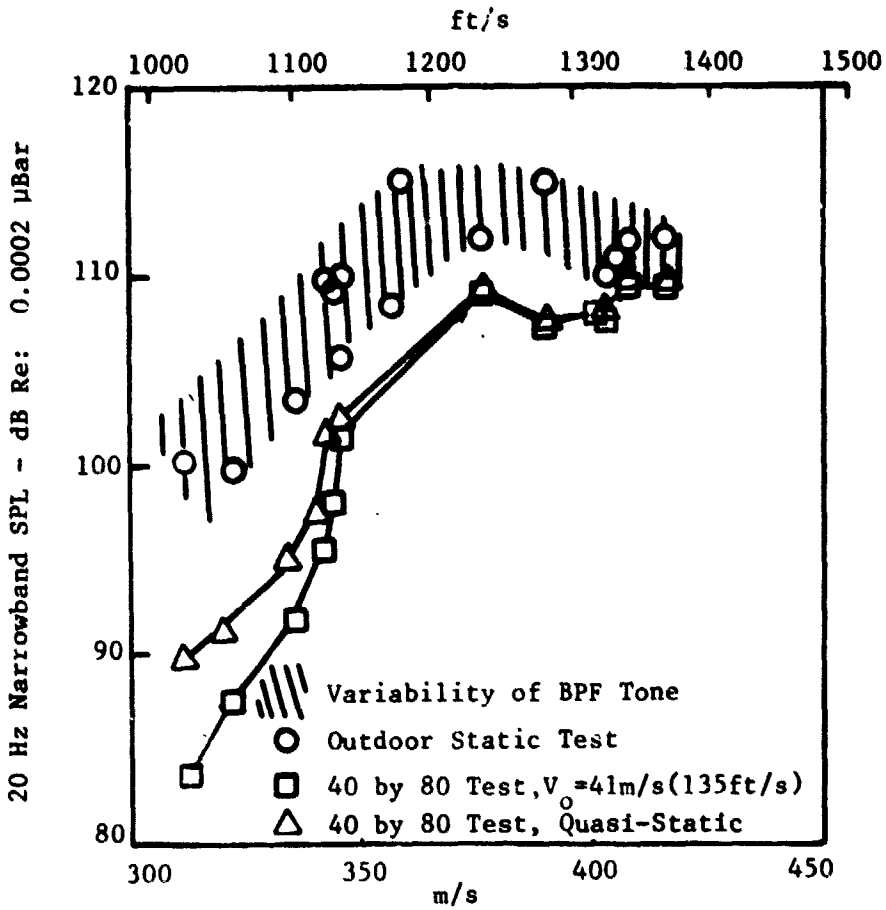

Corrected Fan Tip Speed

- 3.7 m (12 ft) Arc Uncorrected Data

(c) 70° Noise Emission Angle

Figure 51. Narrowband BPF Noise Level Variation with Fan Speed for Baseline Inlet (Concluded).

wind tunnel data at 41 m/s (135 ft/s) will be used since this forward velocity is high enough to be near the design point for both hybrid inlets and is low enough to have background noise levels well below the lowest levels of inlet noise.

4.3.2 Fan Modification Effects

While investigating static-to-flight effects on fan noise using the standard JT15D, Hodder (Reference 2) determined that the interaction between the core inlet guide vanes and the fan-blade wakes was a source of considerable noise in the far field at low corrected fan speed. As a result of this work, NASA ARC contracted with the engine manufacturer to redesign the core inlet guide vanes to reduce or eliminate this BPF tone noise source. This was accomplished in the same way that large turbofan engines are designed: by increasing the number of inlet guide vanes so that the vane/blade ratio exceeds 2.0 so that the noise will not propagate at blade-passing frequency within the fan operating range. An extra benefit was that the spacing between the rotor blade trailing edges and the inlet guide vane leading edges increased (see Figure 4); this reduces the level of the noise that propagates at the harmonics of the blade-passing frequency. The timing of the redesign and modification of the fan was such that the first wind tunnel test (which provided the inlet aerodynamic data), was run with the standard JT15D, and the second wind tunnel test (which provided the noise data) was run with the redesigned JT15D. However, noise data were acquired during the first tests and will be compared with the data from the second tests to demonstrate the effect of the engine modification on the JT15D fan noise characteristics.

The lowest fan corrected speed run with the baseline inlet was just at the lower edge of the speed range where the rotor-alone noise propagates, as was shown in Figure 50. The comparison of the spectra at every 10° between the standard and redesigned JT15D with the baseline inlet is shown in Figure 52 for a forward velocity of 41 m/s (135 ft/s). The format for presentation of the spectra graphically displays the effect of the interaction on the tone directivity pattern. The interaction noise causes high BPF tone levels near the axis but also adds to the rotor-alone noise at the higher angles at this particular corrected fan speed. These results confirm that the standard JT15D has considerable noise, at blade-passing frequency, which is concentrated near the axis of the fan due to the interaction of the fan rotor wakes with the standard core inlet guide vanes.

4.4 HYBRID INLET ACOUSTIC PERFORMANCE

Based upon the acoustic characteristics of the baseline inlet, all the hybrid-inlet acoustic performance results will be determined from the second wind tunnel test data. The throat Mach number, treatment, and angle-of-attack effects will be shown at the forward velocity of 41 m/s (135 ft/s). The forward-velocity effects will be shown at both low and design throat Mach numbers for each inlet at zero angle of attack. A more complete presentation of the data is contained in Reference 3.

ORIGINAL PAGE IS
OF POOR QUALITY

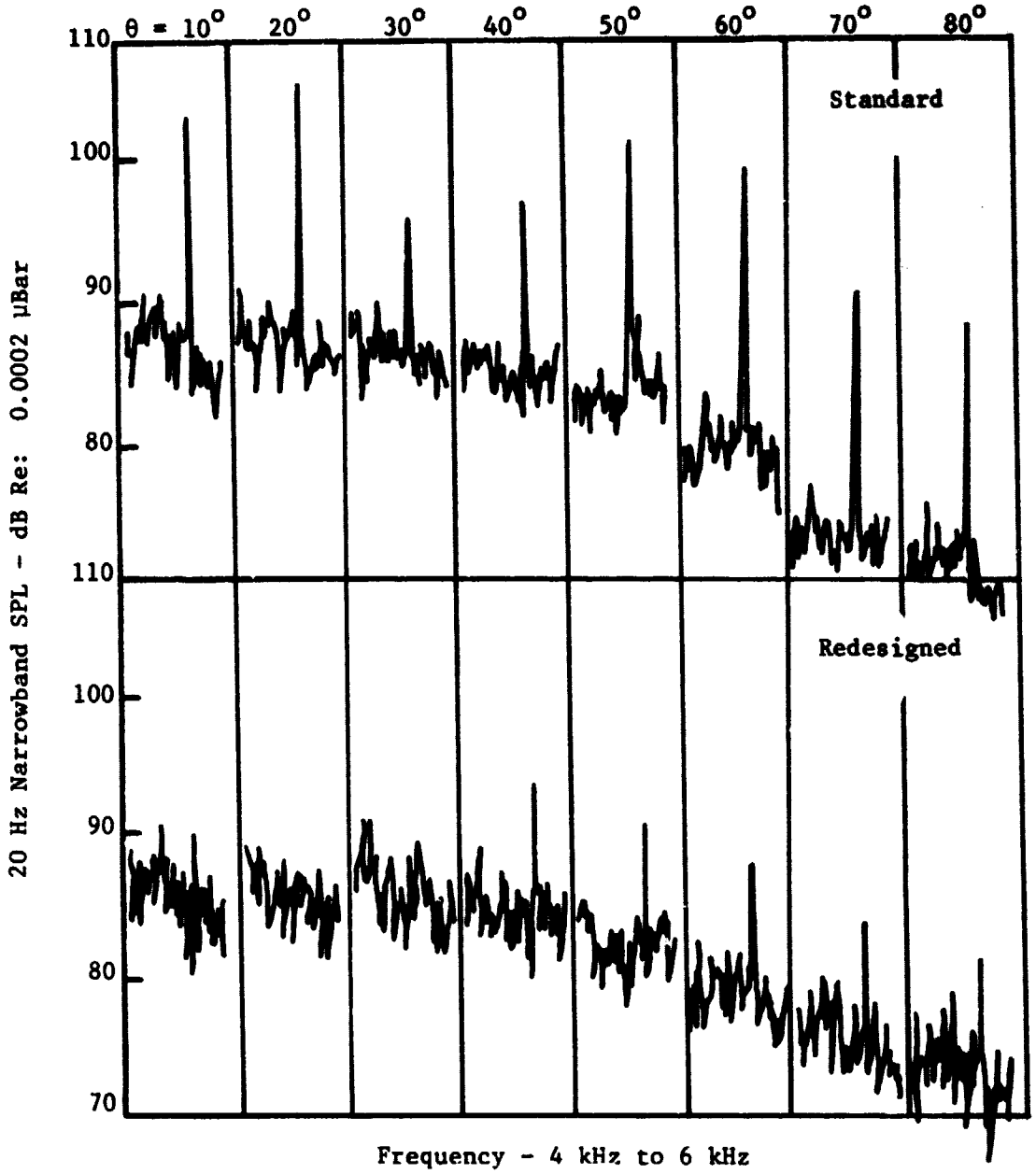

- 3.7 m (12 ft) Arc Uncorrected Data
- 311 m/s (1020 ft/s) Corrected Fan Tip Speed
- 41 m/s (135 ft/s) Forward Velocity

Figure 52. Narrowband Spectra for Baseline Inlet with Standard and Redesigned JT15D Fan.

4.4.1 Comparisons with Baseline Inlet

The fan noise suppression or reduction results are presented as comparisons of absolute sound pressure levels from each inlet rather than as differences in levels from the baseline inlet. These absolute levels are derived from 1/3-octave-band analysis and are plotted as functions of both noise-emission angle and frequency. Narrowband spectra are presented when necessary to provide more detailed explanations of the results. Particular attention is given the frequency region containing the blade-passing tone during analysis of the actual JT15D data. For application of the results to large turbofan engine systems the emphasis is shifted to the extrapolated perceived noise levels (PNL) and the overall sound pressure level (OASPL) at a distance of 61 m (200 ft) parallel to the inlet centerline. For the hybrid-inlet comparisons at zero angle of attack, this distance is referred to as sideline.

Directivity patterns for the 1/3-octave-band containing the blade-passing frequency for four throat Mach numbers and 1/3-octave-band spectra for three angles are shown in Figures 53 and 54, respectively, for the baseline and CTOL inlets. The same type of data are shown in Figures 55 and 56 for the baseline and STOL inlets. The presentation format was chosen to demonstrate the effect of both inlet flow acceleration and acoustic treatment on the fan noise generated at both high and low corrected fan speeds. The same four throat Mach numbers were used for both the CTOL and STOL directivity-pattern comparisons while the lowest and the design throat Mach numbers are used to show the spectral comparisons.

The baseline inlet BPF directivity pattern for the high corrected fan speeds run for the CTOL inlet are all sharply peaked due to the strong presence of rotor-alone noise (Figure 53). The CTOL hard-wall inlet reduces the baseline BPF directivity pattern to a nearly omnidirectional pattern at all throat Mach numbers. The effect of increasing throat Mach number is to continue to reduce the BPF levels at all angles, thus, maintaining the same directivity shape. The addition of treatment to the CTOL inlet reduces the BPF levels at all angles at the lower throat Mach numbers so that the BPF level reduction by the CTOL hybrid inlet is essentially the same at all throat Mach numbers.

The baseline-inlet, 1/3-octave-band spectra exhibit very high levels at frequencies below BPF; this is further verification of strong rotor-alone noise (Figure 54). The CTOL hard-wall inlet substantially reduces the complete noise spectrum at all throat Mach numbers. Because the rotor-alone noise is concentrated at the outer wall of the inlet, which leads to a directivity pattern that peaks near 40° to 50°, the greatest noise reductions occur at higher throat Mach numbers at these angles. The addition of acoustic treatment further reduces the noise at other frequencies as well as at BPF so that the absolute levels over the entire spectrum are essentially the same for the CTOL hybrid inlet regardless of throat Mach number.

The baseline-inlet BPF 1/3-octave-band directivity patterns for the three lowest corrected fan speeds run for the STOL inlet are relatively flat

ORIGINAL PAGE IS
OF POOR QUALITY

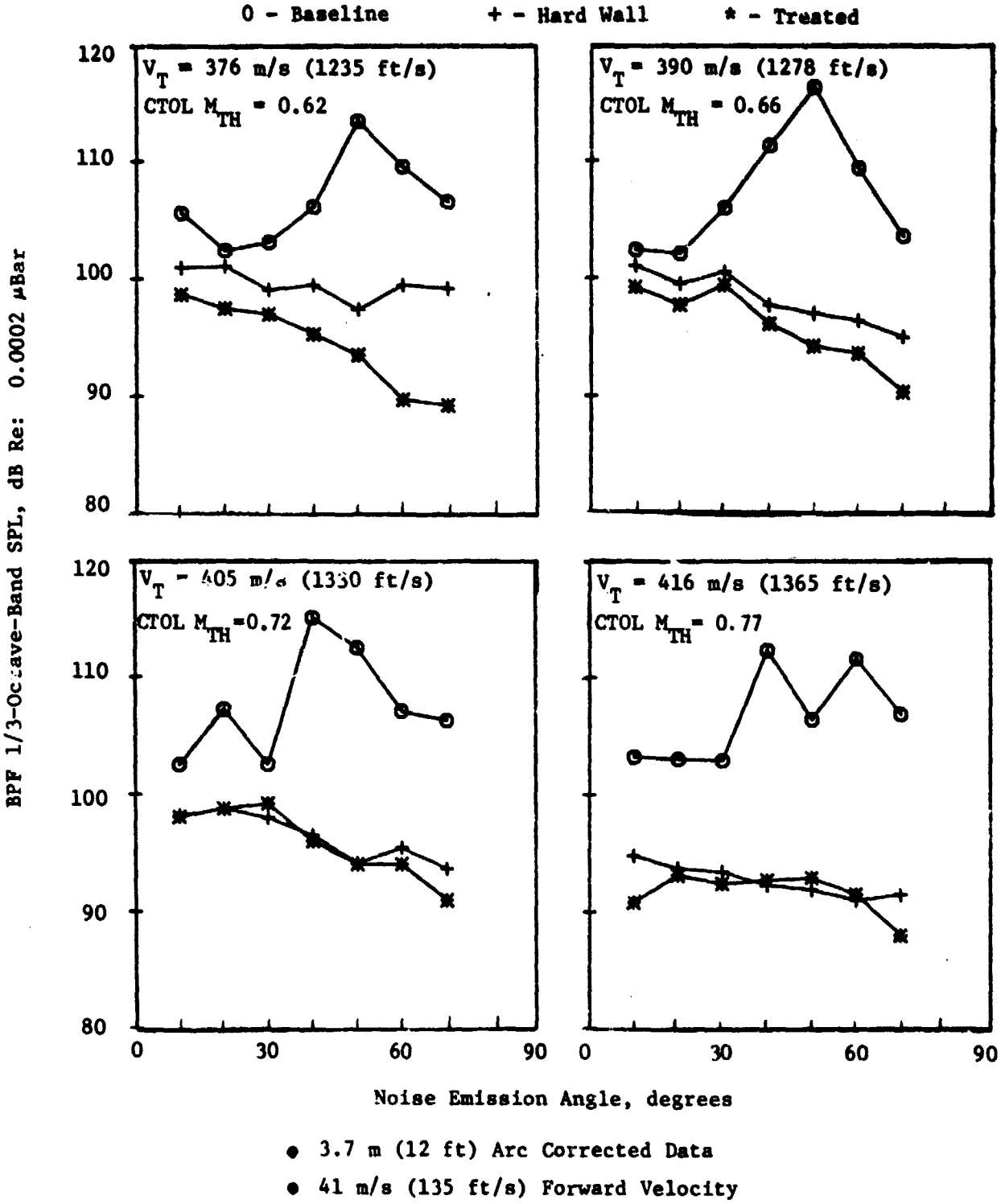

● 3.7 m (12 ft) Arc Corrected Data

● 41 m/s (135 ft/s) Forward Velocity

Figure 53. Blade-Passing Frequency, 1/3-Octave-Band Noise Directivity for Baseline and CTOL Inlets at Forward Velocity.

ORIGINAL PAGE IS
OF POOR QUALITY

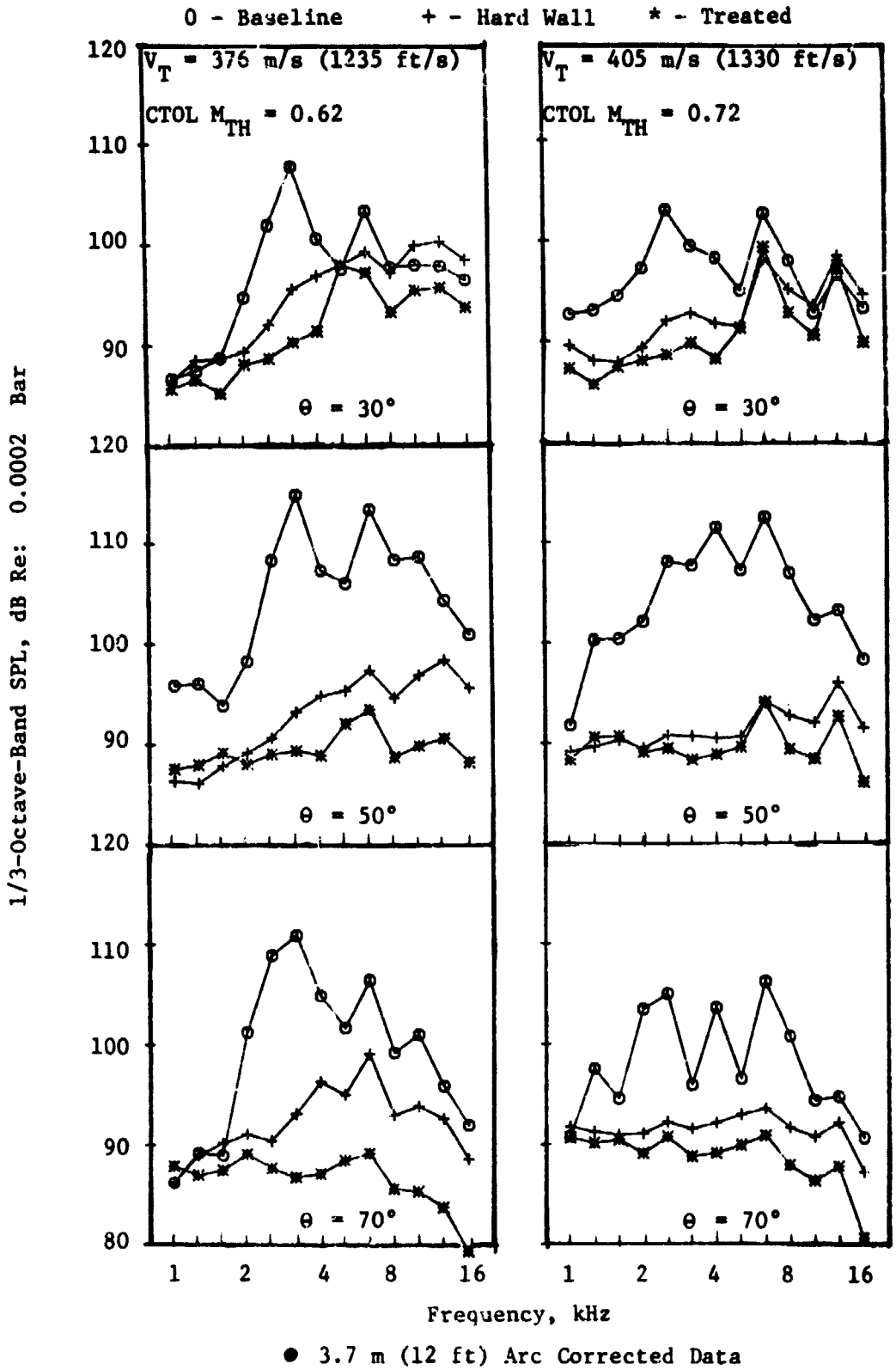

Figure 54. One-Third-Octave-Band Spectra for Baseline and CTOL Inlets at 41 m/s (135 ft/s) Forward Velocity.

ORIGINAL PAGE IS
OF POOR QUALITY

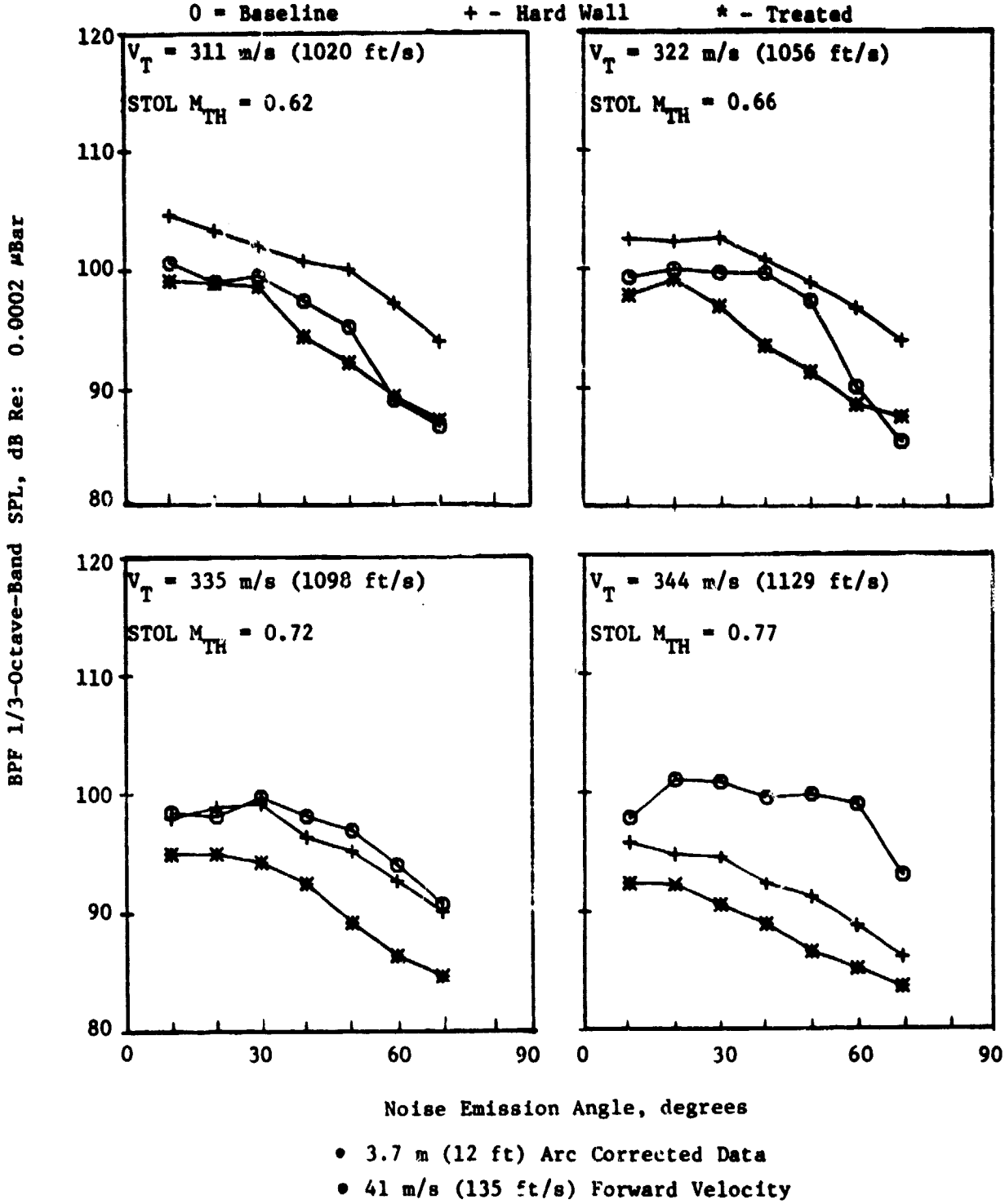

- 3.7 m (12 ft) Arc Corrected Data
- 41 m/s (135 ft/s) Forward Velocity

Figure 55. Blade-Passing-Frequency, 1/3-Octave-Band Noise Directivity for Baseline and STOL Inlet at Forward Velocity.

ORIGINAL PAGE IS
OF POOR QUALITY

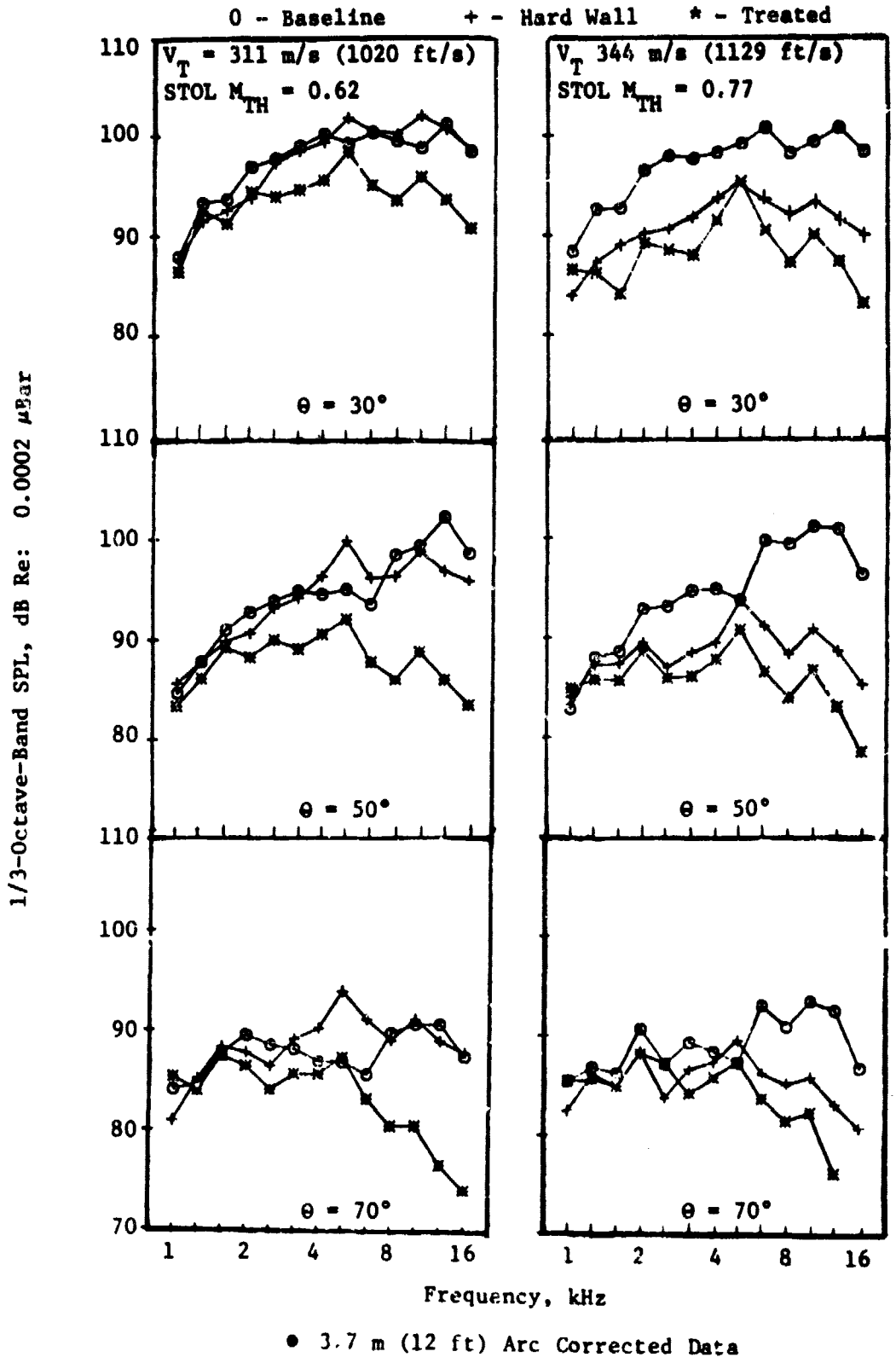

Figure 56. One-Third-Octave-Band Noise Spectra for Baseline and STOL Inlets at 41 m/s (135 ft/s) Forward Velocity.

and characterized by slightly decreasing levels with increasing angle (Figure 55). The pattern for the fan speed run at the STOL design throat Mach number has a quite different shape. The reason for these shapes has to do with the fact that the rotor-alone noise is just beginning to propagate, and the tone levels do not contribute to the 1/3-octave band until highest fan speed. The 20 Hz narrowband spectra shown in Figures 50a and 50b can be used to demonstrate this point. Observe that the broadband noise near the BPF has the same directivity shape as the low-fan-speed points in Figure 55. However, when the BPF tones are greater than 18 dB above the broadband noise, as is the case for Figure 50b, the directively pattern is altered by the tone levels.

The STOL hard-wall inlet BPF directivity patterns have the characteristic shape of broadband noise, at all throat Mach numbers, with the levels decreasing as throat Mach number is increased. However, comparison with the baseline inlet data shows that the levels are increased at the lowest throat Mach number and are not actually reduced until the design throat Mach number. The addition of acoustic treatment uniformly reduces the levels at all angles with a greater effect at low throat Mach numbers. At the lowest throat Mach number the STOL hybrid inlet appears to have little effect on the BPF 1/3-octave-band noise levels (see Figure 56), but at the highest throat Mach number the noise reduction follows the same trends as the CTOL hybrid inlet. The 1/3-octave-band noise spectra from the STOL inlet at these two throat Mach numbers were compared to those from the baseline inlet to determine if these conditions exist at other frequencies.

The baseline-inlet 1/3-octave-band spectra exhibit a general trend of higher levels at higher frequencies with BPF and twice-BPF tone peaks at the higher fan speed. The STOL hard-wall inlet at the low throat Mach number appears to cause the level increase only in the 1/3-octave bands at or near BPF and twice BPF. The fact that this increase is spread over more than one 1/3-octave band indicates that it is broadband rather than tone in nature. The effect of adding acoustic treatment is to reduce the levels at all frequencies at both throat Mach numbers. At the low throat Mach number the reduction increases as frequency increases; the reduction is relatively constant with frequency at the design throat Mach number. The result is that the STOL hybrid inlet reduces the baseline-inlet noise at all frequencies to about the same levels regardless of the throat Mach number.

To provide more detail about the effects of the hybrid inlets on the fan noise at frequencies at or near BPF, as well as to help explain the broadband noise increase caused by the STOL hard-wall inlet, segments of the narrowband spectra are presented in Figures 57 and 58 which correspond to the 1/3-octave band spectra presented in Figures 54 and 56. The fan-noise reduction is achieved for the CTOL hard-wall inlet by virtually eliminating all the per rev tones associated with the rotor-alone noise. At low throat Mach numbers additional reduction is achieved by the action of the acoustic treatment on the broadband noise. However, upon closer inspection of the remaining broadband noise spectra, a "hump" of noise has appeared that peaks approximately 1000 Hz below BPF for both CTOL hard-wall and hybrid inlets at all throat Mach numbers. The hump of broadband noise generated by the CTOL inlet,

ORIGINAL PAGE IS
OF POOR QUALITY

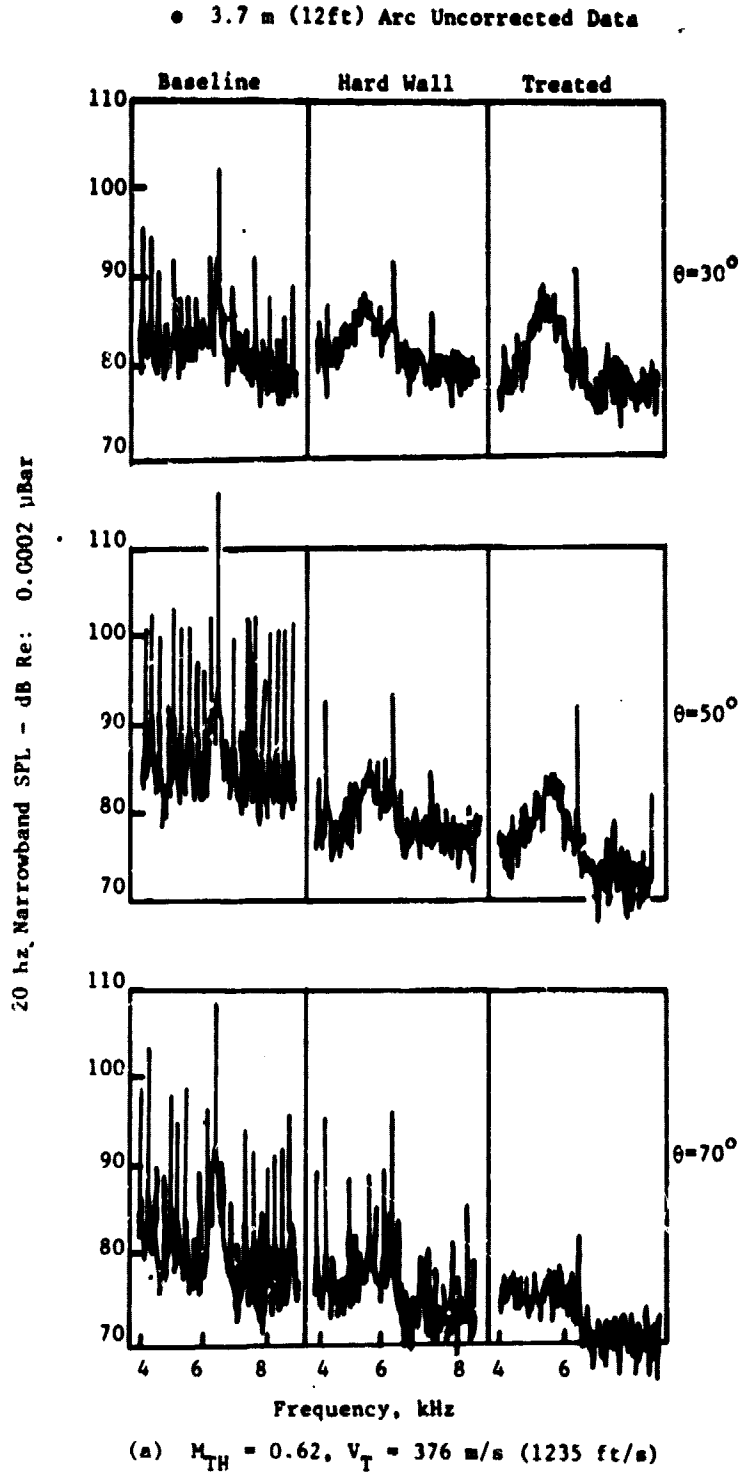

(a) M_{TH} = 0.62, V_T = 376 m/s (1235 ft/s)

Figure 57. Narrowband Spectra for Baseline and CTOL Inlets for 41 m/s (135 ft/s) Forward Velocity.

ORIGINAL PAGE IS
OF POOR QUALITY

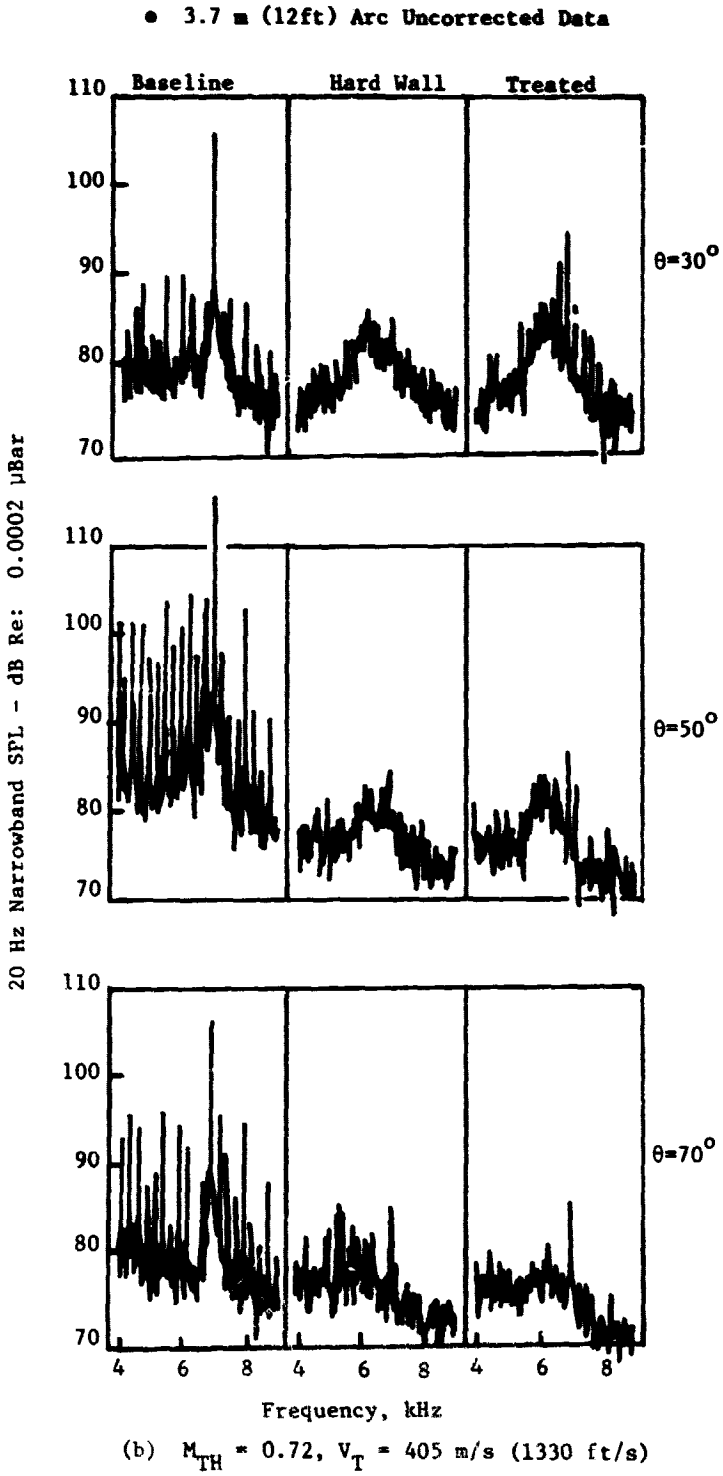

(b) M_{TH} = 0.72, V_T = 405 m/s (1330 ft/s)

Figure 57. Narrowband Spectra for Baseline and CTOL Inlets for 41 m/s (135 ft/s) Forward Velocity (Concluded).

ORIGINAL PAGE IS
OF POOR QUALITY

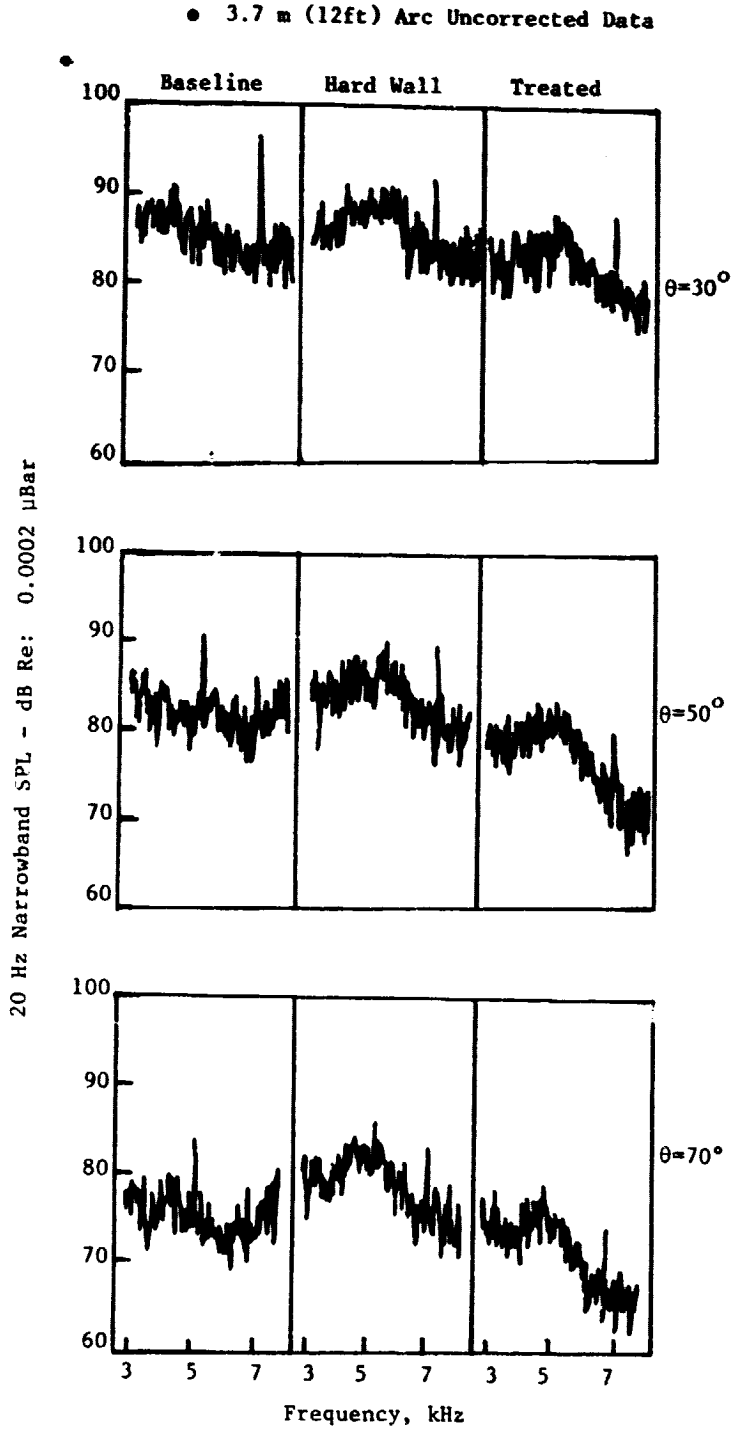

(a) M_{TH} = 0.62, V_T = 311 m/s (1020 ft/s)

Figure 58. Narrowband Spectra for Baseline and STOL Inlets at 41 m/s (135 ft/s) Forward Velocity.

ORIGINAL PAGE IS
OF POOR QUALITY

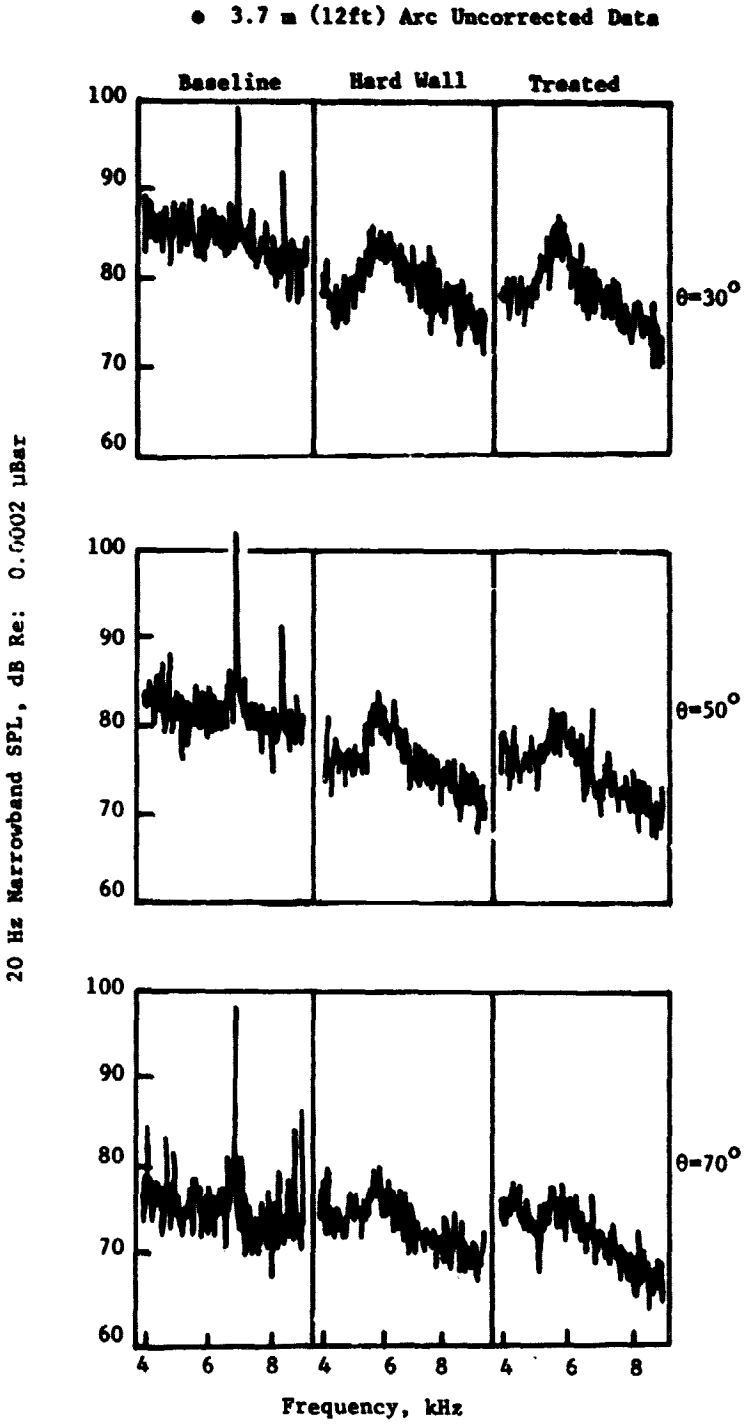

(b) M_{TH} = 0.77, V_T = 344 m/s (1129 ft/s)

Figure 58. Narrowband Spectra for Baseline and STOL Inlets at 41 m/s (135 ft/s) Forward Velocity (Concluded).

rather than residual BPF tone, is the cause of the peaks in the 1/3-octave-band spectra shown in Figure 54. There also is a peak in the 1/3-octave-band noise spectra at twice BPF for the design throat Mach number that is caused by another hump of broadband noise that peaks at twice the frequency of the noise hump near BPF.

Each of the STOL hard-wall inlet narrowband spectra show a similar hump of broadband noise just below BPF (Figure 58). These noise humps are the cause of the BPF 1/3-octave-band noise level increases observed at the low throat Mach numbers in Figure 55. They and the related noise humps near twice BPF are also the cause of the peaks at or near BPF and twice BPF in the 1/3-octave-band noise spectra in Figure 56. The addition of acoustic treatment reduces the noise levels, as previously discussed, but does not remove the humps of broadband noise.

Both CTOL and STOL hybrid inlets cause humps of broadband noise that reduce the suppression levels in the 1/3-octave bands at frequencies at or near BPF and twice BPF. This is shown in the 1/3-octave-band suppression spectra plotted for the noise-emission angle of 50° in Figure 59 for the CTOL hybrid inlet and in Figure 60 for the STOL hybrid inlet. Also plotted in these figures are the suppression spectra as measured at the wall near the throat of each inlet. These data demonstrate that a very good approximation of the peak-angle suppression spectra in the far field can be obtained from inlet wall measurements.

4.4.2 Angle-of-Attack Effects

The effects of angle of attack up to 15° on the acoustic performance of the hybrid inlets are so small they are within the data scatter. The comparisons of 1/3-octave-band spectra at the same three noise-emission angles relative to the inlet centerline for low and design throat Mach numbers at three angles of attack are presented in Figure 61 for the CTOL inlets and in Figure 62 for the STOL inlets. The traverse-microphone data permit direct comparisons at all noise-emission angles to determine if there are any changes in the absolute noise due to angle of attack. The angle-of-attack effects on sideline noise, which are due to rotating the directivity pattern along with the inlet, were not explored. When the STOL inlets were operated at 30° angle of attack the diffuser flow was on the verge of separation, as previously discussed. As a result the 1/3-octave-band noise levels are increased at all angles. However, due to the nature of the flow into the fan at this angle of attack, there are no consistent trends to the increased levels.

4.4.3 Forward Velocity Effects

The acoustic-performance effects of changing forward velocity in the 40 by 80 are shown in Figure 63 for the CTOL hybrid inlets and Figure 64 for the STOL hybrid inlets. The 1/3-octave-band spectra are compared in these figures at three emissions angles for low and design throat Mach numbers at

ORIGINAL PAGE IS
OF POOR QUALITY

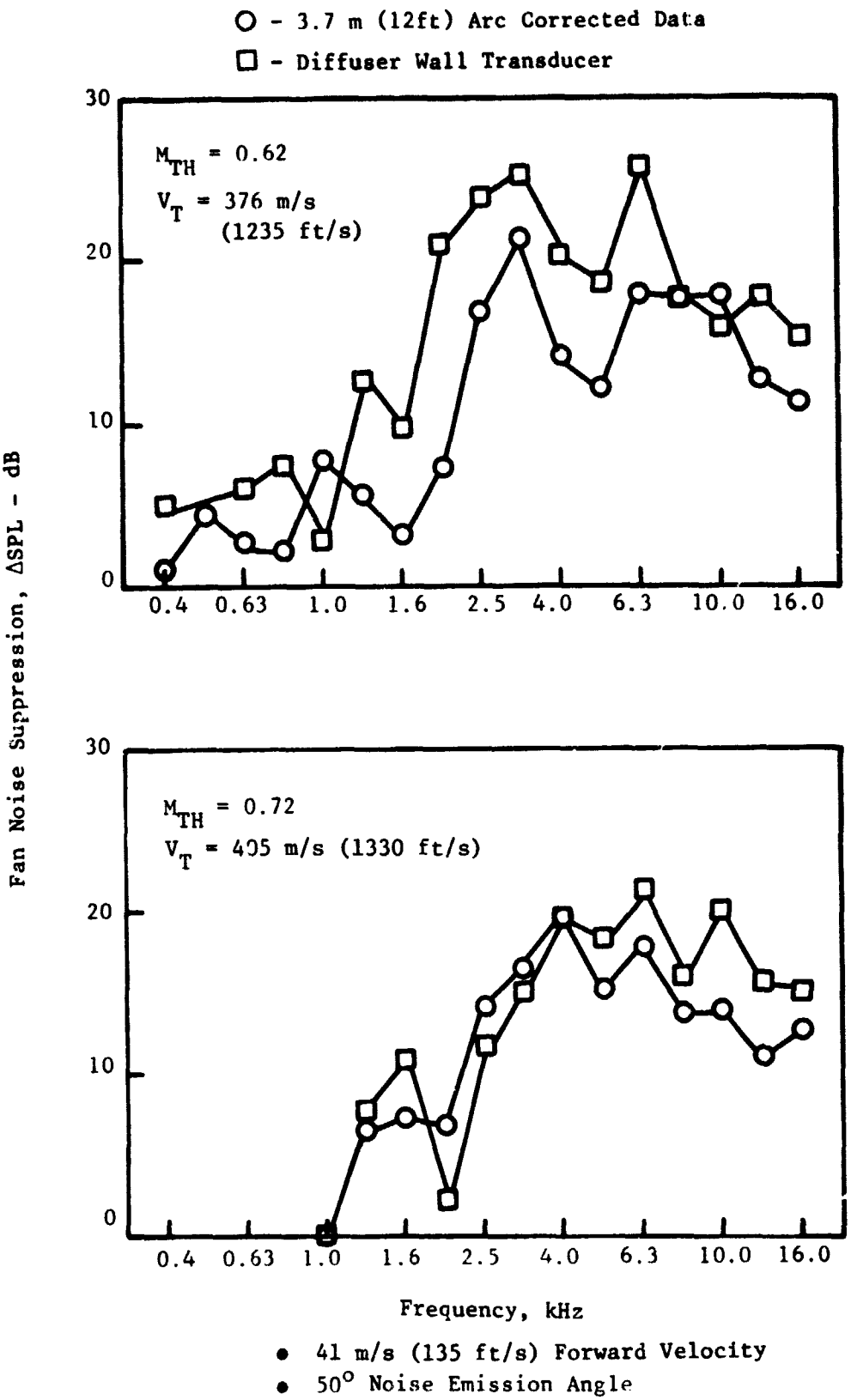

- 41 m/s (135 ft/s) Forward Velocity
- 50° Noise Emission Angle

Figure 59. CTOL Hybrid Inlet Fan Noise Suppression Spectra at Forward Velocity.

ORIGINAL PAGE IS
OF POOR QUALITY

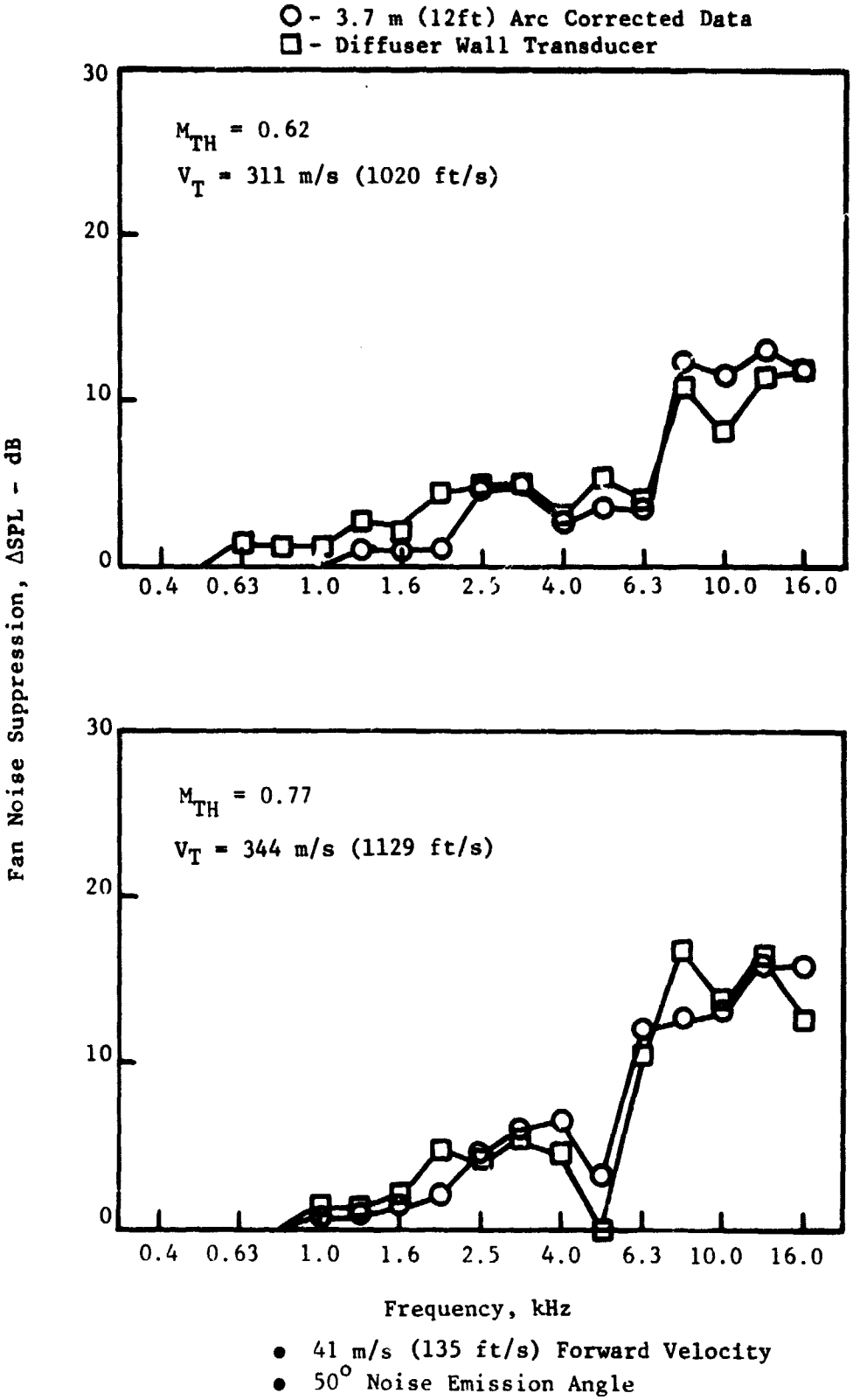

Figure 60. STOL Hybrid Inlet Fan Noise Suppression Spectra at Forward Velocity.

ORIGINAL PAGE IS
OF POOR QUALITY

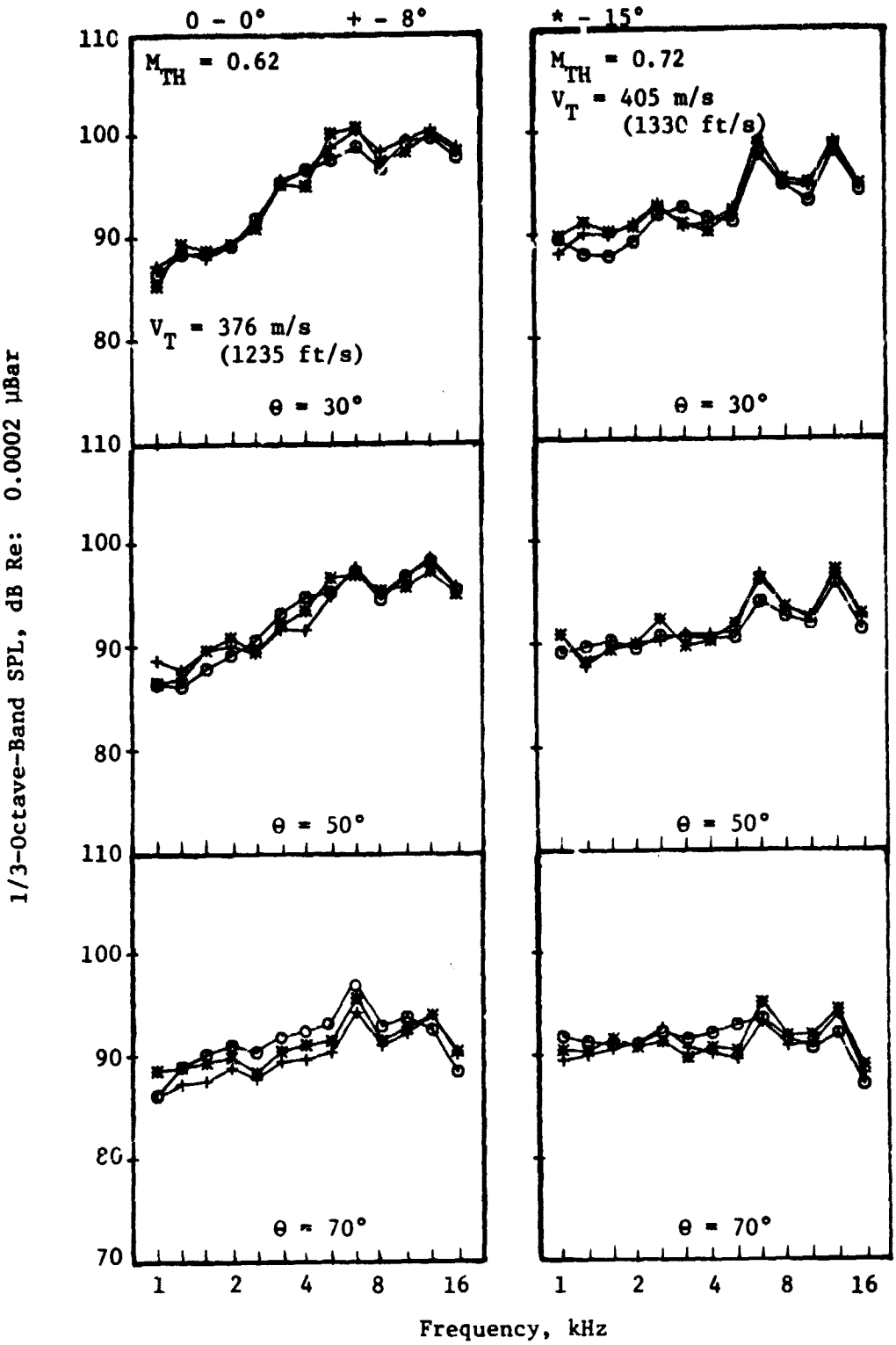

- 3.7 m (12 ft) Arc Corrected Data
- 41 m/s (135 ft/s) Forward Velocity

(a) CTOL Hard Wall Inlet

Figure 61. One-Third-Octave-Band Noise Spectra for CTOL Inlet at Three Angles of Attack.

ORIGINAL PAGE IS
OF POOR QUALITY

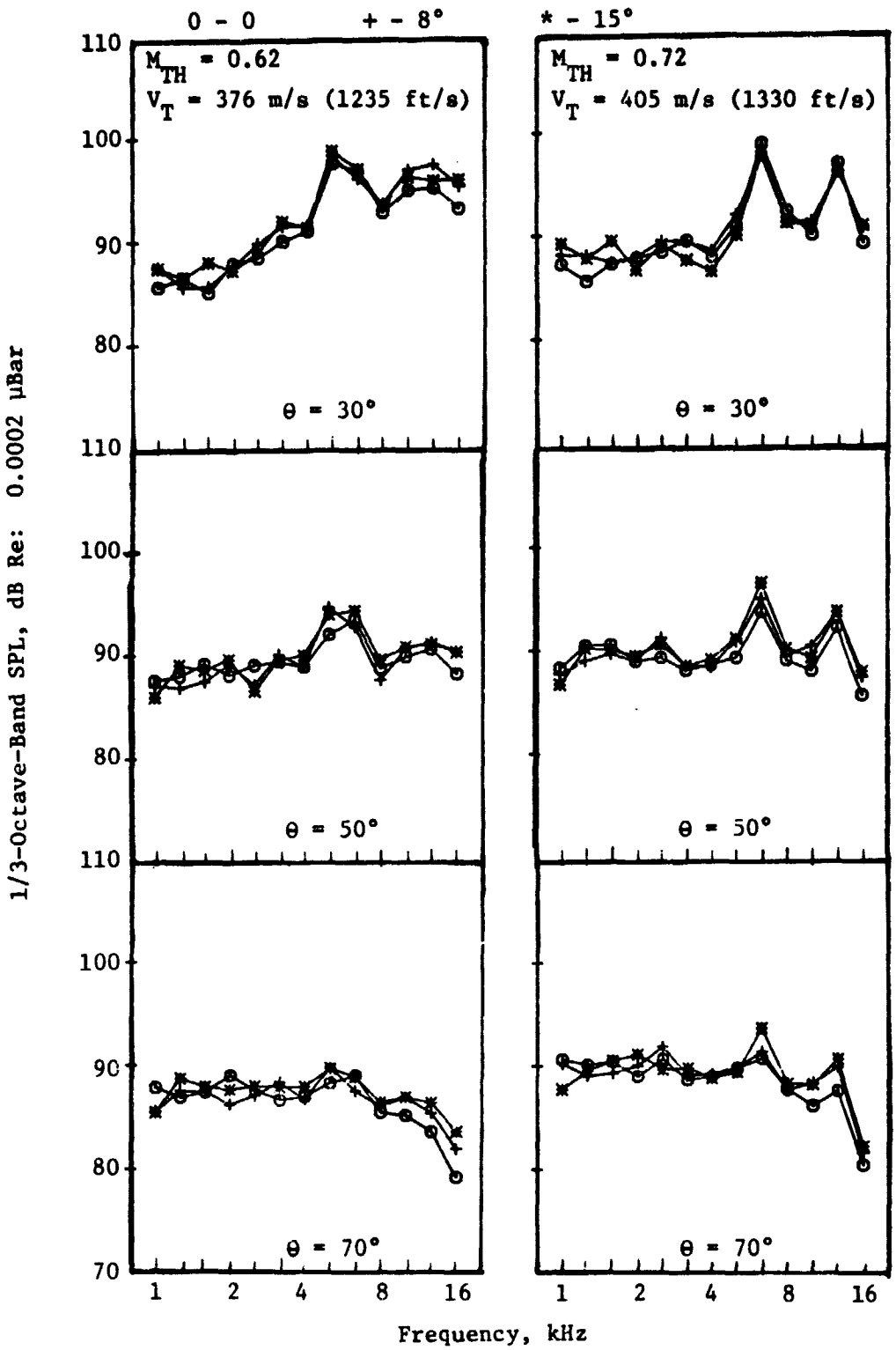

● 3.7 m (12 ft) Arc Corrected Data

● 41 m/s (135 ft/s) Forward Velocity

(b) CTOL Treated Inlet

Figure 61. One-Third-Octave-Band Noise Spectra for CTOL Inlet at Three Angles of Attack (Concluded).

ORIGINAL PAGE IS
OF POOR QUALITY

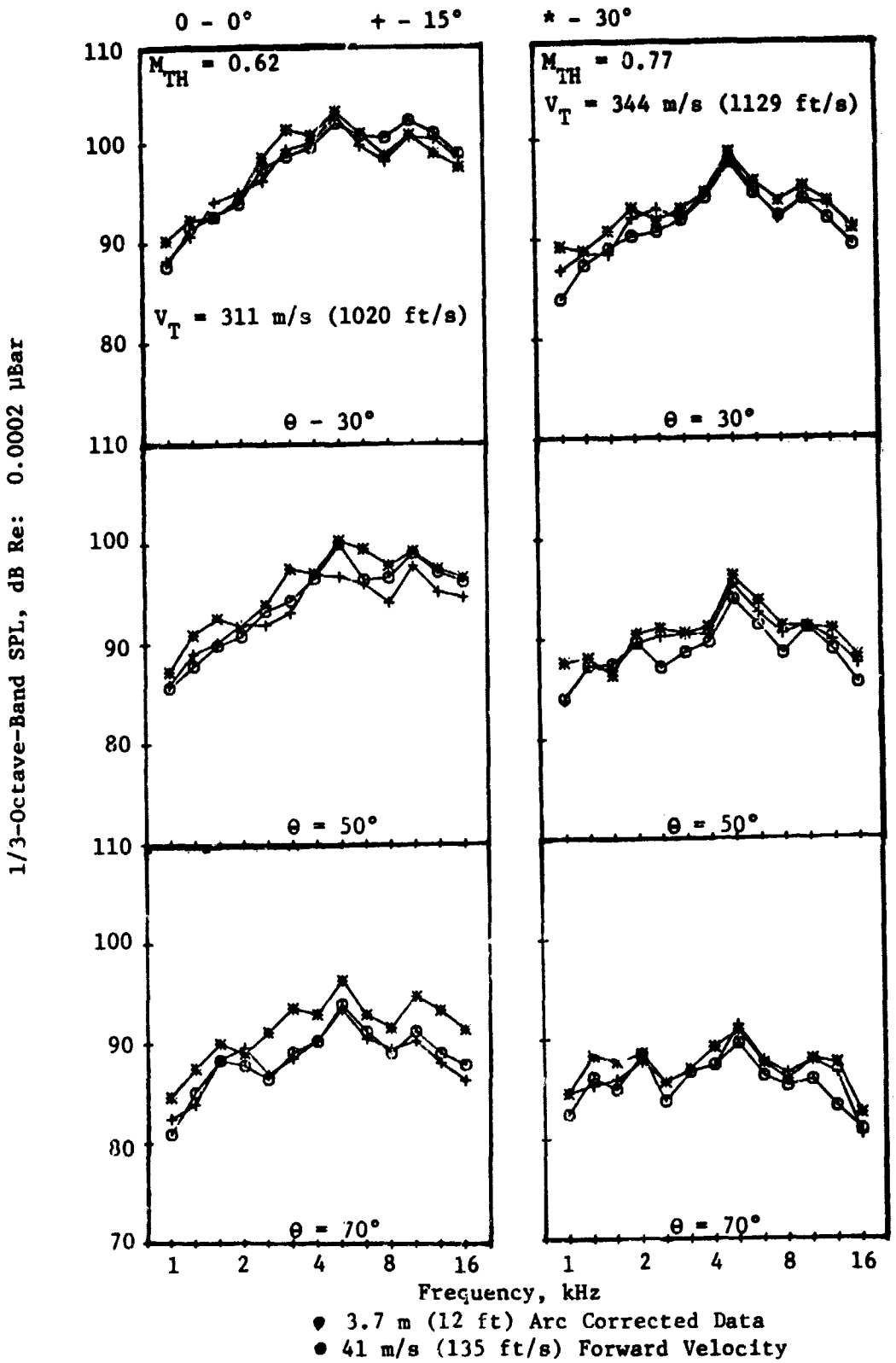

▼ 3.7 m (12 ft) Arc Corrected Data
● 41 m/s (135 ft/s) Forward Velocity

(a) STOL Hard Wall Inlet

Figure 62. One-Third-Octave-Band Noise Spectra for STOL Inlets at Three Angles of Attack.

ORIGINAL PAGE IS
OF POOR QUALITY

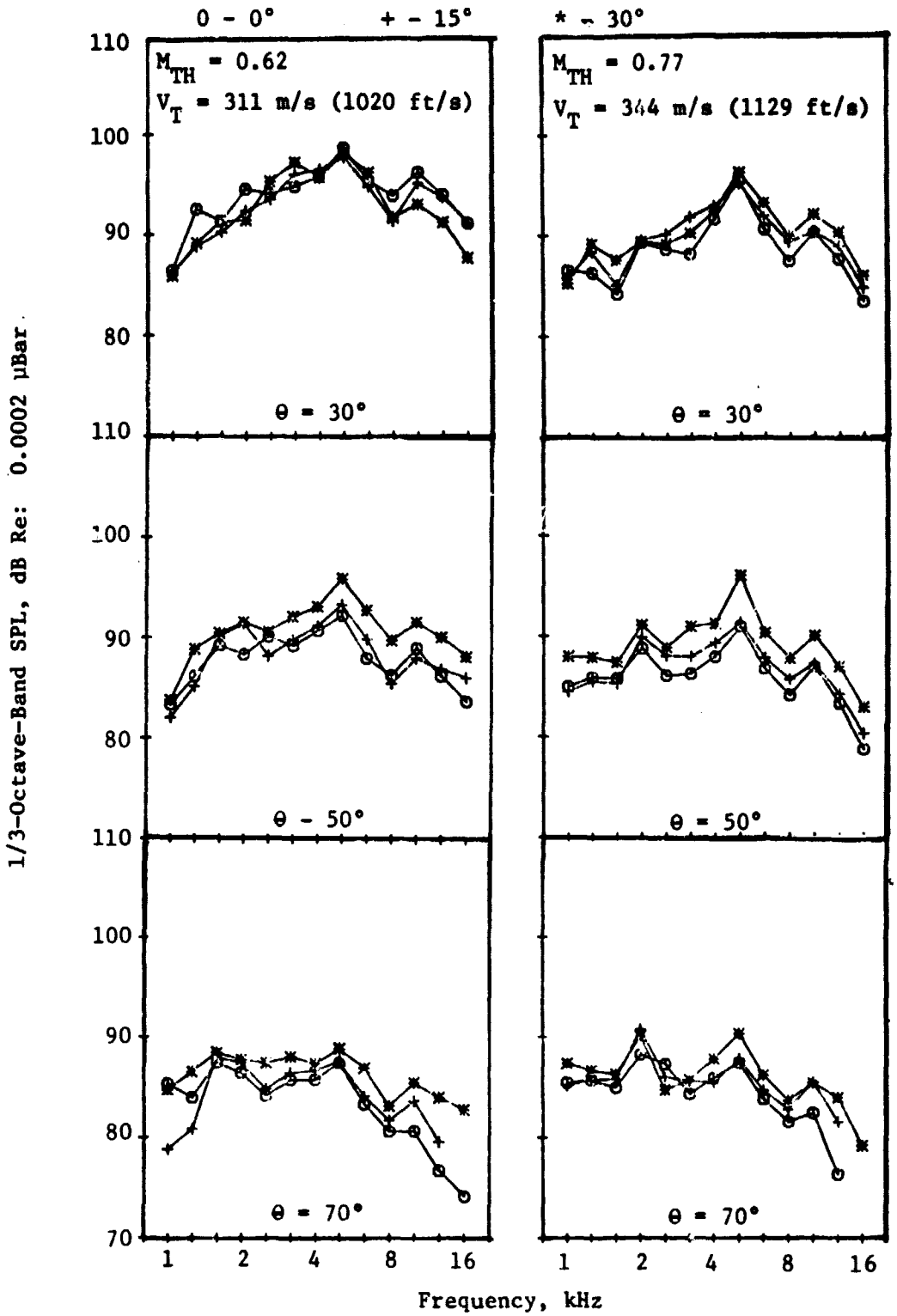

- 3.7 m (12 ft) Arc Corrected Data
- 41 m/s (135 ft/s) Forward Velocity

(b) STOL Treated Inlet

Figure 62. One-Third-Octave-Band Noise Spectra for STOL Inlets at Three Angles of Attack (Concluded).

ORIGINAL PAGE IS
OF POOR QUALITY

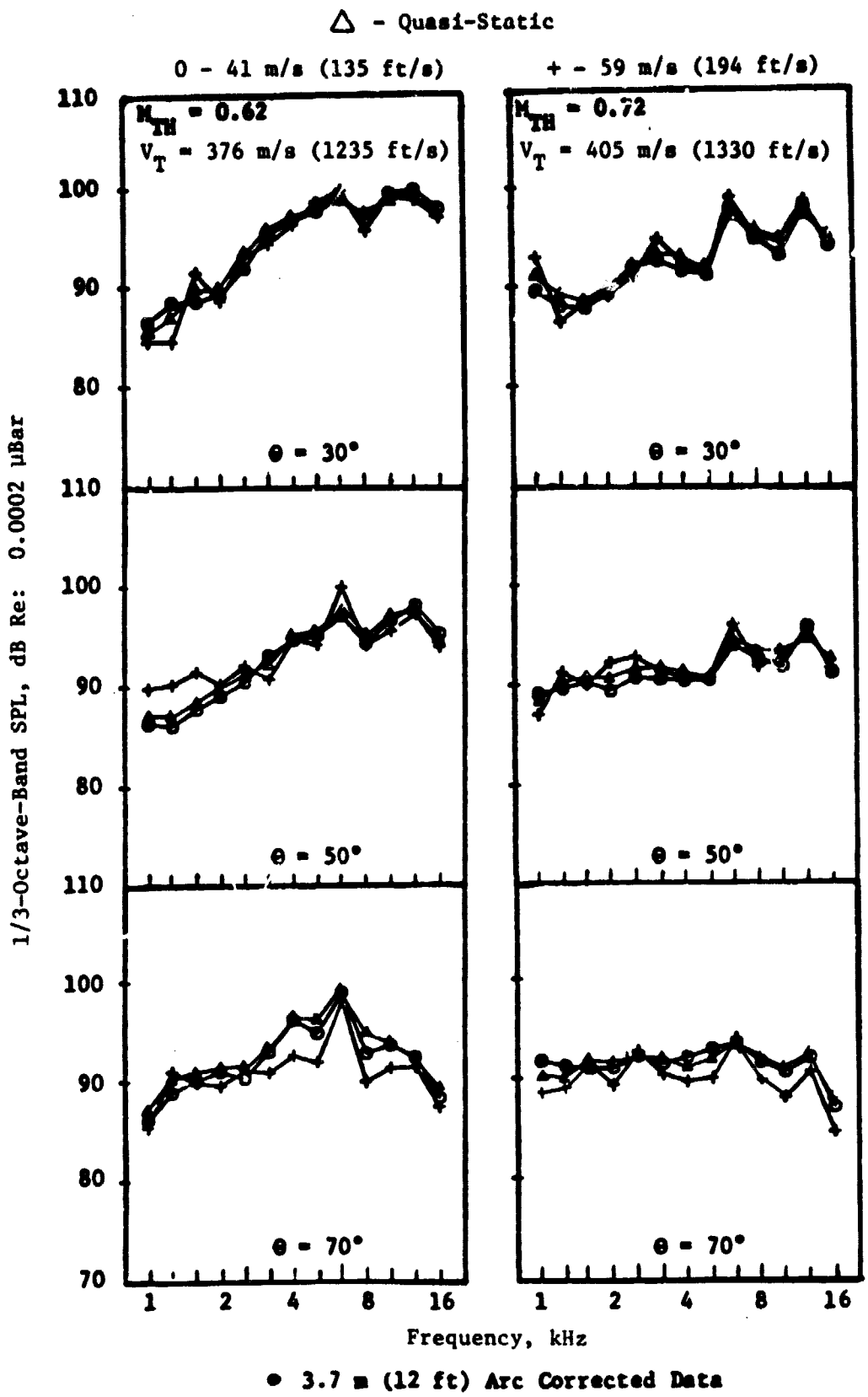

(a) CTOL Hard Wall Inlet

Figure 63. One-Third-Octave-Band Noise Spectra for CTOL Inlet at Various Forward Velocities.

ORIGINAL PAGE IS
OF POOR QUALITY

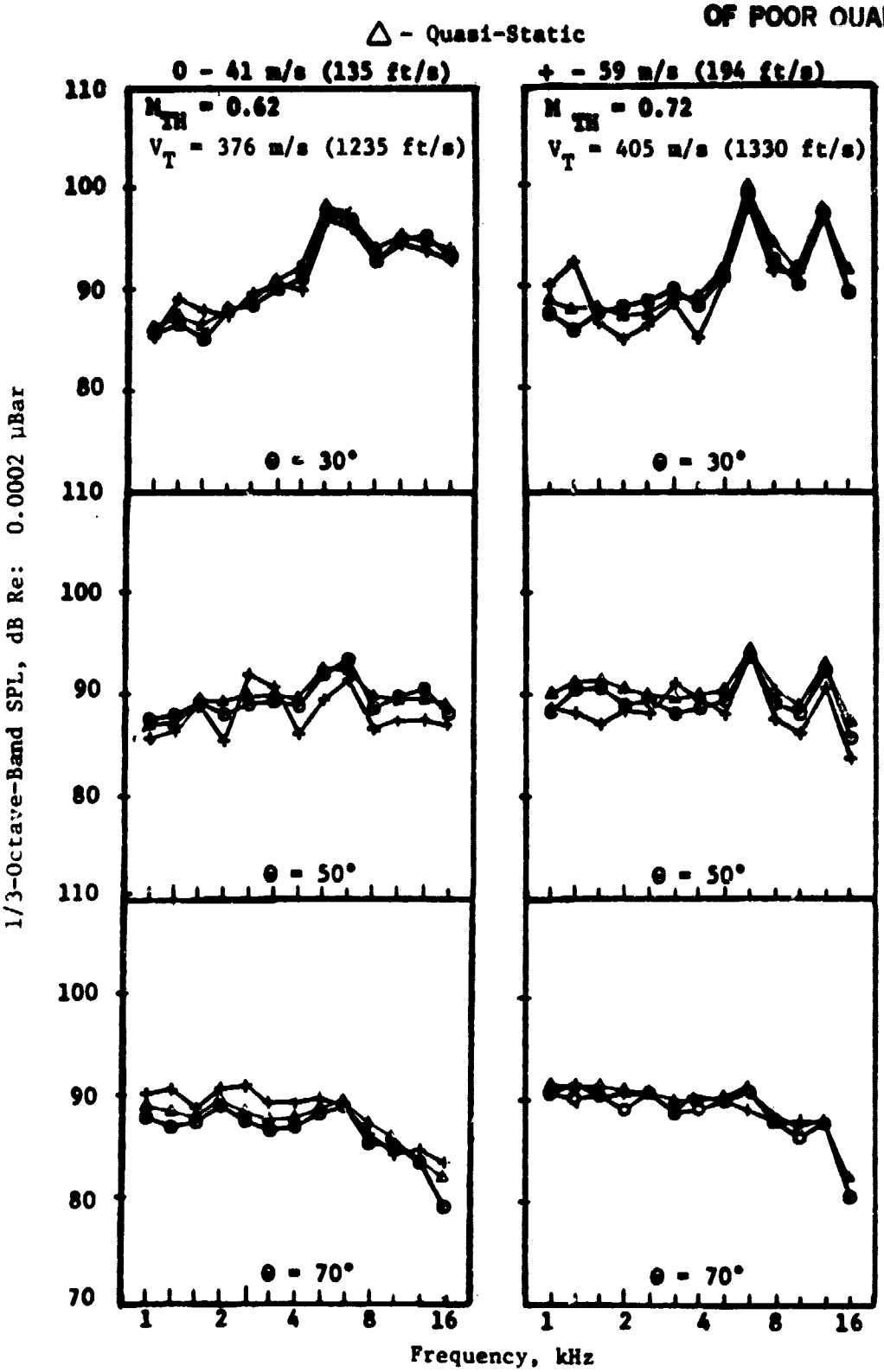

● 3.7 m (12 ft) Arc Corrected Data

(b) CTOL Treated Inlet

Figure 63. One-Third-Octave-Band Noise Spectra for CTOL Inlet at Various Forward Velocities (Concluded).

ORIGINAL PAGE IS
OF POOR QUALITY

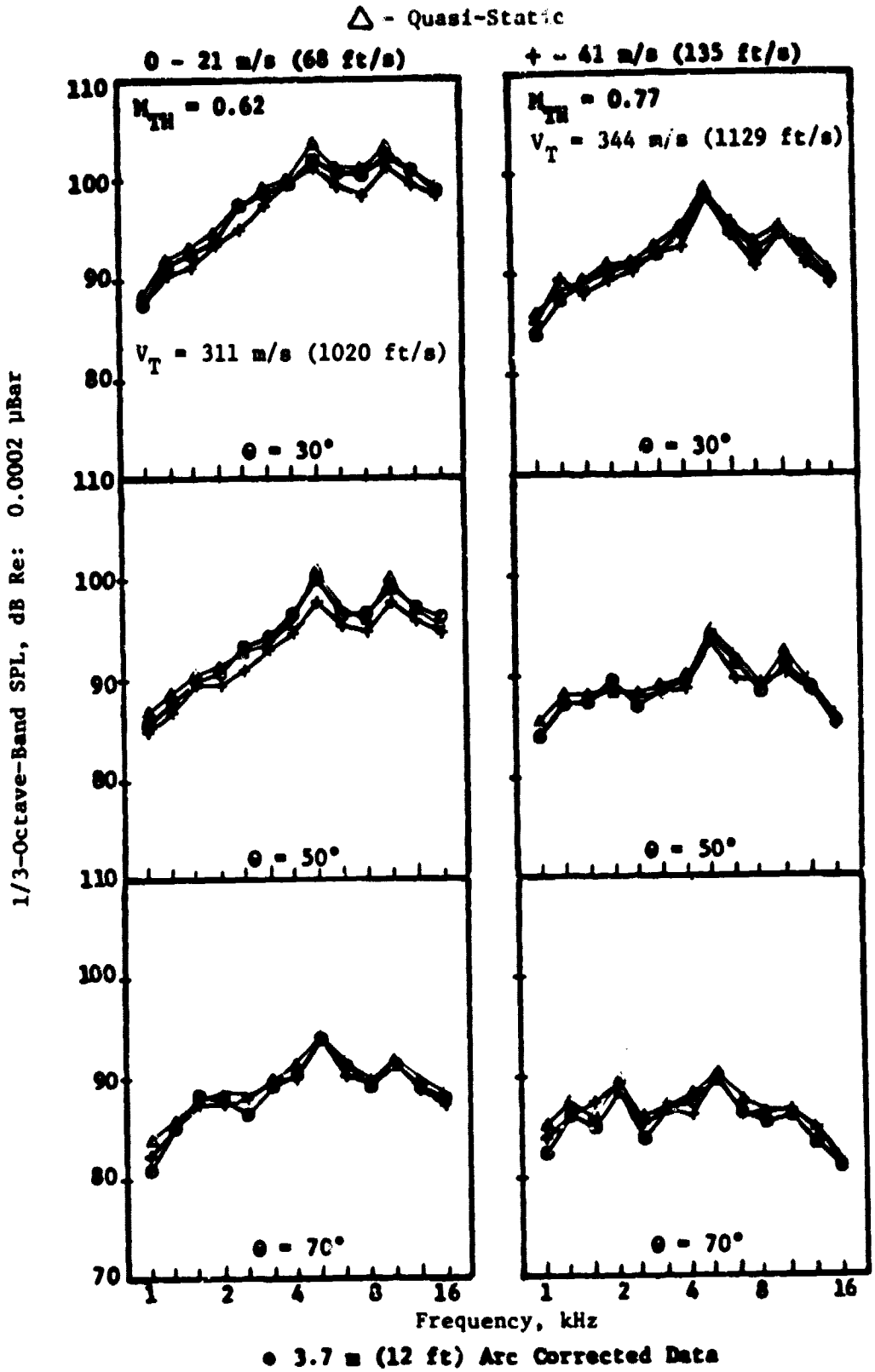

(a) STOL Hard Wall Inlet

Figure 64. One-Third-Octave-Band Noise Spectra for STOL Inlet at Various Forward Velocities.

ORIGINAL PAGE IS
OF POOR QUALITY

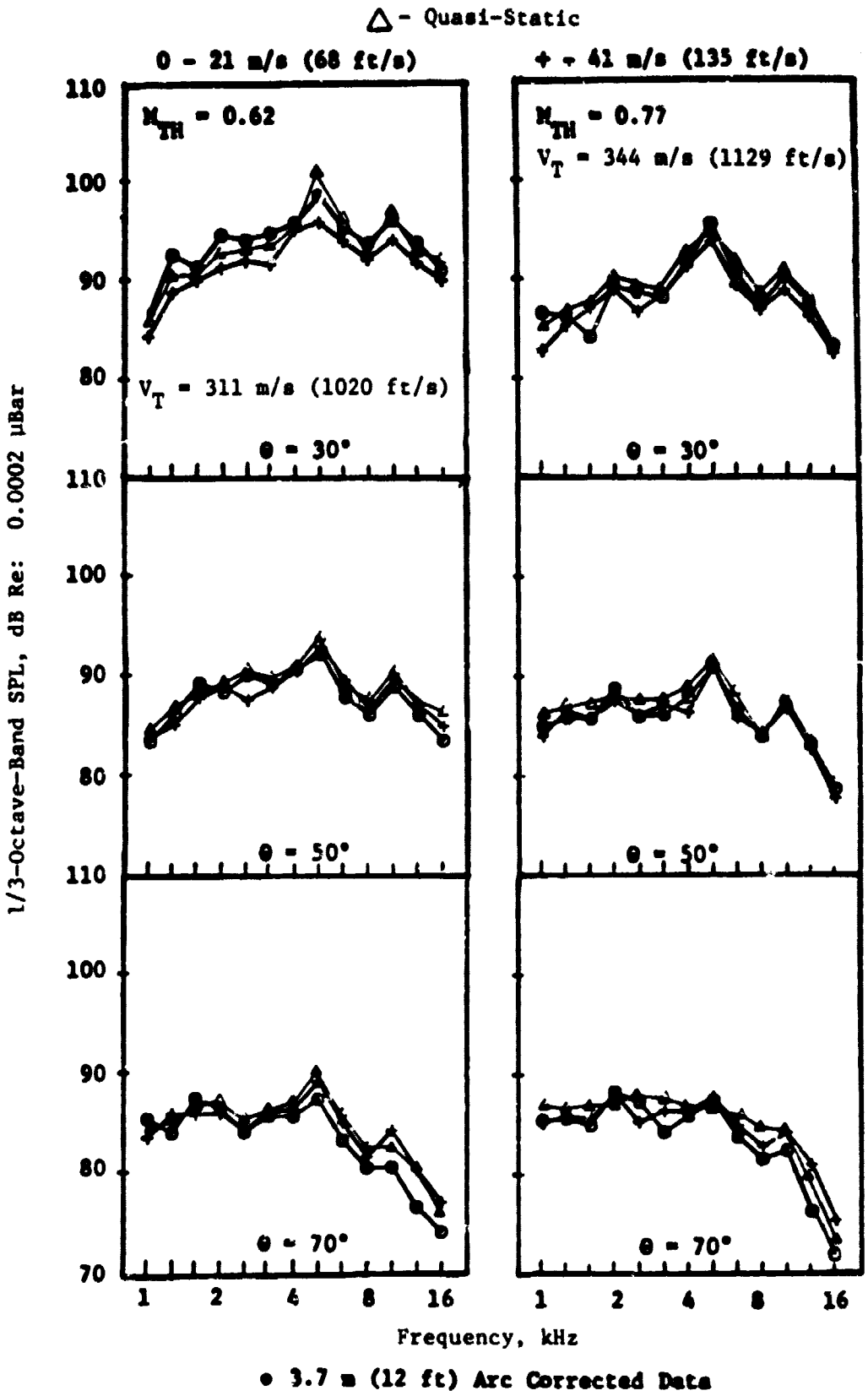

• 3.7 m (12 ft) Arc Corrected Data

(b) STOL Treated Inlet

Figure 64. One-Third-Octave-Band Noise Spectra for STOL Inlet at Various Forward Velocities (Concluded).

various forward velocities including quasi-static conditions, <8 m/s (26.3 ft/s). The CTOL inlet spectra are somewhat scattered at the highest forward velocity due to the high levels of wind tunnel background noise that have been subtracted from the data. However, these data indicate that the hybrid-inlet noise in the 40 by 80 is basically the same at quasi-static and moderate-forward-velocity conditions, even though that is not the case for the baseline-inlet noise. There are two reasons for this apparant anomaly.

First, the tone noise generated by the rotor-turbulence interaction at quasi-static conditions is adequately suppressed by the hybrid inlets expect for the STOL inlet at $M_{TH} = 0.62$ and $\theta = 30°$. Second, the remaining tone levels in the hybrid-inlet data are not high enough above the broadband levels to affect the spectral levels in the 1/3-octave bands containing the fundamental and harmonic BPF's. Therefore, comparisons between hybrid- and baseline-inlet noise from 40 by 80 data to determine suppression results will be affected by forward velocity if the quasi-static data are used. This is due to the fact that the hybrid inlets suppress rotor-turbulence-interaction noise at quasi-static conditions, but at moderate or higher forward velocities the interaction noise is not there to suppress. The conclusion that there are no forward-velocity effects on the hybrid-inlet acoustic characteristics is only valid for forward velocities of 21 m/s (68 ft/s) or higher.

4.4.4 Effects on Large-Scale-Fan Noise

To compare the fan-noise suppression of the hybrid inlets with that from other inlets, the noise data had to be scaled up to the size of the large turbofan engines and extrapolated to a sideline. The noise data for the CTOL inlet and baseline inlet at the high corrected fan speeds were scaled up to a CF6 size engine. In a similar manner, the noise data for the STOL inlet and the baseline inlet at the low corrected fan speeds were scaled up to a QCSEE size engine. The 61 m (200 ft) sideline perceived noise and overall noise directivity patterns are shown in Figure 65 for the CTOL data and in Figure 66 for the STOL data.

The baseline-inlet noise-directivity patterns for all CTOL and STOL corrected fan speeds have the same characteristic. The noise is lowest near the axis, peaks between 40° and 60°, and then drops off toward 90°. The levels for the CTOL corrected fan speeds are much higher due to the contribution of all the per rev tones below blade-passing frequency generated by the rotor-alone noise. This is true for both the weighted perceived noise and the overall noise.

The CTOL hard-wall inlet significantly reduces the noise at the peak angles and, as a result, shifts the noise directivity pattern peak to the higher angles. The acoustic treatment provides additional reduction at the lower throat Mach numbers so that the resultant CTOL hybrid inlet perceived noise levels are essentially the same over the throat Mach number range tested.

ORIGINAL PAGE IS
OF POOR QUALITY

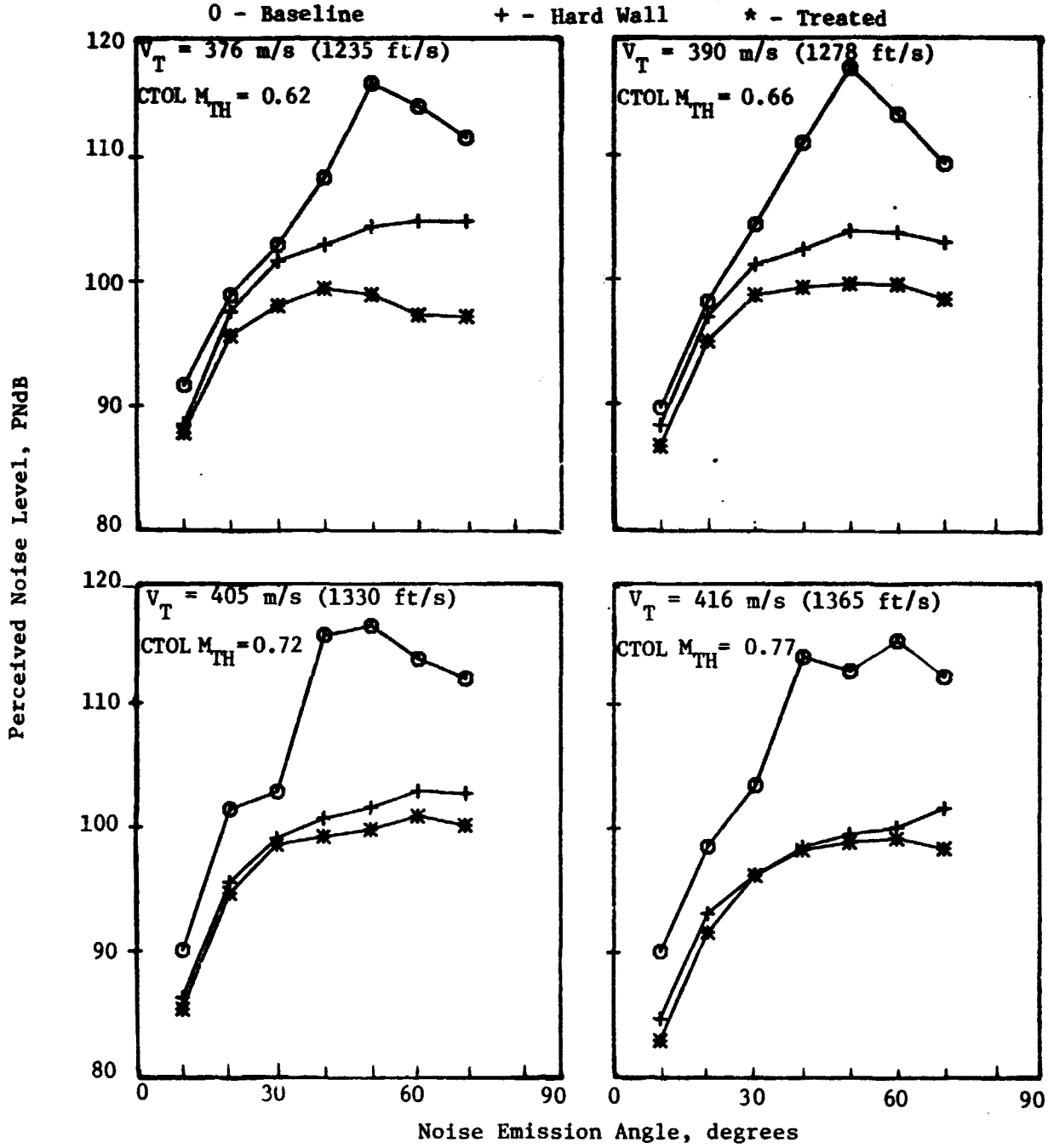

- 61 m (200 ft) Sideline
- 41 m/s (135 ft/s) Forward Velocity

(a) Perceived Noise

Figure 65. CTOL Noise Directivity (CF6 Size) at Forward Velocity.

ORIGINAL PAGE IS
OF POOR QUALITY

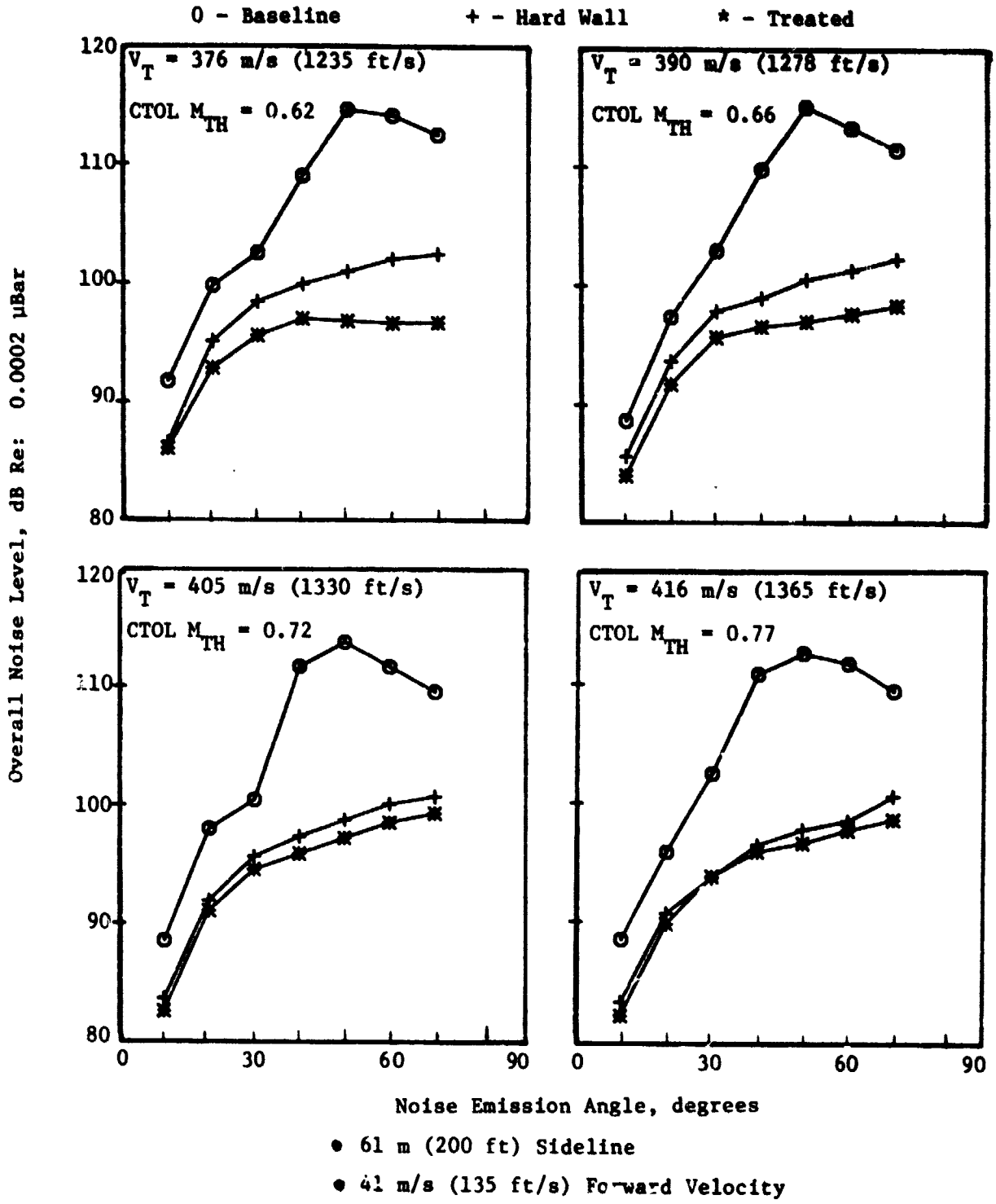

(b) Overall Noise

Figure 65. CTOL Noise Directivity (CF6 Size) at Forward Velocity (Concluded).

ORIGINAL PAGE IS
OF POOR QUALITY

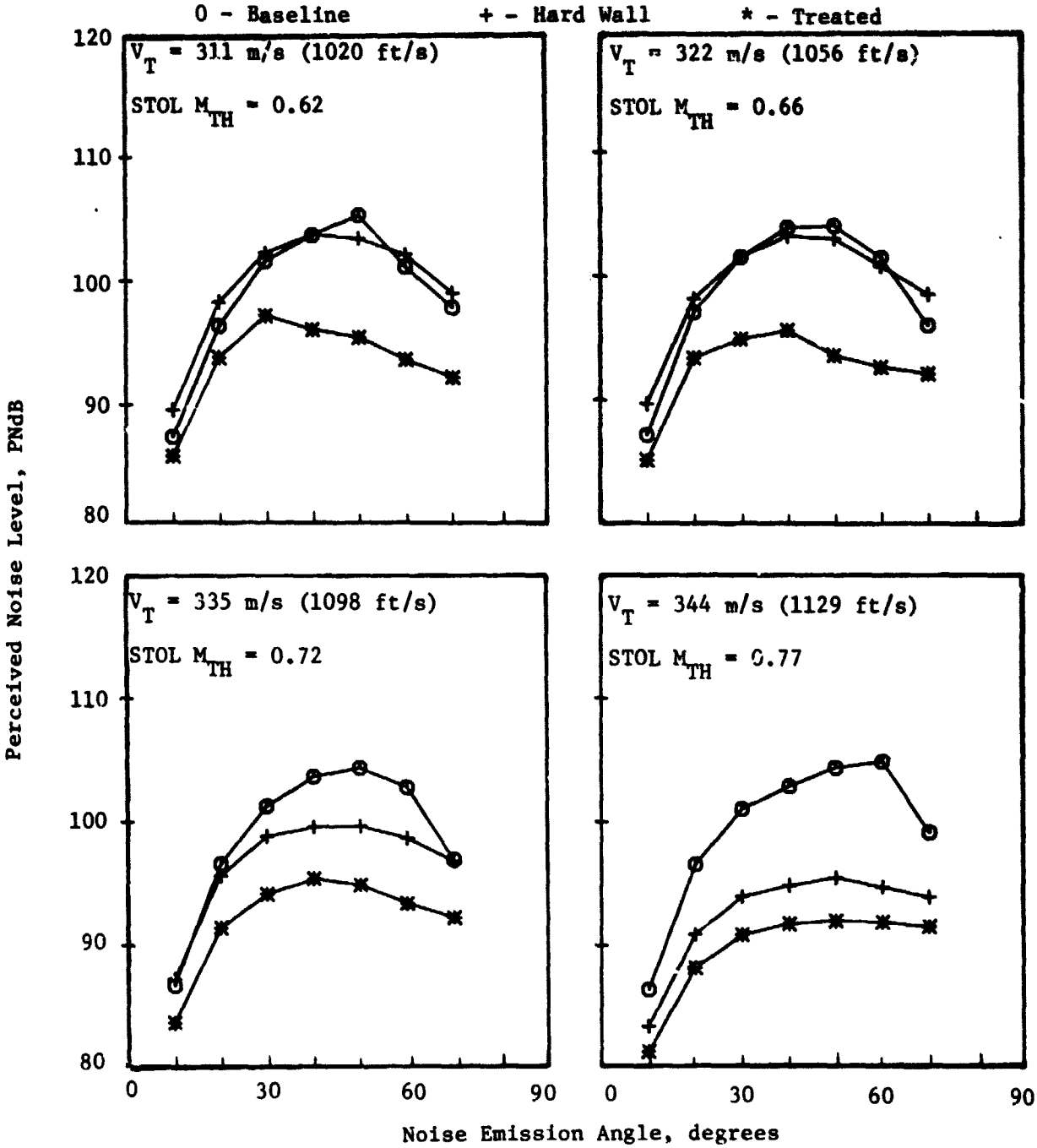

- 61 m (200 ft) Sideline
- 41 m/s (135 ft/s) Forward Velocity

(a) Perceived Noise

Figure 66. STOL Noise Directivity (QCSEE Size) at Forward Velocity.

ORIGINAL PAGE IS
OF POOR QUALITY

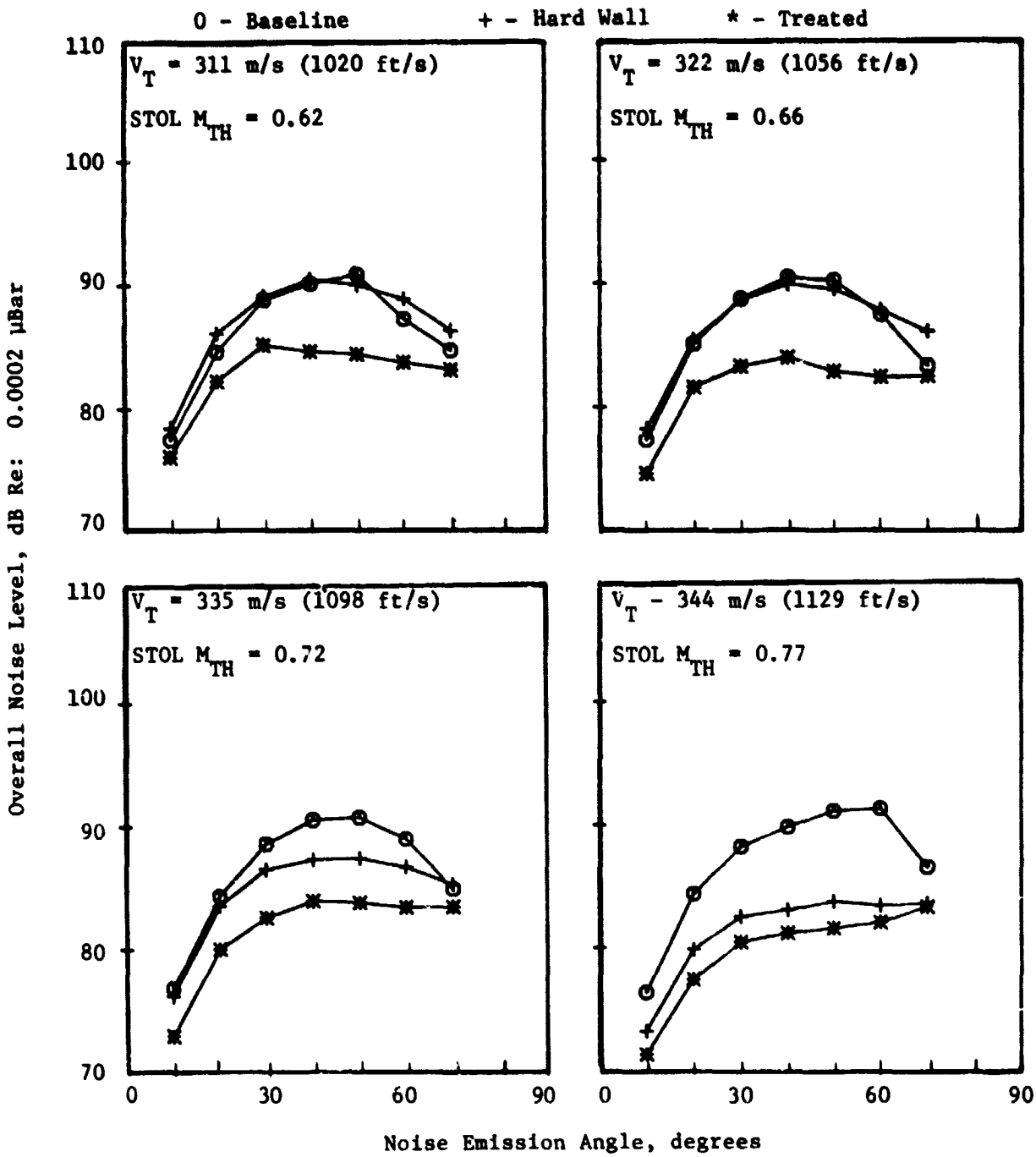

● 61 m (200 ft) Sideline

● 41 m/s (135 m/s) Forward Velocity

(b) Overall Noise

Figure 66. STOL Noise Directivity (QCSEE Size) at Forward Velocity (Concluded).

The STOL hard-wall inlet appears to have little effect on the baseline inlet noise at the low throat Mach numbers. This is the combined effect of summing the noise from 1/3-octave bands where the STOL hard-wall inlet noise was less than the baseline inlet with those that contained the increased levels due to the noise humps. At the higher throat Mach numbers the levels of those noise humps were less, and the result is a reduction of the total baseline inlet noise by the STOL hard-wall inlet.

The acoustic treatment seems to benefit the STOL inlet more than the CTOL inlet at all angles and at all values of throat Mach number. This is an indication of the relative effectiveness of the two noise-reduction mechanisms of the hybrid inlets. Flow acceleration is most effective against the rotor-alone noise, which is characterized by tones, but the acoustic treatment is most effective against the type of fan noise characterized by broadband noise.

4.5 DEFLECTOR INLET ACOUSTIC PERFORMANCE

The acoustic-performance characteristics of the deflector inlet were determined during the second wind tunnel tests. Since throat Mach number was not a test variable, all the data will be presented as a function of corrected fan-tip speed. The fan speeds for the deflector inlet were the same as those run with the baseline inlet; thus, fan-noise suppression could be determined by comparing the results of the two inlets. This provided deflector-inlet acoustic results at fan-tip speeds below as well as above the point where the rotor-alone noise is dominant. The hard-wall and treated deflector-inlet results are compared with those from the baseline inlet at a forward velocity of 41 m/s (135 ft/s). The effects of angle of attack and forward velocity on the treated-deflector-inlet noise characteristics are then discussed.

4.5.1 Comparisons with Baseline Inlet

As with the hybrid inlets, the fan-noise suppression results are presented as absolute sound pressure levels derived from 1/3-octave-band analysis and plotted versus noise emission angle or frequency. Emphasis in the analysis of the actual JT15D data will be on the frequency region containing the blade-passing tone and on the 1/3-octave-band noise spectra at selected angles. When the results are scaled up to large turbofan engine size for comparison with those from other deflector inlets, the emphasis is shifted to extrapolated overhead perceived noise levels (PNL) and overall sound pressure levels (OASPL).

The BPF 1/3-octave-band directivity patterns for four corrected fan-tip speeds are presented in Figure 67 for the baseline and deflector inlets. The shapes of the patterns for the baseline inlet at low tip speeds are typical of broadband noise because, as previously discussed, it dominates the BPF 1/3-octave band at all angles even though the rotor-alone tone is present at the higher angles. However, as soon as the per rev tones from the rotor-alone noise become dominant, the directivity pattern changes dramatically with a

ORIGINAL PAGE IS
OF POOR QUALITY

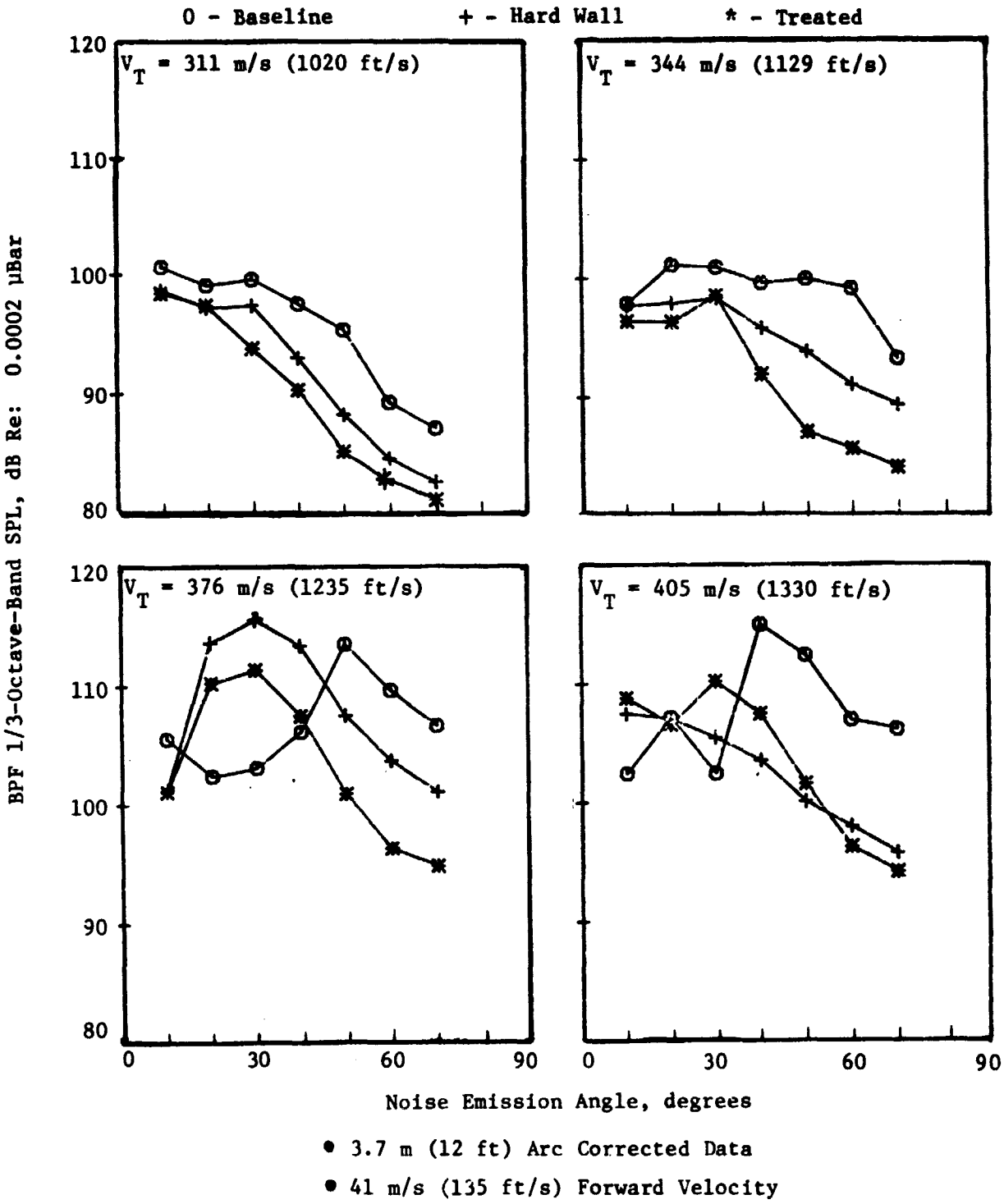

- 3.7 m (12 ft) Arc Corrected Data
- 41 m/s (135 ft/s) Forward Velocity

Figure 67. Blade-Passing-Frequency, 1/3-Octave-Band Noise Directivity for Baseline and Deflector Inlets at Forward Velocity.

sharp peak forming near 50° and moving toward the axis as the tip speed increases. The effect the hard-wall deflector inlet has on these patterns is to translate them to the left so that the peaks appear at lower angles due to redirecting the noise. This has the effect of considerable noise reduction at the higher angles. The addition of acoustic treatment provides further noise reduction at the high angles, particularly at the low fan-tip speeds. To determine if these trends occcur at all frequencies, the 1/3-octave-band spectra for three noise-emission angles at a low and a high fan-tip speed are presented in Figure 68.

The baseline-inlet 1/3-octave-band spectra at the low tip speed are reduced at all frequencies, for the angles shown, by the hard-wall deflector inlet. This indicates that all the noise for each angle is redirected to lower angles. The acoustic treatment then reduces the noise more or less uniformly at all frequencies to increase the effective suppression at each angle. At the high tip speed the effects of the deflector inlet on the baseline noise are quite different. The frequencies below BPF that are dominated by rotor-alone per rev tones do not show the same redirection characteristics as the BPF. These levels appear to remain unchanged at the higher angles by the redirection process. However, when acoustic treatment is added there is substantial reduction of the per rev tone noise at all angles; this was not the case with the BPF tone.

4.5.2 Angle-of-attack Effects

The effects of angle of attack on the 1/3-octave-band noise spectra for the treated deflector inlet are shown in Figure 69 for four fan-tip speeds. Unlike the hybrid inlets, the deflector inlet shows notable change in the spectral levels at all forward angles, particularly at high fan speeds, when the deflector inlet is operated at angle of attack. The noise levels are generally increased with angle of attack, but no consistent trend with frequency or noise-emission angle are apparent. Considering that there were no signficant changes in recovery or distortion of the inlet total pressures at angle of attack (see Figure 46), there appears to be no reason for the changes in noise. However, the deflector inlet does cause a signficant distortion in static pressure at the fan entrance due to asymmetry of the flow field into the inlet. This static pressure distortion is shown in Figure 70 to be slightly altered in level at all angels and in shape at the top or shortest part of the inlet due to adjustment in the flow field at angle of attack. In the following discussion on the canted baseline inlet, the presence of static pressure distortion at the fan entrance is shown to alter the baseline-inlet noise characteristics. If static pressure distortion is responsible for noise, then changes in the distortion, such as with the deflector inlet at angle of attack, can change that noise.

ORIGINAL PAGE IS
OF POOR QUALITY

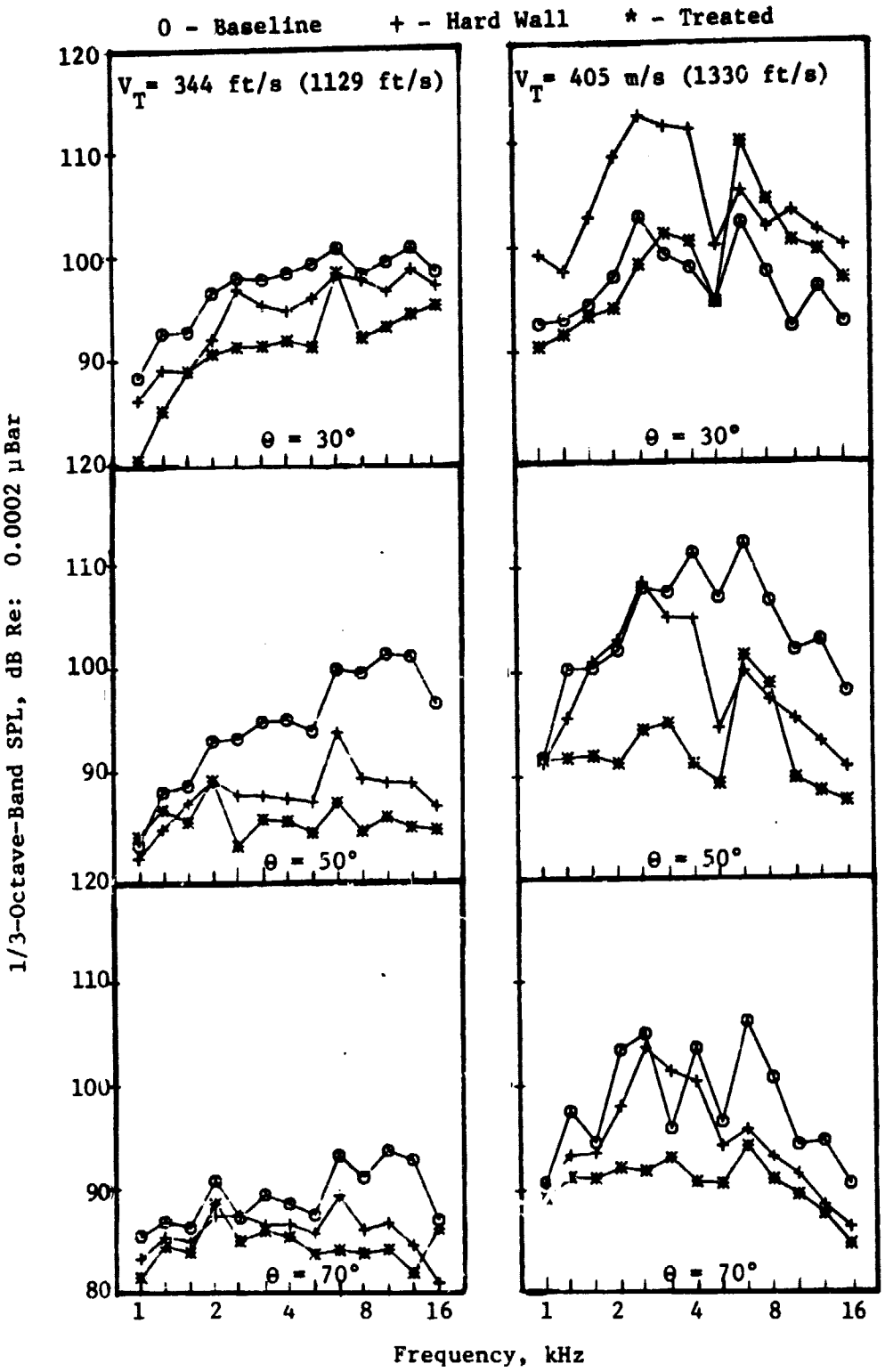

● 3.7 m (12 ft) Arc Corrected Data

Figure 68. One-Third-Octave-Band Noise Spectra for Baseline and Deflector Inlets at 41 m/s (135 ft/s) Forward Velocity.

ORIGINAL PAGE IS
OF POOR QUALITY

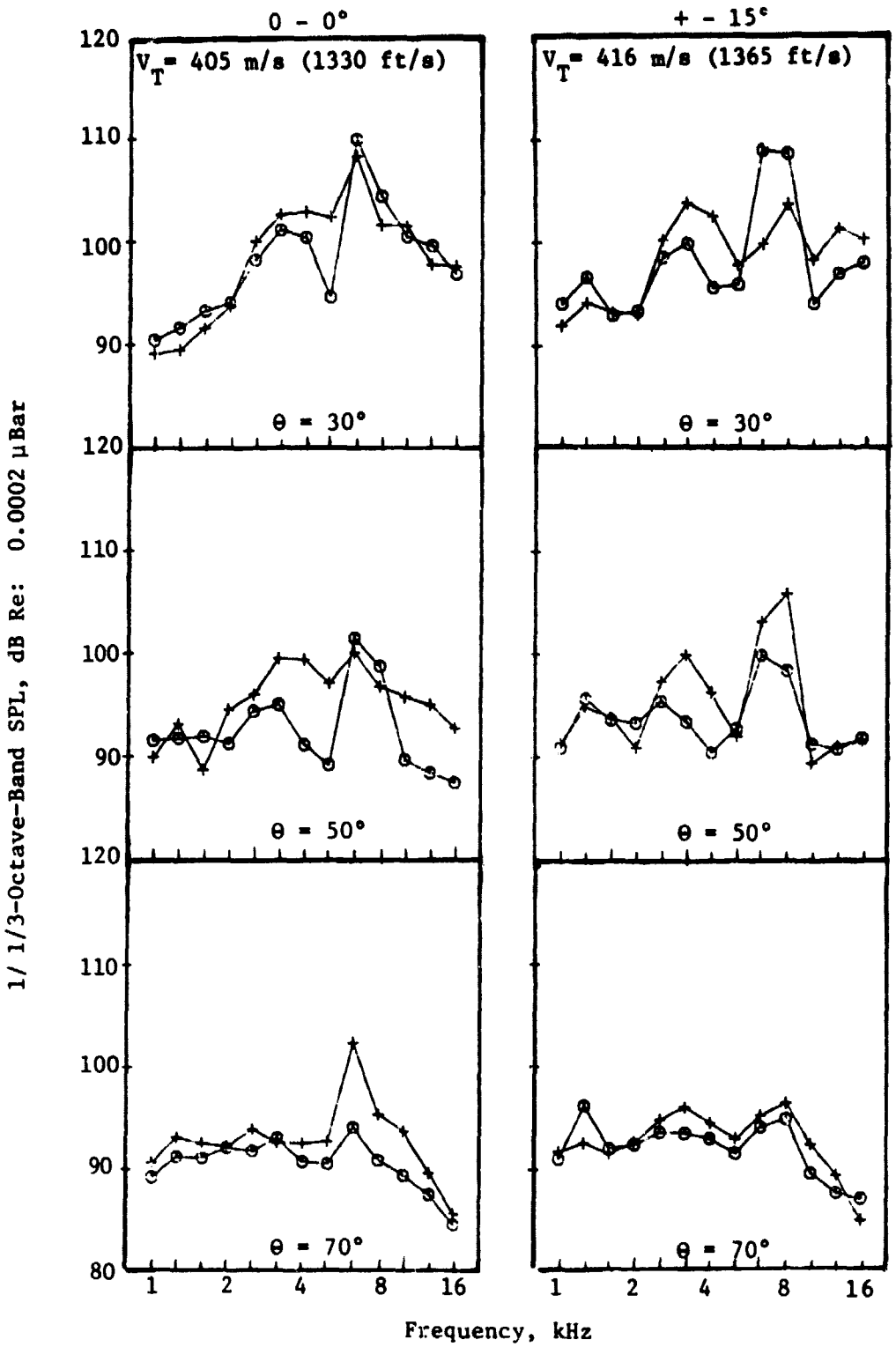

● 3.7 m (12 ft) Arc Corrected Data
● 41 m/s (135 ft/s) Forward Velocity

Figure 69. One-Third-Octave-Band Noise Spectra for Deflector Inlet at Two Angles of Attack.

ORIGINAL PAGE IS
OF POOR QUALITY

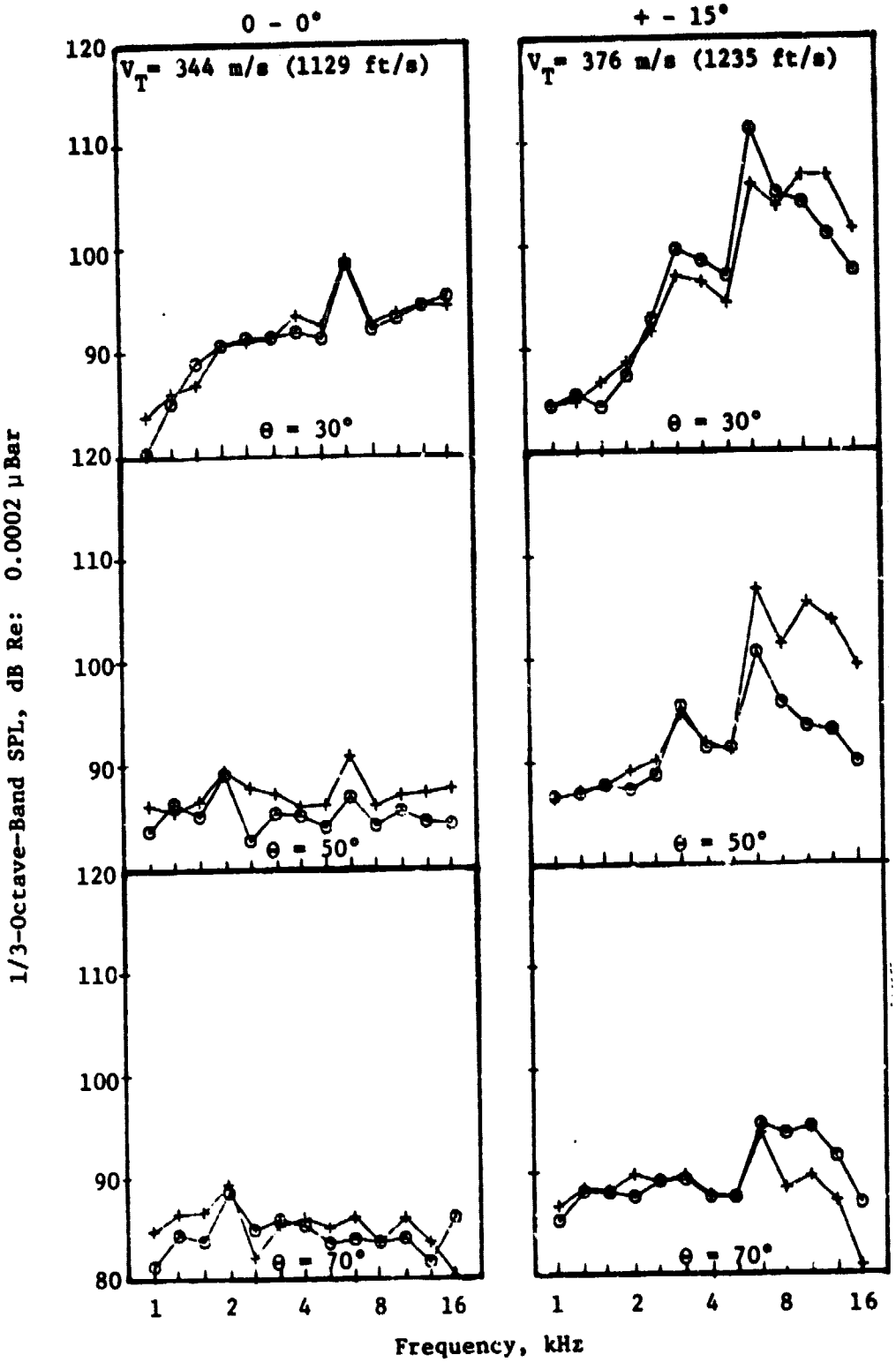

● 3.7 m (12 ft) Arc Corrected Data
● 41 m/s (135 ft/s) Forward Velocity

Figure 69. One-Third-Octave-Band Noise Spectra for Deflector Inlet at Two Angles of Attack (Concluded).

ORIGINAL PAGE IS
OF POOR QUALITY

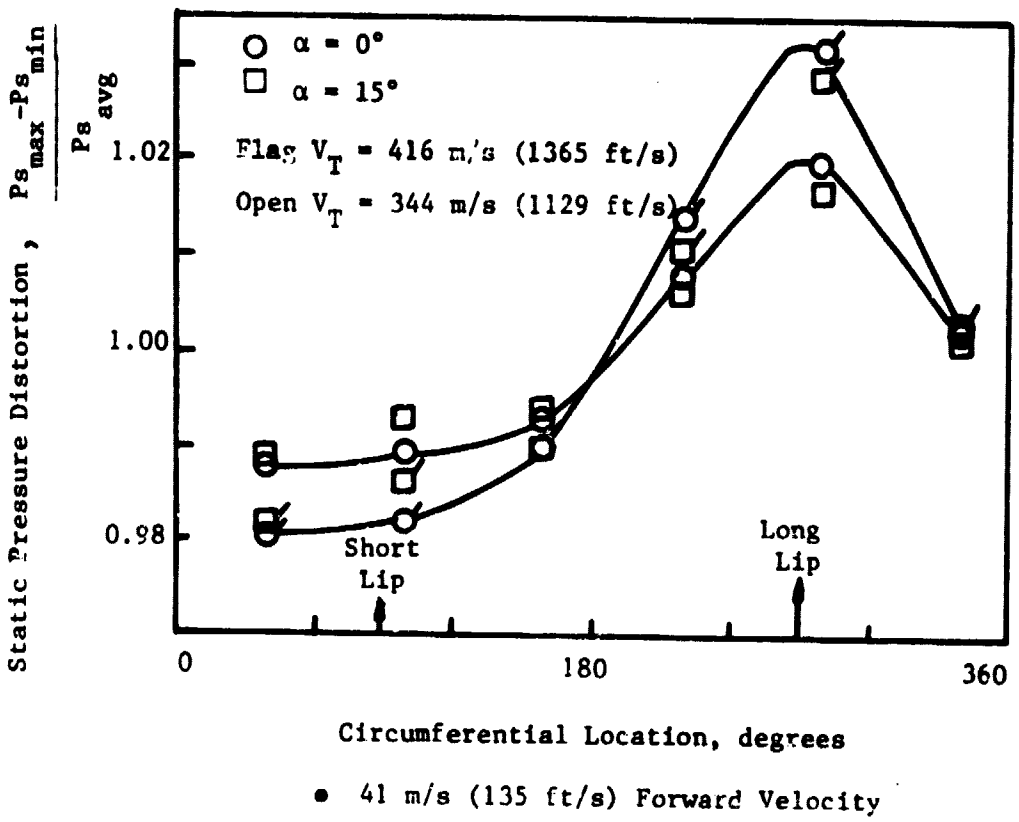

● 41 m/s (135 ft/s) Forward Velocity

Figure 70. Deflector Inlet Fan Entrance Static Pressure Distortion at Two Angles of Attack.

4.5.3 Forward-Velocity Effects

Since the static pressure distortion from the deflector inlet is sensitive to changes in inlet flow field caused by angle of attack, the changes in forward velocity might have similar effects. The static pressure distortion at the fan entrance is shown in Figure 71 to be slightly reduced in level as the forward velocity is increased. As was expected, the fan-noise characteristics of the treated deflector inlet are also changed with forward velocity. The 1/3-octave-band spectra shown in Figure 72 for the three noise-emission angles are notably changed at all fan speeds when the forward velocity is increased. Again there are no particular trends with frequency or angle to the noise level changes.

4.5.4 Effects on Large-Scale-Fan Noise

The noise data for the baseline and deflector inlets have been scaled up to a CF6 size turbofan engine and extrapolated to a distance 61 m (200 ft) parallel to the centerline and directly below the longest part of the deflector inlet. This distance is referred to as the overhead distance since this extrapolation simulates the noise an observer would hear from an aircraft, with deflector inlets, flying directly overhead. The perceived noise and overall noise-directivity patterns resulting from this scaling and extrapolation are shown in Figure 73 for four corrected fan speeds. The redirection effect of the hard-wall deflector inlet in producing fan-noise reduction at the higher angles is very evident. The noise reduction due to the addition of treatment is fairly uniform at each fan speed.

To compare the fan-noise-suppression capability of all the advanced inlets, the hybrid-inlet results were plotted along with the deflector-inlet results in Figure 74. The baseline-inlet data are the same for all three inlets, as are the treated-aft-diffuser and the JT15D fan-noise-source data. As might be expected, the hybrid inlets provide more fan-noise suppression, particularly at low noise-emission angles. The CTOL hybrid inlet is more effective for suppressing the high-tip-speed fan noise at all angles and virtually all frequencies due to the effects of flow acceleration on this type of fan noise. However, the deflector inlet appears to provide as much fan-noise suppression at low fan-tip speeds for the higher noise-emission angles as the STOL hybrid inlet. This is true at all frequencies with the deflector inlet providing more suppression in those frequency bands containing the humps of broadband noise caused by the STOL inlet. These results further indicate that treatment is more effective than flow acceleration for suppression of the broadband noise from low-tip-speed fans.

4.6 CANTED-BASELINE-INLET ACOUSTIC CHARACTERISTICS

One feature of actual aircraft inlets, rarely simulated in inlet/fan-noise testing, is the forward cant of the inlet centerline relative to the engine centerline prevalent in wing-mounted-engine inlet design. The inlet

ORIGINAL PAGE IS
OF POOR QUALITY

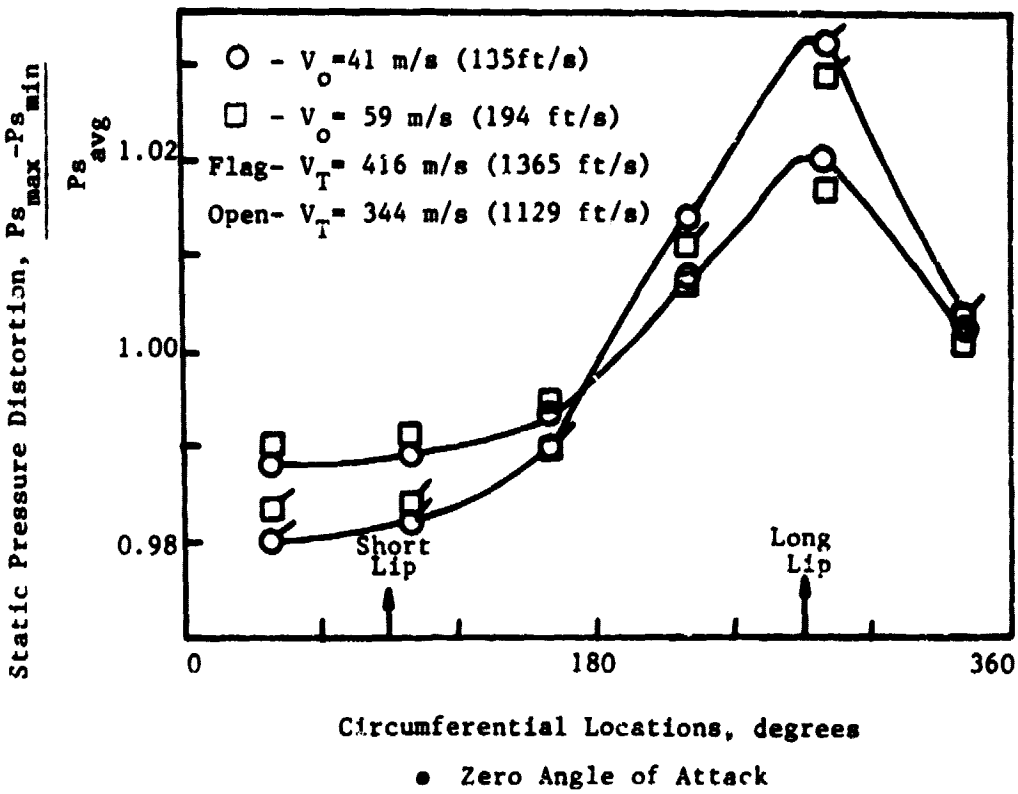

Figure 71. Deflector Inlet Fan Entrance Static Pressure Distortion at Two Forward Velocities.

ORIGINAL PAGE IS
OF POOR QUALITY

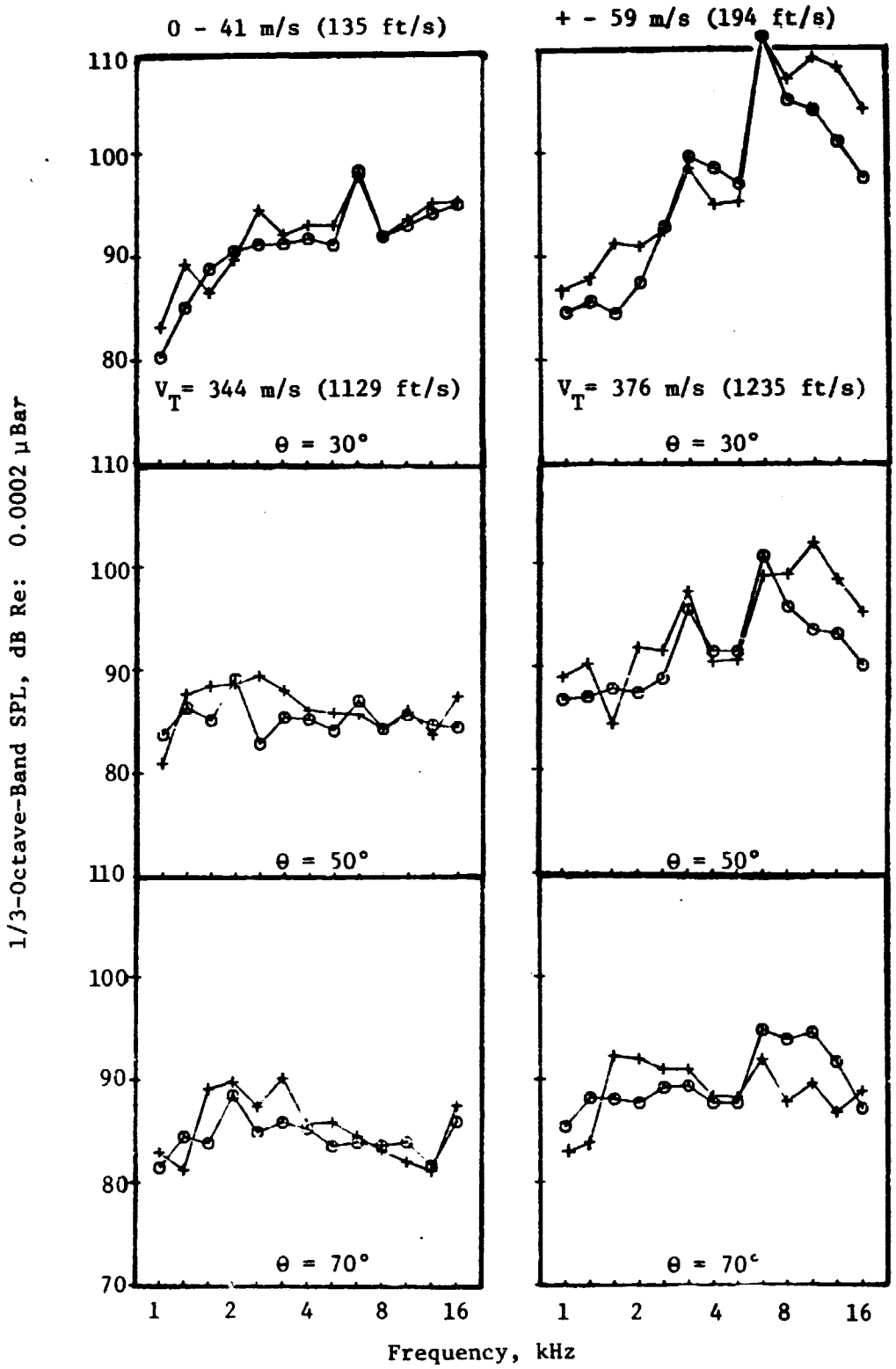

● 3.7 m (12 ft) Arc Corrected Data

Figure 72. One-Third-Octave-Band Noise Spectra for Deflector Inlet at Two Forward Velocities.

ORIGINAL PAGE IS
OF POOR QUALITY

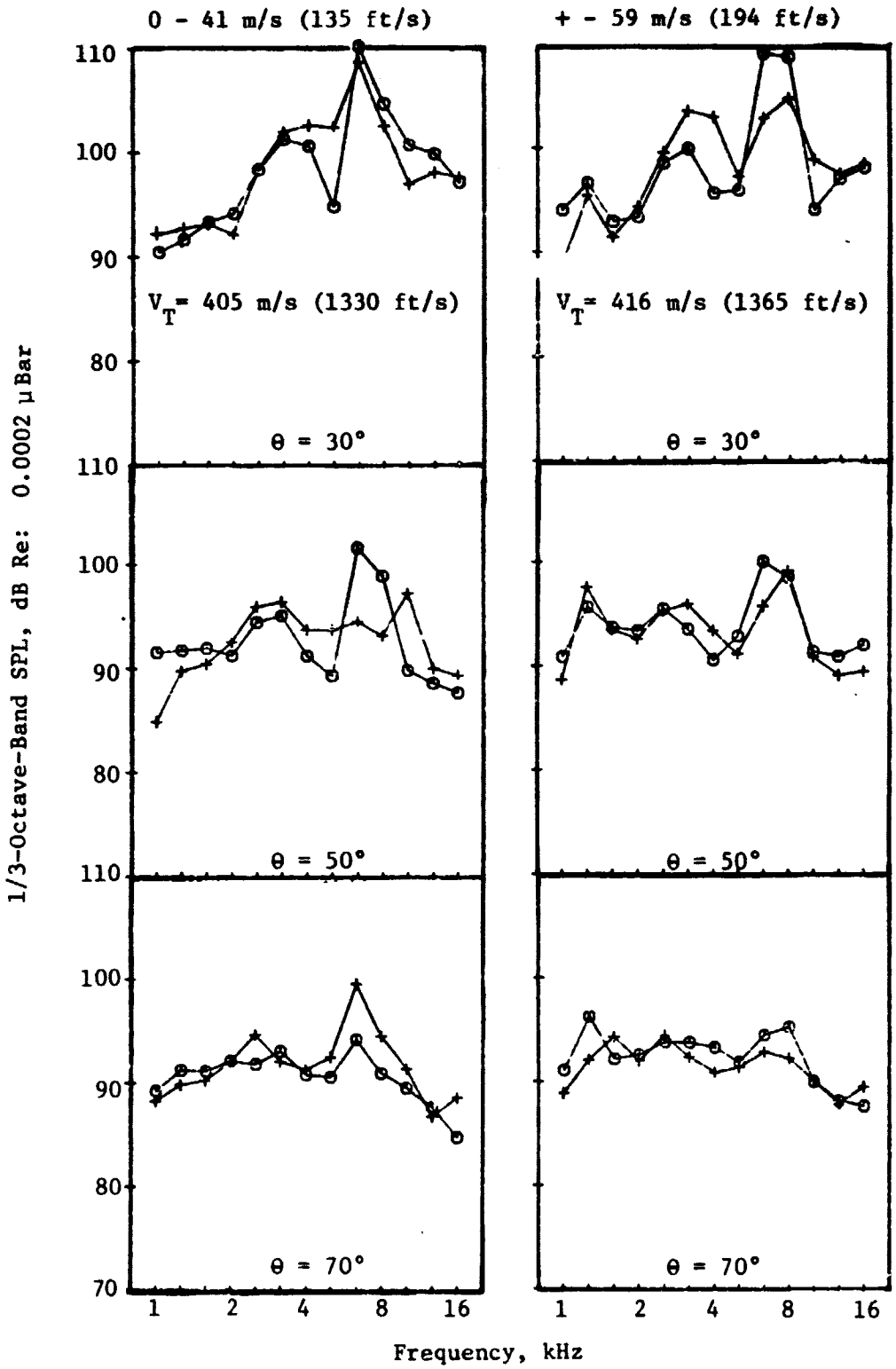

● 3.7 m (12 ft) Arc Corrected Data

Figure 72. One-Third-Octave-Band Noise Spectra for Deflector Inlet at Two Forward Velocities (Concluded).

ORIGINAL PAGE IS
OF POOR QUALITY

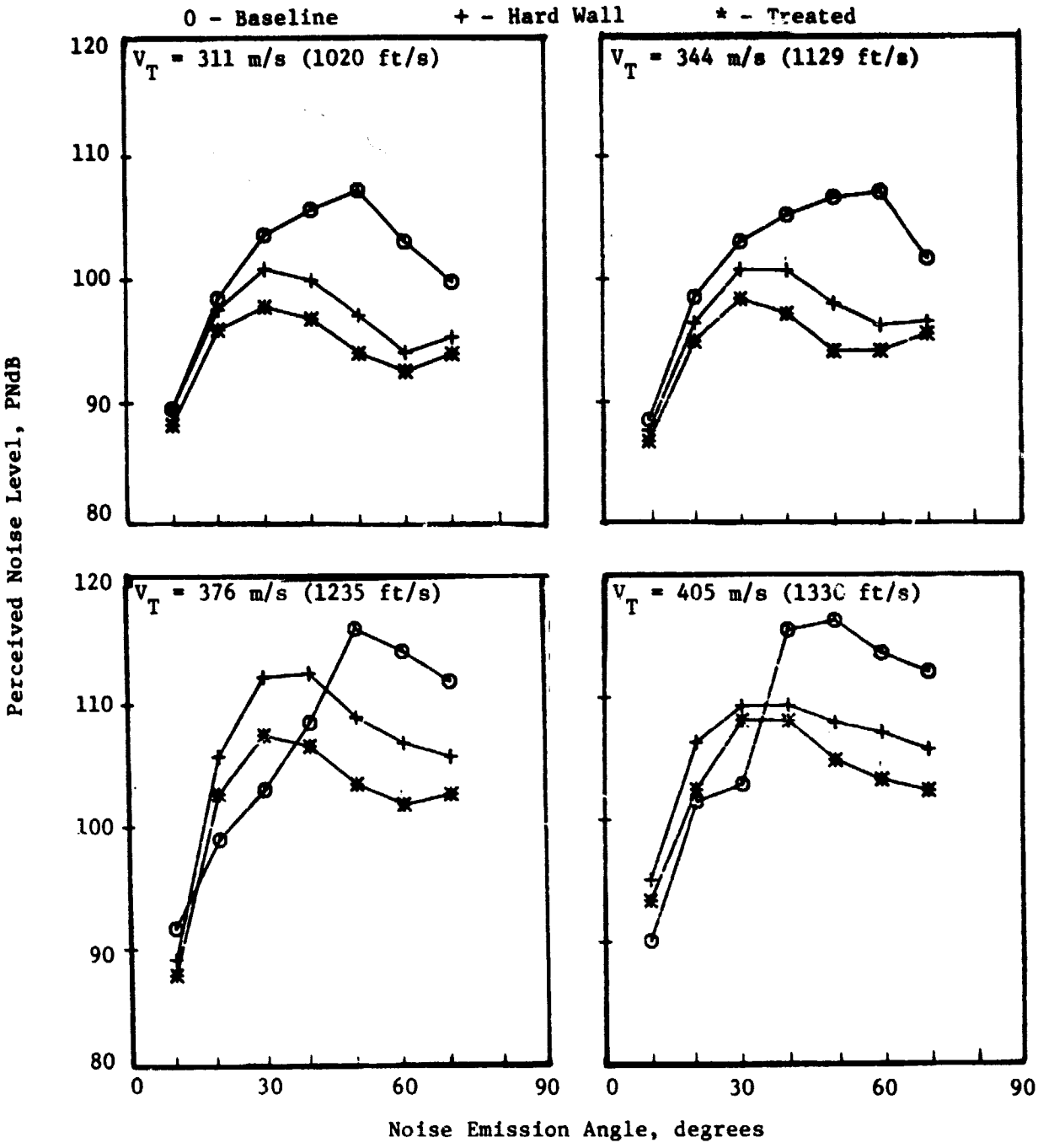

- 61 m (200 ft) Overhead
- 41 m/s (135 ft/s) Forward Velocity

(a) Perceived Noise

Figure 73. Deflector Inlet Noise Directivity (CF6 Size) at Forward Velocity.

ORIGINAL PAGE IS
OF POOR QUALITY

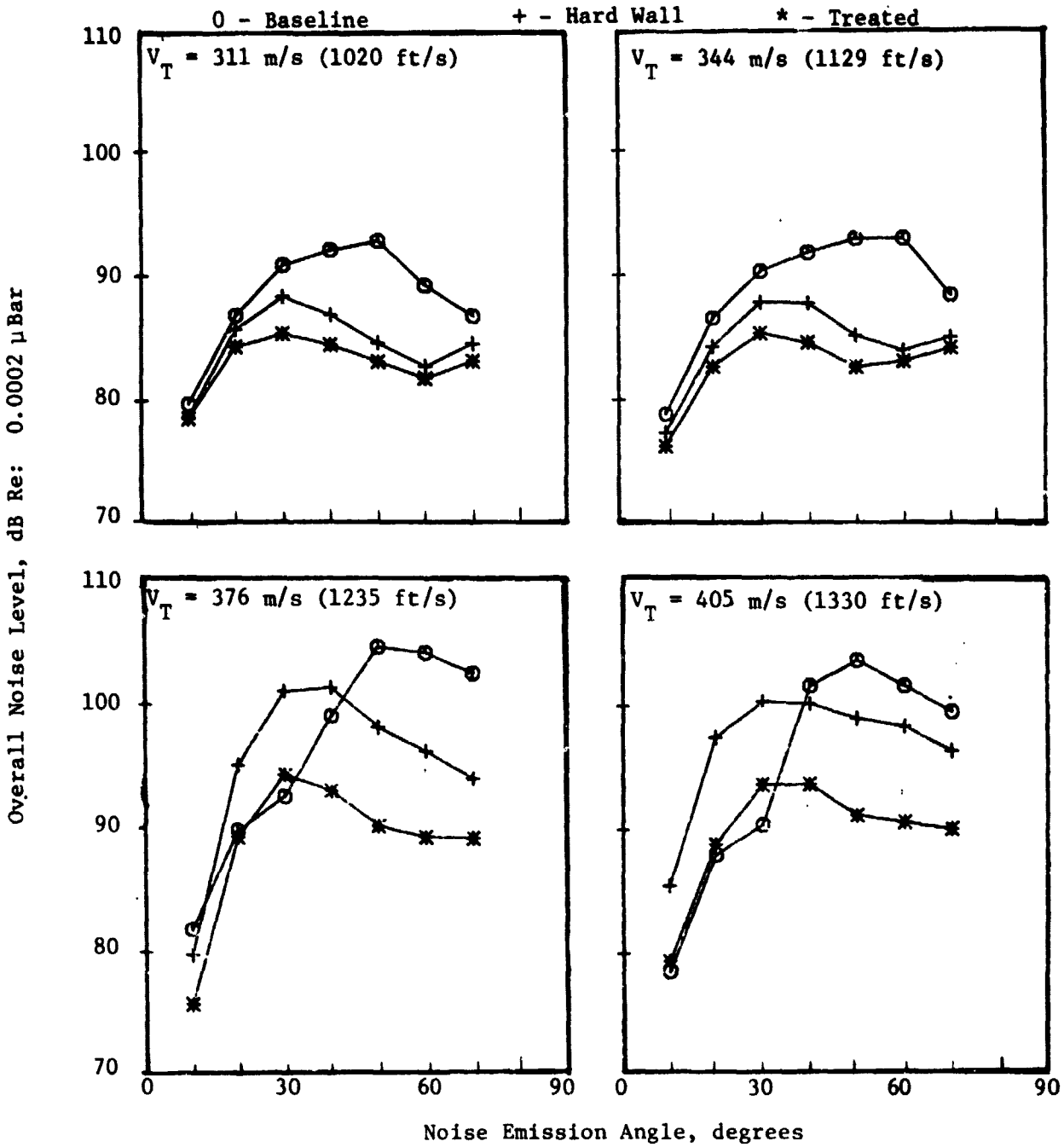

- 61 m (200 ft) Overhead
- 41 m/s (135 ft/s) Forward Velocity

(b) Overall Noise

Figure 73. Deflector Inlet Noise Directivity (CF6 Size) at Forward Velocity (Concluded).

ORIGINAL PAGE IS
OF POOR QUALITY

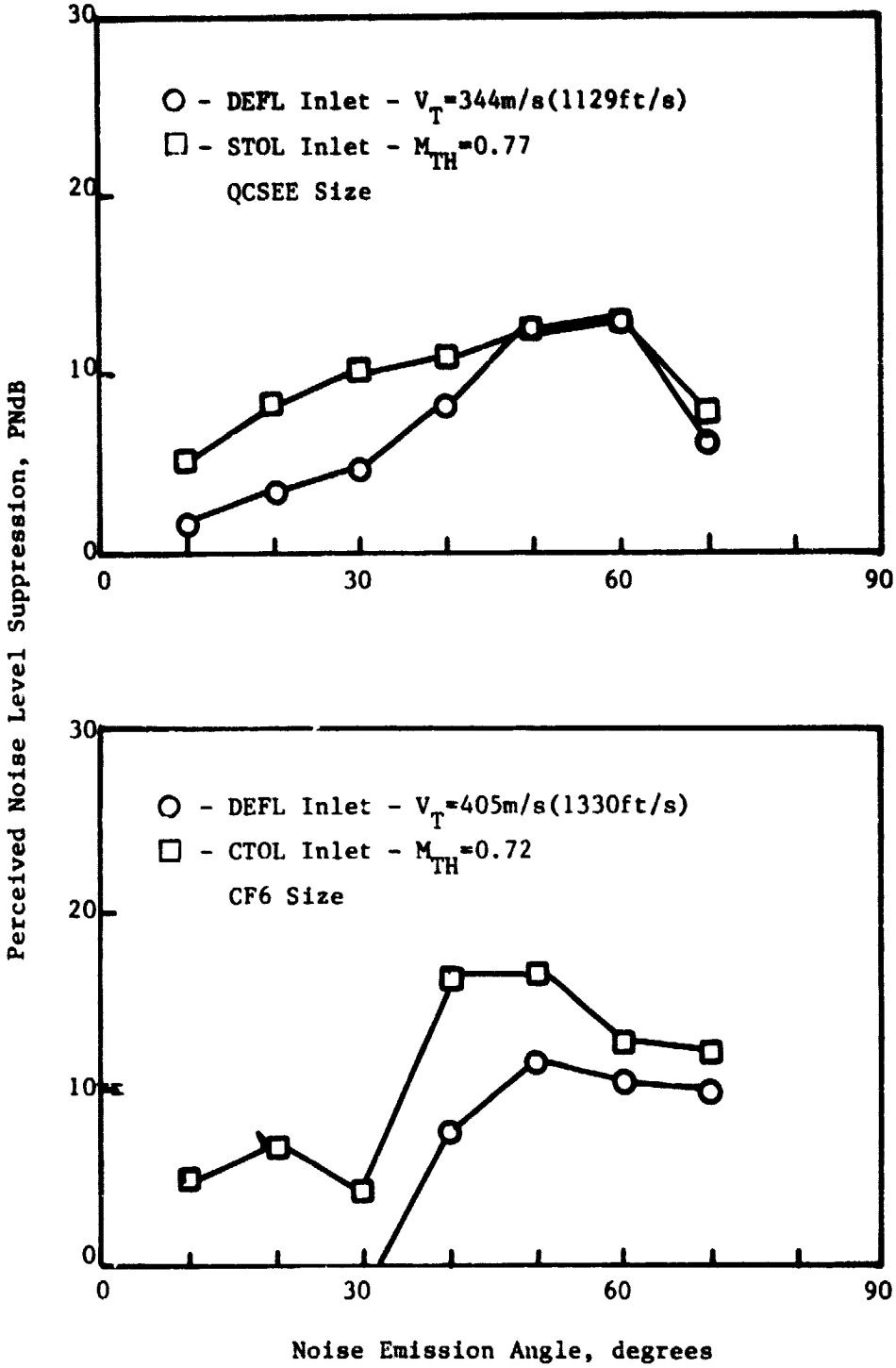

- 61 m (200ft) Sideline or Overhead
- 41 m/s (135ft/s) Forward Velocity

(a) PNL Suppression Directivity

Figure 74. Advanced Inlets Fan Noise Suppression Comparison.

ORIGINAL PAGE IS
OF POOR QUALITY

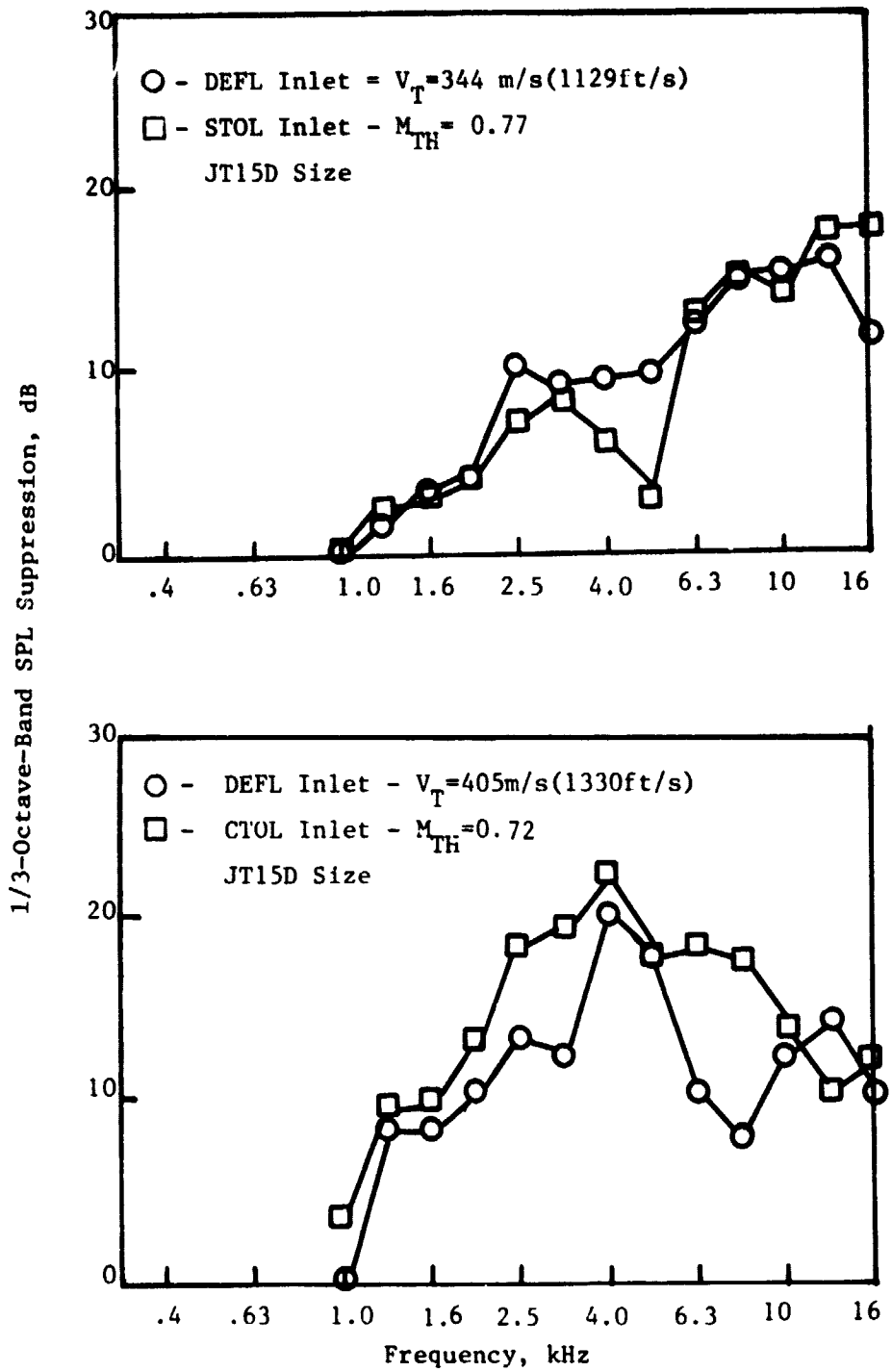

- 50° Noise Emission Angle
- 41m/s(135ft/s) Forward Velocity

(b) SPL Suppression Spectra

Figure 74. Advanced Inlets Fan Noise Suppression Comparison (Concluded).

opening is canted downward 3° to 5° by the aircraft manufacturer to minimize the propulsion system installed performance losses due to the upward flow component, ahead of the engine, imposed by the wing flow field. Although there is no significant fan-entrance total pressure recovery or distortion effects due to canting the inlet, there is a circumferential distortion in the inlet wall static pressure. The level of static pressure distortion has been measured in-flight, on an actual aircraft inlet, to be as much as 5% with a circumferential shape as shown in Figure 75. Since this distortion is at the discharge of the inlet and is due to flow turning, within the inlet to the fan, the levels and shapes of the distortion are dependent upon the inlet internal aerodynamics and not on forward velocity and angle of attack.

To determine if canting the inlet has potential for changing fan noise, a simple wedge was built to cant the baseline inlet 4° downward (see Figure 22). The canted baseline inlet was installed on the JT15D on the 40 by 80 (see Figure 23) and run at a forward velocity of 41 m/s (135 ft/s). The configuration with the aeroacoustic lip was also tested outdoors. Additional pressure taps installed in the wedge (see Figure 29) measured the static pressure distortion just ahead of the fan, and the data are presented in Figure 75. The canted-baseline-inlet static pressure distortion has the characteristic one-per-rev shape and a slightly lower level than was measured in the aircraft inlet. The effects of the static pressure distortion on fan noise are best shown by comparing the canted-baseline-inlet results with those from the baseline inlet.

4.6.1 Comparisons with Baseline Inlet

To compare the effects of canting the baseline inlet on fan noise, the baseline-inlet narrowband BPF tone peak level variation with fan tip speed (Figure 51a) is compared with the same data from the canted baseline inlet in Figure 76. The peak BPF tone levels for both inlets in the 40 by 80 are virtually the same at the lowest and highest fan speeds and undergo a large (20 dB) increase as fan speed is increased. However, the canted-baseline-inlet BPF tone peak level starts increasing and reaches a maximum level at lower fan speeds than the baseline inlet. These changes in noise level are the same for both 0° and 4° angle-of-attack conditions. Note that the changes in the baseline-inlet noise due to canting the inlet are completely obscured by the variations in the rotor-turbulence noise in the outdoor static test data. The explanation of the large increase in BPF tone level for the baseline inlet is that the rotor-alone noise begins to dominate above sonic fan-tip speed. The canted inlet causes a circumferential static pressure distortion into the fan rotor, and this is another source of BPF tone noise. Because this distortion is not purely sinusoidal, the various orders of distortion components interact with the rotor to produce BPF tone noise at subsonic fan-tip speeds. The BPF tone levels begin to increase for the canted baseline inlet as this noise begins to propagate until the rotor-alone noise becomes dominant.

ORIGINAL PAGE IS
OF POOR QUALITY

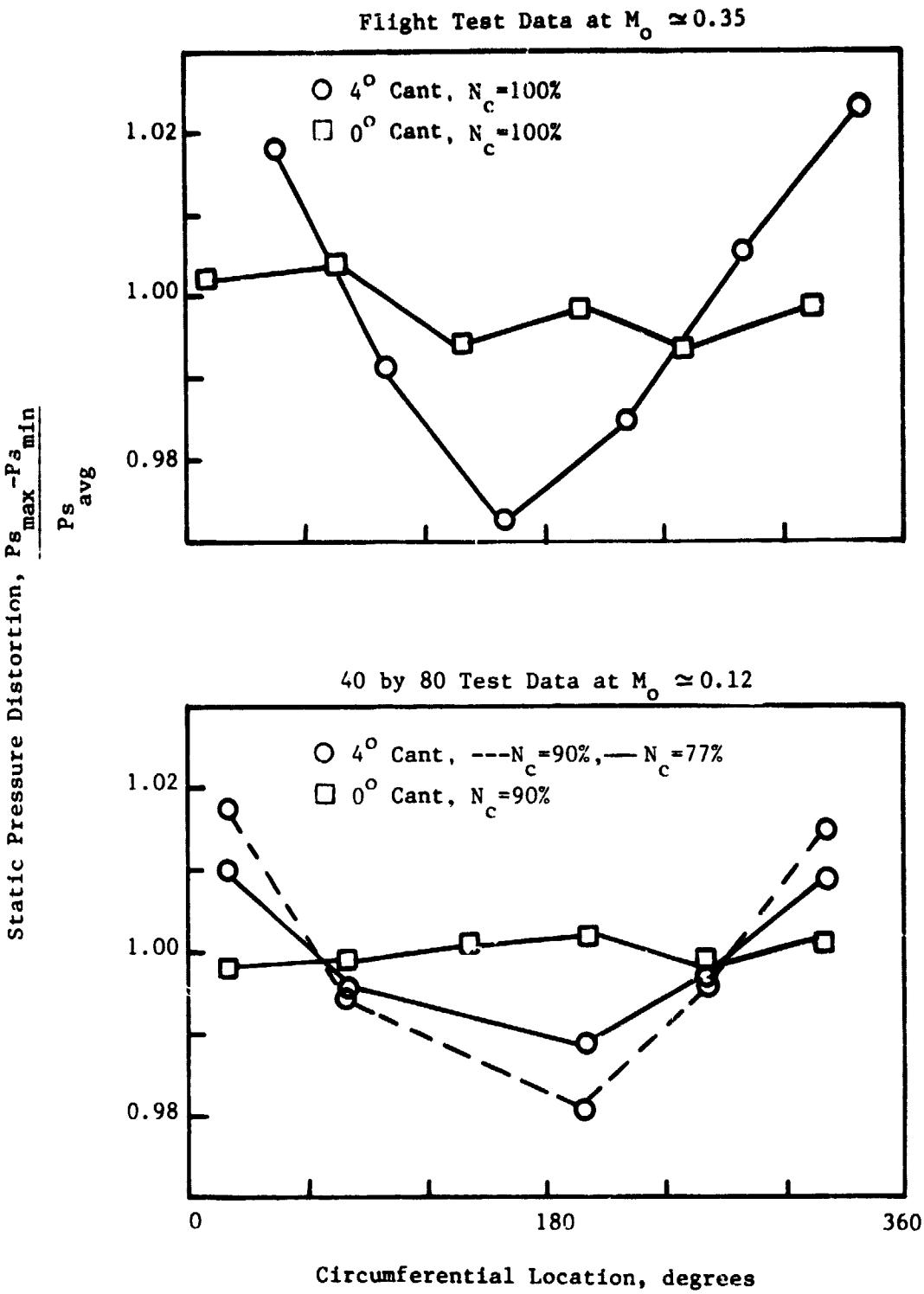

Figure 75. Canted-Inlet Effect on Fan Entrance Static Pressure.

ORIGINAL PAGE IS
OF POOR QUALITY

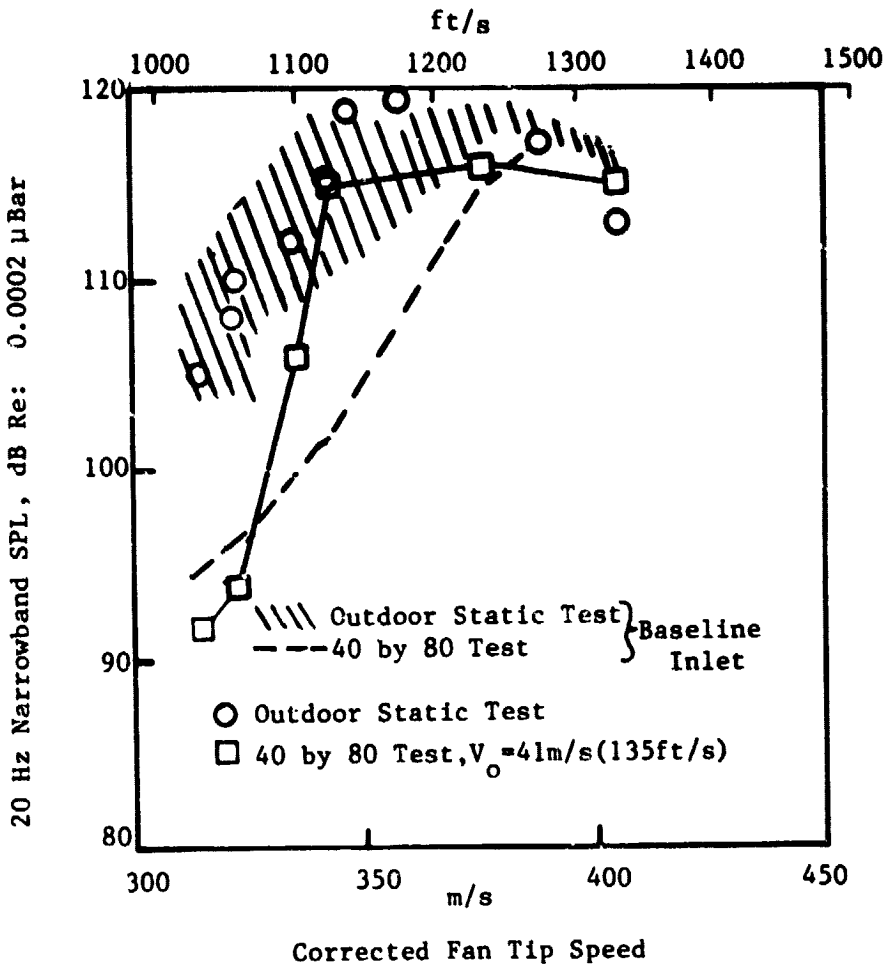

- 3.7 m (12ft) Arc Uncorrected Data
- Peak SPL Angle

Figure 76. Narrowband BPF Noise Level Variation with Fan Speed for Canted Baseline Inlet.

To determine if canting the baseline inlet affects the noise at other frequencies, the 0 to 10 kHz narrowband spectra from both inlets at three noise-emission angles are shown in Figure 77 for the fan speed where BPF tone level separation was the greatest. The presence of tones in the spectra at other than BPF along with the increased BPF tone levels are indications that the static pressure distortion from the canted baseline inlet is indeed interacting with the rotor to generate fan tone noise. This additional noise level is more apparent where the comparisons are made with the 1/3-octave-band spectra.

The 1/3-octave-band spectra for the lowest fan speed and the fan speed that has the greatest canted-inlet effects are presented in Figure 78 for three noise-emission angles. Canting the baseline inlet appears to make no significant difference in any of the 1/3-octave-band noise levels at the low fan-tip speed where the distortion-interaction noise propagation hasn't yet started. However, at the fan speed that showed the most increase in narrowband BPF tone level, the canted baseline inlet causes considerable noise level increases in the 1/3-octave bands below BPF and at twice BPF as well as at BPF for angles of 50° and higher. The BPF 1/3-octave-band noise-level directivity patterns in Figure 79 confirm that the noise levels at angles above 40° are most affected at tip speeds where a downward cant of 4° changed the baseline-inlet noise characteristics.

4.6.2 Effects on Large-Scale-Fan Noise

The question of how much change in large-scale-turbofan noise characteristics will be caused by canting the aircraft inlet still remains unanswered. A partial answer is provided in Figure 80 where the CF6 size turbofan noise directivity for the canted baseline inlet and the baseline inlet are compared. There appear to be very minor changes in either perceived noise or overall noise levels due to canting the inlet at low fan speeds where rotor-distortion noise or the rotor-alone noise is propagating and at high fan speeds where the rotor-alone noise dominates all other fan-noise sources. However, in the range of fan speeds where the rotor-distortion noise is propagating with more strength than the rotor-alone noise, the canted baseline inlet, with its static pressure distortion into the fan, causes as much as 7 PNdB more noise at the critical sideline angles of 50° to 60°. This is a critical fan-speed range in terms of fan noise because current turbofan engines operate at these fan speeds during approach to landing. Whether canting an actual aircraft inlet generates as much additional fan noise as canting the baseline inlet remains to be determined, but the presence of fan noise due to a circumferential distortion of the static pressures entering a fan has been clearly demonstrated.

ORIGINAL PAGE IS
OF POOR QUALITY

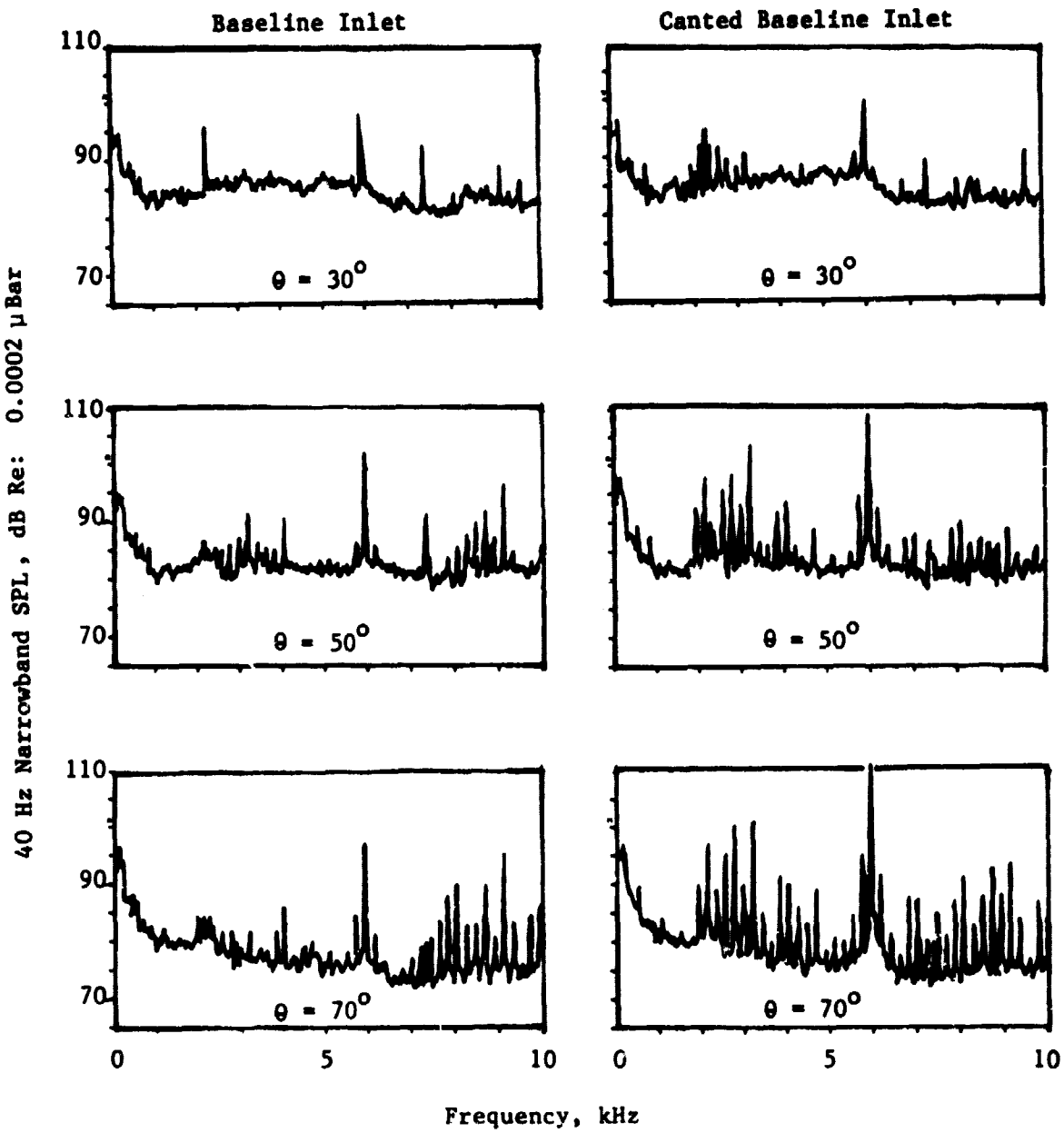

- 3.7 m(12ft) Arc Uncorrected Data
- 41 m/s(135 ft/s) Forward Velocity

Figure 77. Narrowband Spectra for Baseline Inlet and Canted Baseline Inlet at V_T = 344 m/s (1129 ft/s).

ORIGINAL PAGE IS
OF POOR QUALITY

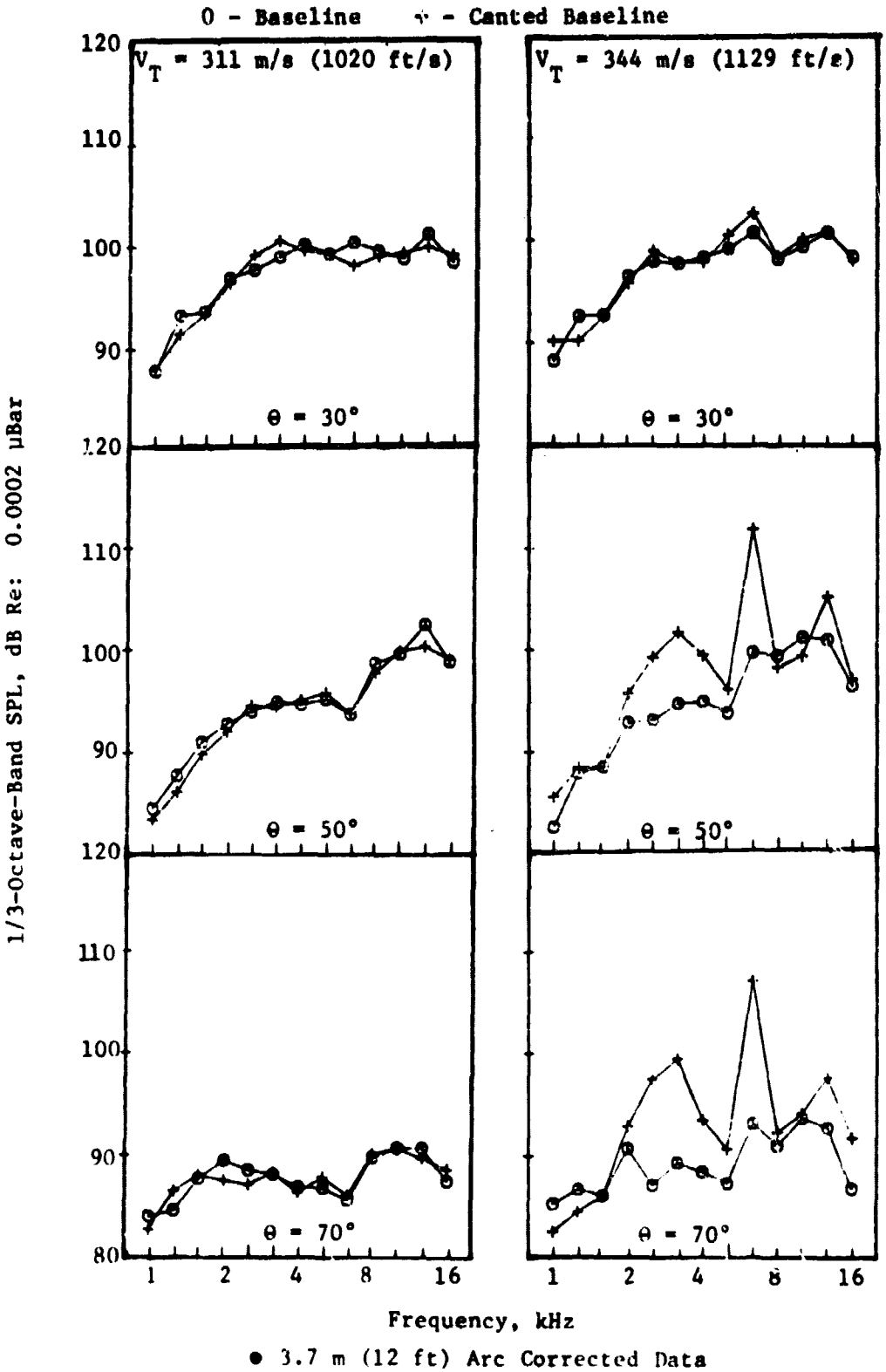

Figure 78. One-Third-Octave-Band Noise Spectra for Baseline and Canted Baseline Inlets at 41 m/s (135 ft/s Forward Velocity.

ORIGINAL PAGE IS
OF POOR QUALITY

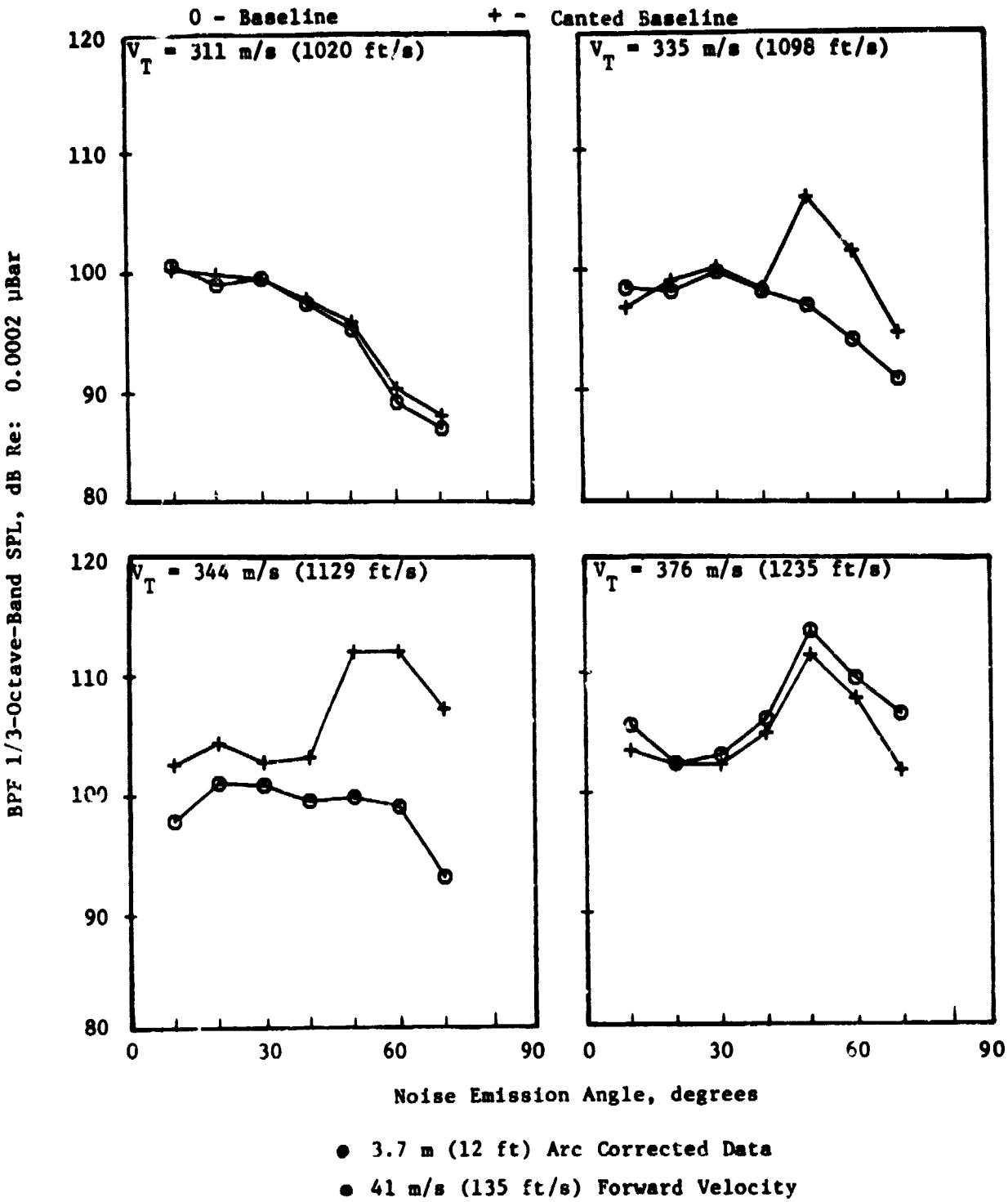

Figure 79. Blade-Passing-Frequency, 1/3-Octave-Band Noise Directivity for Baseline and Canted Baseline Inlets at Forward Velocity.

ORIGINAL PAGE IS
OF POOR QUALITY

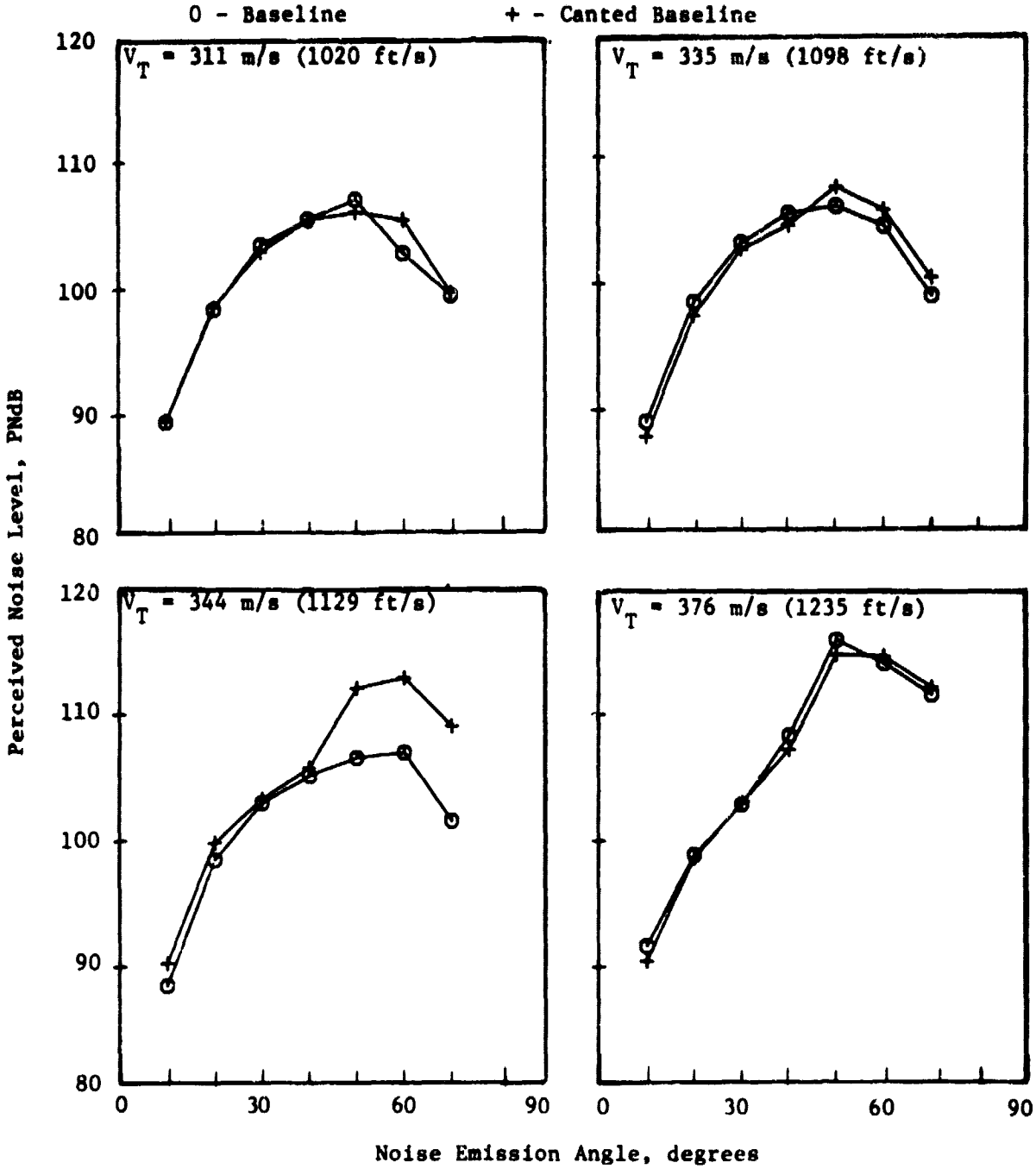

- 61 m (200 ft) Overhead
- 41 m/s (135 ft/s) Forward Velocity

(a) Perceived Noise

Figure 80. Canted-Baseline-Inlet Noise Directivity (CF6 Size) at Forward Velocity.

ORIGINAL PAGE IS
OF POOR QUALITY

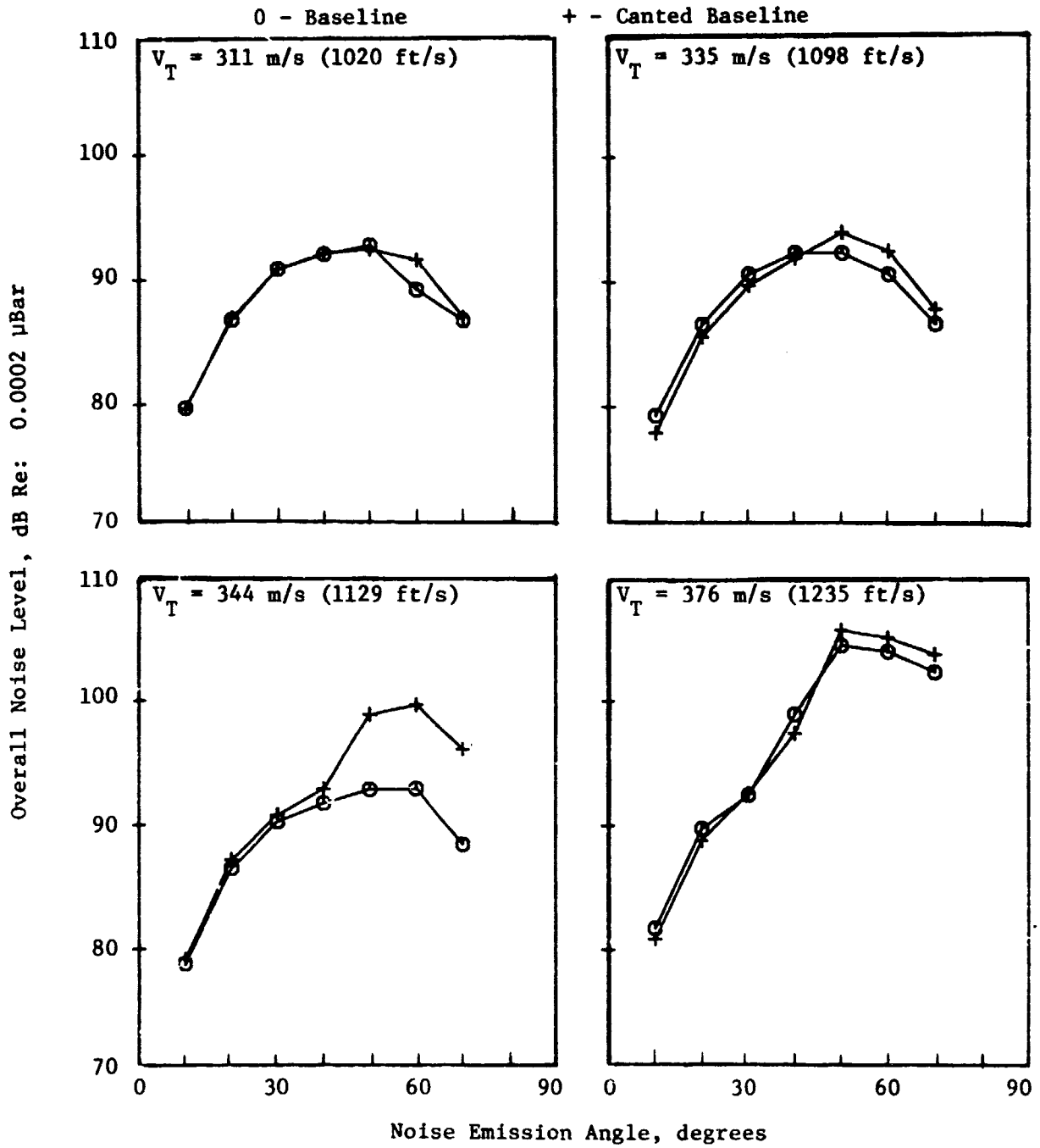

- 61 m (200 ft) Overhead
- 41 m/s (135 ft/s) Forward Velocity

(b) Overall Noise

Figure 80. Canted-Baseline-Inlet Noise Directivity (CF6 Size) at Forward Velocity (Concluded).

5.0 CONCLUSIONS AND RECOMMENDATIONS

Many observations were made during the analysis of the data from the outdoor static and wind tunnel tests and the subsequent presentation of the results. The more significant of these have been grouped into specific areas for discussion. These areas include the fan-noise testing and data acquisition in the simulated-flight environment as well as the suppression of fan noise by advanced inlets.

5.1 FAN-NOISE TESTING TECHNIQUES

There has been recent emphasis placed on fan-noise testing because of the need to further reduce engine noise to meet more rigid requirements. Since recent measurements of fan noise in the actual flight environment have produced results that are quite different than those obtained in static tests, there has also been emphasis placed on the understanding and prediction of static-to-flight effects on fan noise. The results of Hodder's (Reference 2) work and this investigation have led to the main conclusion in the area of fan-noise testing techniques:

- Removal of the noise caused by the interaction of atmospheric or test chamber turbulence with the fan is essential in order to properly assess the sources of fan noise and suppression effects of advanced inlets that will occur in the flight environment.

With the variability of the fan tones generated by the rotor-turbulence interaction during static testing, there doesn't appear to be an accurate method of predicting static-to-flight effects. Two very important noise-source mechanisms would have gone completely undetected had testing the JT15D in a simulated-flight environment not been performed. The tone noise caused by the core inlet guide vanes is one, and the static pressure distortion interaction with the fan is the other.

5.2 FORWARD-VELOCITY TESTING IN THE 40 BY 80

The results of the baseline-inlet and hybrid-inlet testing at forward velocity in the 40 by 80 confirm the following conclusion of Gliebe (Reference 6):

- The NASA ARC 40 by 80 wind tunnel adequately simulates forward-velocity effects on fan noise at velocities of 21 m/s (68 ft/s) and higher by reducing the rotor-turbulence interaction tones below the noise levels from other fan sources so that they make no contribution to the noise spectrum.

There were no forward-velocity effects on the baseline-inlet and hybrid-inlet fan noise as long as testing was conducted at velocities high enough to remove noise due to rotor-turbulence interaction. However, there are two other effects of forward-velocity testing in the 40 by 80 that must be dealt with in the data acquisition and analysis.

The wind tunnel background noise in the 40 by 80 is sufficiently high at low frequencies that fan-noise suppression results from advanced inlets can be in error if the following test guidelines are not used for small fans.

- The forward velocities used during testing should be at least 21 m/s (68 ft/s); this should be sufficient to reduce the rotor-turbulence interaction tone levels below the broadband noise levels.

- The microphone measurements should be made as close to the fan/inlet as possible using the criteria of 10 wavelengths at the lowest frequency of interest. These measurements should be at the engine centerline height, which should be set higher from the wind tunnel floor than the distance to the measurements in order to minimize reverberant reflections.

The above guidelines can easily be satisfied for fans with less than 1 m (3 ft) diameter and 1/3-octave-band data at 250 Hz and higher. The simplest way to satisfy the measurement proximity requirement is to use a circular-arc microphone array. Convection corrections must be made to the levels and locations of the measurements to transform the results to a static equivalent coordinate system so that comparisons can be made between results from static and forward-velocity conditions. This means that spectral comparisons at the same noise-emission angle cannot, in general, be made with fixed-microphone data for different forward velocities or angles of attack. However, the measurements-analysis techniques employed during the 40 by 80 wind tunnel tests solved that problem.

- The circular-arc, traversing-microphone, data-acquisition and reduction system provided spectral results almost continuously around the arc. This enables selection and correction of spectra at equivalent static locations independent of forward velocity and angle of attack. The use of one microphone for angular locations has the added advantage of minimizing measurement errors in the data.

The traversing-microphone system used in the 40 by 80 wind tunnel provided information about the rapidly changing directional characteristics of fan noise on a consistent basis. The traverse data were repeatable because of the stable test conditions provided by the relatively small engine operating in the large airflow environment of the 40 by 80.

5.3 HYBRID-INLET SUPPRESSION AT FORWARD VELOCITY

A primary objective of this investigation was to determine the low-speed-flight effects on the fan-noise suppression characteristics of hybrid inlets by testing them at forward velocity in the 40 by 80. The principal conclusions pertaining to that objective are:

- There are no significant effects on the suppression of either a STOL hybrid inlet on low-tip-speed-fan noise or a CTOL hybrid inlet on high-tip-speed-fan noise due to changes in forward velocity above 21 m/s (68 ft/s) or angle of attack up to 15°.

- When comparing the quasi-static results to those at forward velocity, there are differences in hybrid-inlet suppression due to rotor-turbulence interaction noise that is suppressed at quasi-static conditions.

There are also observations that were made about the basic characteristics of hybrid-inlet fan-noise suppression at forward velocity. These pertain to the various parameters that are important in fan-noise generation and suppression and apply to the specific configurations tested, not necessarily to the general case.

- Low-tip-speed-fan noise that is primarily broadband in nature was suppressed more by the bulk absorber treatment than by flow acceleration.

- High-tip-speed-fan noise that is dominated by tone noise was easily suppressed by either flow acceleration or treatment.

- Suppression levels for the STOL hybrid inlet were 13 PNdB; as much as 18 PNdB was measured for the CTOL hybrid inlet at the higher tip speeds.

- The hybrid-inlet suppression levels were virtually the same at all throat Mach numbers tested because the treatment provided suppression when the flow-acceleration effects were reduced.

- Aerodynamic performance of the hybrid inlets was comparable to low Mach inlets in terms of both inlet pressure recovery and distortion up to 15° angle of attack.

5.4 DEFLECTOR-INLET SUPPRESSION AT FORWARD VELOCITY

Another objective of the investigation was to determine the low-speed-flight effects on the fan-noise suppression characteristics of a deflector inlet by conducting tests at forward velocity in the 40 by 80. The conclusions drawn for the deflector inlet are quite different than those for the hybrid inlets.

- There are considerable effects on the fan-noise suppression of the deflector inlet tested when either forward velocity or angle of attack are changed. The noise characteristics at the higher fan-tip speeds change unpredictably with change in either forward velocity or angle of attack. This is due, in part, to changes in the distortion of the fan entrance static pressures resulting from the asymmetry of the deflector inlet.

The conclusions drawn from the deflector-inlet fan-noise-suppression results are based upon the conditions of 41 m/s (135 ft/s) forward velocity and zero angle of attack. The suppression mechanism of redirecting the fan noise away from the observer and suppressing what is left with treatment was very effective. Comparison of the results with those from the hybrid inlets leads to the following conclusions.

- At low fan-tip speeds the deflector inlet was as effective as the STOL hybrid inlet in suppressing fan noise at noise-emission angles of 50° and higher.
- At high fan-tip speeds the deflector-inlet fan-noise suppression was 3 PNdB to 7 PNdB less than the CTOL hybrid inlet at noise-emission angles of 30° and higher.
- The deflector-inlet fan-noise suppression remained relatively unchanged over the fan-tip-speed range at noise-emission angles of 50° or higher but was reduced at lower angles as fan speed was increased.
- The deflector-inlet aerodynamic performance was better than that of the hybrid inlets in terms of inlet pressure recovery and distortion at all test conditions.

5.5 CANTED-INLET EFFECTS ON FAN NOISE

An important objective of the investigation was to determine whether fan noise was affected by the downward cant of the inlet centerline, relative to the engine centerline, which is typical of wing-mounted turbofan engines. A partial answer to the question was provided by canting the baseline inlet and comparing the results with the baseline inlet at the same test conditions. The important conclusions were:

- The canted baseline inlet causes the same level of static pressure distortion into the fan as actual aircraft inlets.
- The interaction of this level of static pressure distortion with the fan increases the noise levels up to 7 PNdB at the critical sideline angles of 50° and 60° at fan-tip speeds that are consistent with those at approach-power settings on large turbofan engines.

These changes in fan-noise characteristics apply to the baseline inlet (cylindrical, no acoustic treatment). Whether the canting of an actual, treated, aircraft inlet will cause as much noise increase depends upon many parameters. However, the static pressure distortion interaction with the fan has been identified as a source of fan noise, and tests with straight and canted low Mach inlets should be conducted at forward velocity to determine if that source affects the fan-noise-suppression capability of aircraft-type inlets.

APPENDIX - ABBREVIATIONS AND SYMBOLS

α	-	Inlet Angle of Attack
ARC	-	Ames Research Center
BPF	-	Blade-Passing Frequency
Base	-	Baseline Inlet
CTOL	-	Conventional Takeoff/Landing Inlet
Defl	-	Deflector Inlet
ΔSPL	-	Sound Pressure Level Reduction
ΔPNdB	-	Perceived Noise Level Reduction
IGV	-	Inlet Guide Vanes
L/D	-	Length to Diameter Ratio of Inlet
$(L/D)_{TR}$	-	Length to Diameter Ratio of Treatment
Mod	-	Modified JT15D
M_{TH}	-	One-Dimensional Throat Mach Number
N_c	-	Corrected Fan Speed
OASPL	-	Overall Sound Pressure Level
PNL	-	Perceived Noise Level
P_S	-	Inlet Static Pressure
P_T	-	Wind Tunnel Total Pressure
PR	-	Fan Pressure Ratio
QCSEE	-	Quiet, Clean, Short-Haul, Experimental Engine
Red	-	Redesigned JT15D
SPL	-	Sound Pressure Level
Std	-	Standard JT15D
STOL	-	Short Takeoff/Landing Inlet
V_T	-	Corrected Fan Tip Speed
V_o	-	Forward Velocity
$\dot{w}$	-	Corrected Inlet Airflow

REFERENCES

1. Plucinsky, J.C., "Quiet Aspects of the Pratt and Whitney Aircraft JT15D Turbofan," SAE Paper 730289 presented at the Business Aircraft Meeting, Wichita, Kansas, April 3-6, 1973.

2. Hodder, B.K., "Further Studies of Static-to-Flight Effects on Fan Tone Noise Using Inlet Distortion Control for Source Identification," NASA TMX-73, 183, NASA Ames Research Center, Moffett Field, California, December 1976.

3. Moore, M.T., "Forward Velocity Effects on Fan Noise and the Suppression Characteristics of Advanced Inlets as Measured in the NASA Ames 40 by 80 Foot Wind Tunnel, Acoustic Data Report," NASA CR-152329, General Electric Co., Cincinnati, Ohio, December 1979.

4. Anon, "Standard Values of Atmospheric Absorption as a Function of Temperature and Humidity," Society of Automotive Engineers, ARP866A, March 1975.

5. Keith, J.S. et al., "Analytical Method for Predicting the Pressure Distribution About a Nacelle at Transonic Speeds," NASA CR-2217, General Electric Co., Cincinnati, Ohio, July 1973.

6. Gliebe, P.R. and Kerschen, E.J., "Analytical Study of the Effects of Wind Tunnel Turbulence on Turbofan Rotor Noise," NASA CR-152359, General Electric Co., Cincinnati, Ohio, November 1979.